Temporal and spatial variations of nitrous oxide fluxes in Great Britain

Chiara Di Marco

Doctor of Philosophy

The University of Edinburgh

2005

Acknowledgements

My thanks to NERC for funding this work through the GaNE project (NER/T/S/2000/00195).

I would like to thank both my supervisors, Dr. Ute Skiba at the Centre for Ecology and Hydrology, Edinburgh, and Dr. Keith Weston at the Institute of Atmospheric Sciences of the University of Edinburgh, for their invaluable advice, support and encouragement throughout this project. I would also like to thank Dr. Ken Hargreaves for initiating me to the complex world of tuneable laser spectroscopy, Prof. David Fowler and Dr. Eiko Nemitz for their precious advices and for always showing an interest in my work.

I am very grateful to all the people at CEH for the friendly and collaborative atmosphere during these years. Thanks to Massimo Vieno and to Tony Dore for providing the modelling data and for patiently accomplish all my requests, to Mhairi Coyle and Robert Storeton-West for providing more soil and meteorological data, to Stephanie and Sofie for sharing the office and the difficulties of the PhD.

Thanks to Nicole, Genevieve, Jennifer, Cecile, Tim and all the others that encouraged me and made these years an enjoyable experience.

A special thank goes to Daniela for her generous and irreplaceable support as a friend that helped me to survive difficult times in my work and in life, always.

Thanks to Aron for making me smile and keeping my mood up during the last months, even from far away.

Finally, my gratitude goes to my sister Alessia, and to my parents Giuliana and Sergio who have helped and encouraged me through out these years and life in general, and to whom this thesis is dedicated.

Qualche parola in italiano per chi mi ha sempre sostenuta da oltremare durante questi anni.

Grazie a Giovanna, Francesca, Lorenza, Max e a tutti gli amici che mi sono stati vicini nei momenti difficili di questa avventura. Un grazie speciale a Daniela

per il suo sostegno generoso e insostituibile nel lavoro e per la sua amicizia preziosa.

Grazie ad Aron per avermi fatto sorridere e per aver tenuto alto il mio umore negli ultimi mesi, anche se da lontano.

Infine, la mia gratitudine va a mia sorella Alessia e ai miei genitori Giuliana e Sergio, che mi hanno incoraggiato durante tutti questi anni e nella vita in generale, e a cui questa tesi e' dedicata.

Declaration

This thesis has been composed by myself and all work reported herein is my own work except where otherwise stated. This thesis has not been previously presented for any other degree.

Abstract

Estimates of nitrous oxide (N_2O) emissions from grassland at field and national scale are presented. Concentrations of atmospheric N_2O are currently rising due to increasing anthropogenic emissions. This is of concern as N_2O participates in reactions leading to the destruction of stratospheric ozone and adding to radiative forcing. Quantifying these emissions accurately is a challenge complicated by environmentally driven spatial and temporal variability of its main source, microbial production in soils.

In the UK grasslands are the largest source of N_2O. In this project for the first time N_2O was measured from typical intensively managed grassland at Easter Bush, S. Scotland from June 2002 to June 2003 almost continuously. Measurements were made using the micrometeorological eddy covariance technique which couples an ultrasonic anemometer with a Tunable Diode Laser fast response gas Analysis System (TDLAS) to measure the N_2O concentration (precision ±0.9%, frequency 10 Hz). The spatial coverage attainable using long-term eddy covariance N_2O flux measurements (10^3-10^4 m^2) represents a valuable alternative to the commonly used static chamber method (< 1 m^2), overcoming the problem of spatial and temporal variability of N_2O emissions associated with the latter technique. Four fertiliser applications made over this period were investigated in detail together with environmental conditions. Background activity was characterised by small fluxes (± 50 ng N_2O-N m^{-2} s^{-1}). However, N_2O flux varied widely, with a series of daily emission peaks (≤ 3,795 ng N_2O-N m^{-2} s^{-1}) following the fertilisation in June 2002 and less pronounced emissions after the other fertilizations in August 2002, March and June 2003.

A multi-linear regression relating combinations of soil water content, soil temperature and the soil available nitrogen with N_2O fluxes was used to study the seasonal variation of the emissions. Good results (R^2 = 0.83-0.9) were obtained with all the parameters but the best predictors resulted from soil water content and soil temperature at 7 cm depth.

The extraordinarily large pulse observed on the 8th June 2002 immediately after the fertilizer application (120 kg N ha^{-1}) represents 1.6% of the N applied. After this event clear diurnal emission cycles, peaking at noon, were recorded for about 10 days, allowing an analysis of the environmental factors controlling the loss. In this case turbulent parameters such as sensible heat flux and friction velocity were closely related to the N_2O flux suggesting that they could be fundamental drivers in the emissions.

The total budget emission was calculated using a gap filling technique combining two different approaches: a linear interpolation of daily flux averages (calculated over the 30 min measurements) in case of background activity, and the use of a modelled diurnal cycle obtained from the daily pattern of fluxes observed in June 2002 in cases of elevated N_2O emission (daily flux ≥150 ng N_2O-N m^{-2} s^{-1}). The estimate of the total cumulative flux was 5.3 kg N ha^{-1} y^{-1}, representing an emission factor of 1.68%. The data also reveal a small, but significant, uptake during the winter months, highlighting the existence of N_2O sink activity for grassland.

A comparison with static chambers positioned at Easter Bush field in the footprint area of the eddy covariance mast was performed over 3 days of measurements in June 2003. Results showed a reasonable agreement between the two techniques with micrometeorological N_2O hourly fluxes within 50% of those estimated by the chamber method.

The contribution of grassland N_2O emissions to the total GB emissions was assessed by comparison of N_2O concentrations in locations dominated by rural, urban or a mixture of the two activities. Cumulative monthly N_2O concentrations were collected in simple devices between March 2002 and November 2003 from 87 sites across GB. Seasonal variations in locations dominated by grassland agriculture were observed, with summer N_2O concentrations slightly higher than winter concentrations. Overall N_2O concentrations from urban sources were generally higher than from agricultural sources. A preliminary comparison between measured concentrations and N_2O concentrations modelled from average meteorology and a detailed 5x5 km N_2O emission inventory for GB using the Lagrangian atmospheric transport model FRAME (**F**ine **R**esolution **A**tmospheric **M**ulti-pollutant **E**xchange) suggests that our current understanding of the magnitude of total annual emissions in Great Britain is generally correct. The average annual concentration measured at the 55 sites characterised by grassland agricultural N_2O sources was 324 ± 5.7 ppb N_2O and FRAME modelled an annual concentration of 321 ± 0.7 ppb. Therefore, the estimate used in the GB inventory for N_2O emissions from agricultural-grassland sources is broadly accurate.

Table of contents

Chapter 1 Introduction

Nitrous oxide (N_2O) is an important greenhouse gas and plays a role in the destruction of stratospheric ozone (Houghton et al. 1995). Global warming potentials (GWPs) are used to compare the abilities of different greenhouse gases to trap heat in the atmosphere. GWPs are based on the radiative efficiency (heat-absorbing ability) of each gas relative to that of carbon dioxide (CO_2), as well as the decay rate of each gas (the amount removed from the atmosphere over a given number of years) relative to that of CO_2. In the Third Assessment Reports (2001) of the Intergovernmental Panel on Climate Change (IPCC) the published GWP for N_2O is ~290. The current increase rate of 0.2 - 0.3 % y^{-1} (IPCC 2001a) of atmospheric N_2O concentration is mainly attributed to a rise in anthropogenic emissions and agriculture represents one of the main N_2O sources (Kroeze et al. 1999). Due to large spatial and temporal variability, N_2O emissions at the country scale are not quantified very accurately. The current default methodology adopted by the IPCC (IPCC 2001b) to provide estimates for N_2O emissions from managed fertilizer fields assumes that a fixed fraction of nitrogen applied to the soil is emitted as N_2O to the atmosphere. In practice, the fraction of N applied as fertilizer that is emitted as N_2O varies with the type of soil, management and environmental conditions (Smith et al. 1998; Dobbie and Smith 2003). The vast majority of N_2O flux measurements are carried out at low temporal and spatial resolutions, with weekly measurements over small areas (< 1 m^2) being typical. For this reason the scaling up of these measurements to an annual and national estimate of N_2O emissions imposes large uncertainties.

The study presented here is part of the NERC-funded umbrella project GaNE (**G**lobal **N**itrogen **E**nrichment). The thesis aims to provide a better understanding of N_2O emissions at field scale and to provide a method to validate Great Britain's national inventory for N_2O emissions through following objectives:

- Measure N_2O fluxes for one year almost continuously at the field scale using the eddy covariance method.

- Determine the seasonal and diurnal variations of N_2O emissions from grassland and their relationships with environmental conditions.
- Calculate the N_2O annual budget at field scale applying a gap filling technique and improving the accuracy in current N_2O budget calculations.
- Develop a national monitoring network to measure Great Britain's spatial, seasonal and inter-annual variations of N_2O emissions at local, regional and country scale
- Assess the applicability of the monitoring system to validate the national emission inventory for N_2O with the use of the atmospheric transport model 'FRAME'.

1.1 Issues outlined in the study

The thesis begins with a general description of the role of N_2O in the atmosphere and a definition of major known sources of N_2O globally and more specifically in Great Britain (Chapter 2). The processes of N_2O formation in the soil and the relationship of the emissions with the major controlling factors are also presented. The importance of grasslands as a main source of N_2O in Great Britain is discussed.

Chapter 3 describes the micrometeorological methods used to measure and analyses near-continuous N_2O flux measurements at the field scale from typical managed grassland, the Easter Bush field site. The characterisation of the field site, including the description of the experimental set up and instrumentation used, the climatology, and the management of the field, are fundamental for the interpretation of N_2O fluxes (Chapter 4). The results of the measurements are presented in Chapter 5 with a detailed analysis of the quality control of the data and limitation of the technique used. Seasonal and diurnal fluxes are discussed in relation to the controlling factors and the calculation of the annual budget for the field site is explained (Chapter 5). In order to investigate N_2O emissions at the country scale, a national monitoring network was developed to measure concentrations at locations influenced by different N_2O sources (Chapter 6). The measurements from the national monitoring network were used to validate the N_2O emission inventory for

Great Britain by comparison with concentrations modelled by the atmospheric transport model FRAME (Chapter 7). FRAME modelling was provided by Massimo Vieno. Conclusions of the research are presented in Chapter 8.

Chapter 2 Nitrous oxide

2.1 Nitrous oxide in the atmosphere

Besides carbon dioxide (CO_2) the most significant greenhouse gases are methane (CH_4) and nitrous oxide (N_2O) with minor contributions from rarer gases such as chlorofluorocarbons (CFCs and HCFCs). Despite its importance in global warming due to a high GWP (~ 290), a long life in the atmosphere (~120 years) (Houghton et al. 1995) and to its role in destroying stratospheric ozone, the N_2O global budget remains poorly understood at present (Khalil 2000). In the troposphere N_2O is lost by transport to the stratosphere, deposition to the surface and chemical reaction. The loss rate from the troposphere is relatively slow and N_2O is therefore long lived and well diluted. The mixing ratio is relatively constant up to 15-20 km; above that N_2O is decomposed to N_2 and the singlet oxygen atom $O^1(D)$ by photolysis. The chemical reaction in the stratosphere of the N_2O molecule with an excited oxygen atom $O^1(D)$ forms reactive NO. NO naturally reduces ozone in the upper stratosphere to form NO_2 and O_2. The NO_2 then reacts with O to reform NO. In the process, both an ozone and an oxygen molecule are destroyed (i.e., two Ox molecules), while the NO is reformed:

$$NO + O_3 \rightarrow NO_2 + O_2$$

$$NO_2 + O \rightarrow NO + O_2$$

$$\text{NET: } O_3 + O \rightarrow 2\ O_2$$

The increase in N_2O concentration in the atmosphere from ~ 270 ppbv in the early 19th century to about 315 ppbv at present (Bouwman et al. 2000) is related to the increase of anthropogenic emissions. The atmospheric concentration has been increasing at a rate of 0.25% yr^{-1} for several decades (Prather et al. 1995). During the period 1977-1988 rates of increase ranged between 0.5 ± 0.2 ppb yr^{-1} and 1.2 ± 0.1

ppb yr^{-1} and in the 90s the rise was about 0.7 ppb yr^{-1} (Khalil and Rasmussen 1992; Butler et al. 1998). The average atmospheric N_2O concentration in the Northern Hemisphere is 0.8 ppbv greater than in the Southern Hemisphere, which is consistent with 60% of the N_2O emissions occurring in the Northern Hemisphere (Dentener et al. 2001).

The global annual N_2O production of about 16.5 Tg N_2O-N yr^{-1} (Tg = teragram; 1 Tg = 10^{12} g) is extrapolated from the estimates of the stratospheric destruction (~ 12.5 Tg N_2O-N yr^{-1}) and the increase in atmospheric concentration. Although many N_2O sources have been identified, the uncertainty in most of the source estimates is still of a factor of 2 (Bouwman et al. 2000). The uncertainty is generated by the spatial and temporal heterogeneity of soil sources that makes the scaling-up of biogenic flux measurements from these sources very problematic. For anthropogenic sources the scaling-up is linked to political, social, cultural and economic uncertainty factors (Bouwman 1999). Flux measurements have been done quite extensively in North America and Europe but there is still a small availability of measurement data in other parts of the world. To complicate the picture there is a major uncertainty about N_2O production in the atmosphere: Dentener and Kroeze (1994) postulated a formation of N_2O in the troposphere from oxidation of ammonia (NH_3), mainly in the tropics (0.3-1.2 Tg N_2O-N yr^{-1}), and McElroy and Jones (1996) suggested that isotopically-enriched N_2O could be produced in the stratosphere.

Although global climatic changes are direct consequences of environmental alterations, they affect the variation in atmospheric gas concentrations. Studies on ice core sampling could provide important information about the response of the environment to global climatic changes (Fluckiger et al. 1999).

The problem of potential global climate change started to be widely recognised in 1988, when the World Meteorological Organization (WMO) and the United Nations Environmental Programme (UNEP) established the Intergovernmental Panel on Climate Change (IPCC). A main activity of the IPCC is to provide regular assessments of the state of knowledge on climate change. Its Second Assessment Report (SAR), Climate Change 1995 (IPCC 1995) provided key input to the negotiations, which led to the adoption of the Kyoto Protocol to the UN Framework

Convention on Climate Change (UNFCCC) in 1997 (IPCC 1997). The countries that signed the Kyoto Protocol committed to individual targets to limit or reduce their greenhouse gas emissions. The total cut in emissions of at least 5% from 1990 levels is the common commitment in the period 2008-2012.

In order to find mitigation solutions or emissions reduction strategies, a large quantity of flux measurement studies at small and large scale in different type of ecosystems, coupled with empirical/process/transport models, is needed.

The present study focuses on a specific type of ecosystem, managed grassland, which is predominant in Great Britain and a very important source of N_2O emissions.

2.2 Sources and sinks of atmospheric N_2O

The known major sources of N_2O that have been included in global inventories are shown in Table 2.1 (IPCC 2001a). The main natural sources of N_2O emissions are soils under natural vegetation (tropical wet forests and dry savannah, temperate forests and natural grasslands), oceans and river estuaries (although the latter are strongly affected by human activity) and lightning. Principal anthropogenic sources are agricultural soils, biomass burning, fossil fuel combustion, especially in vehicles fitted with catalytic converters, nitric and adipic acid production (for use in fertilizer manufacturing and for production of nylon respectively) (Bouwman et al. 1995). Recently also sewage treatment, animal manure and waste incineration have been identified as potential N_2O sources (IPCC 2001b).

Table 2.1 Estimates of the global nitrous oxide budget (in Tg N yr^{-1}) from different sources as they appear in the IPCC 2001 report.

Reference	(Mosier et al. 1998) (Kroeze et al. 1999)		(Olivier et al. 1998)		SAR[a]	TAR[b]
Base year: Sources	**1994**	**range**	**1990**	**range**	**1980s**	**1990s**
Ocean	3.0	1-5	3.6	2.8-5.7		
Atmosphere (NH_3 oxidation)	0.6	0.3 -1.2	0.6	0.3 -1.2	3	
Tropical soils						
Wet forest	3.0	2.2 -3.7				
Dry savannahs	1.0	0.5 -2.0			3	
Temperate soils					1	
Forests	1.0	0.1 -2.0				
Grasslands	1.0	0.5 -2.0			1	
All soils			6.6	3.3 -9.9	1	
Natural sub-total	9.6	4.6 -15.9	10.8	6.4 -16.8	9	
Agricultural soils	4.2	0.6 -14.8	1.9	0.7 -4.3	3.5	
Biomass burning	0.5	0.2 -1.0	0.5	0.2 -0.8	0.5	
Industrial sources	1.3	0.7 -1.8	0.7	0.2 -1.1	1.3	
Cattle and feedlots	2.1	0.6 -3.1	1.0	0.2 -2.0	0.4	
Anthropogenic Sub-total	8.1	2.1 -20.7	4.1	1.3 -7.7	5.7	6.9a
Total sources	**17.7**	**6.7 -36.6**	**14.9**	**7.7 -24.5**	**14.7b**	
Imbalance (trend)	3.9	3.1 -4.7			3.9	3.8
Total sinks (stratospheric)	**12.3**	**9 -16**			**12.3**	**12.6**
Implied total source	16.2				16.2	16.4

[a] IPCC Second Assessment Report
[b] IPCC Third Assessment Report

About 70% of the global anthropogenic N_2O emissions are estimated to be derived from the agricultural sector (Cole et al. 1997; EIA 1998) e.g. from increased fertiliser use and indirectly by enhanced N deposition inputs (Granli and Bockman 1994) or land use changes (Keller et al. 1993). The use of estimates of global N_2O emissions for the period 1500-1994 as input for a simple atmospheric model resulted in a closed budget over time, showing that the increase in atmospheric N_2O can be primarily attributed to changes in food production systems. The fast expansion of agricultural land, coupled with intensification of land use during the 19th century, have caused a net increase of N_2O (Kroeze et al. 1999). In 2001 the agricultural/animal/human chain processed approximately 227 Tg N yr^{-1}, with over 50% contributed by animal (McElroy and Wang 2005). Predictions indicate that N_2O emissions from agro-ecosystems to the atmosphere would increase by 1.4 times between 1990 and 2020 (from ~6 Tg N yr^{-1} to 9 Tg N yr^{-1}), with the main increase occurring in Asia from increased N input into food production systems. The

consequent increase in atmospheric N_2O concentration will lead to values of 340-350 ppbv in 2020 (Mosier and Kroeze 2000).

Emissions from rivers, estuaries and continental shelves (1.9 Tg N yr^{-1}) (Seitzinger and Kroeze 1998) account for about 35% of total aquatic N_2O emissions, whereas oceanic emissions represent the remainder. Much of the N_2O emissions from the aquatic system is anthropogenic (Seitzinger et al. 2000) and thus contributes to the current increase in atmospheric N_2O. A chart comparing N_2O emissions from aquatic (including rivers, estuaries, continental shelves and oceans) and terrestrial systems is presented in Figure 2.1 from Seitzinger et al (2000).

The deforestation and conversion of wet tropical lands to pasture is regarded as a source of N_2O emissions but the annual estimate of 1 Tg N_2O-N yr^{-1} has a high uncertainty due to the lack of detailed knowledge of the land use history (Keller et al. 1993).

Earlier estimates of anthropogenic N_2O inputs regarded fossil fuel burning as the major source, but power generation is now considered to be a minor source, and N_2O formation in catalytic converters is a rising source (Cant et al. 1998). Updated studies of N_2O emissions from vehicles have shown that these have a global warming impact corresponding to 1-2% of that of the CO_2 emissions from vehicles. Estimates of annual N_2O emission from the global vehicle fleet amount to 0.08 ± 0.04 Tg N yr^1, which represents 1-4% of the atmospheric growth rate of this species (Becker et al. 2000). Disparate results were found in the hypothesis that the entire fleet of existing vehicles were equipped with present day catalysts: N_2O emissions from cars could reach up to 7% (Jimenez et al. 2000) or 32% (Berges et al. 1993) of the atmospheric growth rate.

N_2O is very stable in air and chemical reactions in the stratosphere are regarded as the main processes for removal of N_2O from the atmosphere. These processes include those that control stratospheric ozone concentration (Granli and Bockman 1994; Wrage et al. 2001).

Soil can represent a small sink for atmospheric N_2O under conditions favourable for N_2O reduction, but only a few studies are available in the literature (Freney et al. 1978; Ryden 1981; Flechard et al. 2005) Soil is probably only a minor sink of N_2O at the global scale (Granli and Bockman 1994). A better understanding of the global

sink strength of soils however is required, since it could influence the N_2O residence time in the atmosphere (Cicerone 1989).

Figure 2.2 (taken from Mosier et al., 1998) shows the relationship between N_2O emissions, the agricultural nitrogen cycle and the systems in which N is transported after leaving the agricultural system.

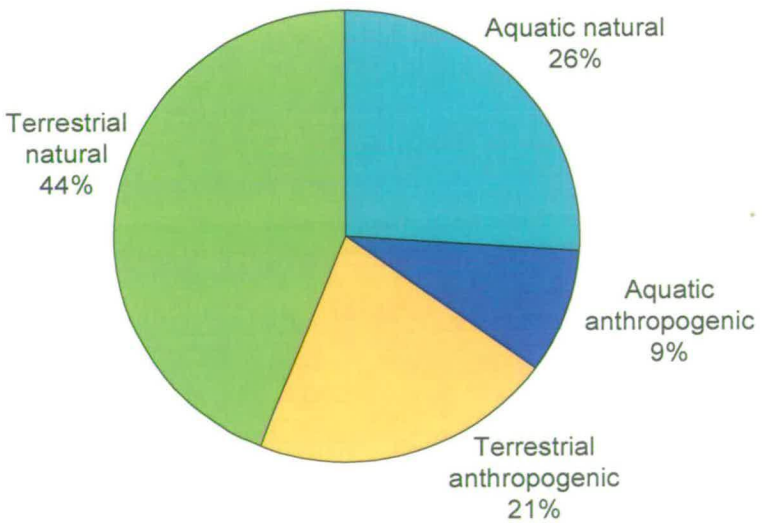

Figure 2.1 Comparison of N_2O emissions from aquatic (rivers, estuaries, continental shelves and oceans) and terrestrial systems. The anthropogenic and natural component of each type is also indicated (redrawn from Seitzinger et al, 2000).

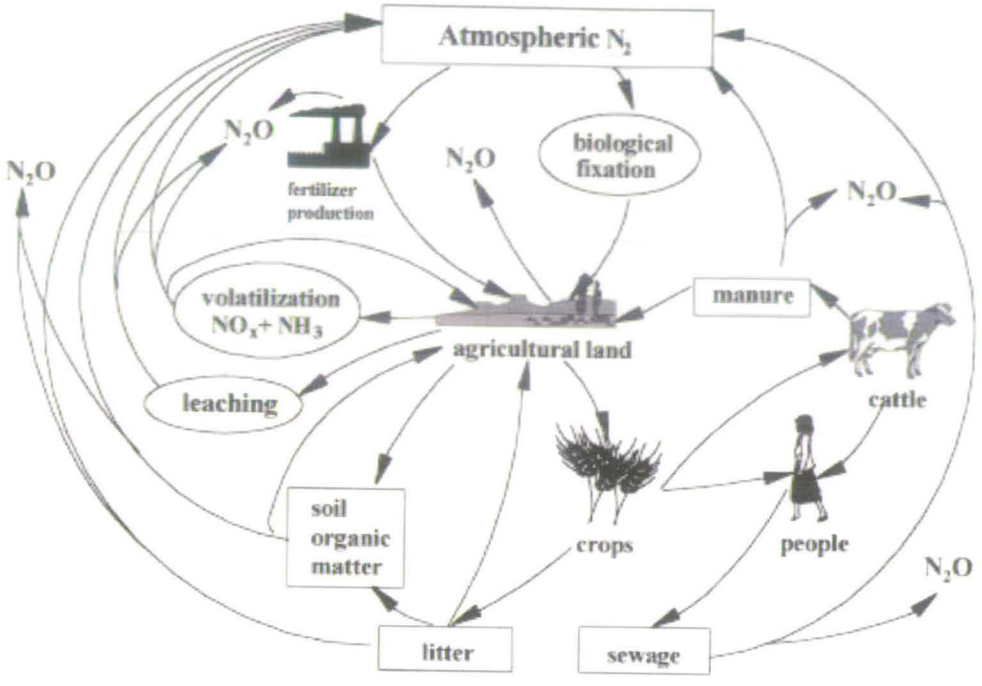

Figure 2.2 Depiction of the nitrogen cycle of agricultural soils and its relationship to N_2O production (by Mosier et al. 1998).

2.2.1 N_2O emissions from the UK

The main emission sources for the UK are agriculture, road transport, combustion and chemical processes (the latter mainly in England) (Goodwin et al. 2001). Overall UK emissions have fallen by 40.5% between 1990 and 2003, driven predominantly by a large reduction in emissions following the installation of abatement measures (Shimizu et al. 2000) at an adipic acid plant in England (Table 2.2). This overall downward trend is offset to a small degree by a rise across the country in N_2O emissions from the transport sector over the period due to increased use of three-way catalytic converters. Agricultural soils represent the main N_2O source and in 2003 produced about 83 kt N_2O y^{-1}. Processes in industry, mainly adipic and nitric acid production, decreased their emission from 94 kt N_2O y^{-1} in 1990 to 10.8 kt N_2O y^{-1} in 2003. On the other hand, during the same period the contribution of fuel combustion from traffic to the total emission increased from 4.3 kt N_2O y^{-1} in 1990 to 16.3 kt N_2O y^{-1} in 2003 (Baggott et al. 2005). The trend in N_2O emissions from principal sources in the UK from 1990 to 2003 in presented in Table 2.2.

Table 2.2 N_2O annual emissions from the UK for the period 1990-2003. Data obtained from the Greenhouse gas emission report for 2005 of the National Atmospheric Emissions Inventory (NAEI).

N_2O source categories	1990	1995	1998	1999	2000	2001	2002	2003
				(kt N_2O y^{-1})				
Energy (fuel combustion, transport)	17.85	20.76	24.67	25.46	26.81	28.16	28.91	28.68
Industrial processes (adipic and nitric acid production)	94.46	61.30	59.45	18.16	20.20	17.40	9.92	10.34
Manure management	4.88	4.82	4.93	4.93	4.64	4.45	4.31	4.26
Agricultural soils	98.10	93.81	94.42	92.56	89.12	83.43	85.22	83.06
Waste (wastewater handling, waste incineration)	3.47	3.46	3.96	3.96	3.94	4.06	4.04	4.05
International bunkers (aviation, marine)	0.92	1.06	1.36	1.28	1.32	1.34	1.25	1.26
Total UK national emissions	**219**	**184**	**187**	**145**	**145**	**138**	**132**	**130**

2.3 Global and regional spatial emission inventories

Currently, for most known sources spatially explicit inventories are available, but for some sources only global estimates are produced with explicit emission fields yet to be obtained (Bouwman et al. 2000). With data for all sources obtained from Bouwman et al. (1995), for oceanic sources obtained from Nevison et al. (1995) and for rivers, estuaries and continental shelves from Seitzinger and Kroeze (1998), Bouwman et al. (2002) present a global geographical source distribution with a 1°x1° resolution. An example of global N_2O emission from soils under natural vegetation and fertilized agricultural fields from data in Bouwman et al. (1995) is presented in Figure 2.3 (source: Global Emission Inventory Activity (GEIA)).

The emission factor (EF) approach is the most widely used method to produce budgets and geographical inventories of N_2O. For soils and oceans, modelling approaches are also used, including process models and simple regressions.

In emission factor approaches, emission estimates are a combination of measurement data and geographic and statistical information. The standard methodology presented by IPCC (IPCC 2001b) for estimating N_2O emissions from fertilised soils is an example of this approach: emissions are calculated as a fraction of N input to the soil, as a result of a simple regression model established by Bouwman (1996), based on 20 long term studies in industrialised countries:

$$N_2O\text{- flux (kg N ha}^{-1}\text{yr}^{-1}) = 1 + 0.0125 * \text{N application} \quad (2.1)$$

where 1 kg N_2O-N $ha^{-1}yr^{-1}$ is the background emission. Further data however showed that the actual range is much wider (0-10%) (Mosier and Kroeze 1999), mainly because variations in soil management, soil type and climate are not taken into account in the calculation but they heavily affect the emissions. Uncertainties related to this type of approach on the global scale are large (50-100%), due to the generalisation of EF, to a lack of measurements or because data do not cover a wide range of environmental conditions, in particular in tropical countries, and to a lack of underlying data (such as soil management, etc.) (Bouwman et al. 2000).

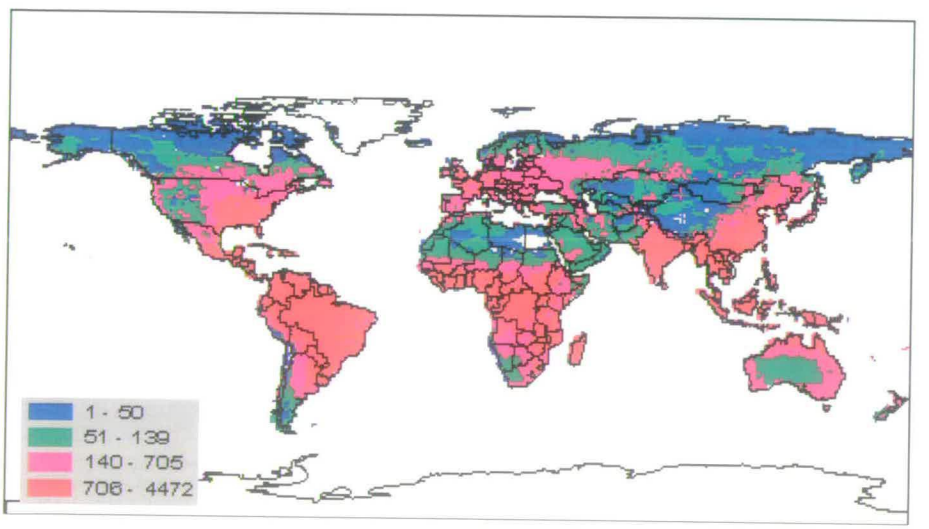

Figure 2.3 N_2O global emission inventory with 1°x 1° resolution for soils under natural vegetation and fertilised agricultural fields. Values are in ton N_2O-N yr^{-1} per 1°square. (Based on data in Bouwman et al., 1995; source: Global Emission Inventory Activity (GEIA)).

In multiple regression methods the emissions are correlated with activities or processes influencing N_2O fluxes, such as changes in soil and climatic characteristics. An example of this approach is given in Section 2.3.1. On the global scale the unreliability of the regression method is mainly caused by the lack of measurement data for particular ecosystems (Bouwman et al. 2000).

Empirical and process models are used to study the system as a combination of elements. The description of the behaviour of the entire system is given through the interaction of its components. An example of results of an empirical model is the

global inventory for oceans (Nevison et al. 1995), whereas examples of process models are the Carnegie-Ames-Stanford (CASA) Biosphere (Potter et al. 1996) and the field-scale process-based Denitrification-Decomposition model (DNDC) (Li et al. 1992). The latter simulates N_2O and NO_x fluxes from decomposition and denitrification in soils, using soil, climate and management data. At large scale DNDC was successfully applied to predict N_2O emissions for agricultural land in the USA (Li et al. 1994).

2.3.1 N_2O emissions inventories in Great Britain

A spatial inventory of N_2O emissions from agricultural and non-agricultural soils in Great Britain, described in Sozanska et al. (2002), was prepared using a simple regression model within a Geographic Information System (GIS) framework and a resolution of 5 km x 5 km. The model, based on data published in literature between 1980 and 1997 (Sozanska 1999), describes emissions as a function of N input, water soil content, soil temperature and land use. Total N_2O emissions from soil in Great Britain were estimated at 127 kt N_2O-N $y^{-1}$and maps of annual and seasonal distributions showed that the largest fluxes occurred in the wetter grassland areas of West Britain (Skiba et al. 2001). The annual emissions predicted by the model for agricultural soils (EF = 2.9%) were higher than those calculated using the IPCC emission factor of 1.25% of N input (Sozanska et al. 2002). The main uncertainty of the linear regression model is due to scaling-up from short-term measurement data (Sozanska et al. 2002).

Another approach was adopted by Brown et al. (2002) to create a UK emissions inventory for N_2O. A new version of the mechanistic model DNDC (Li et al. 1992) has been implemented to improve applicability to UK conditions (Brown et al. 2002) and used as the basis of an inventory of N_2O emission from UK agriculture in 1990. The input for the UK-DNDC model included county scale databases of crop areas, animal numbers and agricultural practices together with environmental data including soil types and daily weather. The estimate of the total emission from UK current agricultural practice in 1990 was 50.9 Gg N including 31.7 Gg from the soil sector, 5.9 Gg from animals and 13.2 Gg from the indirect sector. The EF for fertiliser application (1% of N applied) was lower, but still very close, than the IPCC value EF of 1.25% (Brown et al. 2002). A FOREST version of the UK-DNDC

developed at the Institute of Grassland and Environmental Research (IGER) included data for dominant species of coniferous and deciduous woodland, average tree age and data on the dominant woodland soils in each county. When compared for soil emissions over 19 counties in the UK the results from DNDC approach and the regression method were in good agreement ($R^2 = 0.73$) (Skiba et al. 2005).

A spatially disaggregated inventory of Great Britain N_2O emissions with resolution of 5 km was created for the GANE project using the soil emissions as calculated in the inventory obtained by Sozanska et al. (2002) and emissions from the remaining main sources (transport, industry, rivers, estuaries, manure management and atmospheric N deposition). Emissions from industry, transport, rivers, estuaries and livestock were calculated as advised by the Department for Environment, Food and Rural affairs (DEFRA) and the IPCC, for indirect emissions from atmospheric N deposition the IPCC EF was modified for mineral soils (Skiba et al. 2005). This inventory for Great Britain was used in this thesis as input for the Transport Lagrangian model FRAME in Chapter 7.

2.4 N_2O production in the soil

The production of N_2O results mainly from microbial processes (denitrification and nitrification) of nitrogenous compounds. The microbial transformations are essentially the same whether they take place in soils, wastewater treatment plants, sediments or water bodies (Wrage et al. 2001).

Although pure culture and enzyme studies have clarified the biochemical pathways of nitrification and denitrification, several physical, chemical and biological factors regulate N_2O fluxes, as it is explained by the "hole-in-the-pipe" (HIP) model proposed by Firestone and Davidson (1989) (Figure 2.4), complicating the ecological controls over these processes in nature (Davidson 1991; Groffman 1991). These are:

- the factors, such as changes in soil conditions, that affect the rates of nitrification and denitrification, (rates are identified in the model with the amount of nitrogen flowing through the pipe);

- the factors that affect the relative proportions of the process products, such as the ratio of N_2O and NO or N_2O and N_2 (proportions are illustrated in the model by the size of the holes in the pipe);
- the factors influencing the release of N_2O from the soil to the atmosphere through gaseous diffusion, e.g. site of production in the soil profile, soil texture and soil water content.

The idea expressed metaphorically by the HIP model was of a fluid flowing through a leaky pipe with a flow rate analogous to rates of nitrification and denitrification (Figure 2.4). The NO and N_2O trace gases 'leak' out of holes in the pipe, and the size of holes through which they leak is determined primarily by the soil water content but also affected by the relative abundance of electron donors (soil organic carbon) and acceptors (oxygen, nitrate and sulphate). Soil water content is also important because it controls the transport of O_2 into the soil and the transport of NO, N_2O and N_2 out and into the soil, influencing the diffusive transport of these gases (Davidson et al. 2000).

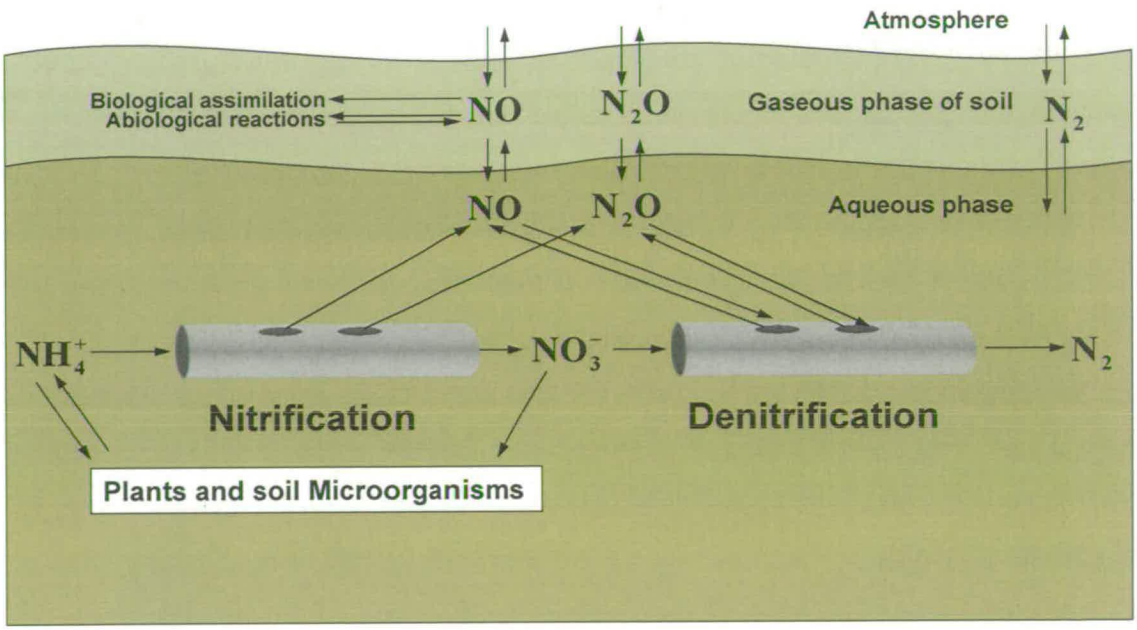

Figure 2.4 Diagram of the "hole-in-the-pipe" conceptual model (redrawn from Davidson *et al.*, 2000).

2.4.1 Nitrification

Nitrification is an aerobic process performed by autotrophic and heterotrophic bacteria. Autotrophic nitrification is the most studied process and produces highest rates of N_2O (Granli and Bockman 1994).

Autotrophic nitrifiers use CO_2 as a carbon source and use ammonium (NH_4^+) and nitrite (NO_2^-) as a source of energy. Nitrification takes place in two steps: the first one is the oxidation of NH_4^+ to NO_2^- with hydroxylamine (NH_2OH) as an intermediate:

$$NH_4^+ + 1.5O_2 \rightarrow NO_2^- + 2H^+ + H_2O + \text{energy}$$

and in the second step NO_2^- is oxidised further to NO_3^-:

$$NO_2^- + 0.5O_2 \rightarrow NO_3^- + \text{energy}$$

The bacteria involved in the first step are called ammonium oxidisers and *Nitrosomonas* species are the best studied (Klemedtsson et al. 1999) in this group. The nitrite oxidisers are the micro-organisms that carry out the second step of the process and representative of the group are *Nitrobacter* species.

The N_2O formation from nitrification has been a subject of debate and two processes are mainly regarded as responsible (Groffman 1991; Granli and Bockman 1994): i) the nitrifier denitrification occurs when NH_4^+-oxidizers use NO_2^- as an alternative electron acceptor at sub-optimal O_2 concentrations and reduce it to NO and N_2O (Firestone and Davidson 1989). This process can be an important source of N_2O under certain circumstances, i.e. high N content, low organic C content, low O_2 pressure and low pH, but it has not been investigated as deeply as the denitrification yet (Wrage et al. 2001); ii) N_2O can be the result of the chemical decomposition of intermediates between NH_4^+ and NO_2^- such as NH_2OH or NO_2^- itself (special form of chemodenitrification).

Heterotrophic organisms use organic carbon as a source of C and energy. More common among fungi than bacteria, it is generally considered to be a minor source of N_2O, although it might produce significant amount of N_2O in conditions of low pH, high oxygen and availability of organic material (Anderson et al. 1993).

At the field scale, nitrification is strongly controlled by ammonium supply either from fertiliser or from mineralization of organic N compounds. Soil water, which is a fundamental regulator of O_2 availability in the soil, is also a strong controlling factor for nitrification, as well as soil pH and soil temperature (Groffman 1991).

2.4.2 Denitrification

Denitrification is the anaerobic process by which fixed N is returned to the atmospheric pool of N_2. Denitrifiers are heterotrophic micro-organisms and facultative anaerobes that are able to use nitrate (NO_3^-) as an electron acceptor in case of low O_2 availability. It is the stepwise reduction of NO_3^- to N_2 with N_2O as regular intermediate (Figure 2.5) (Granli and Bockman 1994; Wrage et al. 2001).

Many soil bacteria are able to denitrify and the end product of denitrification varies: some bacteria produce only N_2, while others generate a mixture of N_2 and N_2O. Important controls for denitrification include nitrate supply, water content (as a mean for anaerobicity) and carbon supply. In environmental conditions favourable to the production of N_2O relative to N_2 (e.g. low temperature, low pH, presence of O_2), the rate of denitrification is usually rather low. Furthermore, N_2O is favoured by lower levels of soil moisture, whereas N_2 is favoured by higher soil moisture (Granli and Bockman 1994; Machefert et al. 2002).

Figure 2.5 Simplified biochemical denitrification pathway (redrawn from Groffman, 1991)

2.4.3 Other processes

The only other significant process is chemodenitrification, which involves chemical reactions between NO_2^- and organic compounds such as amines under acid conditions, to form NO and N_2O and reduction of NO_3^- and NO_2^- by ions such as Fe^{2+} in sub-soils (Smith 1997).

The contribution of nitrification and denitrification to the production of N_2O varies with climate, soil conditions and soil management (Table 2.3). Commonly

high rainfall, small soil diffusion, fine soil texture and high carbon content in the soil will favour denitrification, whereas dry soil, good drainage, aeration and coarse texture will promote nitrification (Groffman 1991). However, because of the very complex interactions of the environmental conditions it is very difficult to distinguish which process prevails in the soil. Furthermore, due to the micro-scale soil heterogeneity the two processes can also occur at the same time in different locations of the soil.

Table 2.3 Soil characteristics that contribute to nitrification and denitrification (from Machefert et al. 2002)

	Nitrification	Denitrification
Substrate availability	NH_4^+, urea	NO_3^-
O_2 concentration	High	Low
Reduced carbon	No effect	High (energy source)
Soil temperature	High (within range)	High (within range)
pH	>5	Low (<5)
Moisture	Intermediate	High
(Water filled pore space)	30-70%WFPS	55-100% WFPS

2.5 Factors controlling N_2O emissions

The principal soil variables that control the emission of N_2O are soil water content, temperature and N availability (see Paragraph 2.5.1-2.5.3), but pH and soil type can also affect the production and emission of N_2O from the soil. Other factors that influence N_2O emissions are related to the land management, grazing, soil drying/wetting, change of land use, etc (see Paragraph 2.5.4).

2.5.1 Soil water content

The variation of water content in the soil influences the production of N_2O in several ways: it promotes microbial processes producing N_2O and regulates the aeration of the soil.

The increase of water reduces aeration and stimulates denitrification although the ratio of N_2O/N_2 decreases with increasing soil water content (Murakami and Kumazawa 1987; Smith et al. 1998; Rudaz et al. 1999). If the soil wetness is at or above the level of *field capacity* (the amount of water that a given volume of soil can

hold against the force of gravitation) the soil pores are filled with water representing a physical barrier to N_2O emission. Furthermore, a prolonged residence of N_2O in the soil increases the possibility of N_2O reduction: N_2O derived in the top soil is more likely to be emitted to the atmosphere than the gas formed more deeply in soil (Granli and Bockman 1994). Also, nitrification is an aerobic process and therefore promoted by the increase of water content up to the point of O_2 limitation (Davidson 1991). The nitrification production ratio N_2O/NO_3^- increases as the conditions become more anaerobic with increasing soil water content.

A physical parameter commonly used in the literature to express the water content in the soil is the *water-filled pore space* (WFPS), defined as:

$$WFPS(\%) = \frac{VWC}{P} * 100 \qquad (2.2)$$

where: VWC is the *Volumetric water content* (vol-%) representing the water volume as a percentage of total soil volume; P is the soil *porosity* (cm^3 cm^{-3}), characteristic of the type of soil ranging between 0.3 and 0.6 for mineral soils and depending on the bulk density and particle density of the soil (refer to Chapter 4 for explanation).

N_2O emissions generally increase with increasing water content until the soil becomes very wet and emissions decrease. Davidson (1991) has illustrated the relationship between soil water, expressed as WFPS, and N_2O and N_2 emissions due to denitrification and nitrification, suggesting that N_2O emissions are at a maximum at a WFPS of 60%. However, later studies on widely contrasting environments suggest that maximum N_2O fluxes occur at a WFPS of 75-85% (Keller and Reiners 1994; Clayton et al. 1997; Veldkamp et al. 1998; Dobbie and Smith 2001) and then decrease at WFPS above 90% due to reduction of N_2O to N_2 (Smith et al. 1998). The influence of soil water content on the N_2O formation processes is strictly related to the type of soil. For example, nitrification rates in fairly wet soils (about 70% of the field capacity) were found higher in loamy soils than in coarse sandy soil, and denitrification rates in sandy loamy soils were very dependent on water content whereas in coarse sandy soil no relationship was observed (Maag and Vinther 1996). As a consequence, the model proposed by Davisdon (1991) is considered a correct

description of the general relationship between fluxes, although the maximum can vary with soil type (Granli and Bockman 1994).

Although rainfall by itself does not provide an accurate estimate of the moisture in the soil, since the latter varies largely depending on the type of soil, it still can offer information about the state of the soil. Correlation between N_2O emissions and rainfall are shown in several studies and suggest a good relationship ($R^2 = 0.7$, $p<0.01$) (Dobbie et al. 1999) between the two factors (Clayton et al. 1994; Brown et al. 2002).

2.5.2 Soil temperature

Soil temperature controls the general microbial activity and nitrification and denitrification rates. The rapid increase in process rate with rising temperature suggests that the response to temperature is primarily a biochemical response (Smith 1997; Machefert et al. 2002). In many laboratory studies the effect of temperature increase on the denitrification and nitrification rate has been investigated and they have all found positive correlation (Macduff and White 1985; Malhi et al. 1990). The denitrification product ratio N_2O/N_2 falls with increasing temperature, whereas the one from nitrification N_2O/NO_3^- tends to rise. The resultant effect is an increase of N_2O emission rate with temperature (Clayton et al. 1994; Granli and Bockman 1994; Smith et al. 2003).

The diurnal and seasonal changes in temperature were found to be directly correlated with N_2O emissions from many soils in temperate climates, although N availability and water content can be limiting factors (Thomson et al. 1997; Dobbie et al. 1999).

2.5.3 N availability

Availability of mineral N (NH_4^+ and NO_3^-) to microorganisms is an important controller of the microbial processes forming N_2O. The increase of NO_3^- content in the soil strongly enhances the denitrification rate up to a level of NO_3^- concentration after which the rate stays constant (Granli and Bockman 1994). NO_3^- usually inhibits or retards the N_2O reduction to N_2, resulting in an increasing N_2O/N_2 ratio. Increasing NO_3^- concentration leads to a rise of N_2O emissions, due to increases of

the nitrification rate and production ratio. N_2O production from nitrification increases with soil NH_4^+ concentration.

N input in the soil is mainly provided by N fertilisation, N atmospheric deposition and N mineralization. The current IPCC (1997) default estimate for atmospheric N deposition assumes that 1% of the N deposited to soils is emitted as N_2O, but experimental studies have shown emission rates significantly above this estimate (Brumme et al. 1999; Machefert et al. 2002).

Applying N fertiliser produces pulses of N_2O emission, in general with no long-term effect (Skiba et al. 1998), and near-background losses are restored when the substrate is depleted, which usually occurs within a few days to several weeks after application (Skiba and Smith 2000; Scanlon and Kiely 2003).

Furthermore, N_2O emissions vary largely depending on the application of different types of fertilisers (McTaggart et al. 1997; Dobbie and Smith 2003).

N mineralization is enhanced by ploughing the soil or during freeze-thaw cycles. Bacteria and fine roots are killed in the freezing soil providing a supply of nutrients which can be used by microorganisms during thawing (Teepe et al. 2004). Several studies showed significant (accounting for 43-52% of the total annual emissions) peaks of N_2O emissions during freeze-thaw periods under conditions of low temperature and fertilizer application (Kammann et al. 1998; Maggiotto and Wagner-Riddle 2001).

2.5.4 Land management practices influencing N_2O emissions

N inputs from mineral and organic N application and N deposition are taken into account by the IPCC (1997) default calculation of N_2O emissions, but many other processes can influence N_2O losses from soils (Skiba and Smith 2000). These include land use change from forestry to agriculture (Keller et al. 1993), biomass burning , ploughing of arable land, grazing and soil drying/wetting. These practices enhance the N mineralization and may temporarily decrease the competition between plants and microbes for N, thereby increasing N_2O losses (Skiba and Smith 2000).

The change in land use, especially deforestation, is a prominent problem in Central and South America, where studies have shown that the actual conversion process of tropical forests to pasture increased substantially emissions of N_2O (from 50-100 $\mu g\ N_2O\text{-}N\ m^{-2}\ h^{-1}$ to 380-580 $\mu g\ N_2O\text{-}N\ m^{-2}\ h^{-1}$) (Keller et al. 1993).

Biomass burning is a source of N_2O during the fire and enhances N_2O emissions afterwards by stimulating N mineralization in the soil. It is estimated that 40% of all savannahs are burned each year (Yienger and Levy II 1995). Higher N_2O fluxes are observed after the practice and they often are persistent for months afterwards (Levine et al. 1988; Weitz et al. 1998).

The practices of tillage and drainage of the soil and ploughing and compacting the soil (with tractors or grazing) change the aeration and modify the process of moisture evaporation, promoting N_2O losses (Skiba and Ball 2002; Skiba et al. 2002; Yamulki and Jarvis 2002). Grazing animals affect the chemical, biological and physical properties of soils, through excretion of urine and dung, and treading. Urine and dung contain mineral N and mineralisable C that control N_2O production in soils (Davidson 1991). Furthermore, the high concentration of NH_3 in the urine patches could provide accumulation of NO_2^- during nitrification, which may amplify N_2O production (Chalk and Smith 1983). Treading by grazing animals compacts the soil increasing the denitrification rate (Douglas and Crawford 1993) and N_2O emission rate (Hansen et al. 1993; Sitaula et al. 2000).

2.6 N_2O emissions from grassland

Globally grasslands cover a large area (~20%) (Bouwman et al. 1995) and in Europe managed grasslands represent between 20% and 30% of the land area, depending on the country, with 37% of the total area managed by agricultural practices devoted to grassland (Soussana et al. 2004).

In a literature study of quantitative estimates of N_2O emission rates from a range of land-uses across Europe, Machefert et al. (2002) showed that the highest rates were from agricultural lands compared to forests and natural grasslands. UK managed grasslands gave one of the highest emission rates (9.35 kg N_2O-N ha^{-1} y^{-1}) compared to forest and natural grassland (0 - 4.9 kg N_2O-N ha^{-1} y^{-1}) in the rest of Europe (Machefert et al. 2002). Furthermore, managed grasslands cover a large area (about 67690 km^2) equivalent to 28% of the UK. They receive large rates of fertiliser (200 – 500 kg N $ha^{-1}y^{-1}$), they tend to be in the wet parts of the country, which cannot be used for arable agriculture, and they are trampled and compacted by animals (Skiba et al. 1996).

During spring, summer and autumn N fertilised and grazed grasslands are generally higher N_2O emitters than fertilized-mown or simply mown ones (Velthof et al. 1996a), by a factor of 4 or 2-3 respectively (Soussana et al. 2004). Also, N_2O emissions from managed grasslands were consistently higher than emissions from crop soils (Smith et al. 1998; Dobbie et al. 1999).

Diurnal cycles of N_2O fluxes have been observed in controlled environment studies (Smith et al. 1998). Maxima were on average 40% (~55 μg N_2O-N m^{-2} h^{-1}) higher than the minimum fluxes and were related to temperature cycles of soil deeper than 10 cm (Thomson et al. 1997). In other sudies the diurnal pattern of N_2O emissions was better related to temperature cycles at the soil surface (Yamulki et al. 1995)

Variations of N_2O fluxes between seasons as well as between soil types are large (Velthof et al. 1996a; Kammann et al. 1998). Similarly, inter-annual variability in N_2O losses can be heavily influenced by the grassland management (Yamulki and Jarvis 2002) and climatic conditions with emission factors ranging from 0.4 to 5.8% of the N input (Velthof et al. 1996a; Dobbie et al. 1999).

Spatial variability of N_2O losses is extremely high (6-222%) in the case of grazing grassland, caused by the uneven compaction by livestock and deposition of excreted N (Yamulki et al. 1995; Flessa et al. 1996; Williams et al. 1999) In addition, N_2O fluxes in mown grasslands can be related to microtopography, e.g. the soil topography at a small scale. In grazed grasslands the animal activity dominates the spatial pattern making the effect of micro-slopes less evident (Velthof et al. 1996b). The study of the topography at field scale is needed when modelling N_2O fluxes from soil (Ambus 1998).

Recognizing the important role played by European grasslands in global warming, the GREENGRASS project was commissioned by the EU (DG Research, V^{th} Framework Programme, Energy, Environment and Sustainable Development) to reduce the large uncertainties concerning the estimates of CO_2, N_2O and CH_4 fluxes to and from grassland and to evaluate mitigation scenarios by up-scaling at European scale. Overall grasslands seem to act as a small sink of greenhouse gas (Soussana et al. 2004), although other studies showed that management practices can determine whether the grassland is a global warming sink or source (Leahy et al. 2004). This

highlights the importance of measuring and studying emissions of the three gases from grassland at the same time.

The role of grassland as an N_2O sink was studied by Ryden (1981). In his study results showed that fertilized fields with water content exceeding 20% (gravimetric moisture) acted as a sink, whereas unfertilized fields were invariably both sink and source when the water content in the soil was > 20%. Although moist to wet soils represent conditions favourable to sink activity, they can restrict N_2O movement from the atmosphere to zones of N_2O depletion within the soil, limiting the sink activity. Negative fluxes rarely exceeded mean weekly rates of 5.8 ng N m^{-2} s^{-1} (Ryden 1981) independently of fertilizer application. This observation suggested that in this case sink activity was limited more by the ease of diffusion of N_2O from the atmosphere to the soil than by the potential for reduction to N_2. More recently, Flechard et al. (2005) have investigated grassland sink activity with long-term N_2O flux measurements and they found that grassland behaved as a sink even in conditions of dry soil (WFPS <50%).

The variability of annual N_2O emission factors from grassland was related to the type of treatment in Jones et al. (2005): in 2002 EF calculated from plots with different management on the same field varied from to 0.4% of N input when urea was applied to the soil to 4.3% of N when sludge pellets were used. Although the same treatments and quantity of N were applied to the soil in 2003 EF varied from 0.1% to1.3%. The inter-annual discrepancy observed was due to different climatic conditions in the two years. Similarly, Clayton et al. (1997) presented emission factors varying for type of fertilisers applied (0.4%-2.2%) and between two consecutive years for the same type of treatment (0.8%-1.4%). In many studies emission factors for N application on agricultural soils were higher than the IPCC default emission factor of 1.25% of N input. Ranges vary from 0.6%-6.8% (Velthof et al. 1996a) and 0.4%-7% (Dobbie et al. 1999) to 0.04%-11.1% (Rudaz et al. 1999).

A recent work that used Scotland as a case study for the development of a new methodology to estimate N_2O emission from N applied to agricultural soils using crop- and climate-dependent emission factors, produced higher values of N_2O emissions than the IPCC default methodology. The significant difference in the total annual N_2O emission (10,662 t N_2O-N yr^{-1} using the new method and 6,796 t N_2O-N

yr^{-1} using the IPCC) is mainly due to the contribution of increased grazed pasture (Flynn et al. 2005). This highlights that the uncertainty in emission estimates for emission inventories highly depends on the variability of the emission factors.

2.7 N_2O flux measurements at field scale

Most of the N_2O flux measurements at field scale have been made using a static chamber technique (Clayton et al. 1994; Christensen et al. 1996), where a small area, less than 1 m^2, is enclosed and the rise in concentration after a period of time, usually 1 hour, is measured and used to calculate the gas emission (Fowler et al. 1997) (see Section 5.3.6 for details). The air samples from inside the chamber are usually analysed by electron capture gas chromatography (GC). An alternative to the GC is a photo-acoustic infra-red gas analyser (Velthof et al. 1997), which has been used successfully for measuring N_2O fluxes from grasslands in the Netherlands. The precision of this instrument is similar to the one for conventional GCs, allowing the measurement of N_2O concentration differences of ~10 ppb(Fowler et al. 1997), but it is more portable than GC and more practical for field measurements.

Some progress in the instrumentation, such as the tunable diode laser spectroscopy (TDL) (Wienhold et al. 1994), the Fourier Transform infrared spectroscopy (FTIR) (Galle et al. 1994) and a modified chromatography technique (Arah et al. 1994), which uses repetitive analyses of the same sample providing a resolution of 1ppb of N_2O, have improved the limit detection up to differences in N_2O concentration <1ppb.

With these new gas analysers micrometeorological techniques, such as eddy covariance and aerodynamic gradient (Christensen et al. 1996), and the mega-chamber method can be used to measure N_2O fluxes (Smith et al. 1994).

Static chamber methods have the advantage that they are cheap, versatile and useful to investigate soil processes. When land uses involve small fields with different crops and fertilizer rates or plots with different treatments chambers are the only real option to successfully measure N_2O flux (Smith et al. 1994; Flessa et al. 1998; Jones et al. 2005). The disadvantages are that covering only a small area the extrapolation of the flux to the field scale can be subject to a limited confidence (Fowler et al. 1997) and a large number of chambers is needed to get a representative

estimate of fluxes from field sites with high spatial variability such as grasslands. Although automatic chambers have been used (Laville et al. 1997), manual chambers are more commonly used and usually they are associated with one or maximum two measurements per day, with the risk of missing an emission peak out of the scheduled measurements.

Micrometeorological methods are well suited for measuring field-scale fluxes. Depending on the technique used and the height at which samples are taken, these methods can integrate a flux over 0.1-1 km^2 (Fowler and Duyzer 1989). The spatial and temporal variability of N_2O emissions that strongly influence the up-scaling of measurements made with chamber technique does not represent a problem for micrometeorological methods: assuming that the area investigated is wide and uniform, micrometeorological methods provide an estimate of the flux coming from a large fraction of the surface. Furthermore, they allow continuous measurements producing a detailed picture of the fluxes even on a daily basis (see Section 5.3). The disadvantages are that the necessary instrumentation is expensive and requires time for setting up and constant attention for keeping the instrumentation going.

N_2O fluxes from grassland have been investigated extensively with chamber method (Clayton et al. 1997; Skiba et al. 1998; Smith et al. 1998; Dobbie et al. 1999; Grant et al. 2004) but only few micrometeorological studies are available, usually short term measurements (Hargreaves et al. 1996; Wagner-Riddle et al. 1996; De Klein et al. 1999; Laville et al. 1999; Griffith et al. 2002), and only one long term (8 months) experiment occurred in Ireland (Scanlon and Kiely 2003; Leahy et al. 2004) using eddy covariance.

TDL spectroscopy (Wienhold et al. 1995) is the only analysis technique currently capable of providing the resolution and speed response (magnitude of 200 ms) required for eddy covariance measurements of N_2O. Contrary to the aerodynamic gradient, eddy covariance is a direct method where the flux is calculated from the measurement of concentration and vertical wind speed and does not involve parameterisation, which is often a source of uncertainty in measurements using the gradient method. However, the advantage of the aerodynamic gradient method is that it does not require a very fast gas analyser (timescales of minutes) and it can be applied using an FTIR spectrometer.

Chambers and micrometeorological methods were compared on several occasions (Smith et al. 1994; Christensen et al. 1996; Laville et al. 1997) with satisfactory results. Laville et al. (1997) measured fluxes ranging from 0.6 to 35 ng N_2O-N m^{-2} s^{-1} with 16 manual chambers and with micrometeorological methods emissions varied from -5 to 50 ng N_2O-N m^{-2} s^{-1}. Christensen et al. (1996) found differences in N_2O fluxes measured with the two methods of only 18%. The difference in N_2O flux estimates obtained with the static chamber method and the values measured with eddy covariance is related to the different magnitude of area investigated by the two methods: the chamber system analyses a more localised area than the large area investigated by eddy covariance and therefore it is more subjected to emission hot-spots and cool spots.

2.7.1 Up-scaling to regional and national scale

The extrapolation of N_2O fluxes to the regional and global scales relies predominantly on results from small chamber measurements since they are the most common, but they are often only made for short periods. In addition the large spatial and temporal variability of N_2O emissions increases the uncertainty of up-scaling to annual and large-scale fluxes (Fowler et al. 1997).

A study of N_2O emissions from Australian grazed pastures using measurements at different scales (Denmead et al. 2000), such as a 0.05 ha plot, a field with area between 25 ha and 5 km^2, and regions of order 100 km^2, showed that micrometeorological approaches are a good tool to improve the quality of large scale emission estimates extrapolated from measurements.

Applying the fractional loss of 2.1%, obtained from measurements in literature (Clayton et al. 1994; McTaggart et al. 1994; Velthof and Oenema 1994; Clayton et al. 1997) Fowler et al (1997) estimated the annual emission from British grasslands to be 16 kt N_2O-N y^{-1}, with grazed grasslands being the largest source, accounting for 60% of total UK soil emissions. Grasslands represent the most spatially variable source of N_2O and have large uncertainty. Flux estimates needs to be improved by long-term and large scale measurements (Fowler et al. 1997). For this reason this thesis has studied long-term measurements of N_2O fluxes using the eddy covariance method, as presented in Chapter 5.

2.8 Mitigation strategies

There is a growing interest in various mitigation options for N_2O emissions (Cole et al. 1997; Velthof et al. 1998; Soussana et al. 2004) from many countries committed to reduce their greenhouse gas emissions for the Kyoto protocol.

Modifying management regimes is a possible solution for mitigating N_2O emissions from grasslands and several options have been suggested. For example, increasing the cutting frequency on non-grazed grassland could reduce N_2O losses by 29% (Kammann et al. 1998). A package of measures including refined N fertiliser application, reduction of NH_3 volatilization (by selecting fertilisers and method of application), restricted grazing, use of maize silage, and the use of clover as an alternative for N fertiliser, has been suggested as policy able to mitigate N_2O emissions from farming systems up to 70% (Velthof et al. 1998).

The contributions of agriculture to the net global fluxes of N_2O into the atmosphere are large. The increasing demand of food by an increasing global population is one of the main external driving forces for increasing N_2O emissions from agriculture. The potential to decrease these emissions is high, although there are large uncertainties in it (Cole et al. 1997). The nitrogen cycle is strictly influenced by the farmer and the major challenges of policy makers are to formulate effective and efficient policies using the potentials of the technical measures proposed so far (Oenema et al. 2001).

Chapter 3 Micrometeorological theory and methods

3.1 Introduction

Atmospheric motions are distinguished by temporal scales ranging from several months to a fraction of second and spatial scales ranging from thousand of km to few millimetres. In general they are classified in three big categories: *macro-scale* with temporal scale of the order of a week and spatial scale greater than 1000 km, *meso-scale* with dimensions ranging from hundreds of km to hundreds of metres and periods of days, *micro-scale* with spatial dimensions ranging from 1 km to 1 mm and temporal scale from the order of a few minutes to a fraction of second. Micrometeorology by definition is concerned with meteorological processes on micro-scale. The small-scale phenomena are so transient in nature that it is impossible to use deterministic methods to study them. Therefore, tools such as stochastic methods and similarity theories are commonly used in micrometeorology.

Exchange and vertical transport between surface and atmosphere mainly occur via swirling motions, also called eddies. Turbulent flows can be thought of as a superposition of eddy-coherent patterns of velocity, vorticity, and pressure spread over a wide range of sizes. These eddies interact continuously with each other and with the mean flow, from which they derive their energy. The "large energy" containing eddies, which contain most of the kinetic energy and are responsible for most of the transport in the turbulence, arise through instabilities in the background flow. The random forcing and the interaction with other eddies provoke instabilities in the eddies themselves that lead to a finite lifetime and to a breaking up into smaller eddies. This process, known as "eddy cascade", is repeated at all scales until the eddies become sufficiently small. It converts the mean kinetic energy into turbulent kinetic energy and then into internal energy (heat) (Kaimal and Finnigan 1994). Basically, in this process of energy conversion three different scales of eddies can be distinguished: the large eddies (*energy-containing range*), which contain the bulk of the turbulent energy, and receive energy from buoyancy and shear; the

medium size eddies (*inertial subrange*), which receive energy from the large eddies and transfer it to the small eddies where the viscous damping becomes the energy loss mechanism (*dissipation range*).

3.2 Atmospheric boundary layer

A definition of the Atmospheric Boundary Layer (ABL) is 'that part of the troposphere that is directly influenced by the presence of the earth's surface, and responds to surface forcing with a time scale of about an hour or less' (Stull 1988). The ABL is the place of turbulent convective motions due to the energy exchange between soil and atmosphere and its depth typically varies between one and two km in the afternoon and hundred metres during the night. It can be divided into two regions:

An *outer layer*, where the shearing stress is variable and the wind structure is influenced by surface friction, temperature gradient and the earth's rotation

A *surface* or *inner layer* of approximately constant (in the vertical) shearing stress, where the flow is not dependent on the earth's rotation and the wind structure is mainly related to the surface friction and the vertical temperature gradient.

The surface layer is the region of interest of this work because it is strictly related to the processes occurring at the surface. From the ground and extending to two or three times the canopy height is the *roughness sub-layer*, directly influenced by the drag of the base. On top of it is the *inertial sub-layer*, where turbulent fluxes and stress vary by less than 10% of their magnitude. This is also called constant flux layer and because of this assumption, measurements of fluxes nearby the surface reflect the values at greater height.

3.3 Spectral characteristics of boundary layer turbulence

To understand the conversion of mean kinetic energy into turbulent kinetic energy in the large eddies, the handing down of this energy to eddies of smaller and smaller scale and its ultimate conversion to heat, it is necessary to observe their behaviour separately. The commonly used method utilizes Fourier spectra and cospectra of the turbulence to associate with each scale of motion the amount of kinetic energy that contributes to the whole, and provides a perspective of the

boundary layer structure. In this way, invoking Taylor's hypothesis (Stull 1988), a frequency n or a wavenumber κ (defined as the inverse wavelength ($2\pi/\kappa$ = u/n) corresponds to a particular scale of motion.

A useful conceptual picture of the description of the energy distribution in frequency, considering turbulence homogeneous in all directions, is given by the power spectral density $S(\kappa)$. For each turbulent variable θ the quantity $S_\theta(\kappa)$ expresses the contribution to the total variance of θ from unit interval of wavenumber κ. Integrating over the whole spectrum yields the total variance and the spectral density is then defined according to:

$$\int_0^\infty S_\theta(\kappa)d\kappa = \overline{\theta'^2} \tag{3.1}$$

where θ' is the turbulent fluctuation of the variable under examination. In analogy, the cospectrum of two variables θ and w ($Co_{w\theta}$) is a convenient tool to investigate the frequencies contributing to the total covariance being:

$$\int_0^\infty Co_{w\theta}(\kappa)d\kappa = \overline{w'\theta'} \tag{3.2}$$

The energy-containing and dissipation ranges have their own characteristic length scales. In the first case it is the Eulerian integral length scale Λ, whereas in the dissipation range a measure of the scale is provided by the so called Kolmogorov microscale η, given by:

$$\eta = \left(\frac{\nu}{\varepsilon}\right)^{1/4} \tag{3.3}$$

where ν is the kinematic viscosity of air and ε is the dissipation rate of turbulent kinetic energy. While Λ could vary between 10 and 500 m, η is of the order of 1 mm.

In the inertial subrange the $S(\kappa)$ is considered varying proportionally to $\varepsilon^{2/3}\kappa^{-5/3}$.

3.4 Atmospheric stability

The vertical gradient of air temperature, also called the *profile* of temperature, plays a fundamental role in the description of the motion of air parcels. In fact, the wind-speed profile and turbulence in the surface layer are strongly dependent on the thermal stratification of the air.

3.4.1 Neutral condition

The temperature stratification that produces the condition of *neutral stability* is identified in meteorology with the adiabatic lapse rate (≅ 1°C/100 m decrease in temperature with height) and is often transitory. In this state the vertical gradient of the potential temperature (θ) is zero ($\partial\theta/\partial z = 0$), the air parcels displaced up and down adiabatically maintain exactly the same density as the surrounding air experiencing no net buoyancy forces. Wind speed increases according to the logarithm of the height.

3.4.2 Unstable condition (mixing convection)

During the daytime the soil and, as a consequence, the layer of air above it, warms up inducing a thermal mixing strongly influenced by the intensity of the radiation received from the surface. In this case the air temperature decreases more rapidly with height than the adiabatic rate, equivalent to a negative gradient of θ, $\partial\theta/\partial z < 0$, and displaced air parcels accelerate vertically away from their original positions, generating a condition of *instability* or *mixed convection.*

3.4.3 Stable condition

During the night the air immediately above the surface cools and mixes progressively upward through the action of the turbulence generated by wind shear, forming in this way a *stable layer.* In this condition the temperature decreases less rapidly with height than the adiabatic rate ($\partial\theta/\partial z > 0$) and displaced air parcels return to their original position, from which the connotation of 'stability'. Flow in a stable layer is characterized by strong wind shear, small eddies, and occasional wave activity.

3.5 Eddy flux

The time series of a turbulent variable such as the wind speed (Figure 3.1) shows superimposed patterns with different time scale periods, predominately a mean pattern varying over several-hour periods, and a turbulent pattern changing with time scales of the order of few minutes and seconds. Following this concept

every turbulent variable ξ can be seen as a sum of a mean term $\overline{\xi}$ and a fluctuating term ξ':

$$\xi = \overline{\xi} + \xi' \tag{3.4}$$

Adopting Reynolds averaging rules (Stull 1988), the statistic covariance of two variables such as temperature (θ) and vertical wind speed (w) becomes the average over time of the product of the two fluctuations θ' and w':

$$\mathrm{cov}(w\theta) = \overline{w'\theta'} \tag{3.5}$$

Equation (3.5) represents the vertical kinematic eddy heat flux, which corresponds to the heat transported by the turbulence. This concept can be then extended to other scalar quantities.

In the case of unstable conditions (Figure 3.2a) a downward moving air parcel ($w'<0$) ends up being cooler than its surroundings ($\theta'<0$), resulting in an instantaneous $w'\theta'$ positive product. Similarly, the upwards moving parcel ($w'>0$) is warmer than surroundings ($\theta'>0$), providing again a $w'\theta'>0$ and therefore the average eddy flux is $\overline{w'\theta'}>0$. The net result is then an upward transport of heat.

In stable condition (Figure 3.2b) instead, a downward moving air parcel is warmer than its surrounding ($w'\theta'<0$) and a upward moving parcel is cooler than surrounding ($w'\theta'<0$), resulting in an average eddy flux $\overline{w'\theta'}<0$, therefore a downward transport of heat (Stull 1988).

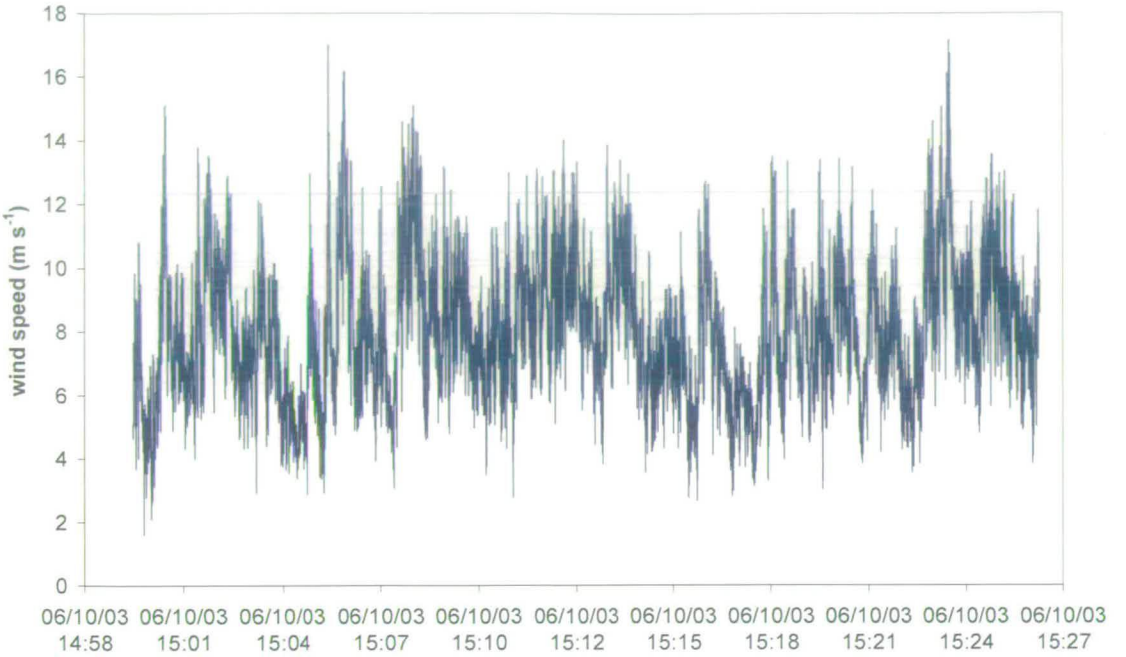

Figure 3.1 Example of 30 min period time series for wind speed recorded at 20 Hz by ultrasonic anemometer at Easter Bush field site.

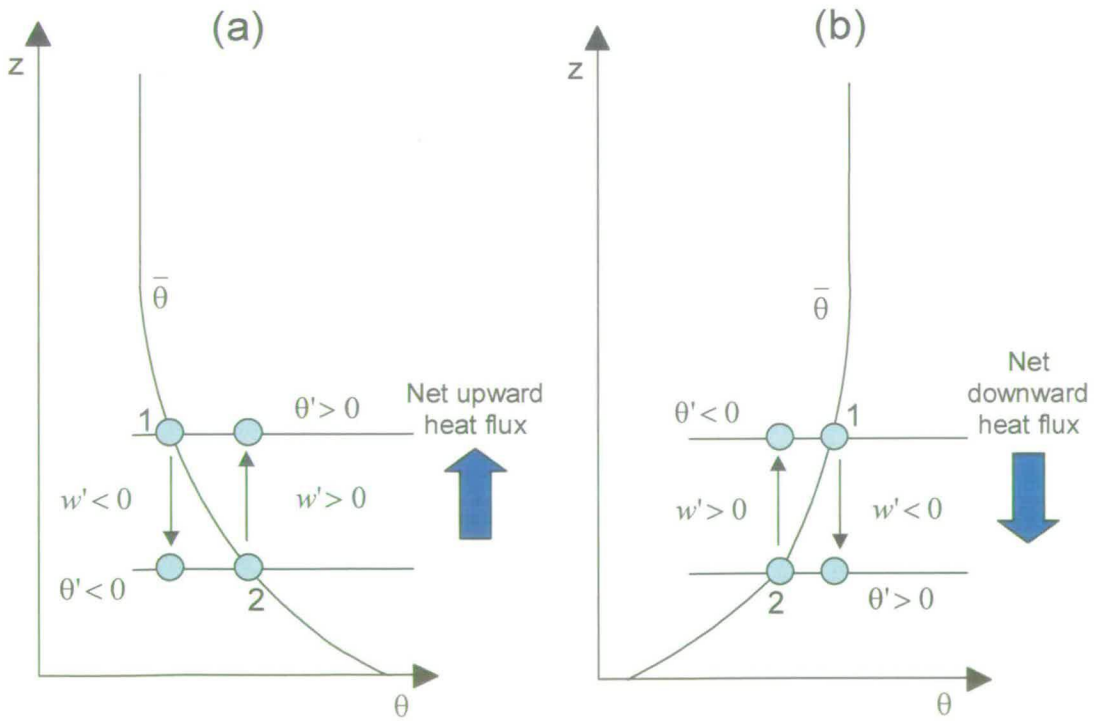

Figure 3.2 Idealization of the eddy mixing processes in (a) unstable condition and (b) stable condition (from Stull, 1988).

3.6 Monin-Obukhov similarity

In many situations the knowledge of the governing physics is insufficient to derive laws based on first principles. However, the characteristics of the surface layer deduced from experimental observations of meteorological variables suggest that the structure of turbulence is determined by a few key parameters as proposed by Monin and Obukhov (1954). In the Monin-Obukhov similarity, several atmospheric parameters and statistics, such as gradients, variances and covariances, can be normalized by the scaling quantities z, the *friction velocity* u_* and the temperature T_* (see below for definition), and then expressed as universal functions of z/L (where L is the Obukhov length). The M-O similarity works only when the winds are not calm and u_* is not zero (Stull 1988). Conventionally it is assumed that u, v, w are the wind speed components along the Cartesian axes x, y, z.

Below are some of the quantities mentioned above:

$$u_* = [-(\overline{u'w'})_0]^{1/2} \tag{3.6}$$

$$T_* = -\frac{(\overline{w'\theta'})_0}{u_*} \tag{3.7}$$

$$L = -\frac{\overline{\theta}(u_*)^3}{kg(\overline{w'\theta'})_0} \tag{3.8}$$

where $(\overline{u'w'})_0$ is the vertical momentum flux at the surface, $(\overline{w'\theta'})_0$ is the vertical temperature flux, k is the *von Karman* constant and g is the acceleration due to gravity.

The quantity L provides information on the stability and it is proportional to the height above the surface at which buoyant factors ($\overline{w'\theta'}$) dominate over mechanical shear $(u_*)^3$ production (Stull 1988). $L<0$ under unstable condition ($\overline{w'\theta'}>0$) and $L>0$ under stable condition ($\overline{w'\theta'}<0$), but it is infinite under neutral condition ($\overline{w'\theta'}=0$).

3.7 Micrometeorological flux measurements

With the development of the similarity theory some techniques to measure the transfer of momentum, mass, and heat through the surface layer were also elaborated.

A common method for estimating turbulent fluxes is the **Aerodynamic Gradient** method. In this case the analogy of molecular diffusion to turbulent transport in the atmosphere is used to express the fluxes of momentum (τ), heat (H), and moisture (E) in terms of vertical gradients:

$$\tau = K_m \rho \frac{\partial \bar{u}}{\partial z} \tag{3.9}$$

$$H = -K_h \rho c_p \frac{\partial \bar{\theta}}{\partial z} \tag{3.10}$$

$$E = -K_q \rho \frac{\partial \bar{q}}{\partial z} \tag{3.11}$$

where K_m, K_h, and K_q are the turbulent exchange coefficients for momentum, heat and moisture respectively; $\bar{u}$, $\bar{\theta}$ $\bar{q}$ are the mean streamwise wind component, mean potential temperature, and the mean specific humidity; ρ is the air density, c_p is the specific heat at constant pressure for moist air. For analogy, the vertical scalar flux of s, F_s, is:

$$F_s = K_s \frac{\partial \bar{s}}{\partial z} \tag{3.12}$$

Two main approaches can be used to determine the transfer coefficients: the first one uses the wind profile to obtain the transfer coefficient K_m and then assumes some relationship between K_m and K_s and the second one utilizes some empirical functions of the stability, related to the similarity theory.

Another micrometeorological method often used to derive the sensible heat flux H and the latent heat flux LE (where L is the latent heat of vaporization) is called the **Bowen Ratio method**. In this case the Bowen Ratio $\beta = H/LE$ is obtained from the ratio of the temperature difference between two measurement heights and the difference in vapor pressure between the same two heights:

$$\beta = \gamma \frac{\Delta\theta}{\Delta e} \tag{3.13}$$

where $\gamma = c_p/L = 0.0004\ K^{-1}$ is the *psychrometric constant*. If the net radiation Rn and the ground heat flux G are also measured, the latent flux LE can be derived from:

$$LE = \frac{Rn - G}{1 + \beta} \tag{3.14}$$

the energetic balance equation at the surface being:

$$Rn = H + LE + G \tag{3.15}$$

A very common micrometeorological method for investigating surface fluxes is the **Eddy covariance method**, explained in detail in Section 3.8

The advantage of the gradient method is that slow response sensors can be used, whereas for the eddy covariance technique instruments must be capable of detecting the high frequency structure of the vertical component of the wind and concentration of the trace gas, requiring a fast response time, usually 10-20 Hz. Unless an instrument has a sufficiently fast response and logging time to resolve the fastest eddies contributing to the turbulent flux, this portion of the flux will not be recorded.

The frequency required for the Eddy Covariance method depends upon the mean eddy size at the sensors. This is a function of surface roughness length z_0 and measurement height z. Larger values of z_0 give larger mean eddy sizes and ease the frequency requirements for the system. Equally, larger values of z give larger mean eddy sizes, having the same effect. So for example, for measurements above a tall canopy with large roughness length z_0 the response frequency needed is smaller than above short canopies, where measurement heights and surface roughness are smaller.

3.8 The Eddy covariance technique

Eddy covariance is the simplest and most direct of the micrometeorological methods used to investigate turbulent air transport in the surface boundary layer of the atmosphere. Because fluxes of momentum, heat, moisture and trace gas are mainly the result of turbulent mixing, it is possible to define them in terms of the turbulent components of velocities and of the properties being transferred. Mean flux across any plane implies correlation between the wind component normal to that plane and the variable investigated (Kaimal and Finnigan 1994).

Paw et al. (2000) distinguished two theoretical lines of logic in the literature, for interpreting flux covariance and exchange for a scalar. One school is derived from the classical definition of Reynolds: total average F of an atmospheric quantity such as a density of a trace gas ρ_c (kg m^{-3}) can be defined as(McMillen 1988):

$$F = T^{-1} \int_0^T U \rho_c dt \tag{3.16}$$

where U is the total wind vector and T is the averaging time.

Applying Equation (3.4) in Equation (3.16) the total flux can be seen as composition of a mean flux and a turbulent term. Assuming the horizontally homogeneous conditions for the mean scalar and for the mean velocity field near the surface, and aligning the coordinate system of the anemometer with the x axis along the main wind direction, the equation for the vertical flux becomes:

$$F = \overline{w}\,\overline{\rho_c} + \overline{w' \rho_c'} \tag{3.17}$$

At this point a rotation of the coordinate system of the anemometer is applied by most micrometeorologists to set $\overline{w}$ to zero, eliminating the mean flux term from Equation (3.17):

$$F = \overline{\rho w' s'} \tag{3.18}$$

where ρ_c is replaced by the product of the air density ρ (kg m^{-3}) and the mixing ratio s of the trace gas.

The other school of thought (Lee 1998; Paw et al. 2000) derives the eddy covariance equation from the conservation of mass of species c:

$$\frac{\partial \rho_c}{\partial t} + \frac{\partial (u_i \rho_c)}{\partial x_i} = S_c \tag{3.19}$$

where u_i is the velocity component in direction i, and S_c is the Eulerian source term for the scalar, in units of kg m^{-3} s^{-1}. After applying Reynolds decomposition and averaging, this equation becomes

$$\frac{\partial \overline{\rho}_c}{\partial t} + \frac{\partial \left(\overline{u}_i \overline{\rho}_c\right)}{\partial x_i} + \frac{\partial \overline{\left(u_i' \rho_c'\right)}}{\partial x_i} = \overline{S}_c \tag{3.20}$$

using 'Einstein' notation where the repeated indices i indicate summation over the values i = 1,2,3. In meteorological notation it is: $u = u_1$, $v = u_2$ and $w = u_3$. The first term represents the variation in time of the scalar (storage), the second term is a divergence term and corresponds to the mean advection, and the third term is the eddy covariance term.

Although this relationship may be not valid in cases of strongly heterogeneous terrain, a further simplification, based on scale analysis, can be made assuming:

$$\frac{\partial(\overline{u}\,\overline{\rho}_c)}{\partial x} >> \frac{\partial(\overline{u'\rho_c'})}{\partial x} \tag{3.21}$$

The following equation then results:

$$\frac{\partial \overline{\rho}_c}{\partial t} + \overline{\rho}_c \frac{\partial \overline{u}}{\partial x} + \overline{u}\frac{\partial(\overline{\rho}_c)}{\partial x} + \overline{\rho}_c \frac{\partial \overline{w}}{\partial z} + \overline{w}\frac{\partial(\overline{\rho}_c)}{\partial z} + \frac{\partial(\overline{w'\rho_c'})}{\partial z} = \overline{S}_c \tag{3.22}$$

With the assumptions of steady state conditions (the first term is zero), of horizontally homogeneous conditions for the mean scalar (the third term is zero) and for the mean velocity field near the surface (the second, fourth, and fifth terms are zero), the equation reduces to (3.18).

In contrast to Webb et al. (1980) that stated the assumption of complete horizontal homogeneity, omitting the horizontal advection terms and accounting for the air density flux term in the vertical, Lee (1998) assumed that incompressible flow existed such that the air density could be assumed as a constant, but allowed a form of vertical advection, arising from a mean vertical velocity, which near the surface could only occur with a horizontal gradient in the mean horizontal velocity field.

Following this line, Paw et al. (2000) distinguished two major forms of horizontal homogeneity. The first is horizontal scalar homogeneity where the mean horizontal gradients of scalars and horizontal covariances are negligible, but the horizontal gradient of the longitudinal velocity are still possible. The second form is the complete horizontal homogeneity and simply assumes that all horizontal gradients of the means and covariances of the velocity field are zero (Webb et al. 1980).

Discussions about the horizontal scalar gradients arising even under source homogeneity conditions (Lee 1998; Finnigan 1999; Lee 1999), suggest that in some cases the horizontal scalar advection should be directly measured, although it is difficult to accomplish.

The average vertical fluxes of momentum (τ) or shearing stress, sensible heat (H) and moisture (E) are expressed as:

$$\tau = -\rho\overline{u'w'} = \rho u_*^2 \tag{3.23}$$

$$H = \rho c_p \overline{w'\theta'} \tag{3.24}$$

$$E = \rho \overline{w'q'} \tag{3.25}$$

In 1980 Webb et al. (1980) addressed a relevant problem: most sensors do not measure mixing ratio (s), rather they measure the density of the scalar quantity under investigation (ρ_c) and in this circumstance sensible and latent heat fluxes cause vertical gradients in air density that result in an apparent vertical flux. They noted that if the total vertical speed w could be measured accurately, then the flux F would not require correction and would be given by Equation (3.17), but in practice $\overline{w}$ is too small to be measured with sufficient accuracy; therefore they provided an expression to quantify the error. Equation (3.17) now becomes (Webb et al. 1980):

$$F = \overline{w'\rho'} + (\overline{\rho}_c / \overline{\rho}_a)[\mu/(1+\mu\sigma)]E + (\overline{\rho}_c / \overline{\rho})H / c_p \overline{\theta} \tag{3.26}$$

where $\overline{\rho}_a$ is the density of dry air, μ is the ratio of molecular weight of dry air to that of water vapour, σ represents the ratio of density of water vapour to the mean density of air, E is the latent heat flux, $\overline{\rho}$ is the total density of air, H is the sensible heat flux, c_p is the specific heat of air at constant pressure and θ is the air temperature.

In the present work the classical approach is used and no Webb correction was applied because the scalar quantity measured by the gas analyzer was the N_2O mixing ratio (ppbV) and not density (kg m^{-3}). Although the temperature at the measuring cell in the gas analyser is different from the one initially at the sonic, the mixing ratio does not vary, unlike the density, which changes with temperature.

3.9 Applicability and limitations of micrometeorological measurements

The application of the eddy covariance technique is convenient because flux densities are directly measured, they can be measured at an arbitrary point and the technique is suitable for short– as well as long-term measurement periods, but, as stated above, some requirements for its applicability are needed.

3.9.1 Fetch and footprint

Although the flux measurements are made in the inertial sub-layer and fluxes can be assumed constant with height, the surface investigated should be homogeneous to allow the surface layer of the atmosphere to be considered a constant-flux layer. Changes in the land cover or in the topography or a presence of obstacles contribute to undermine this homogeneity and to increase the depth of an internal boundary layer. At the base of this layer is the much thinner equilibrium layer (δ_e), where the momentum and the flux balance is dominated by the eddy flux divergence and the advection terms are negligible in comparison. A rule of thumb for the depth of the this layer is $\delta_e \sim X/100$ where X is the distance from the measurement location to the point of the change in surface (Finnigan and Paw 2001). The distance downwind between the point of inhomogeneity and the measurement point is called the *fetch*. Over short vegetation in general a ratio of the measurement height to fetch of 1:100 is required (McMillen 1988).

The portion of the surface that contributes to the measured flux, or effective fetch, is called the *footprint*. Several approaches exist to calculate this area. In a recent paper Schmid (Schmid 2002) presented an extensive review of footprint modelling approaches and theoretical foundations of the footprint concept, identifying some limitations of the applicability of this concept to micrometeorological measurements. An early concept of footprint was related to considerations of internal boundary growth, in response to changes of the thermal or mechanical surface forcing (Elliott 1958). Afterwards the problem of surface inhomogeneity was extended to two-dimensional surface patchiness. This was addressed with an analogy between the developing zone of influence downwind from a surface element, and a diffusing Gaussian plume of a scalar emitted at that surface element (Pasquill 1972). Gash (1986) provided an analytical solution for the basic diffusion equation, later modified by Schuepp et al. (1990), which defined the cumulative normalized contribution to the flux measurement (CNF) at height *(z-d)* (where *d* is approximately 2/3 the total height of the canopy) and downwind distance x_L from the point of observation as:

$$\mathrm{CNF}(x_L) = \int_0^{x_L} f(x)dx = \int_0^{x_L} \frac{U}{u_* kx^2} \exp(-U / ku_* x)dx = \exp(-U / ku_* x_L) \tag{3.27}$$

where U is the average wind speed between the surface and measuring point obtained from the logarithmic expression of the wind profile in neutral stratification; k is the von Karman's constant and u_* is the friction velocity. This one dimensional approach can be adequate for simple and homogeneous terrain but it suffers from the restriction of neutral stratification.

Other methods were applied based on a more general solution of the diffusion equation using Monin-Obukhov similarity (Horst and Weil 1992), providing analytical solutions to the advection-diffusion equation (Schmid 1997; Haenel and Grunhage 1999). In order to extend the concept of footprint to complex and non homogeneous conditions, descriptions and applications using Lagrangian and Eulerian approaches were further developed (Leclerc and Thurtell 1990; Schmid 1994; Baldocchi 1997).

Kormann and Meiner (2001) presented an analytical model, which apply also to non-neutral stratification. The calculation of CNF at upwind distance x_L and height *(z-d)* becomes:

$$\mathrm{CNF}(x_L) = \int_0^{x_L} f(x)dx = \int_0^{x_L} \frac{1}{\Gamma(\mu)} \frac{\xi^{\mu}}{x^{1+\mu}} \exp\left(\frac{\xi}{x}\right) dx \tag{3.28}$$

where:

$$\xi = \frac{U_c}{r^2} \frac{(z-d)^r}{k_c}$$

$\Gamma(\mu)$ is the value of the Gamma function in μ

$\mu = (1+m)/r$

$r = 2+m-n$ is the so-called *shape factor*

$m = \frac{u_*}{k} \frac{\varphi_m}{u(z-d)}$ is the exponent of the power law for the vertical profile of the horizontal wind velocity:

$u(z-d) = U_c(z-d)^m$,

where the constant $U_c = u/(z-d)^m$, u is derived from Monin-Obukhov similarity profile for horizontal wind (Kormann and Meixner 2001) and φ_m is the stability function:

$$\varphi_m = \begin{cases} 1+5z/L & \text{for } L>0 \\ (1-16z/L)^{-1/4} & \text{for } L<0 \end{cases}$$

$$n = \begin{cases} \dfrac{1}{1+5(z-d)/L} & \text{for } L > 0 \\ \dfrac{1-24(z-d)/L}{1-16(z-d)/L} & \text{for } L < 0 \end{cases}$$ is the exponent in the eddy diffusivity equation:

$K(z-d) = k_c(z-d)^n$, the constant $k_c = K/(z-d)^n$ and K is derived from Monin-Obukhov similarity profile for eddy diffusivity (Kormann and Meixner 2001).

The approach of Kormann and Meixner (2001) was adopted in the present work for studying the footprint during the measurements at the Easter Bush field site because it overcomes the limitation of the neutral atmosphere case, which is the common in the other approaches.

3.9.2 Stationarity and homogeneity

Stationarity, which means that statistics do not vary in time, is one of the assumptions for the determination of surface fluxes. Since this condition cannot be realized in its strictest sense, because of changes of measured components with the time of the day or changes of weather pattern, it is one of the most serious problems in turbulence measurements. For most applications the process can be treated as a sequence of steady states. In this way a major simplification is allowed, to introduce time averages that represent the properties of the process and not those of the averaging time, following Taylor's hypothesis (Kaimal and Finnigan 1994).

The homogeneity means that statistics do not vary in space. This requirement is almost impossible to fulfil during measurements, although a careful examination of the measuring site could reduce the risk of obstacles and roughness influence. The occurrence of inhomogeneity is reflected in non stationary processes.

Several tests to investigate non-stationary data are proposed in the literature. A principle proposed by Foken and Wichura (1996) is based on the comparison of covariance (flux) obtained with a different averaging period: the covariance of a parameter (s) with the vertical wind speed (w) over the whole averaging period (30 minutes) (Equation (3.29)) is compared with the covariance obtained dividing the time series in M intervals (M = 6 is usually adopted corresponding to a time interval of 5 minutes), containing N data points (Equation (3.31)):

$$\left(\overline{s'w'}\right)_{30\,\min} = \frac{1}{M(N-1)}\left[\sum_i\left(\sum_j s_j w_j\right)_i - \frac{1}{NM}\sum_i\left(\sum_j s_j \sum_j w_j\right)_i\right] \tag{3.29}$$

$$\left(\overline{s'w'}\right)_i = \frac{1}{(N-1)}\left[\sum s_j w_j - \frac{1}{N}\sum_j s_j \sum_j w_j\right] \tag{3.30}$$

$$\left(\overline{s'w'}\right) = \frac{1}{M}\left[\sum_i \left(\overline{s'w'}\right)_i\right] \tag{3.31}$$

The difference between the two covariances is:

$$RN_{\mathrm{cov}} = \left|\frac{\left(\overline{s'w'}\right) - \left(\overline{s'w'}\right)_{30\,\min}}{\left(\overline{s'w'}\right)_{30\,\min}}\right| \tag{3.32}$$

and when RN_{cov} is less than a threshold value (typically 30%) the time series is considered stationary.

A second test is based on the fact that in stationary conditions the integral function of the covariance $f(t) = \int_0^T \overline{w'\chi'}dt$ will be linearly dependent on time (Affre et al. 2000). A linear regression is then calculated from the function f; if the standard deviation of the integral function with respect of the linear regression is called σ_f, then a parameter of the degree of stationarity of the measurements is given by:

$$C_{rs} = \frac{2\sigma_f}{\overline{w'\chi'}}$$

Another approach is provided by the study of the Ogive function (Spirig et al. 2004), which is defined as the cumulative integral of the cospectrum (e.g. of the flux) over all frequencies:

$$Og_{wx} = \int_{\infty}^{f_0} Co_{\overline{w'\chi'}}(f)df \tag{3.33}$$

Under ideal conditions and well-developed turbulence, the Ogive function starts at zero and monotonically approaches the total covariance (flux) with increasing frequency. Generally flux contributions at the low and high end of the spectrum are small and the frequencies between 0.01 Hz and 0.1 Hz dominate, providing a S-shape curve of the Ogive function. Significant deviations from this form reflect disturbances of the eddy flux. At times the Ogive curve may show turning points as a

result of dominating fluxes in the opposite direction, indicating a violation of the stationarity or homogeneity. As the raw cospectra exhibit a large scatter with high frequency, a frequency smoothing is applied before using the Ogives or cospectra as a quality criterion. The number of significant turning points becomes the parameter for detecting non-stationarity conditions (Spirig et al. 2004). This is equivalent to counting the number of positive and negative points in the cospectra. When the cospectrum is alternatively between positive and negative values its sign is poorly defined.

For the measurements at Easter Bush the approach described by Foken and Wichura (1996) was used.

3.9.2.1 Storage and advection

As a consequence of non-stationarity and inhomogeneity, the flux divergence is investigated with the *storage* and the *advection* terms as they are described in Fowler and Duyzer (1989).

Considering an imaginary unit cube of air above the ground the upper surface represents the measurement reference level and the lower surface represents the site of release (or uptake). Any change in concentrations with time will result in a change in storage of the trace gas in the air below the measurement level. The storage term ΔF_s is the height integral of the difference in concentrations with time and calculated as:

$$\Delta F_s = \int_{z_1}^{z_2} \frac{d\chi}{dt} dz = \frac{d\chi}{dt}(z_2 - z_1) \tag{3.34}$$

where z_1 and z_2 are the ground and the measurement height respectively, and χ is the gas concentration.

Similarly, if a horizontal gradient in a trace gas concentration exists, the advection term ΔF_χ will describe the contribution to the total vertical flux of the difference between the flux entering the upwind surface of the cube and the one leaving the downwind face:

$$\Delta F_\chi = \int_{z_1}^{z_2} U \frac{d\chi}{dx} dz = U \frac{d\chi}{dx}(z_2 - z_1) \tag{3.35}$$

3.9.3 Spectral corrections

The physical response frequency for an instrument, the separation between sensors (e.g. sonic and gas analyser) and the attenuation of turbulent fluctuations due to the long inlet tube, are all critical factors that influence the investigation efficiency of the system at some specific frequencies. In some circumstances a loss of information at high frequencies occurs. In such cases, some form of correction must be applied. Several methods of correction exist, mainly spectrum-related.

A possible correction method is the application of a series of transfer functions defined for each correction term (Moore 1986; Lenschow and Raupach 1991; Massman 1991; Horst 1997).

Another approach frequently used in micrometeorology is the application of spectral corrections based on the comparison of the (hopefully) ideally measured sensible heat cospectrum (Co_{wT} see paragraph 3.3 for the definition) and the degraded cospectra of the other scalars measured (Horst 1997). This second approach was followed in the present work.

The general spectral correction equation for a correction factor R is:

$$R = \frac{\int_0^\infty Co_{wc}(f)df}{\int_0^\infty h_c(f)Co_{sc}(f)df} = \frac{\int_0^\infty Co_{wc}(f)df}{\int_0^\infty Co_{swc}(f)df} \tag{3.36}$$

where Co_{wc} is the actual cospectral density function for the vertical velocity and the gaseous concentration c, Co_{swc} is the sensor's cospectral density function, which integrated over frequency f provides the measured eddy flux, and h_c is the transfer function for the sensor. R represents the inverse of the fraction of actual covariance which the sensor measures.

Assuming that the actual cospectrum for sensible heat Co_{wT} is the same as for other scalars, and that the sensor-based sensible heat flux covariance Co_{swT} is considered an ideal measurement, the transfer function is:

$$h_c = \frac{Co_{swc}(f)}{Co_{wsT}(f)} \tag{3.37}$$

Horst (1997) suggested an expression for a cospectral transfer function for corrections related to the slow response time of the sensor (τ_c) and to the frequency *f*:

$$h_c(f) = \frac{1}{1+(2\pi f \tau_c)^2} \tag{3.38}$$

In this work the transfer function obtained from the measured cospectra using Equations (3.37) and (3.38) was multiplied to the covariance Co_{wT} to obtain a 'damped' sensible heat cospectrum that could fit the Co_{wc}, then the areas below the two curves were compared. The difference between the areas is proportional to the eddy flux that could not be detected by the system at high frequencies. The weakness of this method is the use of a hypothesized time response τ_c (in the current study τ_c = 0.2 s) to predict a 'real' time course of the scalar based on the measured value. For this reason the correction factor was not applied to the flux values studied in this thesis, but was applied to estimate the possible underestimation of the total cumulative flux.

3.9.4 Integral turbulence test

The behaviour of σ_w in the surface layer is fairly well understood (Merry and Panofsky 1976) under the neutral and unstable atmospheric conditions. Panofsky et al. (1977) parameterised the ratio $\frac{\sigma_w}{u_*}$ as a function of *z/L* for unstable conditions as:

$$\frac{\sigma_w}{u_*} = 1.25(1+3\cdot\left|\frac{z}{L}\right|)^{1/3}$$

assuming that the ratio under stable condition was the same as the near-neutral value of 1.25. Over the years numerous studies have been conducted that assess mean, normalized turbulence statistics under different thermal stratification regimes. A commonly assumed value for $\frac{\sigma_w}{u_*}$ in near neutral conditions is 1.3 (± about 5%). The integral turbulence characteristics may be used to check whether the turbulence is well developed according to the similarity theory of turbulent fluctuations.

Foken and Wichura (1996) have investigated this parameter and introduced a test called Integral Turbulence Characteristics (ITC) (Foken and Lee 2004). The tool consists of the calculation of the normalized difference between a modelled

$\left(\frac{\sigma_w}{u_*}\right)_{model}$ and the measured $\left(\frac{\sigma_w}{u_*}\right)_{measurement}$ characteristics of turbulence. The data quality is good if the calculated value is smaller than 30%. The expression for ITC is:

$$ITC_\sigma = \frac{\left|\left(\frac{\sigma_w}{u_*}\right)_{model} - \left(\frac{\sigma_w}{u_*}\right)_{measurement}\right|}{\left(\frac{\sigma_w}{u_*}\right)_{model}}$$

where:

$$\left(\frac{\sigma_w}{u_*}\right)_{model} = 0.21 \cdot \ln\left(\frac{z_+ \cdot f}{u_*}\right) + 3.1$$

where $z_+ = 1$ m, f is the Coriolis parameter ($2\Omega\sin\lambda$), Ω is the angular velocity of the Earth (= 7.2921x10-5 rad s^{-1}), λ is the site latitude (radians). For Easter Bush λ = 55.86°N and $f = 1.2\text{x}10^{-4}$.

3.10 Data acquisition and treatment

At Easter Bush the three components of the wind velocity were all measured by an ultra-sonic anemometer, whereas the gas concentration was measured with a fast gas analyzer, Tuneable Diode Laser (TDL) (see Section 4.4 for description).

For data acquisition, the analogue signal output of the TDL was fed into the analogue input of the ultrasonic anemometer and recorded at 20 Hz, together with the wind data, using a computer logging program written in LabVIEW 6.1 (National Instruments), already in use at the Easter Bush site for CO_2 and other gas flux measurements. Preliminary 15 min average fluxes and some micrometeorological parameters such as friction velocity (u_*), were calculated online to provide an immediate picture of the measurements.

The data were reprocessed off-line with a LabVIEW program, created by E. Nemitz (CEH Edinburgh). In the program N_2O and heat fluxes were calculated using the eddy covariance formulation in Equation (3.18) adopting an averaging period of 30 minutes. The fluxes were a result of an average over about N = 36400 points after: a) a despiking process was applied to eliminate values > 3σ, mainly due to electronic noise; b) a double rotation of the coordinate system of the sonic was performed every

30 min period to align the x axis along the main wind direction and setting $\bar{v} = \overline{w} = 0$ (Finnigan 2001). Lag time between the gas analyser and the sonic was calculated as a dynamic value, by finding the lag-time of the maximum covariance between concentration and vertical wind speed over a user-specified window (Moncrieff et al. 1997), usually between 0 and 10 s. Data were not detrended.

Spectra and cospectra were calculated using a fast Fourier transformation to transform the time series into the frequency domain. To use spectra and cospectra as tools to assess the quality of the data, a frequency smoothing was applied. The averaging interval is exponentially increased with increasing frequency, yielding a similar number of data points for each frequency decade (Kaimal and Finnigan 1994).

Chapter 4 Easter Bush field site characterisation

4.1 Introduction

Measurements of N_2O fluxes began on 06/06/2002 and were continued until 23/06/2003, a period of 1 year of almost continuous measurements. Intensively-managed grassland was chosen as the type of ecosystem to investigate the influence of fertiliser and animal trampling on the variability of N_2O exchange. The absence in the literature of long-term continuous N_2O measurements on agricultural soils was also a reason for interest in carrying out this experiment. This Chapter provides some details of the measurement site, the instrumentation used and the measurements undertaken.

4.2 Site description

The measurement site was located at an Edinburgh university-owned field (Easter Bush) in Scotland, 10 km south of Edinburgh (55°52'N, 3°2'W, Grid Ref: NT245641, elevation 190m above the sea). The instruments were situated on the boundary between two grassland fields (Figure 4.1) of approximately 16 ha in total. The position of the instrumentation was such that micrometeorological flux measurements were carried out utilizing SW wind directions over one field and NE wind directions over the other field, the two predominant wind directions at this site. The two fields are referred to as 'South' and 'North' field, respectively. The fields consist of a clay loam soil mainly covered (>90%) with *Lolium perenne* (Milford (2004), based on C. Pitcairn, Pers. comm.), partially grazed by cattle and sheep and fertilized about three times per year with NPK fertiliser (see Section 4.12 for full management details). The surrounding fields are also intensively-managed grasslands with analogous management. Two farms are in the vicinity: Easter Bush is 400 m east of the measurement site and Easter Howgate Farm is 500 m from the field site (Figure 4.2). Figure 4.3 shows the Ordinance Survey 1:50000 map containing the Easter Bush site.

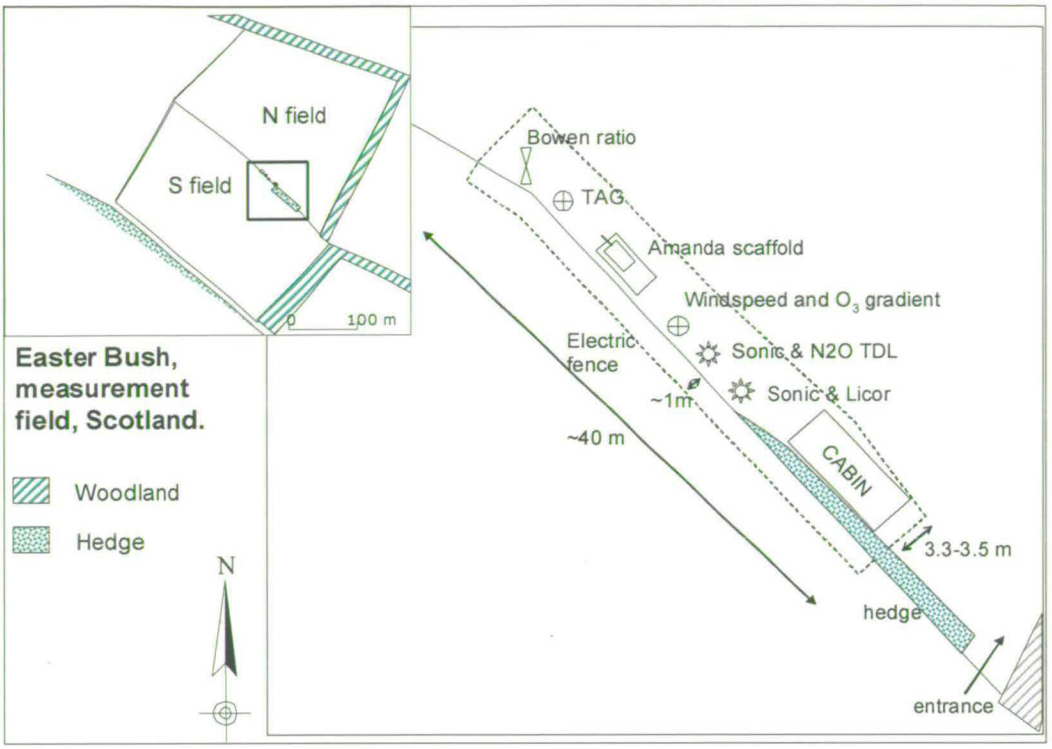

Figure 4.1 Site diagram showing the location of the instruments on the boundary of the two fields.

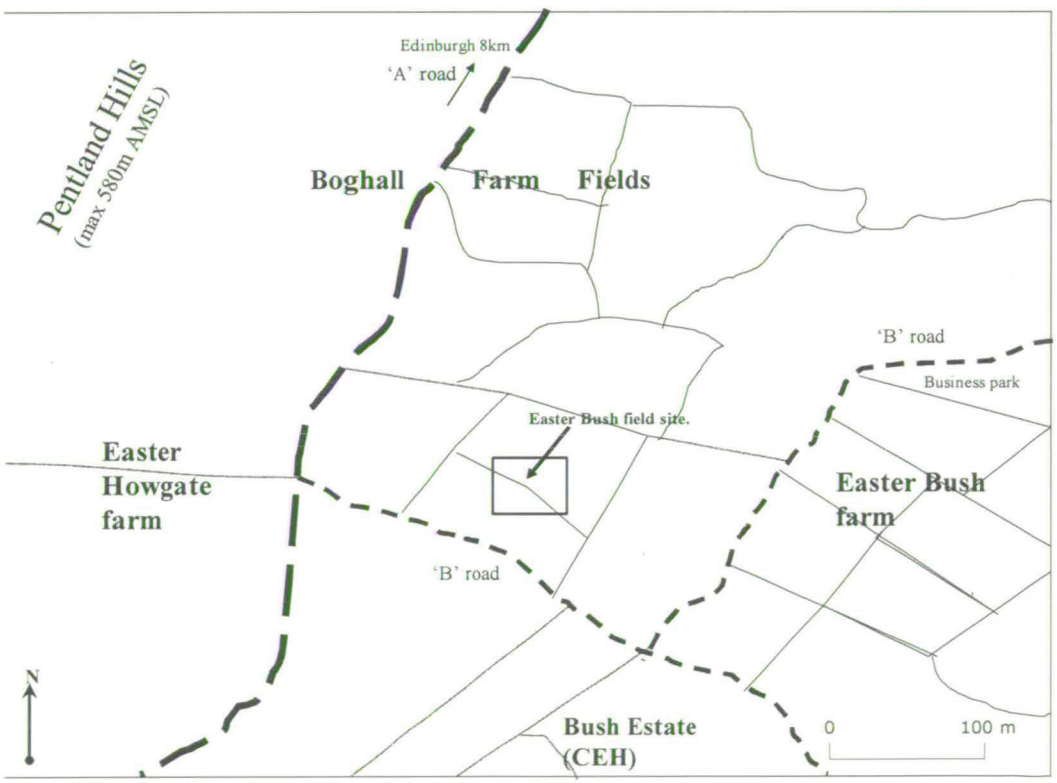

Figure 4.2 Site diagram showing the location of the field site and the surroundings.

Figure 4.3 Ordinance Survey map 1:50000. The blue area represents the Easter Bush field.

4.3 Instrumentation

The Easter Bush site has been used for continuous measurements since early 2001. Micrometeorological measurements of atmospheric turbulence, and fluxes of O_3, CO_2, H_2O and NH_3 have been made along with rainfall, surface wetness, soil temperature, soil heat flux and net radiation. A summary of the instrumentation available and the measurements carried out at Easter Bush at the same time as the experiment described in this thesis is shown in Table 4.1.

Table 4.1 Micrometeorological, soil and vegetation measurements conducted at Easter Bush in 2002-2003.

Measurements	Instrumentation	Model and supplier
N_2O concentration	TDL (trace gas analyzer)	(Aerodyne Res. Inc. Billerica, Mass, USA)
O_3 concentration	O_3 UV absorption analyzer	TE49C, Thermo Instruments, USA
CO_2 concentration	CO_2-H_2O analyzer	LI-7000 and LI-7500 (LI-COR, Lincoln, NB, USA)
H_2O concentration	CO_2, H_2O analyzer	LI-7000 and LI-7500 (LI-COR, Lincoln, NB, USA)
NH_3 concentration	AMANDA[a] (NH_3 analyzer) TAG[b]	
Aerosol concentration	AMS[c] analyser	(Aerodyne Res. Inc. Billerica, Mass, USA)
Sensible heat flux	Ultrasonic anemometers	USA-1 (Metek GmbH, Germany) and 1012RA (Gill Instruments, UK)
Turbulence parameters (e.g. u*)	Ultrasonic anemometer	USA-1 (Metek GmbH, Germany) and 1012RA (Gill Instruments, UK)
Wind speed	Ultrasonic anemometer	USA-1 (Metek GmbH, Germany) and 1012RA (Gill Instruments, UK)
Wind speed profile (5 heights)	Cup anemometers	(Vector Instruments, Ltd, UK
Wind speed direction	Ultrasonic anemometer Wind vane	USA-1 (Metek GmbH, Germany) and 1012RA (Gill Instruments, UK) W200P (Campbell Scientific, UK)
Air temperature	Ultrasonic anemometer	USA-1 (Metek GmbH, Germany) and 1012RA (Gill Instruments, UK)
Air temperature profile	Thermocouples	Fine Gauge Chromel-Constantan, 0.003" (Campbell Scientific, UK)
Net Radiation	Net radiometer	Q-7 (Campbell Scientific, UK)
Solar Radiation	Solar radiometer	SP1110 (Campbell Scientific, UK)
Precipitation	Tipping bucket rain gauge	(Campbell Scientific, UK)
Soil temperature and soil heat flux	Thermocouples and soil heat flux plates	Fine Gauge Chromel-Constantan, 0.003" (Campbell Scientific, UK)
Soil wetness	TDR CS616	(Campbell Scientific, UK)
Canopy height	Direct measurement	

[a]AMANDA (Ammonia Measurement by Anular Denuder sampling with online Analysis)
[b]TAG (long Time Averaged Gradient)
[c]AMS (Aerosol Mass Spectrometer)

4.4 N_2O flux measurements: the Tuneable Diode Laser Spectroscopy

The N_2O flux measurements were conducted by the eddy covariance technique, using the fast gas analyser referred to as TDLAS (Tuneable Diode Laser Absorption Spectrometry) (Wienhold et al. 1994) to measure N_2O concentration and an ultrasonic anemometer (USA-1, Metek GmbH, Germany) to measure the three components of the wind speed. The advantages of this technique and its comparison with other N_2O measurement techniques have been described in Chapter 2 and Chapter 3. The TDLAS analyser is ideally suited for micrometeorological measurements because of its low detection limit and high precision and high time resolution. The high time resolution of this gas analyser allows the use of the eddy covariance method to run continuous measurement (e.g. as in the period presented here of 12 months), providing a remarkable improvement on the chamber-based methods, allowing a more detailed investigation of diurnal and seasonal variability of the exchange of N_2O (Zahniser et al. 1994).

4.4.1 Principle of operation

In tuneable diode laser spectroscopy, highly specific mid-infrared trace gas absorption arising from fundamental rotational-vibrational molecular transitions is monitored using solid-state tuneable lead salt lasers. These narrow-band light sources resolve single lines of the absorption bands for many trace gases at reduced pressure. In practice, several monochromatic light streams emitted by a laser diode go through a gas sample and the transmitted light intensity for each wavelength is detected and revealed in an absorption spectrum.

The fraction of light intensity transmitted through the gas is given by the Lambert-Beer law:

$$I = I_0 e^{-\sigma(\nu)LC} \tag{4.1}$$

where I and I_0 are the transmitted and incident intensity of light respectively; L is the absorption path length; C is the concentration of the absorbing gas; and $\sigma(\nu)$ is the molecular absorption cross section of the absorbing species, depending on radiation frequency (ν).

The absorbance *(a)* of the gas sample is defined as the logarithmic ratio between the incident (I_0) and the transmitted *(I)* light:

$$a = \log(I_0 / I) \tag{4.2}$$

and it is also:

$$a = \sigma(\nu)LC \tag{4.3}$$

From Equation (4.3) it is noticeable that for a given path length, the concentration is proportional to the absorbance *a*. The best detection sensitivity is achieved when both L and σ are as large as possible.

Considering the absorption of a single rotational-vibrational line at a definite wavelength, important characteristics are: the spectral line strength (*S*), defined as the integral of the absorption cross section $\sigma(\nu)$ over the wavenumber range of the line, the line shape and width. The value of *S* for any given line depends on the temperature but not on the pressure of the gas. The absorption cross section and line shape and width, however, depend both on temperature and pressure.

For pressures above 100 mbar in the mid-infrared region, the collision of molecules induces a broadening of the spectral line, which is defined by a Lorentzian function. This enlargement increases the measurement sensitivity but involves a progressive overlapping and blending of the molecular absorption lines of other molecules.

Reducing the pressure below 10 mbar, the line shape and width are essentially defined by Doppler broadening arising from random thermal motion of the gas molecules. In this case the line shape can be described by a Gaussian function. The selectivity of the line is enhanced as interferences from other species are minimised, but the low intensity of absorbed radiation leads to a poor measurement sensitivity (Schiff et al. 1994).

The optimum sampling pressure for TDLAS is a compromise between sensitivity and selectivity, in other words, between maximizing the line centre absorption cross section and minimizing interferences from other species. As the sampling pressure is reduced, the sensitivity does not fall significantly with respect to atmospheric pressure conditions as long as the ratio between Lorentzian and

Gaussian line widths ranges between 0.5 and 1, typically for pressures of 10-50 mbar (Figure 4.4).

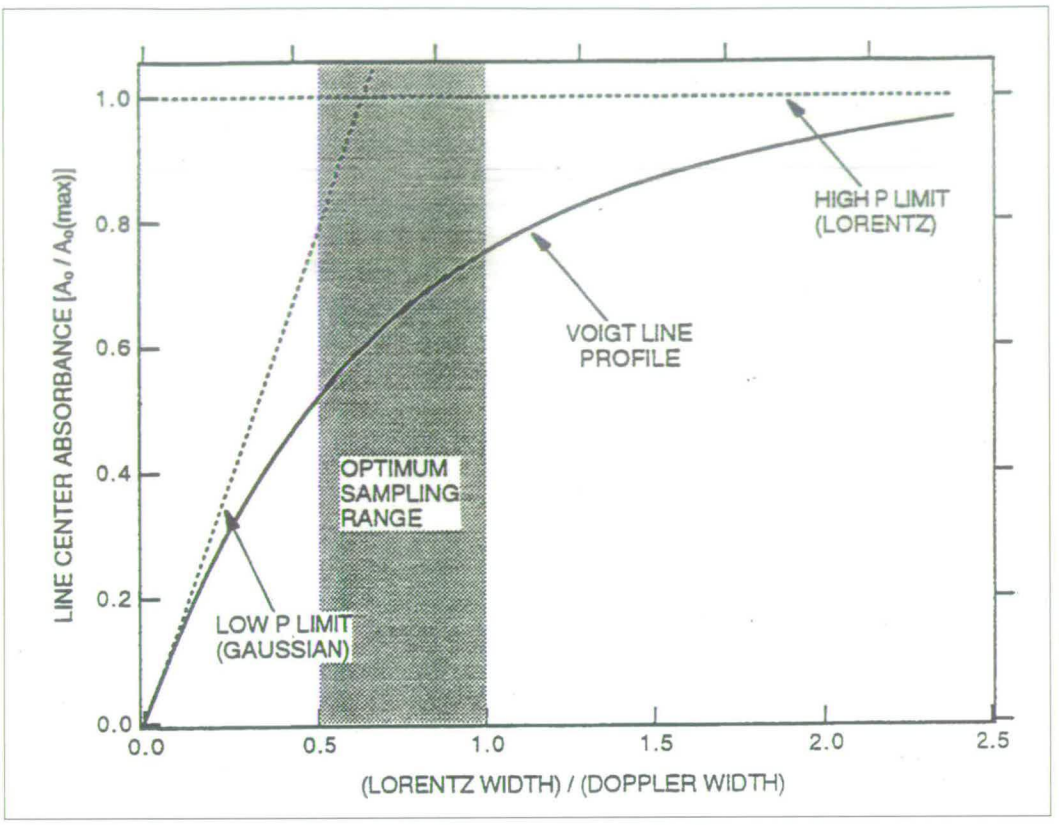

Figure 4.4 Line centre absorption as a function of line width ratio. From (Zahniser et al. 1997).

The Voigt line can be described as a convolution of Lorentizian and Gaussian line shapes and it is used to fit the shape and width of the absorption line when operating in such pressure conditions, which are ideal for the TDLAS operation (Werle 1998).

4.4.2 Description of the TDLAS system

The TDL system set up for measurements requires: a diode laser with tuneable emission frequency; a temperature control system; a current control and modulating system; an optical bench to direct the light through the air sample; an optical path long enough to guarantee a good sensitivity to the measurement; a detector to measure the light intensity; a computer to control the system and to visualize, elaborate and store the data.

Tuneable diode lasers operating in the mid-infrared region (2.5-25 μm) are semiconductors consisting of lead salts (PbS, PbSe, PbTe) and their mixed alloys

with themselves and with tin salts (e.g. SnS or SnSe). These semiconductors form p-n junctions with small energy band gaps that result in emissions in the 3-30 μm spectral region, depending on the composition of the alloy. The application of a forward bias current (typically 0.1-1.0 A) to the p-n junction produces population inversion between the nearly empty conduction band and the nearly full valence band, providing the gain mechanism through which stimulated emissions occurs via electron-hole recombination (Schiff et al. 1994).

Like other semiconductor lasers, the wavelength of lead salt lasers changes with temperature. In particular, molecular spectra are particularly complex in the mid infrared region and the ability to generate a narrow laser line and tune its wavelength can be useful. Thus lead salt lasers are designed to provide wavelengths that are temperature-sensitive and are packaged so that their output can be temperature-tuned. The population inversion in proximity of the junction is achieved for currents higher than the threshold value: at room temperature such current value is very high; therefore the diodes are operated in cryogenic conditions (Hinkley et al. 1976).

The diode laser used for the measurements at Easter Bush was operating at temperatures around 86-87 K with injection of current lower than 500 mA. In order to maintain this operating condition, the diode was located in a Dewar vessel and cooled with liquid Nitrogen (LN_2) (T = 80 K), which was periodically (every 20 hours) poured into the vessel. The temperature tuning rate of most diodes is greater than 1 cm^{-1} K^{-1}, requiring temperature stability in the order of 10^{-3} K. Up to four diodes can be held on a cold-finger in a cryocooler. Temperature control and tuning is provided by a heating element used in combination with a semiconductor temperature sensor attached to the diode inside the Dewar (Laser Photonics controllers). Temperature tuning of a diode permits coarse wavelength variations over a range of about 200 cm^{-1}, in the specific case between 2195 and 2220 cm^{-1}.

Once the thermal stability in the Dewar is reached, the diode emission can be tuned with adjustments of the density of the current, typically with steps of $5x10^{-3}$ cm^{-1} for each mA. In practice, temperature or current tuning of the diode results in a series of continuous portions 1 – 2 cm^{-1} wide, separated by gaps where no emissions occurs, phenomenon known as "mode hopping" (Schiff et al. 1994) (Figure 4.5). Even for predominant single-mode laser, small spurious side modes are evident and

conditions of multi-modes (more than one output laser wavelength detected at the same time) can occur. For this reason the concentration value obtained cannot be considered an absolute concentration value unless calibrations are made regularly. A saw-tooth modulation waveform of sufficient amplitude to tune the laser across the infrared absorption line is applied to the laser current and is repeated at a rate of 6 to 1.5 kHz. The ideal combination of temperature and density of current provides the strongest line signal.

From the Dewar the laser light, in a narrow beam, is directed through the optical module to a sample cell that provides the absorption path, and then to the detector. The optical module of the instrument is shown in Figure 4.6 and it consists of an optical bench of 0.61 x 0.76 m, where a microscope objective, a dichroic beam-splitter and a pinhole are situated. A parallel visible optical system aids alignment and setup of the optical assembly. A red visible (678 nm) "trace" diode laser beam passes through a dichroic beam-splitter and thus is co-aligned with the infrared beam associated with it, as guaranteed by focussing both visible and infrared beams through the common input aperture (200 μm pinhole). To increase sensitivity, ambient air is pumped at reduced pressure (~36 mbar) through the multiple reflection cell that provides an optical absorption path length of 36 m. The cell used for the measurements at Easter Bush (Figure 4.7) is an astigmatic Herriott cell with two astigmatic mirrors placed at the base of a glass cylinder: the laser beam is injected through a hole in one mirror in an off-axis direction and it re-circulates 182 times on 20 cm base length for a total of 36 m path, before exiting through the coupling hole. The gas exchange time in the cell is 0.2 s (Zahniser et al. 1995).

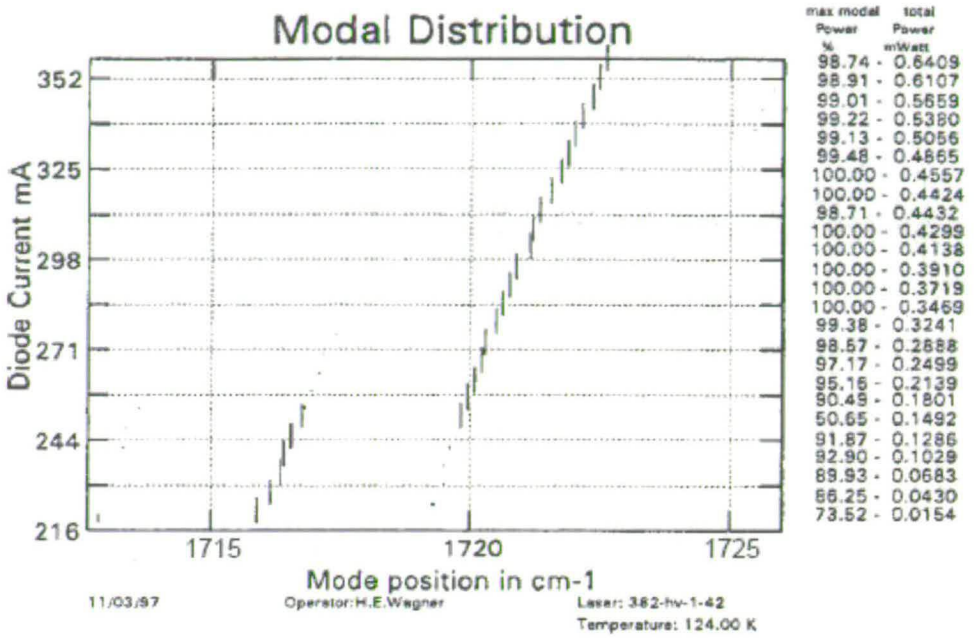

Figure 4.5 Example of a tuneable diode laser mode map. Although it represents a good single mode diode, it is still possible to notice small gaps where there is no emission.

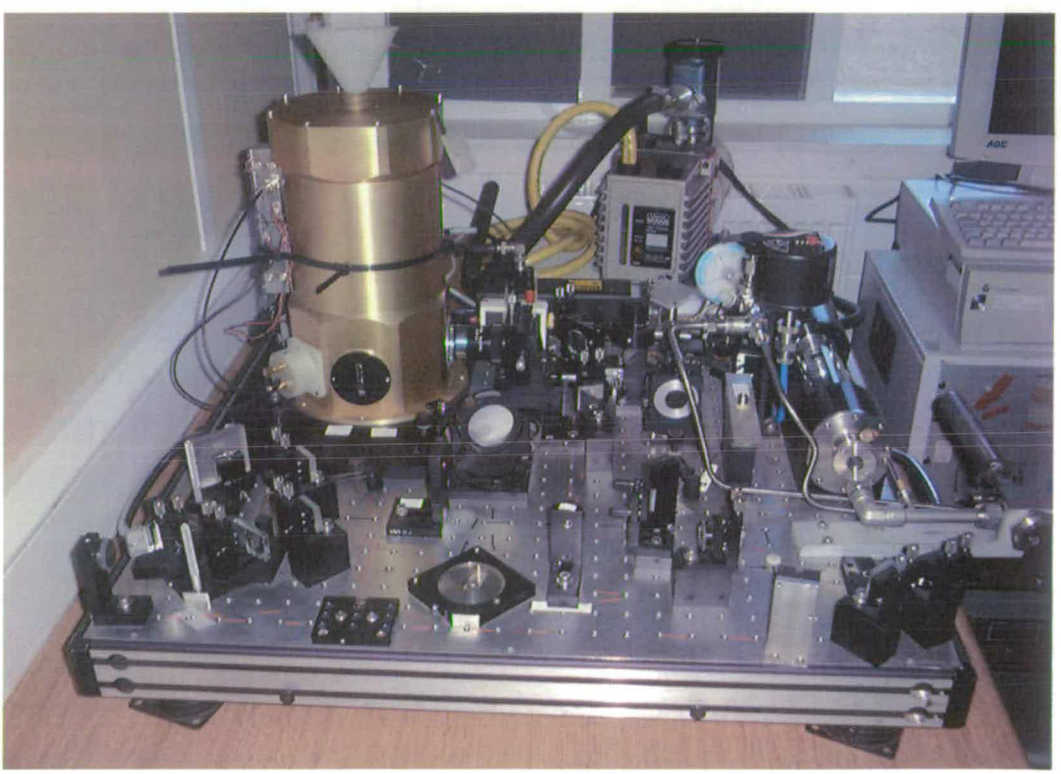

Figure 4.6 The optical bench in the TDL analyser. The diode and the detectors are enclosed in the golden Dewar

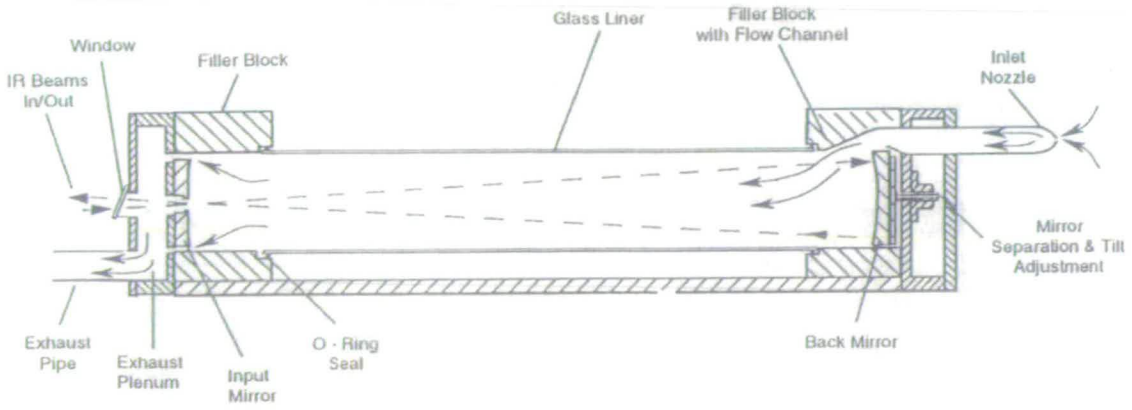

Figure 4.7 Multi-pass absorption cell used in the TDL.

Figure 4.8 shows the scheme of the optical module. The red line from the diode in the Dewar to the detector, passing through the multi-pass cell, represents the principal laser beam path; this beam provides the absorption spectrum. The grey line defines the path of a secondary beam that goes through a cell with high N_2O concentration; the detected beam gives a reference spectrum, useful to identify the position in the characteristic N_2O absorption spectrum.

The detectors used are photoconductive and photovoltaic HgCdTe. The light revealed by the detector is converted to a signal which goes through an analogue to digital card and subsequently is processed by a computer.

4.4.2.1 Signal processing

The data acquisition method is based on direct measurement of the absorption by a rapid sweep integration of the spectra.

The problems encountered with TDLs are mainly due to limitations in stability of the laser output and frequency, as a result of fluctuations in operating temperature. These are reflected in the degree of reproducibility of the spectra, which affects the determination of both transition frequencies and line shapes.

The laser current is saw-tooth modulated and phase-locked to the signal averager. Laser temperature and current are adjusted to sweep the desired spectral interval. The result is a spectrum in which all points are scanned for any period of time sufficient to reduce the noise to an acceptable level. Once the laser mount temperature reaches an equilibrium with the average injection current, it generally remains stable over periods much longer than the scan time so that the spectra are reproducible, and no smearing of lines occurs during a scan (Jennings 1980).

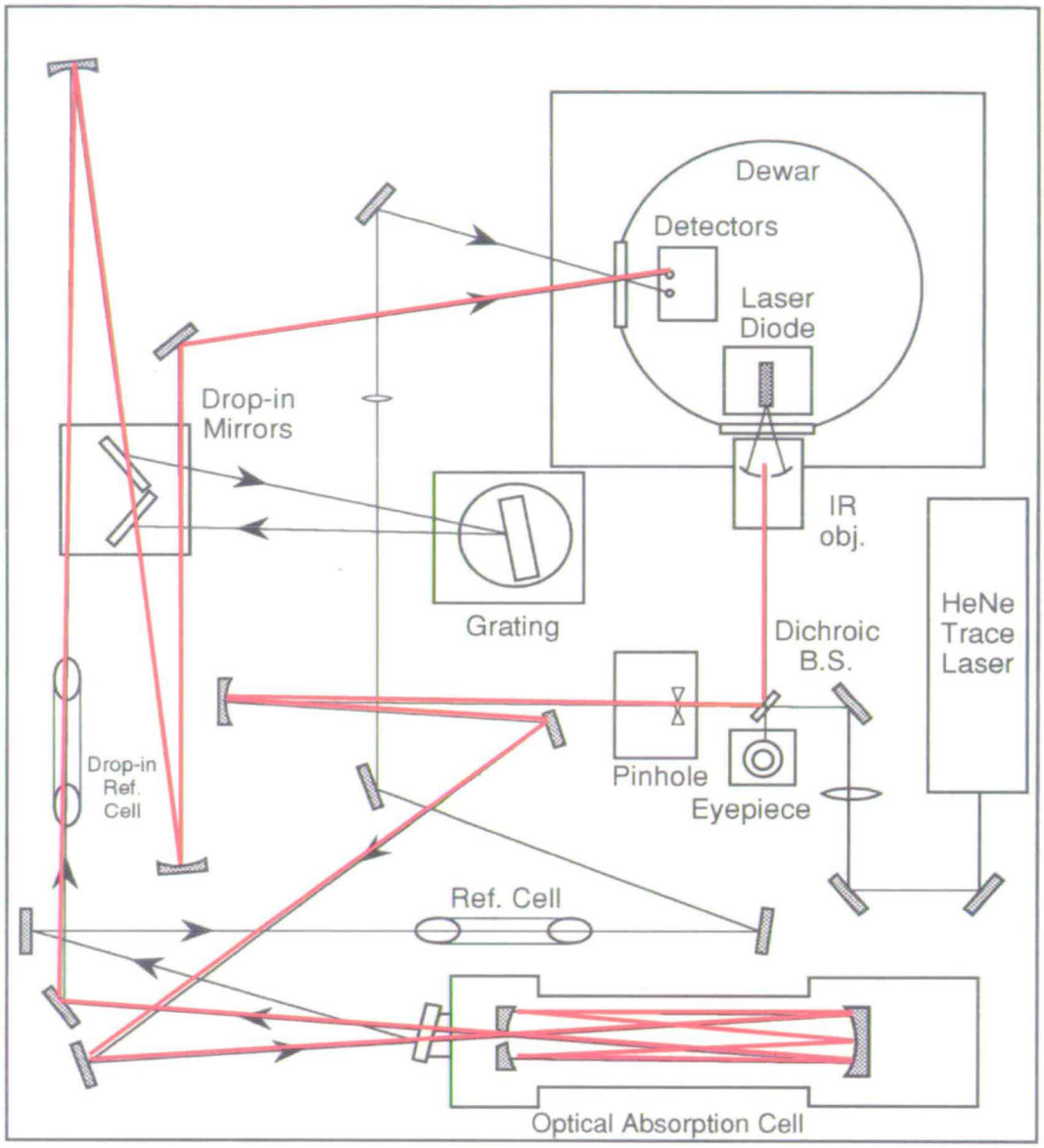

Figure 4.8 Optical path scheme of the TDL

This spectral information is analyzed in real time with a nonlinear least squares fitting routine, which returns both the spectral line Voigt profile and laser intensity spectrum (baseline). The area between the absorption line and the baseline, together with the known absorption coefficient for the line (from the HITRAN spectral database line parameters), temperature and pressure in the cell are used to calculate the concentration of the species observed (Figure 4.9).

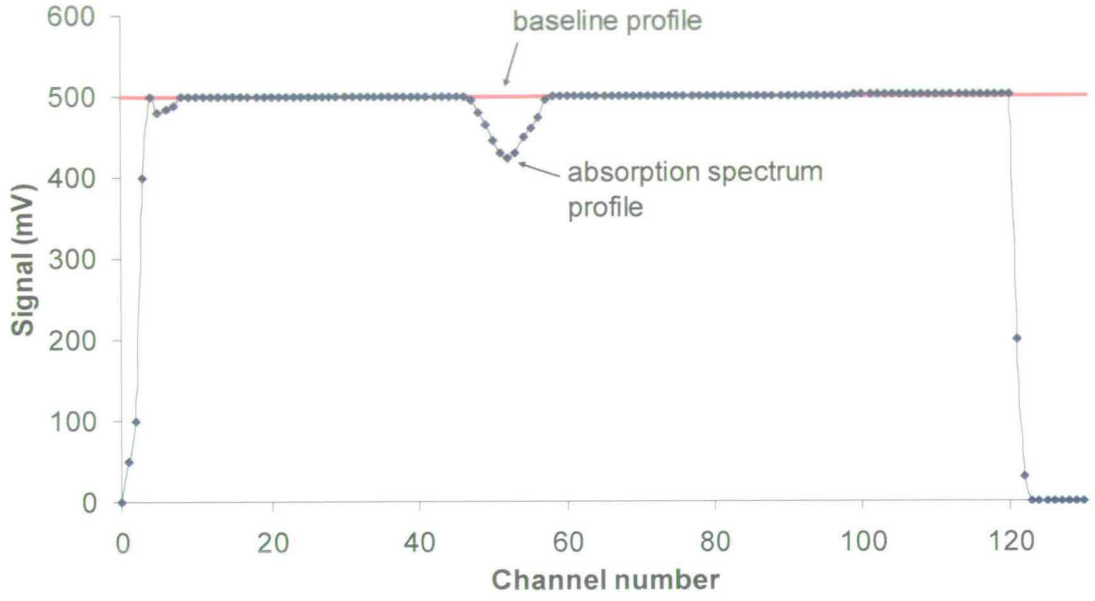

Figure 4.9 Scheme of a TDL absorption spectrum with a Voigt profile fit.

For the measurements at the Easter Bush field the N_2O absorption line λ=2209.466 cm^{-1} was used most of the time. Under field conditions the measurement precision in the fast response operating mode is typically about 0.8-0.9 % (rms) of ambient N_2O concentrations with a signal averaging time of 0.1 s (10 Hz).

The multi-mode condition of the diode laser used for Easter Bush caused often a shift in the frequency emission. In this case the area defined by the baseline and the absorption line for a fixed concentration could be modified causing a drift in the evaluation of the absolute N_2O mixing ratio in the long term. A regular gas calibration (1 every hour) could have avoided this problem, but a rejection of a 30 min-flux every hour would have been necessary, implying a big loss of data. Furthermore, the automatic calibration option in the version of the TDL software used was not always working correctly. A calibration of the instrument was done

about once a month but the concentration drift was checked and re-adjusted every time that the dewar was filled with liquid nitrogen (about every 20 hours).

4.5 Ultrasonic anemometer

A USA-1 ultrasonic anemometer (Metek GmbH, Germany) was mounted at a height of 2.5 m to measure the three wind velocity components and air temperature at 20 Hz. The use of the sonic anemometer in combination with a fast gas analyser is ideal for eddy covariance measurements.

The functioning principle of ultrasonic anemometer is the measurement of propagation time of ultra sound waves in the atmosphere. Three pairs of transducers at a set distance *(d)* work intermittently as emitters and receivers, propagating ultra sound waves at high frequency (Figure 4.10). There are therefore two signals travelling in opposite direction for each direction along the same path. From the wave transit times t_1 and t_2:

$$t_1 = \frac{d}{c+v} \qquad t_2 = \frac{d}{c-v} \tag{4.4}$$

where c is the speed of the sound, the wind speed component (v) along the path is calculated:

$$v = \frac{d}{2}\left(\frac{1}{t_1} - \frac{1}{t_2}\right) \tag{4.5}$$

By arranging the three pairs of transducers in different orientations, the direction and magnitude of the airflow is determined. From Equation (4.4) the speed of the sound (c) can be calculated as a function of t_1 and t_2:

$$c = \frac{d}{2}\left(\frac{1}{t_1} + \frac{1}{t_2}\right) \tag{4.6}$$

The measurement of the air temperature is based on the relationship between the speed of the sound and environmental conditions such as air composition pressure, temperature and humidity:

$$c^2 = 403T(1 + 0.32e/p) \tag{4.7}$$

where e is the vapour pressure of the water in air at T and p is the atmospheric pressure. The sonic temperature T_s of the air is then computed (Kaimal and Gaynor 1991):

$$T_s = \left(\frac{L^2}{1612}\right)\left[\left(\frac{1}{t_1}+\frac{1}{t_2}\right)\right]^2 + \frac{v_n^{\,2}}{403} \tag{4.8}$$

where v_n is the component of wind speed normal to the transducers line. The temperature obtained by the sonic measurement approximates the virtual temperature T_v of the air:

$$T_v = T(1+0.38e/p) \tag{4.9}$$

since the sonic temperature can also be written as:

$$T_s = T(1+0.32e/p) \tag{4.10}$$

The difference between the two is due to ratio of specific heats included in the sonic temperature calculation not included in the virtual temperature. When the sensible heat flux H is measured with a sonic anemometer a correction for the moisture effect need to be applied (Stull 1988):

$$\overline{w'T'} \approx \overline{w'T_s'}/(1+0.06/\mathrm{B}) \tag{4.11}$$

where B= H/LE is the Bowen ratio. In the present work this correction was done in the reanalysis program.

The inlet of the TDL spectrometer used to measure N_2O concentration was fixed on the same mast as the anemometer (Figure 4.10) with a little funnel to avoid obstructions and water access into the tube. A Teflon® tube of 20.5 m length and 6.35 mm internal diameter (calculated flow ~ 4 ℓ/min) was connected the inlet from the mast to the instrument, which was positioned 10 m from it in an electrically powered portacabin. The analogue signals coming from the TDL and sonic anemometer are converted and processed synchronously by using a LabVIEW (National Instruments Inc.) program (see Section 3.10). Figure 4.11 shows the field set-up.

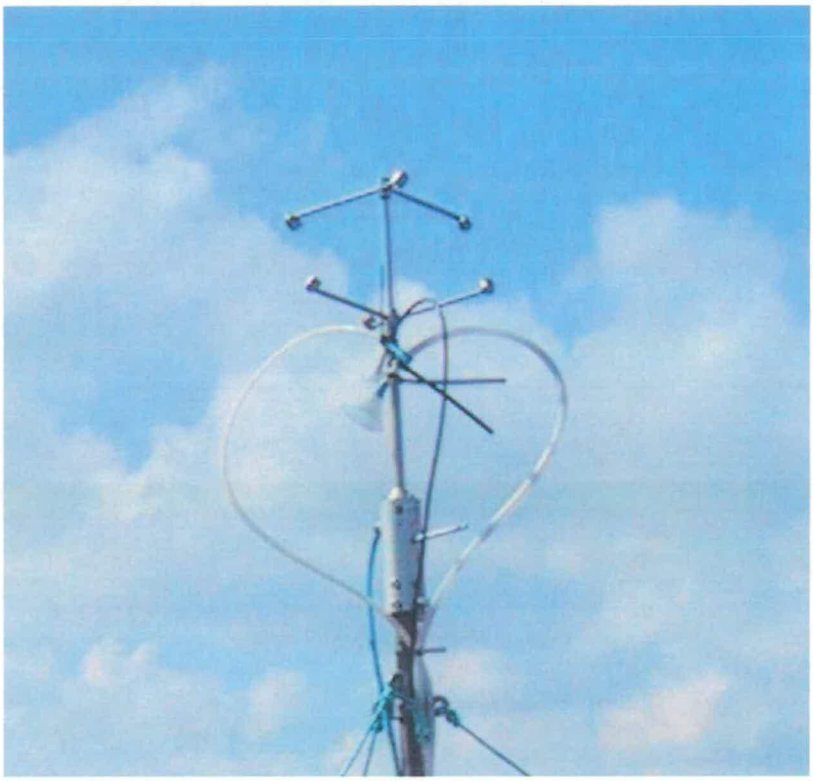

Figure 4.10 Easter Bush field set up showing the N_2O eddy covariance system mast, with the ultrasonic anemometer and the TDL Teflon® inlet.

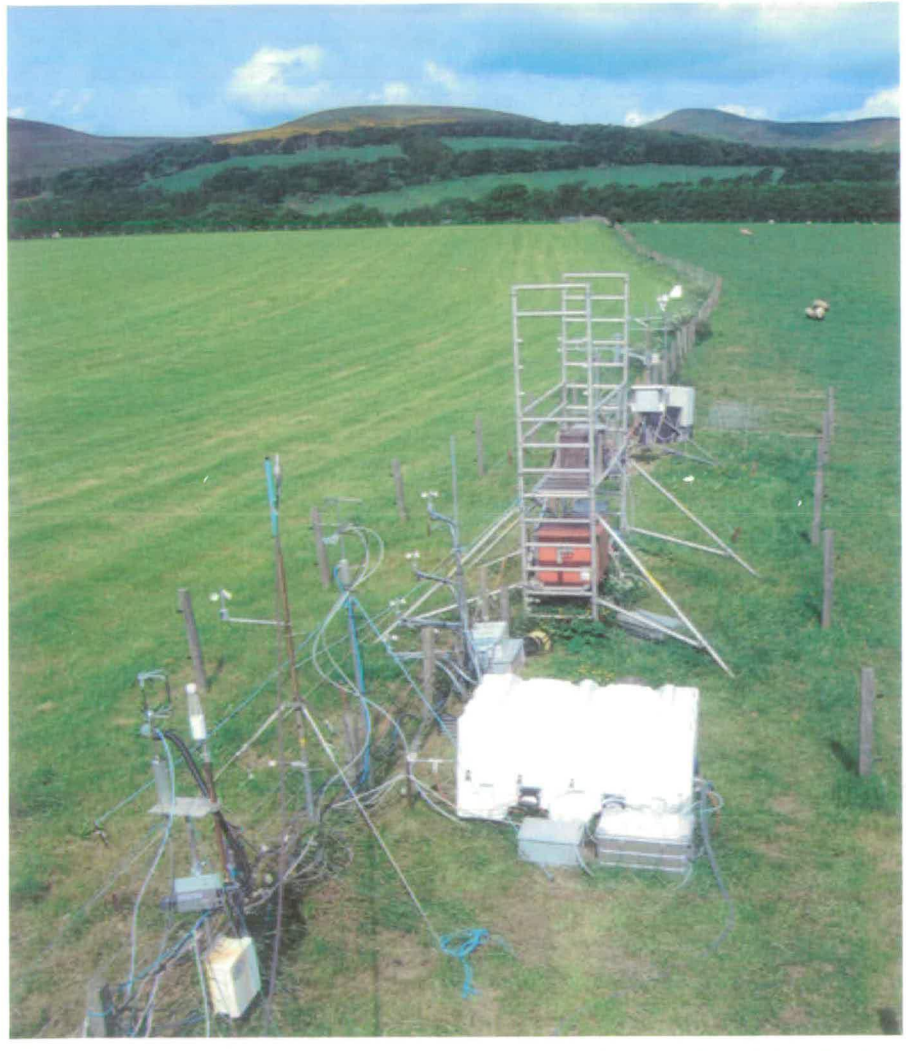

Figure 4.11 Easter Bush field set up showing from the left to the right, i) the CO_2 eddy covariance system on the first mast, ii) the aerosols eddy covariance system, iii) the N_2O and NH_3 eddy covariance system, iv) the O_3 gradient system, v) the AMANDA NH_3 gradient system on the scaffolding, vi) the Bowen Ratio weather system and vii) the TAG-NH_3 gradient system on 14/6/2003. The left field is the S field and is cut and the right field is the N field and is uncut on this date.

4.6 Other meteorological instrumentation

A description of some additional meteorological instrumentation operating at Easter Bush is presented here. Some data from measurements carried out by CEH, overlapping in time with the N_2O fluxes measurements by eddy covariance, were used to enlarge the investigation and to provide a wider picture of the exchange processes between soil and atmosphere.

A Bowen Ratio (BR) system (023A, Campbell Scientific, Loughborough, UK) provided gradients of air temperature and water vapour. Air temperature was measured using fine gauge chromel-constantan (E-type) thermocouples with diameters of 0.003 inch. Water vapour pressure and dew point temperature were measured using a dew point hygrometer. The height of the lower measurement was between 0.4 m and 0.8 m above ground, depending on the canopy height, and the top measurement was about 2.13 m above ground.

Measurements of net radiation, solar radiation and rainfall were made using a Q-7 Net Radiometer, SP1110 Pyranometer sensor and an ARG100 tipping bucket rain gauge (all supplied via Campbell Scientific, Loughborough, UK). Soil temperature was measured at 2 cm and 10 cm depth at two different locations in the soil using TCAV chromel-constantan (E-type) thermocouples probes (Campbell Scientific, Loughborough, UK). Soil heat flux was measured at 10 cm depth at two locations using soil heat flux plates (Campbell Scientific, Loughborough, UK).

Soil moisture was measured with a Time Domain Reflector (TDR100) probe (Campbell Scientific, Loughborough, UK) from the 25/06/2002 at four different depths in the soil, 3.5-7.5-15-30 cm, in both fields. From 06/05/2003 soil temperature profile at the same depths was also recorded using thermocouples.

4.7 Vegetation and soil measurements

As part of the routine measurements at the Easter Bush field site vegetation and soil parameters were measured in addition to the standard meteorological parameters in order to aid the interpretation of gas exchange. Measurements were carried out on

both north and south fields to detect the differences between the two fields, since the timing of the management was not exactly the same for both fields.

4.7.1 Soil profile description

The soil is a fundamental element in the process of production and exchange of N_2O, and is usually carefully analysed in studies of N_2O fluxes. Therefore a description of some soil measurements made at Easter Bush, part of a programme of regular measurements conducted at the field (Milford 2004), are presented here. Some soil characteristics, such as soil type and texture, change only over a long time scale and it is possible to investigate them only once every few years. Other variables, such as mineral N supply, vary on a short time scale and were measured once per month.

4.8 Record of management activities

The Easter Bush grassland is intensively-managed for silage and grazing. As a consequence of this, a wide variety of agricultural management occurs. To completely characterise the site, detailed data on treatments and management activities during the measurement period were recorded, but also information about management in the preceding 10 years were collected, since the history of the grassland has an important influence on its present status.

4.9 Site characterization: results

Measurements of micrometeorological parameters and site characteristics are essential in order to calculate and interpret fluxes of trace gases. The characterisation of type of soil is very useful in understanding the processes that regulate the production and emission of nitrous oxide from the soil to the atmosphere.

4.9.1 Comparison of meteorological parameters from two different measuring systems

In order to assess the reliability of the meteorological measurements used during the study presented here, a comparison was carried out with measurements from other instruments, set up on the same field or very close. Turbulent parameters, such

as $u*$ and H, and meteorological variables, such as wind direction and rainfall, are compared, as they are the parameters used in this study.

*4.9.1.1 H and u**

To evaluate the consistency of $u*$ and H data, measurements from another eddy covariance system, installed at the same field site (Figure 4.1) and measuring at the same time, were analysed. This eddy covariance system was used to measure CO_2 fluxes from the Easter Bush field site and was composed of an ultrasonic anemometer 1012RA (Gill Instruments, UK) and a LI-7500 analyzer (LI-COR, Lincoln, NB, USA) (Table 4.1) to measure CO_2 concentrations. The mast was located 1 m from the mast used by the eddy covariance system for measuring N_2O and the sampling height was slightly lower at 2.15 m.

In Figure 4.12 an example of comparison of time series of H, measured by the two eddy covariance systems from 31/08/02 to 03/09/02 is plotted. Figure 4.13 shows a similar comparison for $u*$. These results show quite close agreement. Figure 4.14 shows the comparison for the period of August 2002 between the sensible heat flux measured with the Metek system (H_{metek_system}) and the sensible heat flux measured with the Gill system (H_{Gill_system}), ($H_{metek\_system} = 0.9H_{Gill\_system}+3.2$, $R^2 = 0.89$ n = 858). The regression over the one year measurement period is: $H_{metek\_system} = 0.82H_{Gill\_system}+0.45$, $R^2 = 0.68$, n = 9960. Figure 4.15 shows similar results for $u*$. In general, the Gill system slightly overestimates the turbulent parameters compared to the Metek sonic system. This can be due to the different structure of the two instruments: the Gill is provided with a support that could cause wake interference in specific wind directions.

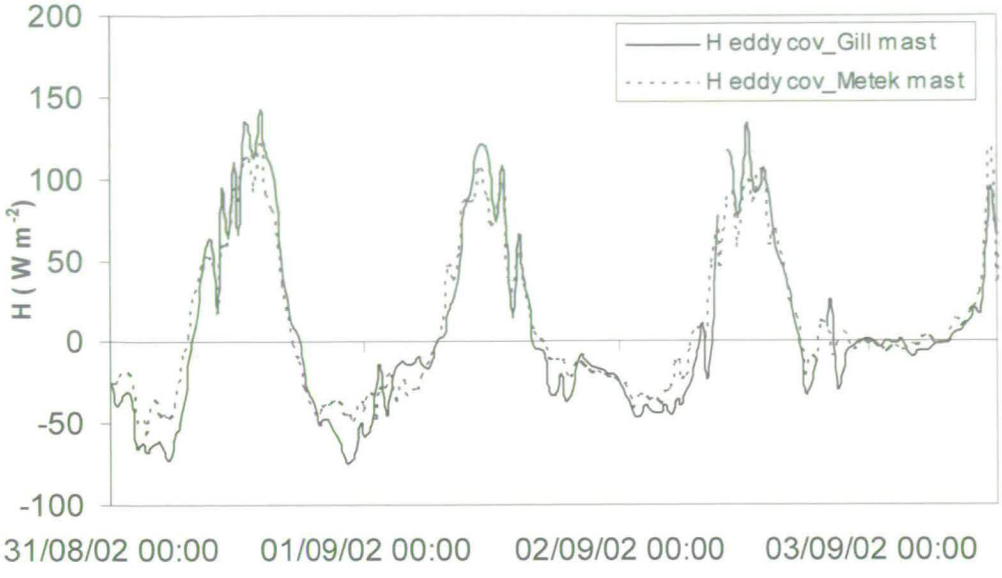

Figure 4.12 Comparison of sensible heat flux (*H*) measurements made with the Gill and the Metek ultrasonic anemometers, 31/8/2002-3/9/2002

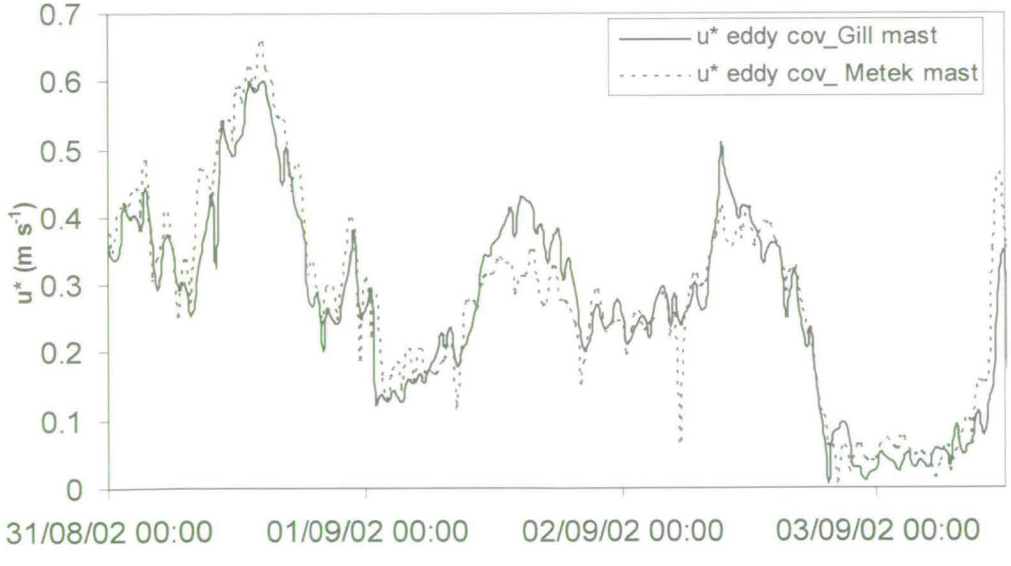

Figure 4.13 Comparison of friction velocity (*u) measurements made with the Gill and the Metek ultrasonic anemometers, 31/8/2002-3/9/2002.**

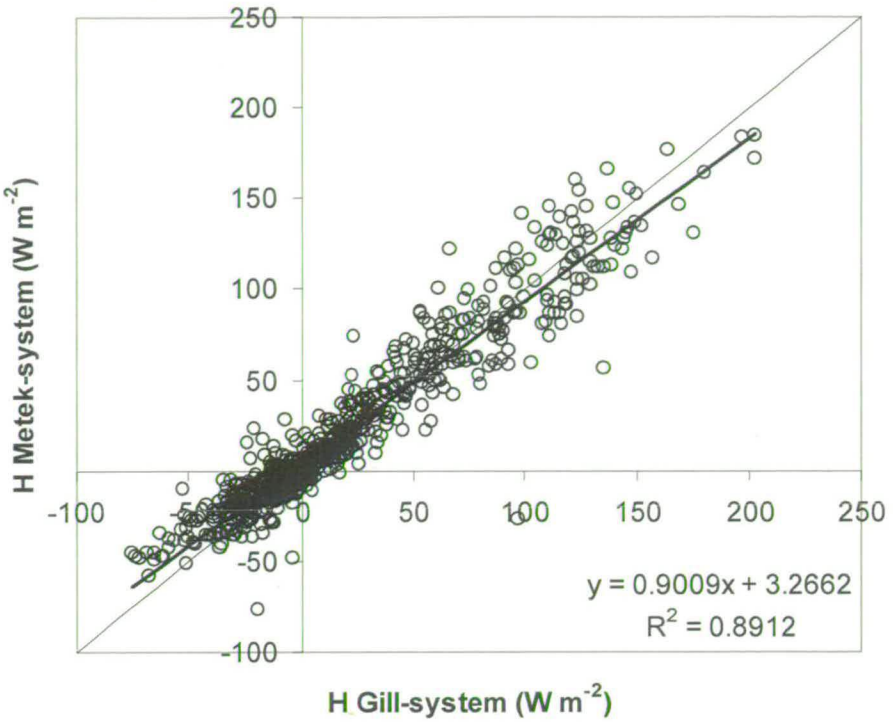

Figure 4.14 Correlation between *H* measurements obtained from Metek system and Gill system for the period 1-31/08/2002. The thin black line represents the 1:1 line.

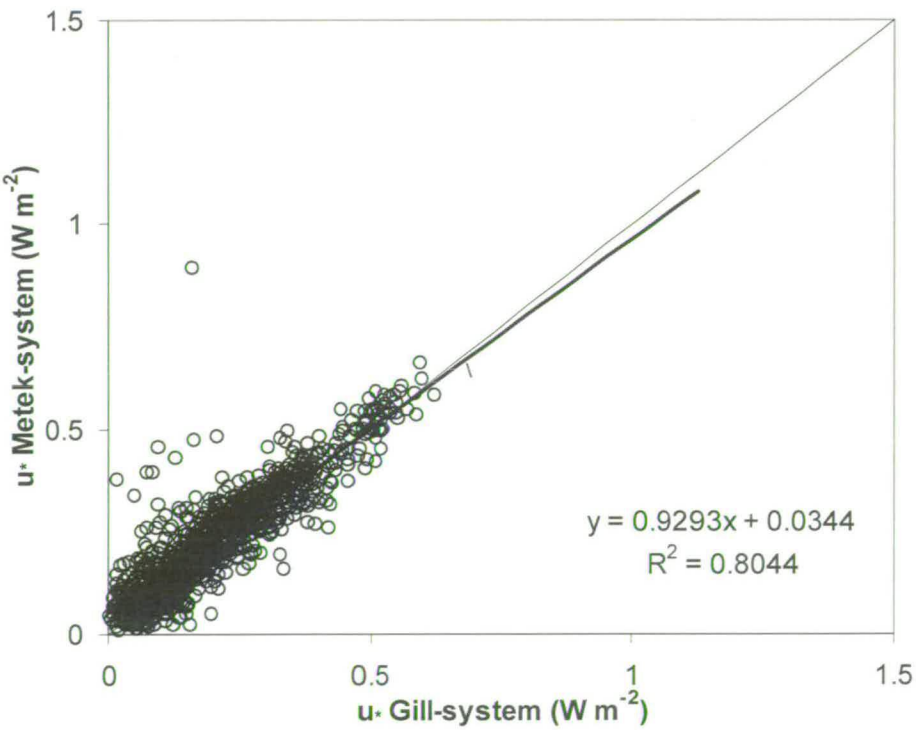

Figure 4.15 Correlation between *u measurements obtained from Metek system and Gill system for the period 1-31/08/2002. The thin black line represents the 1:1 line.**

4.9.1.2 Wind direction

The same two measuring systems used for investigating the agreement of turbulent parameters were used to compare the wind direction measurements. In Figure 4.16 the wind direction from the two ultrasonic anemometers is taken into consideration for the period 09/06/02-19/06/02.

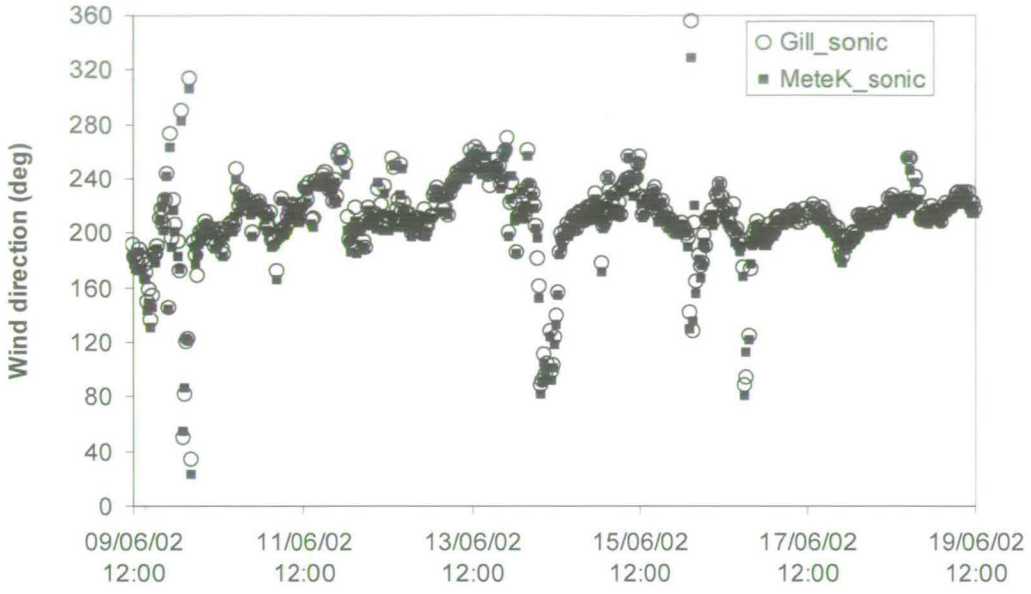

Figure 4.16 Comparison of wind direction measured at the field site with the Gill anemometer and with the Metek anemometer

Since the wind direction is the direction of the wind vector, a different approach than a regression of one wind direction against another is used. From the definition of scalar product for two vectors X and Y, $X \cdot Y = |X||Y|\cos\theta$, where θ is the angle between the vectors in radians. Studying the cosine of the angle (θ) between the two different estimates of wind direction will provide information about the agreement of the two sets of data. In fact, for two identical vector directions $\cos\theta = 1$, whereas for perpendicular vectors $\cos\theta = 0$ and for anti-parallel vector directions $\cos\theta = -1$. Figure 4.17 shows the time series of the cosine of the angle θ for the same period taken into consideration in Figure 4.16. In this case 99% of the time cos θ was >0.95, which corresponds to an angle of 18 degrees. Over the entire period of measurements cos θ was >0.95 in 88% of the cases. Figure 4.18 shows the cosine of the angle θ for a six-month period in 2003.

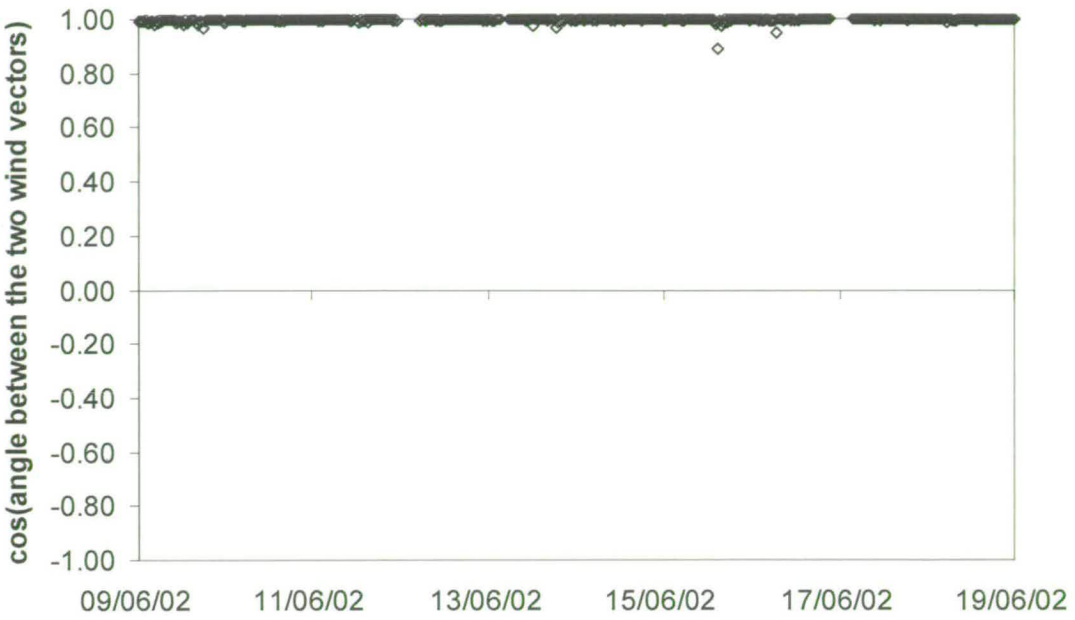

Figure 4.17 Time series of the cosine of the angle (in radians) between the wind vectors measured with the Metek anemometer and the Gill anemometer for the period 09/06/02-19/06/02.

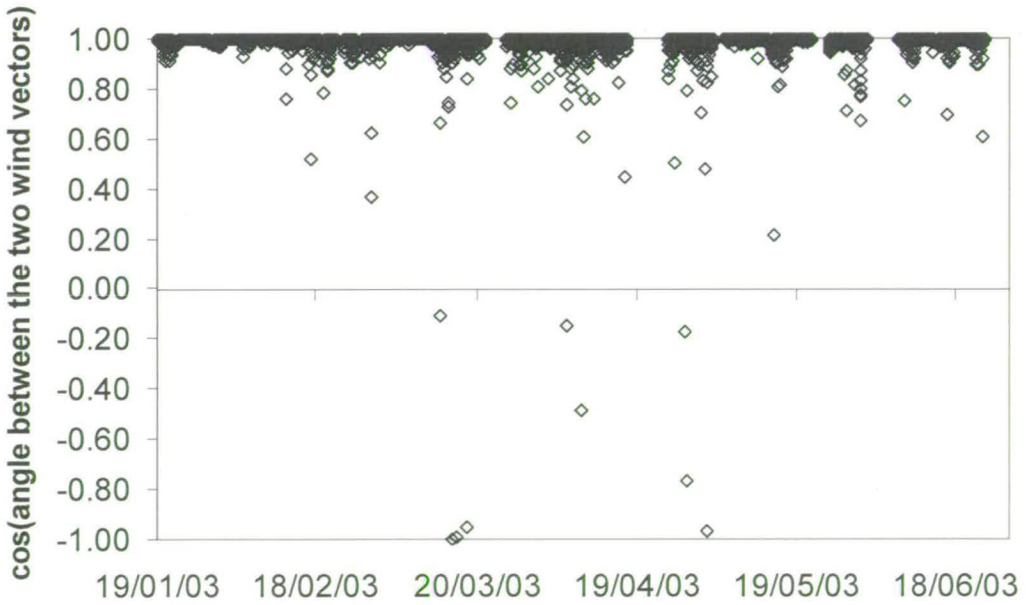

Figure 4.18 Time series of the cosine of the angle (in radians) between the wind vectors measured with the Metek anemometer and the Gill anemometer for the period 19/01/03-18/06/03.

4.9.1.3 Rainfall

The importance of soil wetness in analysing N_2O fluxes was described in Chapter 2 and the soil wetness is very dependent on rainfall. Precipitation was measured using a tipping bucket rain gauge at the field site. Measurements were compared with rainfall data acquired at another monitoring cabin located 400 m south from the field site.

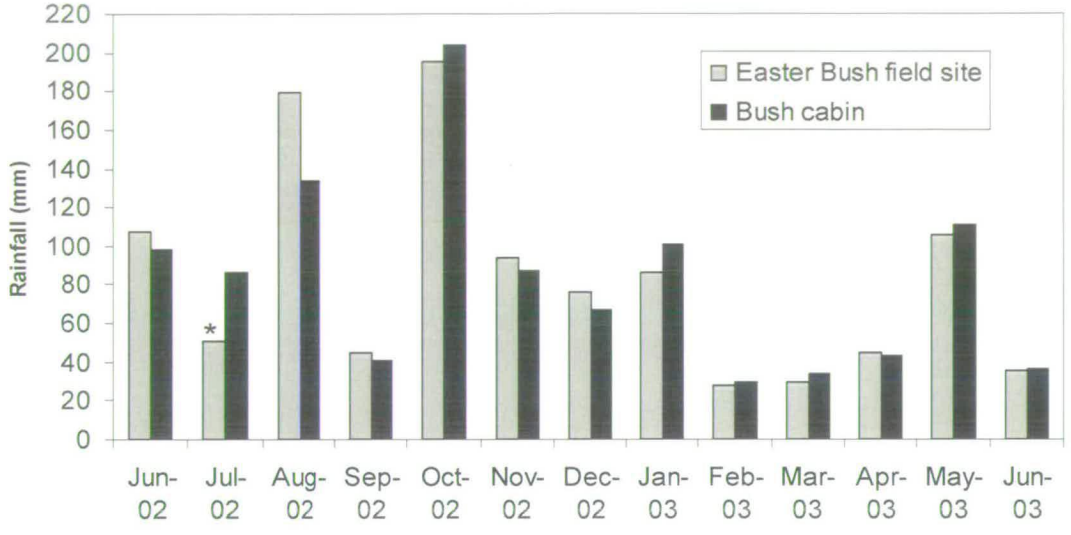

Figure 4.19 Comparison of monthly rainfall measured at the field site against rainfall measured at a monitoring cabin located 400 m south from the field for the period 1/6/02-1/6/03. (*) Data for July 2002 contain a gap of a week in the measurements (from 17/7/02 to 24/7/02).

The comparison in Figure 4.19 shows a good agreement between field site data and Bush cabin measurements. The rainfall over the period of comparison (1/6/02-1/6/03) was 1078 mm at Easter Bush field site and 1072 mm at the monitoring cabin, with a difference of 0.5%. For the period 17/7/02-24/7/02 data at Easter Bush field site were missing, so the values from the monitoring cabin were used.

4.10 Wind frequency distribution, fetch and footprint

From the topography of the site and the position of the instrumentation, the estimate of the fetch was between 175 m and 200 m for the wind directions 180°-305° and 315°-55°. The wind direction frequency distribution for the Easter Bush field site for the 12-month period of measurements is shown in Figure 4.20. From the wind rose it is clear that the main wind direction is from the SW direction. The red

line in the plot defines the position of the fence line where the instruments are located (140°-310°). The low frequency of wind blowing along this direction makes the instruments set up on the field ideal for micrometeorological measurements, resulting only in a small loss of data. The data were filtered excluding the wind sector 80°-170°, where the laboratory-cabin was an obstacle for the wind. This area is indicated with the shadowed sector in Figure 4.20. The rest of the instruments along the fence line towards NW did not affect the measurements, as it is shown in Figure 4.21, where the angle θ of vertical rotation applied to the anemometer axis is plotted against the wind direction over the entire period of measurements. The influence of obstacles on the field site is indicated by the clear and systematic decrease of the values in the sector 80°-170°.

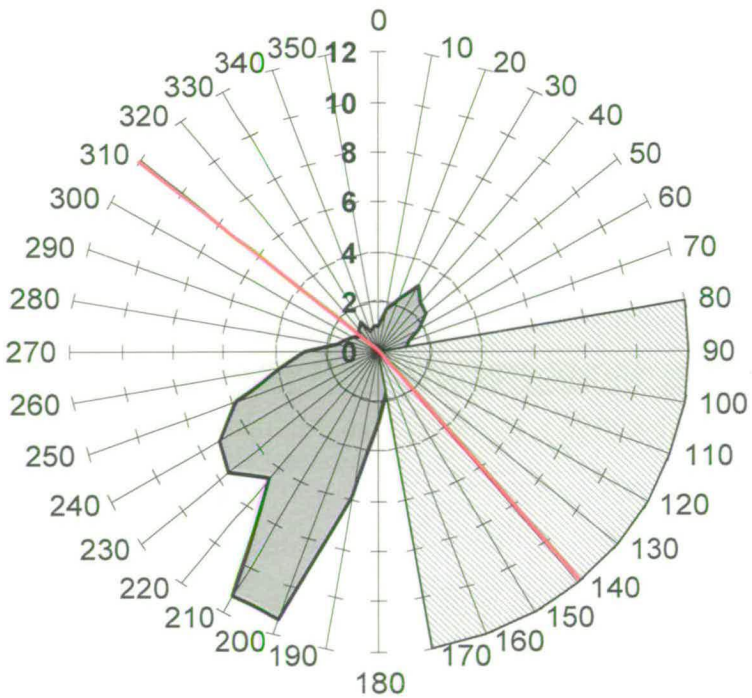

Figure 4.20 The grey area represents the wind direction frequency distribution (as % of time) for Easter Bush for the full measurement period (06/06/02-23/06/03). The red line indicates the position of the instrumentation on the field and the shadowed area is the wind sector rejected in the data filtering.

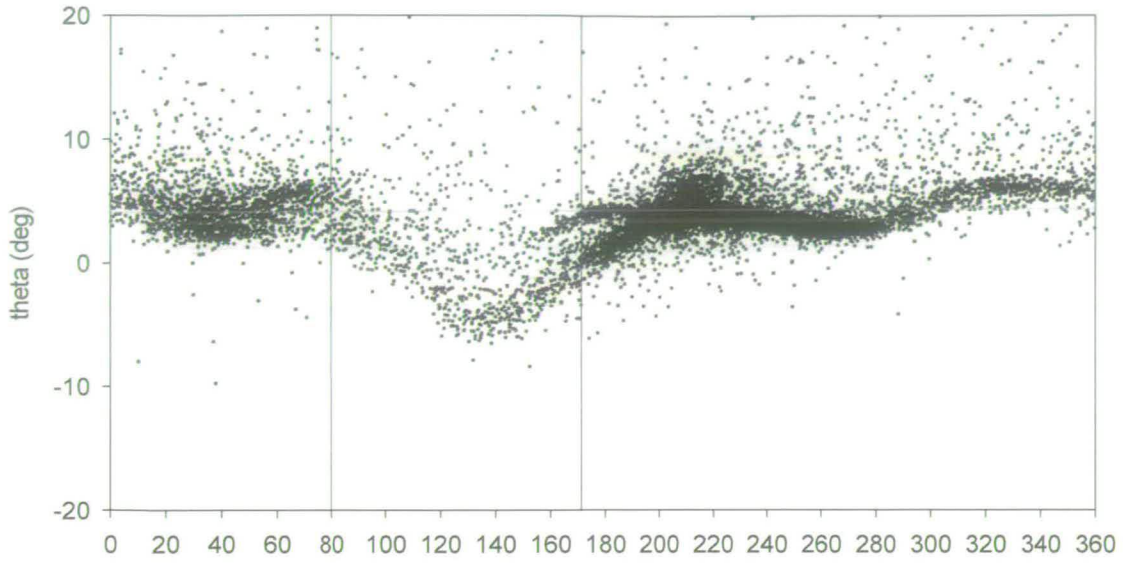

Figure 4.21 The angle theta (θ), which corresponds to the vertical rotation applied to the anemometer's axis, in order to make $\overline{w} = 0$, is plotted versus the wind direction sectors for the full measurement period 06/06/02-23/06/03. The two vertical lines show the wind sector rejected.

Figure 4.20 shows that the wind was blowing from the S field for the majority of the time (72.2%) and more specifically 55.5% of the time from a narrow sector (190°-260°); wind blew from the N field only 25.1% of the time.

As explained in Section 3.9.1 the quantification of the portion of fetch in practice contributing to the measurements is given by the cumulative normalised footprint (CNF). The average over the total duration of the measurements of CNF was 65% and the median was 74%. In 63% of the time CNF was >65%. The stability of the atmosphere strongly influences the footprint (area where the measured flux originates) and changes the size of it. Generally this area is described as an elliptic shape(Schmid 2002). In unstable conditions this ellipse is smaller than in stable conditions when it becomes larger and stretches along the downwind direction (Kljun et al. 2003). As a percentage of the footprint within a given fetch (e.g. Easter Bush field) the CNF in stable conditions is expected to be smaller than in unstable conditions. In Figure 4.22 an example of CNF for Easter Bush is plotted as a function of upwind distance from the measurement mast for neutral, stable and unstable conditions. The overall average CNF for fluxes in stable conditions was 68% and it

was 80% in unstable conditions. These values were calculated taking into account only the CNF for the filtered flux measurements. In summer days the change from stable conditions at night to unstable conditions during the day is more accentuated than in the winter when the difference in stability between night and day is smaller. As a consequence, the daily variation of CNF in summer months is often larger than in winter: at Easter Bush field it was about 30-40% in the summer and less than 20% in the winter. CNF monthly values for fertilisation periods described in Chapter 5 ranged from 74% in August 2002 to 85% in June 2002 (Table 4.2).

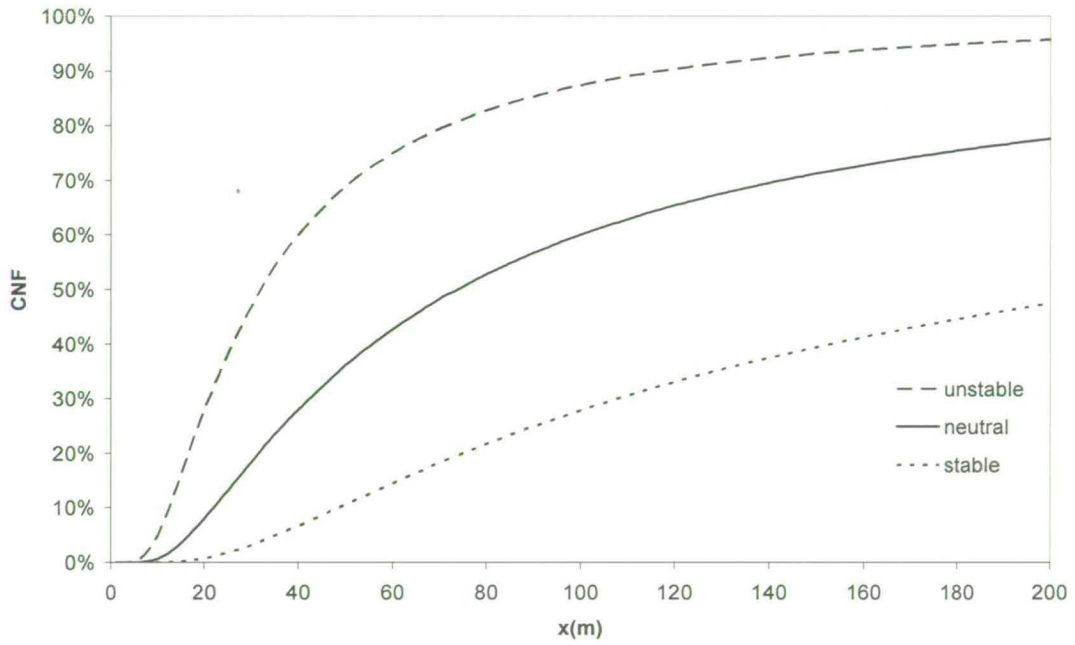

Figure 4.22 Cumulative normalized footprint (CNF) for Easter Bush versus the upwind distance from the measurement point in unstable (L=-5), stable (L=5) and neutral (L=0) conditions. In all the three calculations u_*=0.26 m s^{-1} and z_0=0.02 m.

Table 4.2 Monthly values of CNF for the events described in Chapter 5.

Month of fertiliser application	CNF(%)
June 2002	**0.85**
August 2002	**0.74**
Winter (24/01/03-16/02/03)	**0.77**
March 2003	**0.83**
June 2003	**0.78**

4.11 Climatology

Some climatologic parameters for the Easter Bush site are analyzed in Figure 4.23, Figure 4.24 and Figure 4.25. The lowest mean minimum temperature recorded was -7.7 °C in February 2003 and the highest mean maximum temperature was 22.6 °C in May 2002, with a monthly average temperature over the period (June 2002-June 2003) that ranged between 1.4 °C and 12.9 °C. During the period from October to April the mean minimum temperature is below freezing.

The main mechanism for rain generation at Easter Bush is frontal. Monthly rainfall shows a fairly wet first half period of measurements, with 156 mm of rainfall in August 2002 and 200 mm in October 2002, and a drier second part, with February and March 2003 driest months with 29 mm and 32 mm of rainfall respectively. The total rainfall for the year (June 2002-June 2003) was 1078 mm, as mentioned in section 4.9.1. The 1989-1998 annual average rainfall recorded at the closed Met Office meteorological station, Bush House, about 1 km South-West to Easter Bush field, is 920 mm. The maximum monthly air pressure occurred in September 2002 (999 hPa) and minimum in November 2002 (979 hPa). Monthly averaged wind speeds are usually above 2 m s^{-1}.

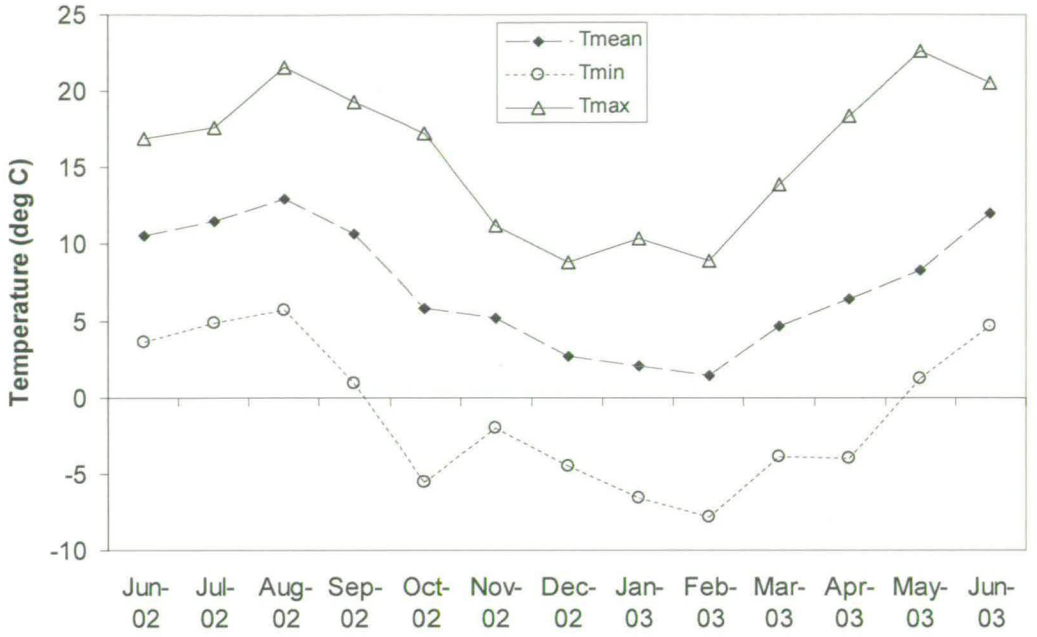

Figure 4.23 Monthly average of mean, minimum and maximum air temperature measured with thermocouples at the cabin located 400 m south from the field site

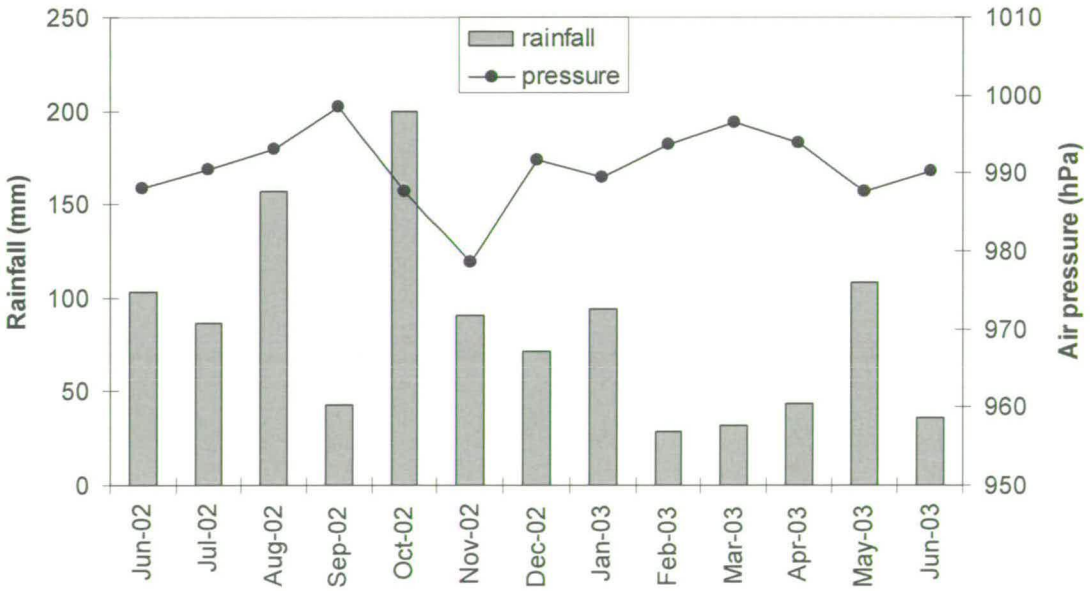

Figure 4.24 Monthly rainfall and monthly average of air pressure at the Easter Bush site for the period 01/06/02-31/06/03.

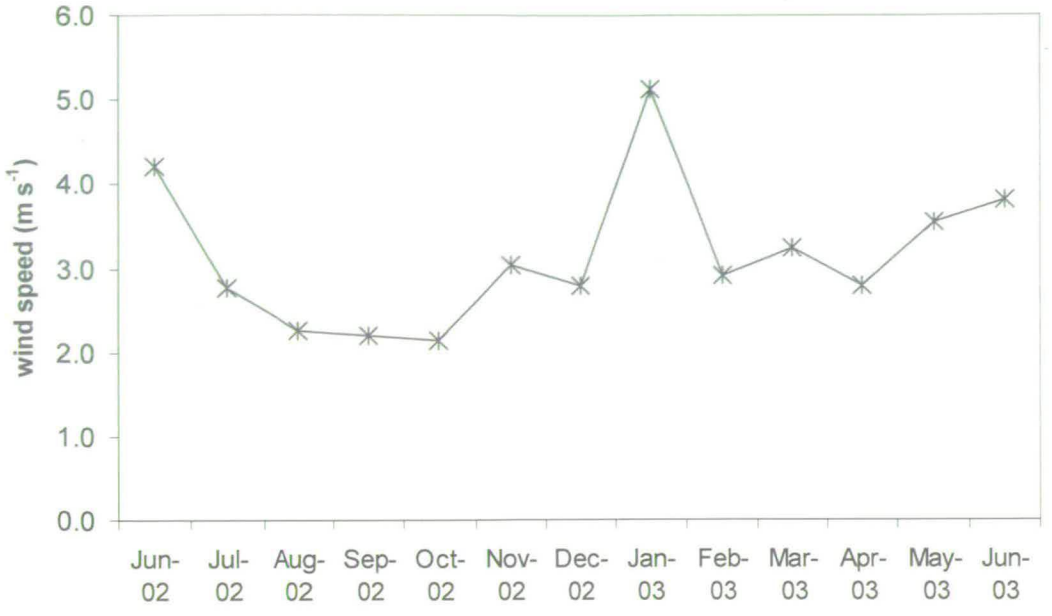

Figure 4.25 Monthly average of wind speed measured with a Metek ultrasonic anemometer (2.5 m) at Easter Bush site for the period 01/06/02-31/06/03.

Figure 4.26 shows the energy balance for the Easter Bush field for three days (27/05-30/05/03). Most of the energy supplied by the net radiation (R_n) is used to heat the air with the sensible heat flux (H) and to add heat to the soil (G), whereas the latent heat flux (LE) measured with the Bowen ratio station is very small for the three days. This could be due to the dry week preceding the days shown here.

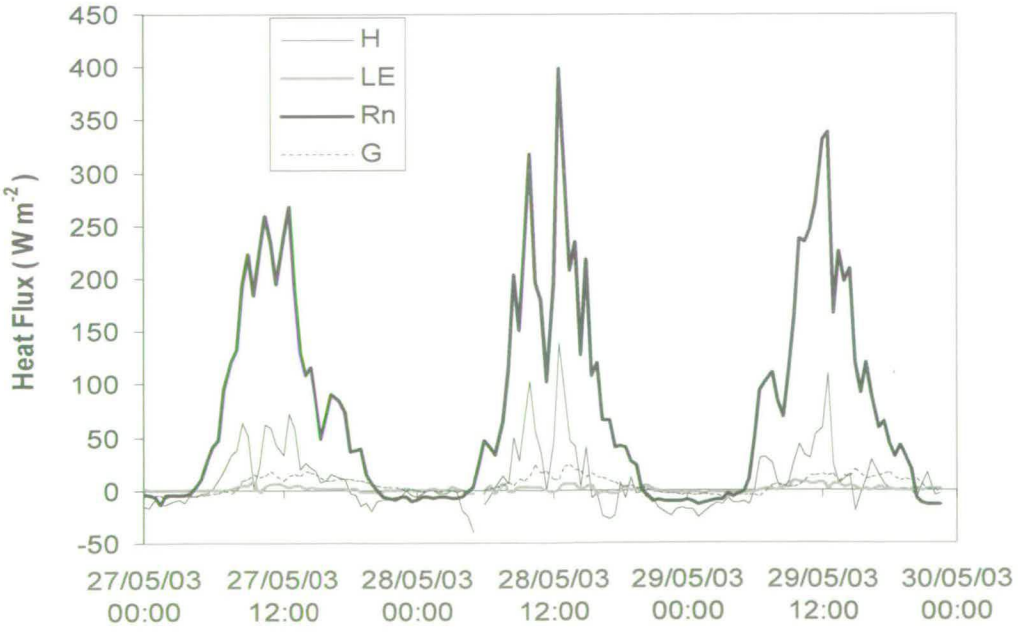

Figure 4.26 Example of energy balance for Easter Bush site for the period 27/05/03-30/05/03.

4.11.1 Soil measurements

4.11.1.1 Soil profile study

A soil pit was excavated by digger to 1 m at Easter Bush in the SW field on 12/11/02 and a soil profile description conducted by B. Rees, from the Scottish Agricultural College (SAC) Edinburgh, following Hodgson (1974) (Milford 2004) (Table 4.3).

Four replicates of soil sample were taken at 3 depths (0.0 m-0.10 m, 0.10 m-0.3 m and 0.3 m-0.5 m) to investigate some of the soil characteristics here described. The sampling devices used were coring cylinders of known volume (200.8 cm^3). The cores were weighed and dried for 24 hours at 110°C.

Table 4.3 Soil profile description from a measurement at Easter Bush site on 12/11/02. (Milford 2004)

Horizon	Depth (m)	Description
A1(g)	0-0.18	Brown (5YR 3/2) occasional mottling; sandy loam, coarse crumb, friable few medium rounded stones; abundant fine roots; gradual change into:
A2(g)	0.18-0.31	Brown (7.5 YR 3/2) mottling, sub-angular blocky; firm; roots many fine; stones small-medium, common; clear change into:
B1(g)	0.32-0.79	Grey-Brown (10YR 4/2) abundant mottling (7.5 YR6/1-10YR 6/8); sandy clay loam poor blocky; plastic; stones moderate, small-large rounded-sub-angular; few fine roots; gradual change into:
B2(g)	0.79-1.00	Grey-Brown (7.5 YR 4/3) strongly mottled (7.5 YR 5/8); clay loam; poor blocky; plastic; stones moderate small-large rounded-sub-angular; very fine roots; water tables at 85 cm.

4.11.1.2 Soil texture

The distribution of the size of soil particles influences strongly chemical and physical properties of the soil (Rowell 1994). Particularly affected by the variability of the size of soil particles is the drainage of the soil and the ability of the soil to hold water and nutrient for plant use.

The particle size distribution was investigated at Easter Bush in three soil layers; the results are given in Table 4.4. The analysis was carried out at SAC Edinburgh. The soil is classified as sandy clay loam according to these results.

Table 4.4 Easter Bush particle size distribution

Soil layer depth	Clay (%) <2 µm	Fine silt (%) 2-20 µm	Coarse silt (%) 20-50 µm	Fine sand (%) 50-200 µm	Coarse sand (%) 200 µm-2 mm
0 - 0.1 m	21	17	10	25	27
0.1 - 0.3 m	20	16	10	26	28
0.3 - 0.5 m	20	17	10	25	28

4.11.1.3 Bulk density

The bulk density of the soil is defined as the mass of oven-dried soil present in a given volume (g dry soil cm $^{-3}$) and it is a significant parameter in the determination of hydrological soil characteristics.

A profile of bulk density was determined at Easter Bush The soil was dried for 24 hrs at 110° C and then weighed. The results are shown in Table 4.5.

Table 4.5 Easter Bush soil bulk density

Soil layer depth	Bulk density (g dry soil cm^{-3})
0 – 0.1 m	1.22
0.1 – 0.3 m	1.58
0.3 – 0.5 m	1.68

4.11.1.4 Soil organic nitrogen and carbon content

The content of organic nitrogen and carbon in the soil changes on a long time scale. Although the chemistry of soil organic matter is complex, its composition is broadly similar in all the soils. In particular, for agricultural soils in temperate regions the ratio C:N is close to 10:1 (Rowell 1994). Chemical analyses were performed at INRA (Institut National pour la Recherche Agronomique) on the soil samples from the three different depths for a one-off measurement and the total organic C, total N, nitrogen available as NO_3 and NH_4, and soil pH for Easter Bush site are given in Table 4.6. Regular soil chemical measurements were made almost every month at two layers (0-10 cm and 10-20 cm) providing estimates of soil water content and available soil N.

Table 4.6 Soil chemical properties at Easter Bush site.

Soil layer depth	Total N (%)	Organic C (%)	NO_3-N (%)	NH_4-N (%)	pH
S field					
0 – 0.1 m	0.23	4.2	0.08	3.3	5.0
0.1 – 0.3 m	0.21	3.0	0.23	2.8	
0.3 - 0.5 m	0.21	2.4	0.35	1.8	
N field					
0 – 0.15 m	0.33	4.5	0.07	5.6	5.0
0.1 – 0.3 m	0.19	2.7	0.16	1.9	
0.3 - 0.5 m	0.19	2.7	0.26	2.5	

4.12 Management information

The description of the management of the Easter Bush site for the duration of the measurements is shown in Table 4.7. The fields have been used as grassland for 15 years; they usually receive 270-320 kg N ha^{-1} $yr^{-1}$and yield two cuts of silage per year. For 2003 the management was slightly different, with a smaller use of fertiliser on the N field and a longer grazing period. The type of animals used for grazing were: dairy heifer calves (4-10-month old, weighing 40 kg when born and gaining about 0.75 kg d^{-1}), sheep (c. 3-4 year old, weighing about 35 kg ewe^{-1}), and lambs. The number of calves was close to 50 animals, whereas sheep number varied between 30 and 120. The total fertiliser applied on the N field was 112 kg N ha^{-1} and on the S field was 242 kg N ha^{-1}.

Table 4.7 Description of the management events on Easter Bush field for the duration of the measurements.

Event	N field	N supply kg N ha^{-1}	S field	N supply kg N ha^{-1}
Cutting	01/06/02			01/06/02
Fertilising	07/06/02	60 (fertiliser Kemira:N-P-K, 24:5:10)	08/06/02	60 (fertiliser Kemira:N-P-K, 24:5:10)
Grazing started	19/06/02			
Cutting			05/08/02	
Fertilising			10/08/02	50 (fertiliser Kemira:N-P-K, 25:5:5)
Grazing started			31/08/02	
Fertilising	17/03/03	52 (fertiliser Nitram, (NH_4NO3))	20/03/03	84 (fertiliser Kemira N-P-K, 24:5:10)
Grazing started	30/04/03			
Cutting			29/05/03	
Fertilising			10/06/03	48 (fertiliser Kemira N-P-K, 24:5:8)
Total N supply		**111.74**		**242**

4.13 Summary

In this chapter a description of Easter Bush field and instrumentation on site was presented with a thorough explanation of the principle of functioning of the TDL and ultrasonic anemometer, which are the two instruments used for the measurements studied in the following chapter.

In order to check the reliability of the meteorological parameters measurements, widely used during the study, comparisons with data from other instruments available on the field were made, providing good agreement for wind direction, sensible heat flux, rainfall and friction velocity. A study of the wind field and a brief overview of the typical annual climatology for Easter Bush were also provided with the description of some of the filters applied to the turbulent data.

Chapter 5 Long-term N_2O flux measurements from managed grassland: analysis and interpretation of the data

5.1 Introduction

The measurements of N_2O fluxes at the Easter Bush site were carried out by eddy covariance (Section 3.8) almost continuously between 6 June 2002 and 21 June 2003. The gaps in the data are due to two causes: short interruptions were due to problems with the measuring system, power cuts, or as a result of filters application, which are discussed in this Chapter. Longer gaps in the charts occurred when breaks of measurements happened for practical reasons (e.g. the TDL was committed to other measurements).

The high temporal resolution of the N_2O flux data allowed a detailed investigation of seasonal and diurnal variations of the fluxes (3,320 hours) that are presented in Section 5.3. The N_2O annual budget for Easter Bush and a comparison of eddy covariance measurements with static chamber measurements are presented in Section 5.3.5 and Section 5.3.6 respectively.

Part of the data set presented in this Chapter have already been discussed in Di Marco et al. (2004)

5.2 Data processing and quality control

The measurement height was 2.5 m above ground. N_2O fluxes were calculated using the LabVIEW program, already described in Section 3.10, adopting an averaging period of 30 minutes. The program included a despiking process to eliminate strange values, a double rotation of the coordinate system of the sonic to align the x axis along the main wind direction (Finnigan 2001), and the lag time calculation by finding the lag-time of the maximum covariance between concentration and vertical wind speed (between 0 and 10 s, apart for few cases of longer time lag discussed further in this Chapter).

To quantify the sensitivity of the system, the standard error (SE) of the flux measured by the eddy covariance method was estimated using the equation suggested by Edwards et al. (2003):

$$SE = \sum \sqrt{\frac{Sw(f)Sc(f)}{4\pi f P}} \tag{5.1}$$

where P is the measurement period (e.g.1800 s), $Sw(f)$ is the variance of the vertical wind speed w, and $Sc(f)$ is the variance of the concentration signal from the TDL at frequency f. If $Sc(f)$ represents the gas analyser noise with zero variance in the concentration time series, SE is the contribution of the analyser noise to the standard error of the flux measured by eddy covariance. To have the condition of almost constant concentration (assuming a TDL noise of 2 – 3 ppb – see Section 4.4), N_2O flux data of a month period in winter 2003, when N_2O fluxes were almost zero due to the small emission activity, were taken into analysis. The eddy covariance flux detection limit was estimated at about 20 ng N_2O-N $m^{-2}s^{-1}$ with wind speed ranging from 1-9 m s^{-1}. A similar result was obtained applying the error propagation formula to the same data (Laville et al. 1997):

$$\Delta F = \frac{1}{\sqrt{N}} \sqrt{\sigma_w^2 \cdot (\Delta c)^2 + \sigma_c^2 \cdot (\Delta w)^2} \tag{5.2}$$

where N is the number of data used for the flux estimate (N = 36400) and σ_w^2 and σ_c^2 are the vertical wind and N_2O concentration time series variance, respectively. Δw (0.01m s^{-1}) and Δc (3 ppb) are the precision of the sonic and gas analyser respectively.

After the flux calculation filters were applied to the data using the information on the topography and the wind rose at the field site, excluding some malfunctioning period of the instrumentation, and applying the stationarity test. Further analysis of the quality of the data included a post-field quality tool (ITC) described by Foken and Wichura (1996), storage and spectral corrections.

5.2.1 Filters applied to the data

The wind sector selected for the data rejection due to obstruction (80°-170°) is discussed in Section 4.10. Fluxes calculated from a small number of data points (N<34000) per 30-min intervals were rejected (for 30-min interval N=36000, at 20

Hz), as well as wind speed (u) smaller than 0.5 m s^{-1} to exclude the non-turbulent data. The integral turbulence test (see Section 3.9.4 for detailed explanation) was applied and when the ITC value was < 30% fluxes were rejected.

Table 5.1 shows a summary of the effect of the application of these filters to the N_2O fluxes.

Table 5.1 Results of applying filter criteria to N_2O flux data (filter for non-stationarity is not applied here).

Filter criteria	No. of valid N_2O flux data points remaining (30-min average)	Retained fluxes (%) after filter application
Obstructed wind sector (excluding 80°-170°)	8,472	92%
Number of sampling point N< 34000	8,928	97%
u (2.5 m) < 0.5 m s^{-1}	8,800	96%
ITC	9,035	98%
Malfunctioning of the TDL (negative concentration, power failure, etc.)	7,785	85%
Total (applying all the filters in the list)	**6,641**	**72%**

5.2.1.1 Stationarity

As stated in Chapter 3 (Section 3.9), stationarity is a fundamental requirement for the application of the eddy covariance technique.

During the post-processing analysis two tests were applied to detect non-stationarity in the N_2O flux measurements at Easter Bush. The first one is based on the study of the sign of the cospectrum Co_{wN2O} between vertical wind speed w and N_2O concentration, which is equivalent to investigating the number of significant turning points in the Ogive function Og_{wN2O} for the same variables (Spirig et al. 2004) (see section 3.9). When the difference between the number of positive and negative Co_{wN2O} values was more than 20%, the uncertainty on the sign of the covariance was small and the 30 min measurement was considered stationary. Figure 5.1 shows the N_2O flux cospectrum for a case of non-stationary (**a**) and a case of stationary conditions (**b**). The red dots represent the negative values converted to positive to include them in the chart, and the blue dots are the positive values. The principle of this stationarity criterion is explained by the difference in number of values of the same sign in the two cases: in the non-stationary case 45% of the values were negative, whereas in the stationary one only 25% were negative, providing a

more reliable estimate of the sign of the total flux, which is positive in this particular case.

The other test for detecting non stationary N_2O flux measurements at Easter Bush was derived from the one proposed by Foken and Wichura (1996) and explained in detail in Section 3.9.2: following the analysis of Foken and Wichura (1996), the requirement that the difference between fluxes calculated with an averaging period of 30 minutes and fluxes obtained using an averaging period of 5 minutes (RN_{cov}) should be less than 30% in case of stationary conditions. This is equivalent to saying that the value of Og_{ws} relative to the corresponding frequency 0.0033 Hz (~ 5 minutes), i.e. the cumulative flux for frequency from 0 to 0.0033 Hz, should be smaller than 30% of the total flux (30 minute averaging period), i.e. only 30% of the flux is due to events at frequencies lower than this.

Both tests excluded about 50% of the data (Table 5.2), but the test derived from Foken's principle filtered out more of the largely negative N_2O flux, which did not seem reliable. Mainly due to non-stationarity in the N_2O concentration measurements, these negative fluxes with magnitude varying between -700 to -200 ng N_2O-N m^{-2} m^{-1} were not related to any evident change in meteorological parameters, but were more likely caused by sudden changes in pressure in the TDL cell, in the range of the signal or other not well identified reasons. A filter on the raw data could be more suitable than a post processing filter to eliminate these events, but because an explanation of the causes for the events was not always identified an appropriate method was difficult to find. As a consequence, the post processing stationarity filter was used for this purpose. Table 5.2 shows the effect of the application of the two stationarity filters on the N_2O flux measurements at Easter Bush, already filtered for wind sector, wind speed and ITC. Both stationarity tests filtered more than 50% of the fluxes but the second filter was chosen for this analysis as it was the most restrictive.

The effect of the application of stationarity criterion on the frequency distribution of fluxes is shown in Figure 5.2, which shows a normal distribution, slightly skewed to the right. The Kolmogorov-Smirnov (K-S) test was used to confirm the normality of the distribution. A small increase in positive flux (emission)

is evident after the rejection of negative fluxes for the application of the filter of stationarity, although the shape of the distribution did not change significantly.

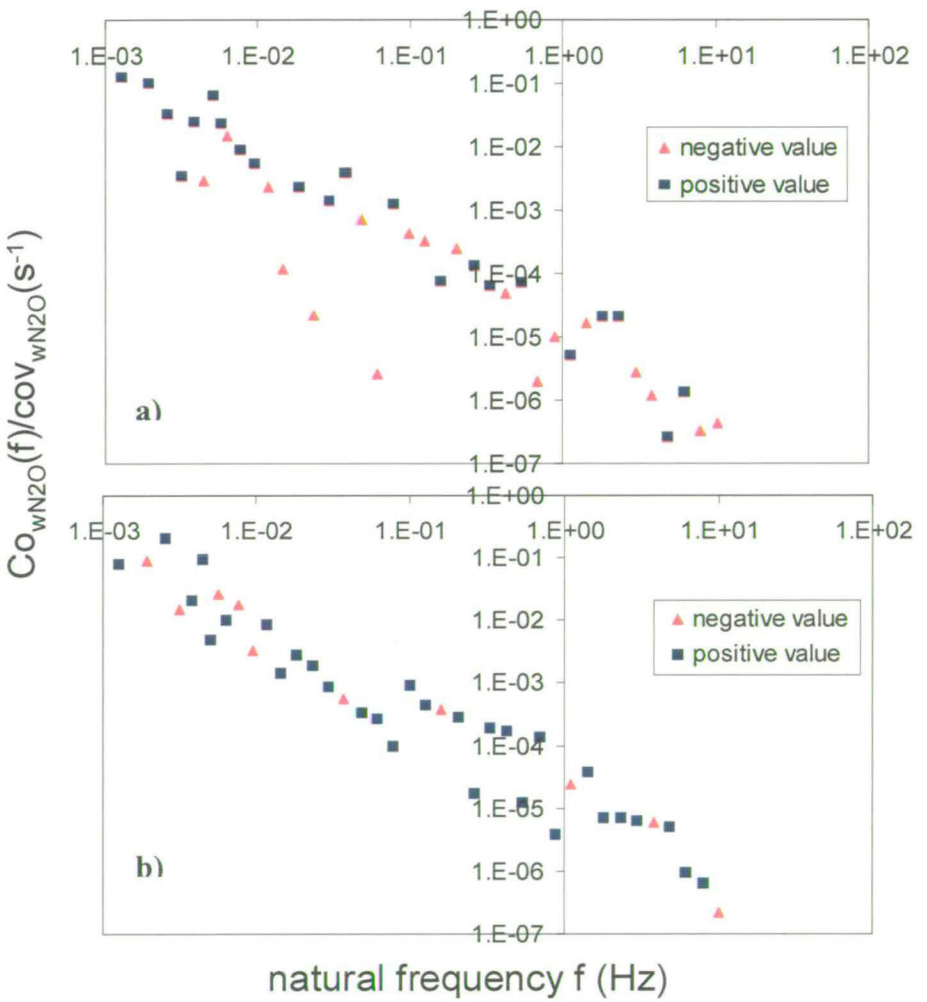

Figure 5.1 Stationary test I: example of cospectra in a stationary (a) and non-stationary case (b). Red dots represent the negative values turned into positive in order to use the logarithmic scale in the chart.

Table 5.2 Effect of the application of the stationarity criteria to the N_2O flux measurements.

	After filtering for wind sector, wind speed, ITC and TDL malfunctioning (see Table 4.1)	After applying stationarity filter I (using cospectrum)	After applying stationarity filter II (derived from Foken's principle)
N of 30 min fluxes	6641	3451	3277
Retained data	-	52%	49%
Tot flux average of remaining data (ng N_2O-N m^{-2} s^{-1})	20	32	40
Tot flux median of remaining data (ng N_2O-N m^{-2} s^{-1})	10	19	14
Tot positive fluxes	54%	58%	57%
Tot negative fluxes	46%	42%	43%

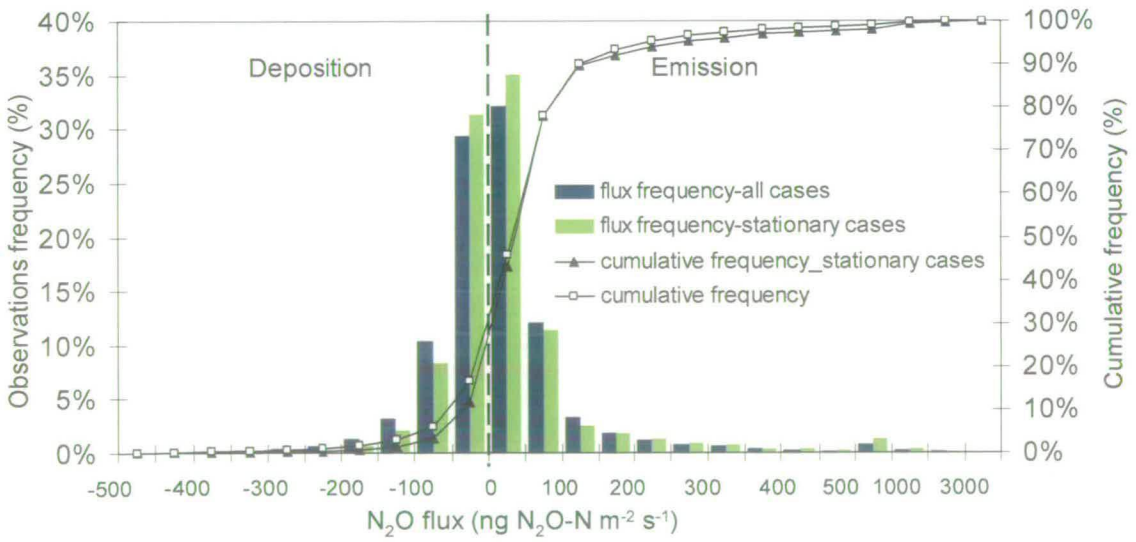

Figure 5.2 Frequency distribution and cumulative frequency of 30 min fluxes measured from 07/06/02 to 21/06/03 for all cases (blue bars and white symbols) and those fulfilling the stationary criterion (green bars and black symbols).

5.2.2 Storage and advection

The contribution of storage to the measured flux was estimated using the method described in Section 3.9.2.1. After calculating the error with the Equation (3.34), the storage correction was added to the measured flux. The modulus average correction was of ± 3 ng N_2O-N m^{-2} s^{-1} that corresponds to a modification of the measured flux of 15%. An example of the correction effect on 3 days of measurements (from 11/06 to 14/06/02) is shown in Figure 5.3. Although the average did not vary a lot with the wind direction, a slightly larger average (20%) was noted for wind directions from the north than for other wind directions.

Advection errors, mainly due to horizontal gradients, can only be estimated from multi-point measurements, which were not available for this study. Therefore, error from advection was not calculated and only storage error was considered.

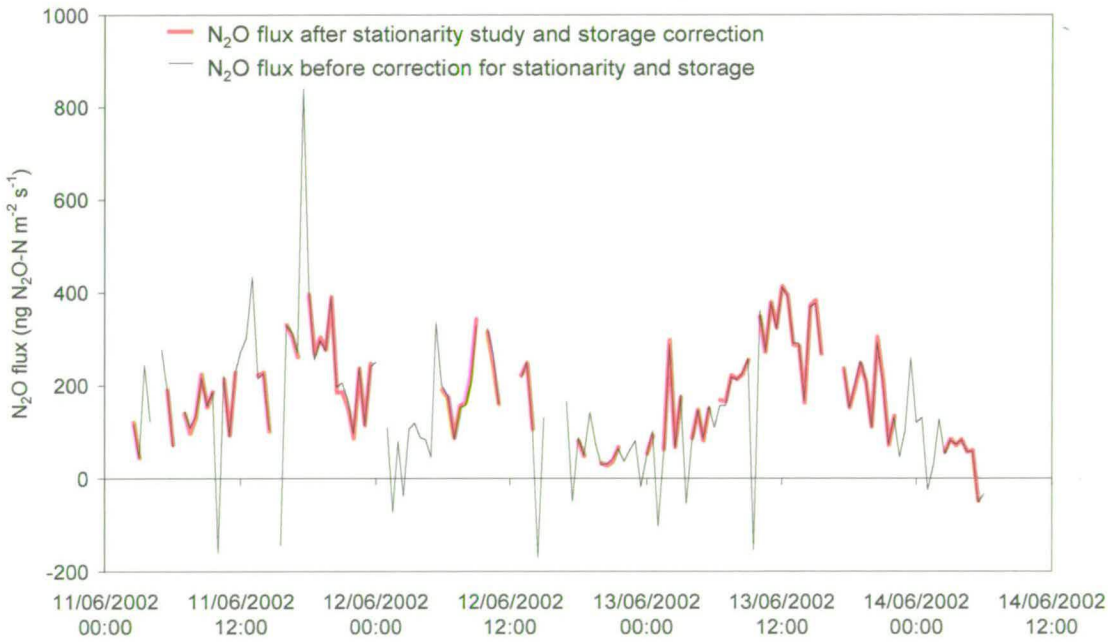

Figure 5.3 Comparison of stationary N_2O flux corrected for storage and uncorrected and unfiltered flux for 3 days from 11/06/02 to 14/06/02.

5.2.3 Spectral corrections

Spectral analysis was performed as a powerful tool for the quality check of the eddy covariance system. The ideal turbulent signal has a well defined spectrum shape (see Section 3.3), which can be approximate with each limited time series. The spectral analysis was performed with a standard FFT routine (Stull 1988) using a LabVIEW (National Instruments Corporation) program (Section **3.10**).

Examples of power spectra for vertical wind speed, temperature and nitrous oxide mixing ratio, obtained averaging 30 min measurements between 12h and 13h GMT on 08/06/02, are shown in Figure 5.4.

The natural frequency f multiplied with the power spectrum $S_x(f)$ itself is plotted against natural frequency and both axes are logarithmic. In this representation the power spectrum should ideally decrease linearly with a $f^{-2/3}$ slope in the inertial sub-range according to Kolmogorov's law (Kaimal et al. 1972). Spectral similarity exists between the spectrum of temperature and the spectrum of a scalar quantity such as nitrous oxide. This similarity means that the spectral and cospectral curves of different variables are similar in the ideal case.

In Figure 5.4 both the temperature (S_t) and wind speed (S_w) spectra follow the theoretical $f^{-2/3}$ slope for inertial sub-range, although at frequencies higher than 3 Hz the spectrum of temperature fluctuations decreases faster than the ideal slope. Also a presence of white noise is noticed at frequencies close to 10 Hz in the temperature spectrum. This can be seen as the small rise in the spectrum, approaching an f^{+1} slope in Figure 5.4 and it is due to sporadic spikes in the signal from frequency interference, which is difficult to eliminate (Kaimal and Finnigan 1994). However, this noise should not be correlated with w and thus does not contribute to the measured flux (Lenschow and Kristensen 1985). The nitrous oxide spectrum (S_{N2O}) starts to follow the $f^{-2/3}$ slope at 0.1 Hz and then shows a damping loss for frequencies bigger than 1Hz.

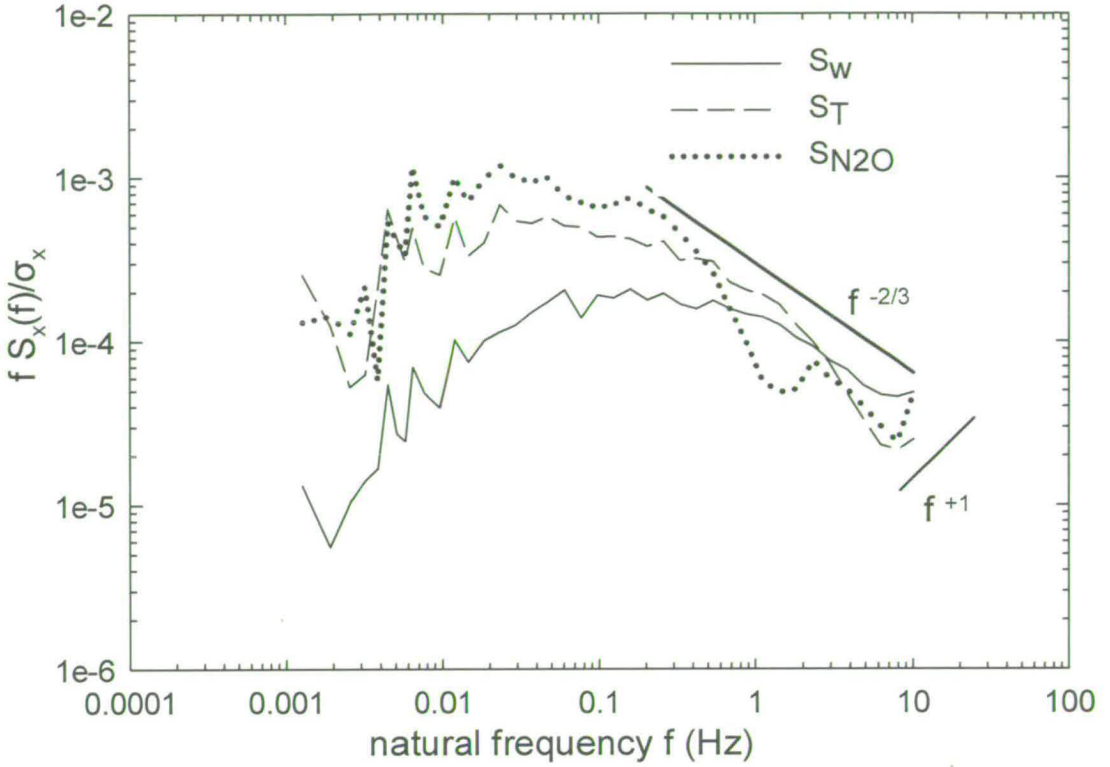

Figure 5.4 Power spectra produced from 30 min data averaged over 1 hour (from 12h to 13h) on 08/06/2002. The theoretical slopes of inertial subrange $f^{-2/3}$ is given, as well as the f^{+1} slope indicating the high-frequency noise of the sonic anemometer temperature spectrum.

Figure 5.5 shows the cospectral density for N_2O flux (Co_{N2O}) and sensible heat flux (Co_{wT}) measurements for the same period as in Figure 5.4. The horizontal wind speed was 2.8 m s^{-1}. Up to frequencies of 0.3 Hz the Co_{wT} and Co_{N2O} show a very similar behaviour, but for higher frequencies the sensible heat flux cospectrum follows well the theoretical $f^{-4/3}$ slope (Kaimal et al. 1972), whereas the N_2O flux spectrum shows a clear degradation, as it was expected from the spectrum pattern in Figure 5.4. Since in this representation the area under the cospectral curve is equal to the covariance (Stull 1988), the deviation of the N_2O cospectrum from the ideal behaviour means that there is a flux loss at high frequencies. This is possibly due to a combination of factors, such as the separation of the sensors and the increase of the response time. During the measurements a pump failure was observed and data for this period were rejected, but other small malfunctioning of the pump could have occurred without being recorded causing a laminar flow and associated flux loss.

From Figure 5.5 it is evident that the sensible heat flux cospectrum provides a suitable reference to estimate the flux loss, using the procedure for spectral corrections explained in Section 3.9.3. However, since N_2O fluxes were most of the time very close to background values (±50 ng N_2O-N $m^{-2}s^{-1}$) and without a clear diurnal pattern, an analysis with this approach for the entire period of measurement was not possible. Analyses of the cospectral density were only made for several example days with a clear, neutral and unstable stratification ($z/L \leq 0$) and significant sensible heat flux, on 08/06, 15/06 and 16/06/02.

The calculated underestimation of N_2O flux was of 12% on 8/06/02, 23% on 15/06/02 and 14% on 16/06/02. On 11/08/02 the time lag calculated was about 70 s with a consequent laminar flow, likely caused by a small blockage in the inlet. The flux loss in this case was estimated to be 26%.

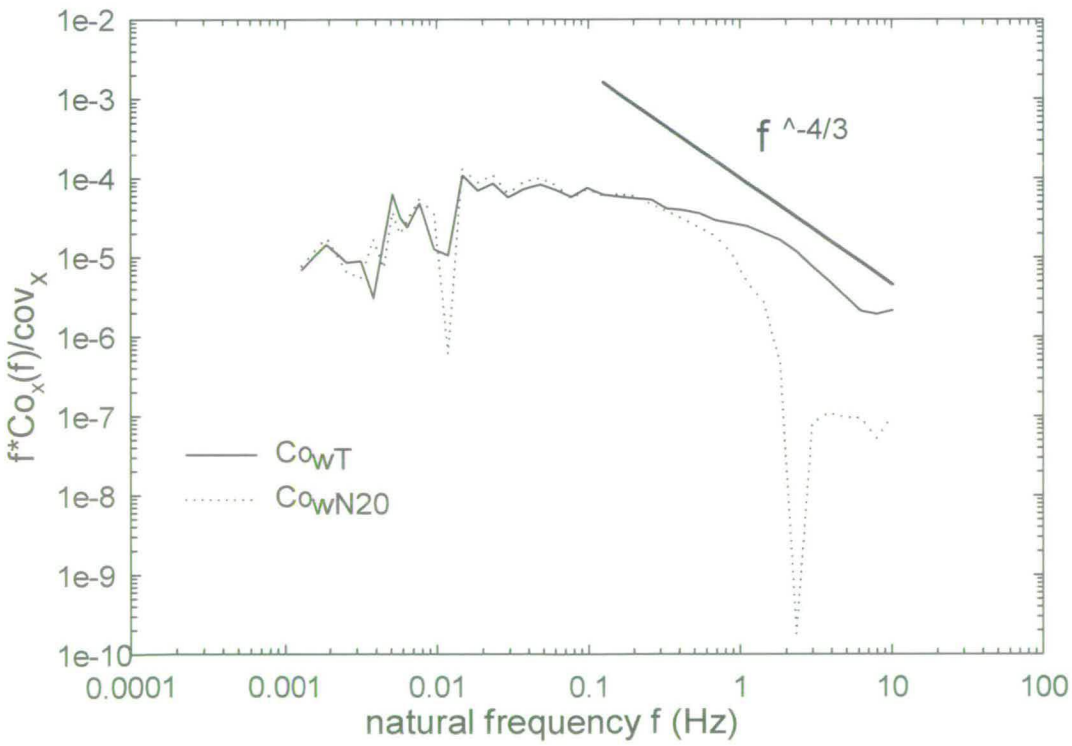

Figure 5.5 Cospectral density function of the frequency *f* for N_2O flux and sensible heat flux measurements. Result of an average over 1 hour of 30 min period measurements (from 12h to 13h) on the 08/06/2002 for data in neutral and unstable stratification conditions ($z/L \leq 0$). Negative values were inverted so that they could be plotted in a logarithmic scale. The average horizontal wind speed was 2.8 ms^{-1}

5.3 Results and discussion

5.3.1 General statistics

Over the entire period N_2O stationary fluxes ranged from -544 to 3800 ng-N_2O m^{-2} s^{-1}, with a median of 14 ng-N_2O m^{-2} s^{-1} and an average of 40 ng-N_2O m^{-2} s^{-1}, where positive values represent emission and negative values deposition. Table 5.3 and Table 5.4 show the statistics for the data before and after the application of the stationarity criterion respectively: as a result of this filter the total percentage coverage of the data over the year decreased from 38% to 19% and the average N_2O flux almost doubled from 22 to 40 ng N_2O-N $m^{-2}s^{-1}$, mainly because many negative fluxes were rejected. The monthly coverage of measurements ranged from a minimum of 11% to a maximum of 31% of the time (Table 5.4).

N_2O flux varied widely in time over the year of measurements with a series of daily peaks of emission (up to 3800 ng-N_2O m^{-2} s^{-1} during the fertilization in June 2002) and longer periods of time characterized by "background" activity. This is reflected in the frequency distribution of fluxes (Figure 5.2), which shows a normal distribution, positively skewed to the right. Figure 5.2 confirms also a small increase in positive flux (emission) after the rejection of negative fluxes for the application of the stationarity criterion, although the shape of the distribution did not change significantly. As it appears in Figure 5.2, 66% of the measured fluxes were between -50 and +50 ng N_2O-N m^{-2} s^{-1} whereas substantial emissions (> 50 ng-N_2O m^{-2} s^{-1}) were measured for 22% of the time.

Uptake (deposition) fluxes were regularly observed during the measurements and they occurred for 43% of the time and up to values of about -500 ng N_2O-N m^{-2} s^{-1}. Although some of these large negative fluxes were found to be associated with non-stationary conditions, 19% of them remained in the data set even after all the filtering processes and no evident reasons were found to omit them from the data set. Monthly average and median values were mainly positive (Table 5.4) denoting emissions from the field for most of the time, but for some months (such as January and February 2003) negative average and median values indicate that deposition occurred as well. Deposition fluxes have been reported in previous studies. Ryden

(1981) measured mean weekly sink activity up to -5.8 ng N_2O-N $m^{-2}s^{-1}$ and N_2O depositions were found in a 2-year study on emissions from grasslands by Clayton et al (1997). Small negative fluxes were also measured by Yamulki et al.(1995) (daily flux of -3 ng N_2O-N $m^{-2}s^{-1}$), Velthof et al. (1996a) (-4.4 ng N_2O-N $m^{-2}s^{-1}$) and Skiba et al. (1998) (range of -0.2-1.7 ng N_2O-N $m^{-2}s^{-1}$). Glatzel and Stahr (2001) measured the exchange of N_2O in the soil-plant system in grasslands using closed chambers and they found uptakes of -11 ng N_2O-N $m^{-2}s^{-1}$, which compare well with the values presented in Table 5.4. In many previous studies with chambers N_2O uptake from grasslands occurred only occasionally (Yamulki et al. 1995; Clayton et al. 1997) and more frequent negative fluxes were found in temperate forests (Butterbach-Bahl et al. 1998; Goossens et al. 2001), where Mediterranean forest soils appeared to be a significant sink (-0.5 kg N ha^{-1} y^{-1}) (Rosenkranz et al. 2005). Nevertheless, high frequency of negative fluxes were reported in Verchot et al. (1999) in tropical pasture ecosystems during the wet season (30-40% of measurements) and the dry season (55-65% of measurements) and Flechard et al. (2005) measured large negative fluxes (between -0.1 and -0.5 kg N_2O-N ha^{-1} y^{-1}) using static chambers over managed grassland in Switzerland. Flechard et al. (2005)observed uptake in 41% - 44% of the measured fluxes and the frequency distribution of the observations is very similar to the distribution shown in the present study in Figure 5.2 (uptake 43% of measurements). Although it has been measured in many studies, N_2O uptake has not been described very thoroughly. However, it seems an interesting factor to take into account in budget calculation and in N_2O production process studies as well.

Figure 5.6 shows the complete period of N_2O flux measurements. A clear response to fertilization was observed the day after the 7-8 June N application (daily average emission of 1800 ng N_2O-N $m^{-2}s^{-1}$) and after the 10 August N application (daily average emissions were up to 880 ng N_2O-N $m^{-2}s^{-1}$). Gaps in data were caused by unsuitable wind direction, power cuts and problems with TDL behaviour. Daily fluxes were obtained by averaging the available data.

Table 5.3 Monthly N_2O flux (non-stationary cases included) statistics (flux unit: ng-N_2O $m^{-2}s^{-1}$) for 30 min measurements at Easter Bush site.

Month	N data point	Coverage	Mean	Median	Stdev
Jun-02	704	49%	149	73	397
Jul-02	332	22%	-11	-12	148
Aug-02	495	33%	63	18	240
Sep-02	307	21%	5	13	63
Oct-02	595	40%	9	14	85
Nov-02	406	28%	9	14	54
Dec-02	321	22%	4	12	74
Jan-03	292	20%	-7	-26	57
Feb-03	688	51%	-1	2	64
Mar-03	684	46%	3	7	95
Apr-03	495	34%	4	2	84
May-03	748	50%	2	4	57
Jun-03	574	40%	-7	-3	76
Total	**6641**	**38%**	**22**	**10**	**169**

Table 5.4 Monthly N_2O flux (only stationary cases included) statistics (flux unit: ng-N_2O $m^{-2}s^{-1}$) for 30 min measurements at Easter Bush site.

Month	N data point	Coverage	Mean	Median	Stdev
Jun-02	447	31%	216	110	468
Jul-02	134	9%	-2	9	145
Aug-02	237	16%	136	29	302
Sep-02	152	11%	3	13	42
Oct-02	255	17%	5	14	58
Nov-02	224	16%	7	12	43
Dec-02	167	11%	9	19	72
Jan-03	212	14%	-12	-27	52
Feb-03	329	24%	-4	-8	44
Mar-03	295	20%	4	5	69
Apr-03	172	12%	-4	0	33
May-03	351	24%	2	2	40
Jun-03	302	21%	1	-2	54
Total	**3277**	**19%**	**40**	**14**	**213**

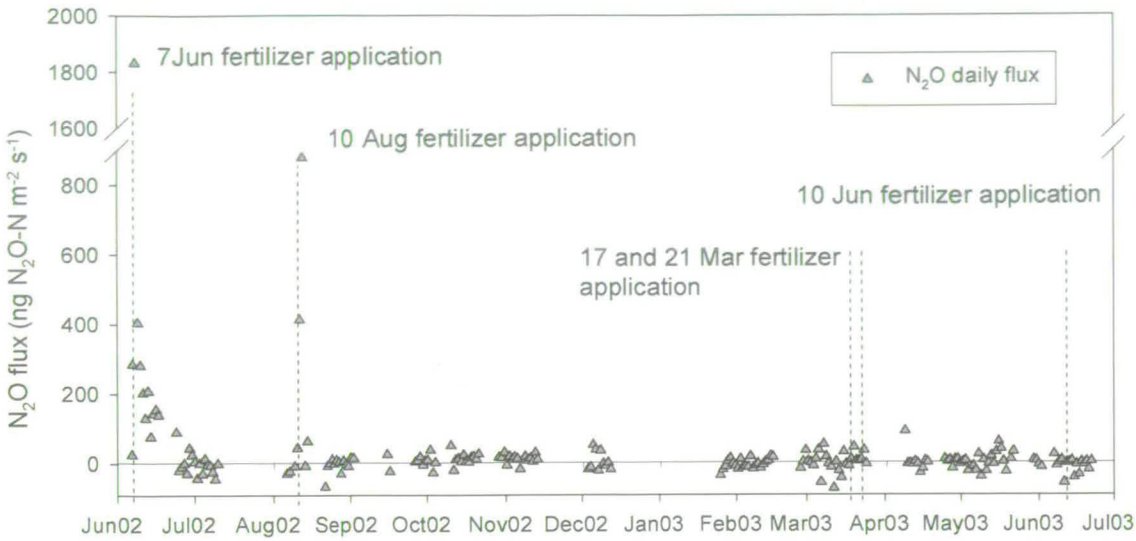

Figure 5.6 Daily average N_2O fluxes on Easter Bush field from June 2002 to June 2003.

The dependence of N_2O emissions on the wind direction was investigated in order to detect spatial influencing factors, such as farms in the surrounding area or anomalies in the topography. Results are shown in Figure 5.7. The large fluxes measured just after the fertilization events occurred during NE wind direction resulting in large average emissions in sector 0°-60° (Figure 5.7-a). To help the interpretation of Figure 5.7-a the frequency of the observation per wind sector is also shown again in Figure 5.7-b. The largest emissions did not occur along the most frequent wind direction, but along directions with 5-8% of frequency. The same analysis was done excluding fluxes from periods after fertilisation events to avoid the bias due to large N_2O emissions and it is shown in Figure 5.8. The median obtained presents a spatial pattern similar to the median shown in Figure 5.7-a, suggesting that N_2O fluxes with air coming from the N sector were higher than for other directions. This phenomenon could be due to a bigger N_2O production and emission occurring in the N sector compared to the rest of the field, but horizontal advections coming from adjacent fields cannot be excluded. Although the effect of these advection events on the measured flux cannot be estimated with only one tower measurement, as already mentioned in section 5.2.2, the absence of big changes in the horizontal

wind speed and the coincidence of large peaks with the fertiliser application on Easter Bush, suggest that these substantial fluxes are not due to advection, but they are real emissions from the field.

No relationship between negative fluxes and wind sector was found, excluding the hypothesis of artefacts or obstacles that could provide systematic negative fluxes. However, fluxes with air coming from the W sector were smaller than for the other directions (Figure 5.8).

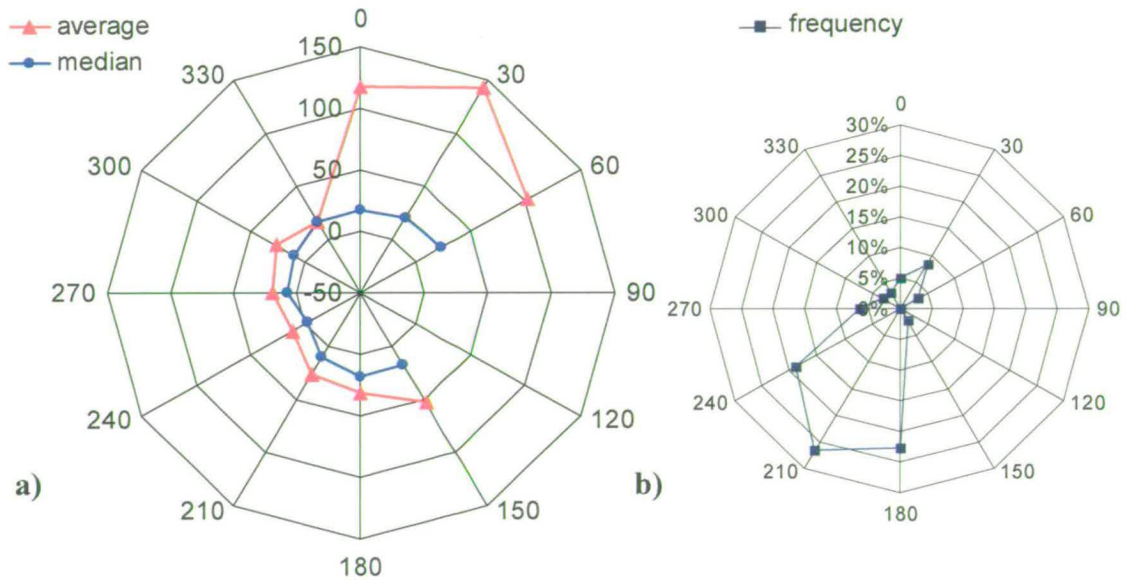

Figure 5.7 Wind sector dependence of N_2O emissions. a) Average and median values for N_2O flux calculated for each 30° wind sector. On the radial axis is the flux measured in ng N_2O-N m^{-2} s^{-1}. b) frequency of the measured flux per wind sector.

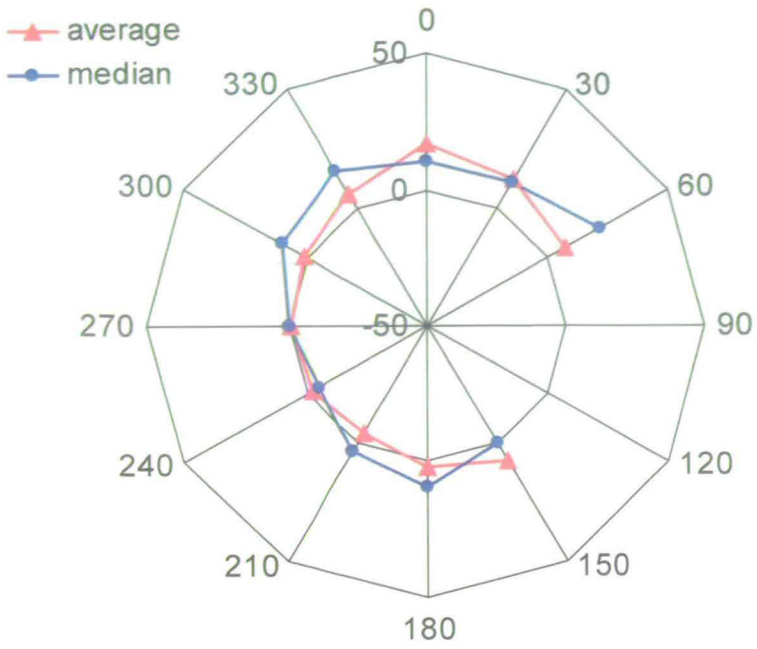

Figure 5.8 Wind sector dependence of N_2O emissions. Average and median values for N_2O flux calculated for each 30° wind sector excluding periods after fertilisation. On the radial axis is the flux measured in ng N_2O-N m^{-2} s^{-1}.

5.3.2 Seasonal variability of N_2O fluxes

A description of the main events that occurred during the measurement period is reported in this section. The largest N_2O emissions on Easter Bush field occurred during sporadic peaks, generally triggered by fertiliser application.

5.3.2.1 June 2002

The bulk of the emissions from the field over the year of measurements occurred after the application on 7 and 8 June 2002 on the N and S fields respectively of 60 kg N ha^{-1} in the form of Kemira N-P-K (24:5:10), a few days following the first cut of the season on the field on 1 June 2002.

Figure 5.9 shows the N_2O emissions from the two different fields at Easter Bush site, soil and air temperatures, wind speed and rainfall for the period after the fertilization in June 2002. The small gaps in the chart are due to rejection of data after the filtering process or to problems with the logging system, such as the case of the night between 8 and 9 June. From 17 to 24 June the instrument was used for other measurements.

A very high emission peak from the N field occurred on 8 June, with a maximum of 3800 ng N_2O-N $m^{-2}s^{-1}$ at 15:00 GMT, a few hours after the fertiliser application which happened in the afternoon of 7 June on this field. This pulse was equivalent to 1.6% of the N fertiliser applied to the north field. The increase of the flux coincides with a rise in soil and air temperature up to 17.5°C and 19.5°C respectively, which represent the maximum temperature values for the following 10 days. Although the 'pulse' on 8 June represents a clear and quick response to the fertiliser application, the increase in temperature and the significant rainfall event (about 10 mm) which occurred on 7 June could have aided the large production and emission of N_2O seen on that day. During the following days N_2O fluxes decreased significantly. Figure 5.10 shows in detail hourly and daily emissions for the period before and just after the trigger event, from 6/06/2002 to 16/06/2002. In the days following the fertilization, emissions decreased to daily averages ranging between 64 ng N_2O-N $m^{-2}s^{-1}$ and 360 ng N_2O-N m^{-2} s^{-1}. A daily pattern of the flux approaching a diurnal cycle is noticeable for most of the days from 11 to 16 June, when emissions were still consistently above background values. The diurnal variation of flux in these cases (e.g. on 15-16 June) was almost twice the variation for days characterized by background emissions, such as 6 June, the day before the fertilization, as it can be seen from the length of the error bars in Figure 5.10. The only exception is represented by the 14 June when emissions close to background occurred in correspondence with a decrease of soil temperature of about 2°C and of a precipitation event that lasted about 12 hours for a total of 18 mm of rain (Figure 5.9).

About 17 days after the fertiliser application, from 24 June until 30 June, N_2O losses decreased to a daily average ranging from -57 ng N_2O-N $m^{-2}s^{-1}$ to 37 ng N_2O-N $m^{-2}s^{-1}$(Figure 5.9).

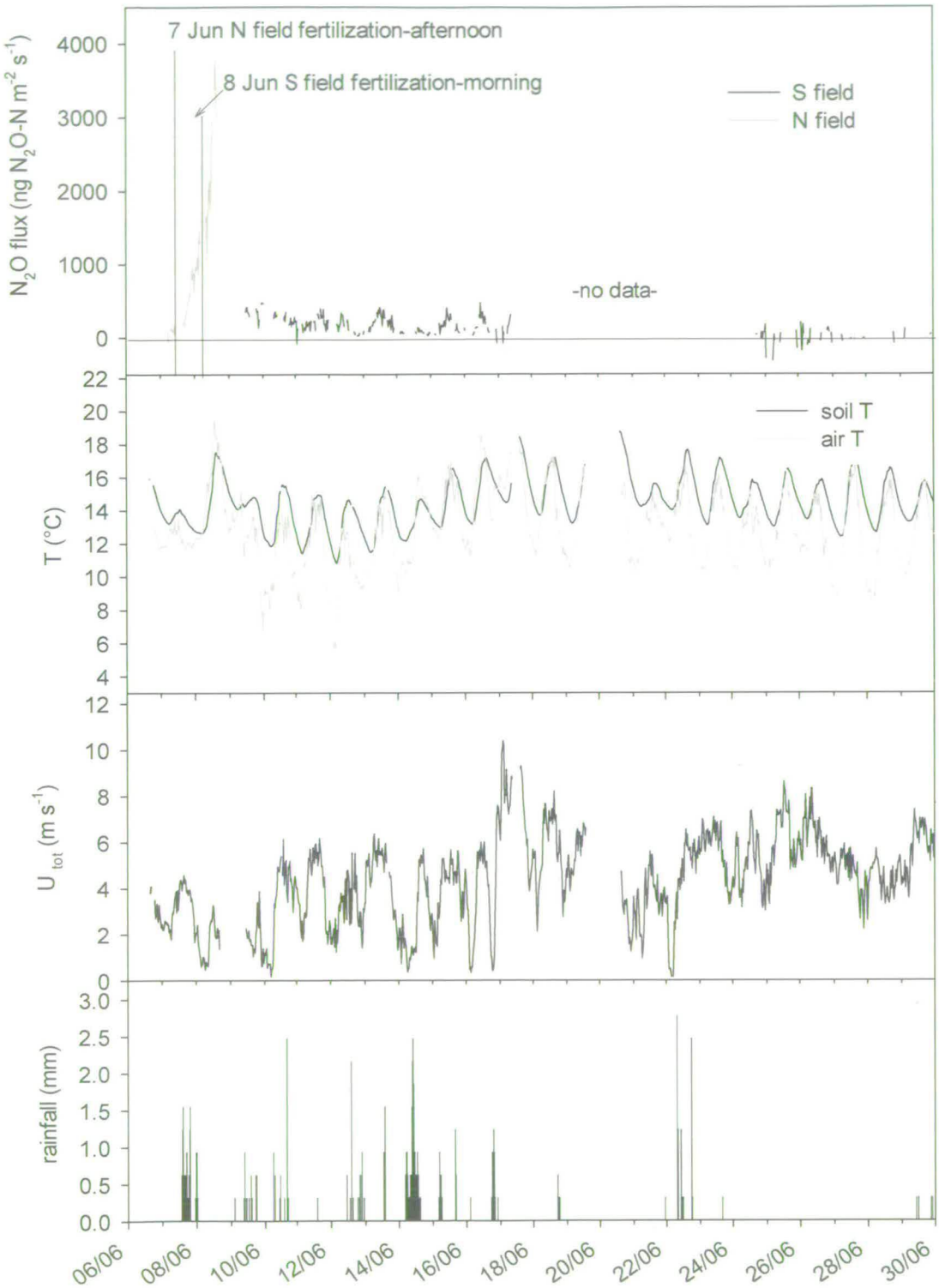

Figure 5.9 Time series (30 min average) of N_2O fluxes, soil (5 cm) and air temperature, wind speed and rainfall measured at Easter Bush site during the fertiliser application in June 2002.

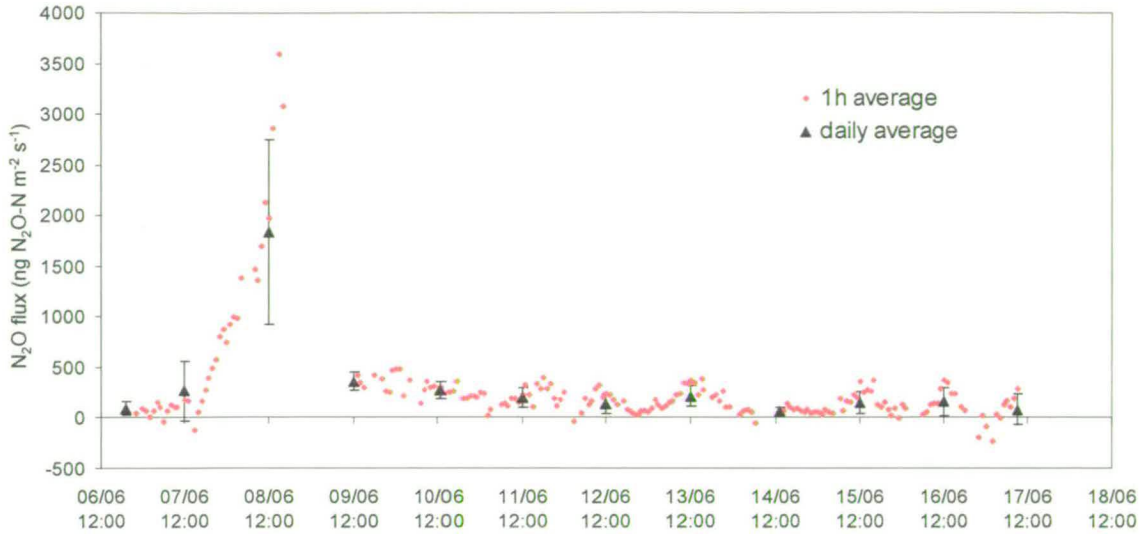

Figure 5.10 Hourly and daily N_2O fluxes at Easter Bush in June 2002. Error bars show the variation (standard deviation) in the daily average flux.

5.3.2.2 August 2002

The second fertiliser application on the south field occurred on 10 August 2002 with 50 kg N ha^{-1} in the form of Kemira N-P-K (25:5:5). The north field was not fertilized in August. Figure 5.11 shows N_2O hourly fluxes from the Easter Bush field for the period from 6/08 to 27/08/02, as well as soil and air temperature, rainfall and wind speed for the same period. The gap in the data between 6/08 and 10/08 is due to some problems with the TDL: the compartment where the diode is mounted inside the dewar is not perfectly under vacuum, and at times a thin layer of ice is created on the diode surface due to the low temperature (see Section 4.4); this layer decreases the infra-red emission efficiency of the diode with a consequent rapid decline of the signal and increase of the noise, so measurements were not taken into account. The gap of a day between 11 and 12/08 is due to problems with the logging system at Easter Bush field, whereas the data missing between 14 and 22 August are due to a break in the measurements.

In Figure 5.11 hourly N_2O fluxes with air coming from the south field (white dots) are distinguished from the fluxes with air coming from the north field (black dots). The increase of emission on 11/08 started at 16:00 on the north field then continued on the south field up to values of 1380 ng N_2O-N m^{-2} s^{-1}at 01:00 at night, coincided with a significant quantity of rainfall which started at 14:00 on 11/08. This suggests that the rainfall could have been the trigger for this fertilization induced

emission event. For the rest of the month fluxes were mostly background, as it can be seen in Figure 5.11 from 20/08 onwards. The increase of N_2O emissions measured on 11/08 at 14:00 was in coincidence with air coming from the north field, which was not fertilised in August. This could be due to the fertiliser application to the south field. In fact, during the previous night and until 13:00 on 11/08 a condition of atmospheric stability occurred with weak wind (1 m/s on average) coming from the fertilised field (south field). N_2O from the fertiliser application could have been transported towards the north field during this time. At 13:00 of 11/08 the wind changed direction blowing from the north field until midnight of the same day with an average speed of 1.6 m/s (period of time when the flux in Figure 5.11 comes from the north field).After midnight the wind changed direction back to the south field with higher wind speed (2.5 m/s on average) and more unstable conditions from the early morning of the 12/08 (flux from the south field in Figure 5.11). One explanation could be that an advection event transported N_2O from the fertilised field to the north field and that N_2O appeared to be emitted from the north field during the following hours. Unfortunately the gaps in the data for the days before the emission peak on the 11/08 prevent a more detailed analysis. This interpretation of the data is also supported by the fact that the only known event on the field that could have caused such increase in N_2O emissions was the fertilisation of the south field.

The average air temperature over this month was 15°C with a wide variation (about 10°C) between night and day. By contrast the soil temperature did not vary largely over the day (only less than 2°C) and the monthly average was 15°C. So the temperature was not a main variable influencing flux variations during August 2002.

In August the rainfall measured at Easter Bush during the period of fertilization showed days with high rates of rainfall (from 5 to 20 mm) alternated by dry days.

During the flux reanalysis for this period a large time lag window was used (0-75 s) since it was noticed that for about 5 hours (from 15:00 to 20:00 on 11/08/02) the correlation function used for the time lag calculation had its maximum value in correspondence of time lags of 72 s. As said in Section 5.2.3, this could be due to some obstruction in the inlet tube. The resulting laminar flow could have caused an underestimation of N_2O emissions from August fertilization.

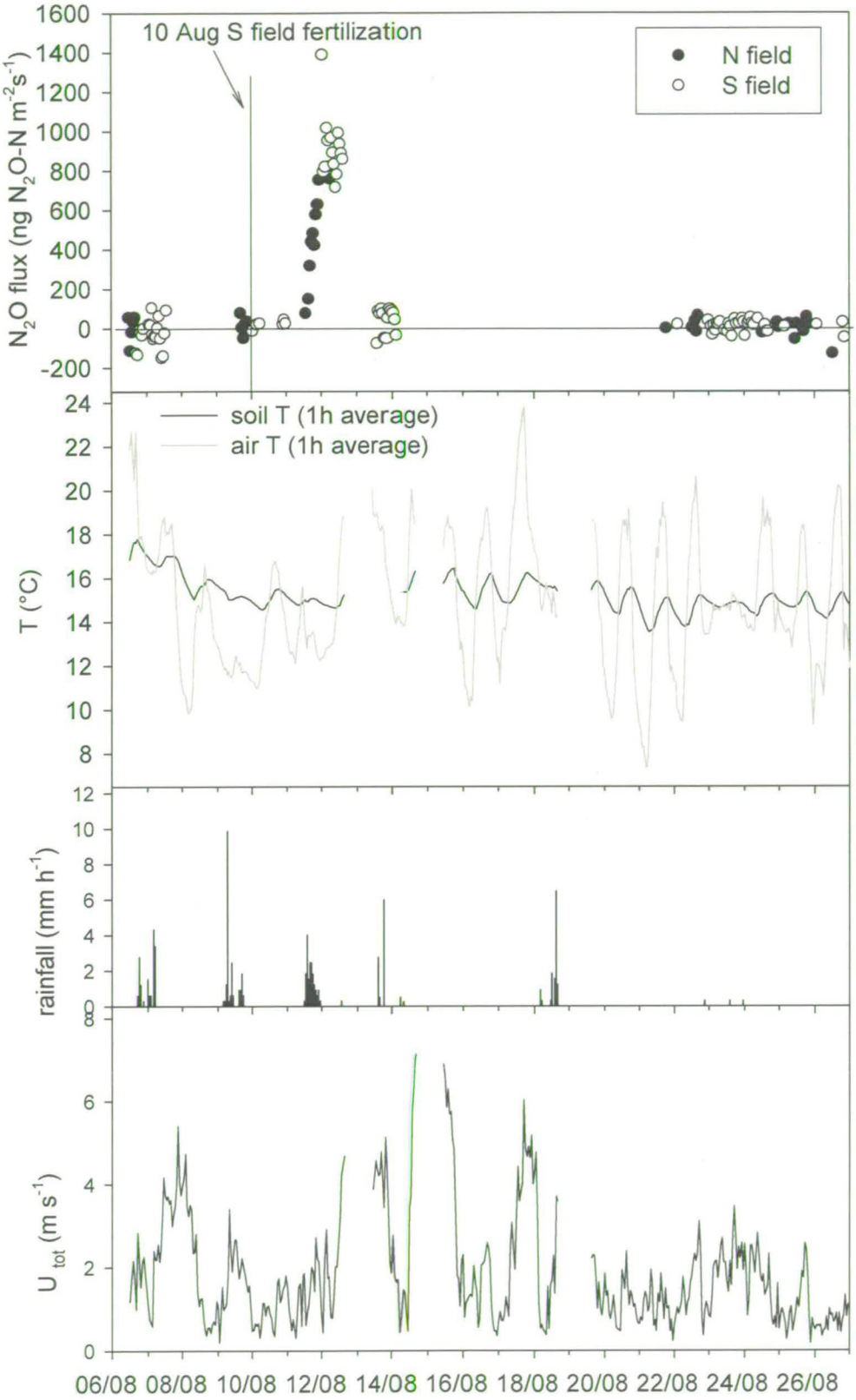

Figure 5.11 Hourly average N_2O fluxes, soil (5cm) and air temperature, rainfall and wind speed at Easter Bush field after the fertiliser application on 10 August 2002.

5.3.2.3 March 2003

In March 2003 the N field was fertilized on 17/03 with 54.71 kg N ha^{-1} in the form of Nitram (NH_4NO_3) and the S field on 20/03 with 84 kg N ha^{-1} in the form of Kemira N-P-K (24:5:10). In Figure 5.12 hourly N_2O fluxes show a clear and short-lasting reaction to the fertiliser application on the north field (black dots), but on the south field they are only of background magnitude (white dots). A maximum flux of 548 ng N_2O-N m^{-2} s^{-1} was recorded on 23/03/03 and some minor peaks occurred on 18 March (135 ng N_2O-N m^{-2} s^{-1}) and 19 March (184 ng N_2O-N m^{-2} s^{-1}). The small fluxes on 20 to 22 March occurred in correspondence with a fairly high wind speed (with a maximum of 6 m s^{-1}). The average soil temperature was about 5-6 °C, providing a pretty cool environment. The only rainfall event occurred fairly close to the fertilization was during the week preceding the fertilization on 11 March (about 8 mm), which is not included in the plot in Figure 5.12.

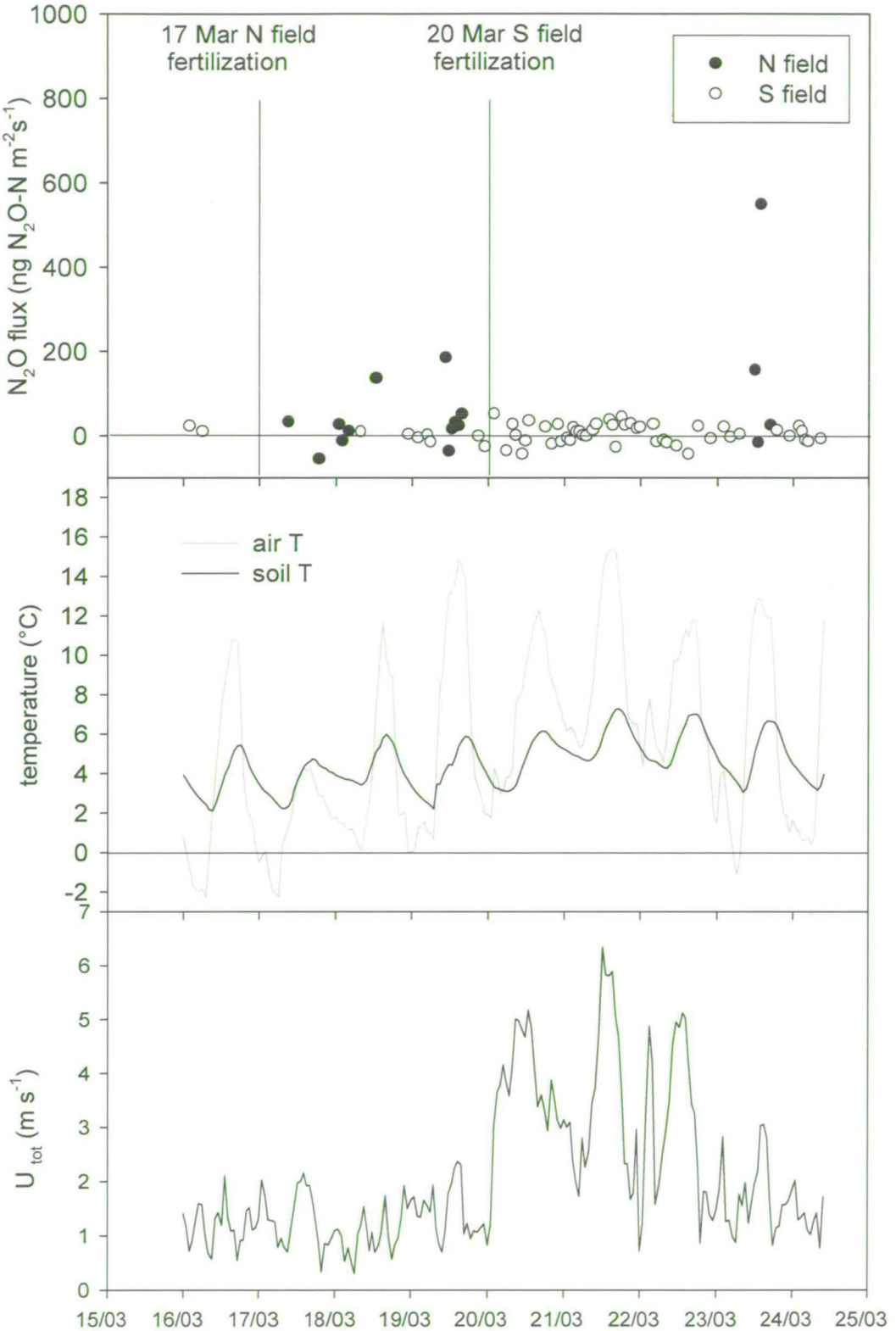

Figure 5.12 Hourly average N_2O fluxes and soil (5cm) and air temperature on Easter Bush field after the fertiliser application on 17 and 20 March 2003. No rainfall events occurred during that period.

5.3.2.4 June 2003

During summer 2003 the fertiliser application at Easter Bush site occurred only on the south field with a total of 48 kg N ha^{-1} as Kemira N-P-K (24:5:8).

The unusually dry and warm weather in June 2003 inhibited the N_2O emissions, which were very small even after the fertiliser application (Figure 5.13). The monthly average air temperature and the soil temperature (at 5 cm depth) were similar at about 15 °C and 14 °C respectively. The maximum air temperature touched 24 °C. There were 2 days with a little rain (7 mm on 8 June and 3 mm on 12 June), but the elevated temperature helped to dry the soil quickly.

N_2O emissions were very small for the entire month, apart from a slight increase in losses immediately after the fertiliser application on 10 June. Towards the end of the measurements period fluxes appeared variable with some large emission of the same magnitude as the uptake (about ±180 ng N_2O-N m^{-2} s^{-1}).

5.3.2.5 Winter time

Measurements continued over the winter, and the period from 24/01 to 17/02/2003 is shown in Figure 5.14. After about 5 months from the last fertiliser application, N_2O losses were almost zero or of 'background activity' magnitude. In 80% of the cases shown in Figure 5.14 fluxes ranged between -50 to 50 ng N_2O-N m^{-2} s^{-1}. Some cases of large uptake were recorded on 6, 7 and 8 February 2003, as well as the presence of a large positive N_2O flux possibly associated with the increase in air and soil temperature on 7/02/02.

The soil average temperature for the period shown in the figure was 3°C, whereas the air average value was 4°C and the total rainfall was 14 mm.

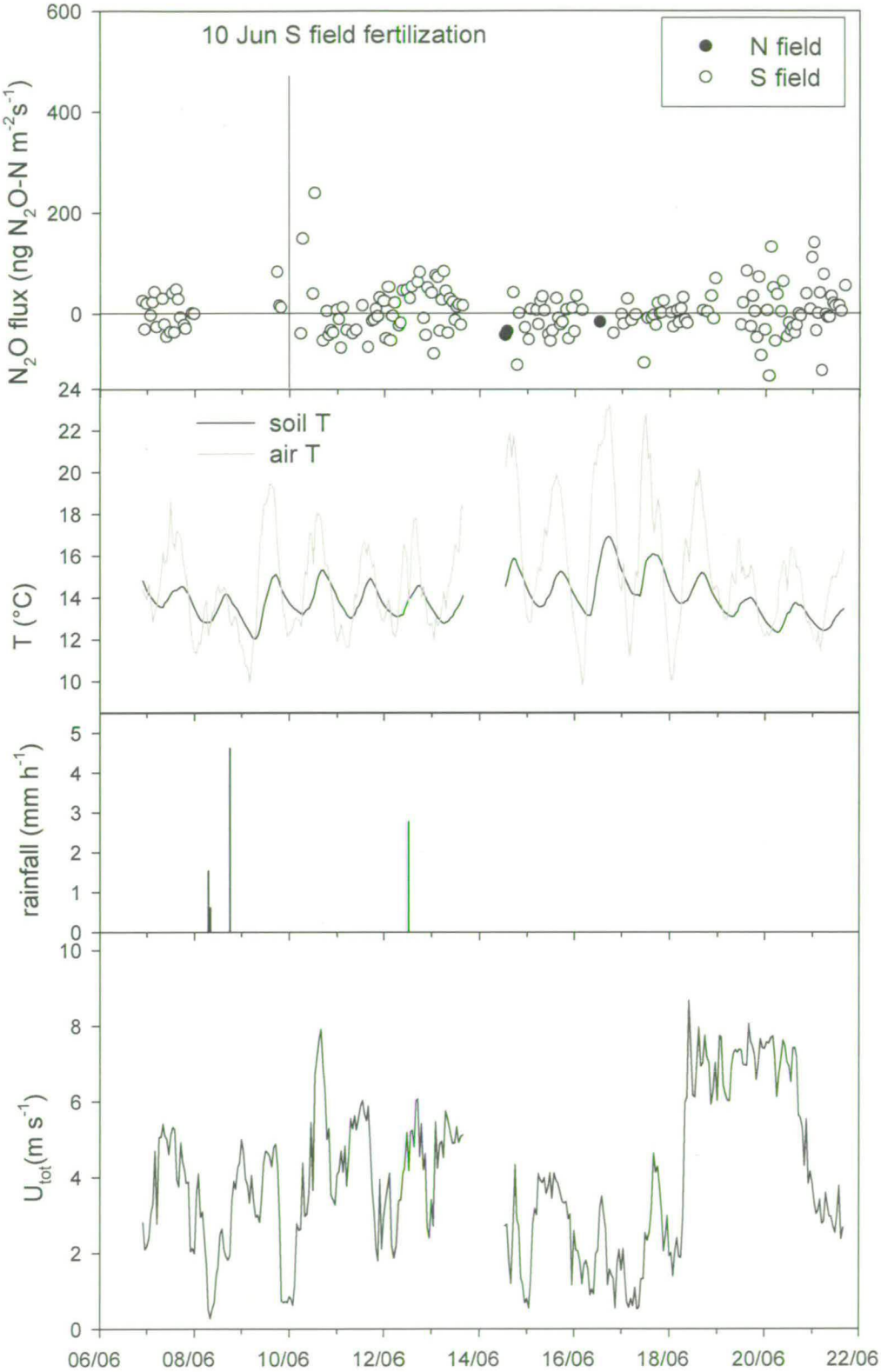

Figure 5.13 Hourly average N_2O fluxes, soil (5cm) and air temperature, rainfall and wind speed on Easter Bush field after the fertiliser application on 10 June 2003.

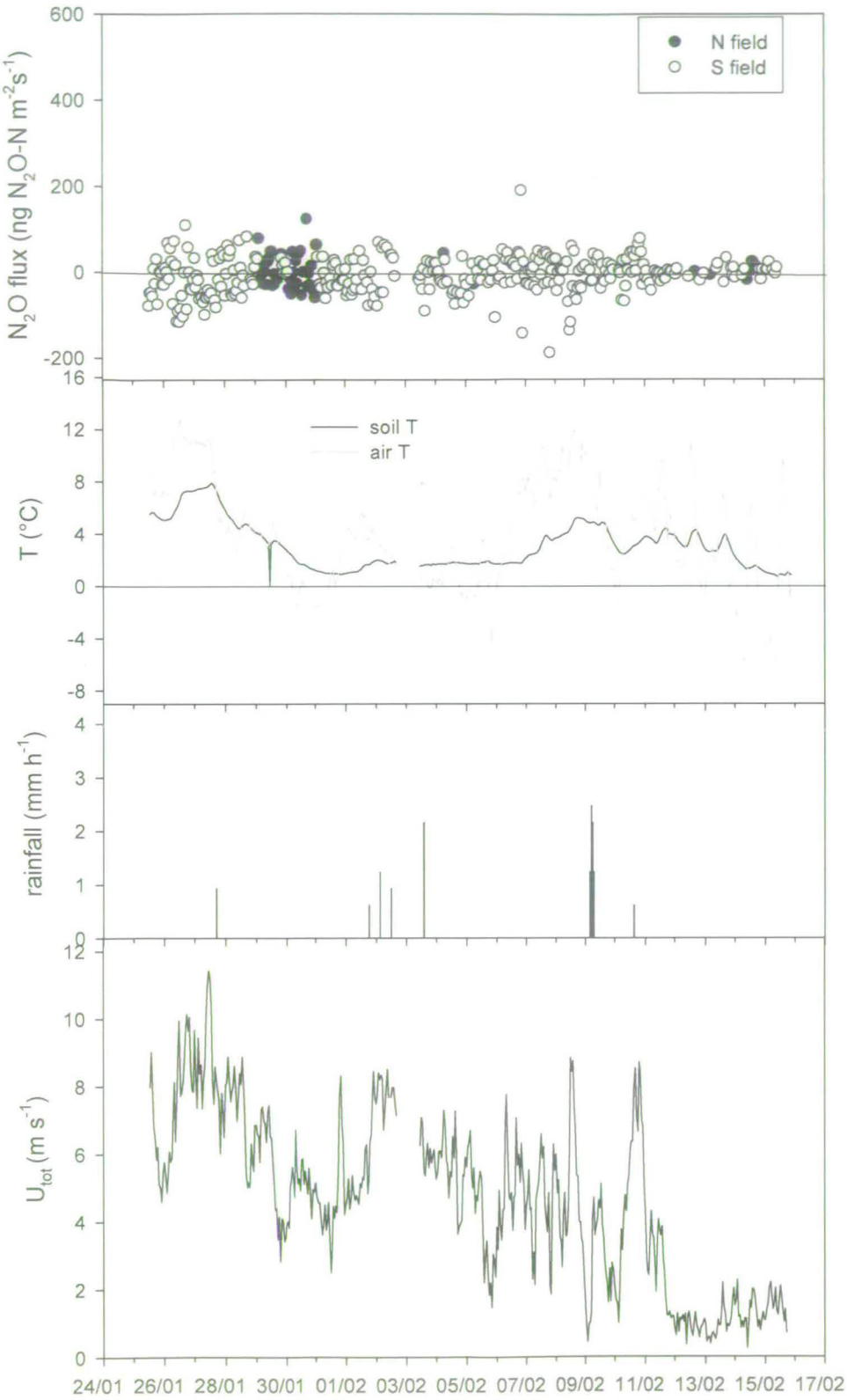

Figure 5.14 Hourly average N_2O fluxes, soil (5cm) and air temperature, rainfall and wind speed on Easter Bush field during winter time from 24/01/03 to 17/02/03.

5.3.3 Influence of control factors on seasonal variability of N_2O fluxes

It is evident that N_2O emissions from managed grassland vary largely over the year (Velthof et al. 1996a), depending on management and environmental conditions, which contribute to induce or inhibit emissions. Rudaz et al. (1999) presented seasonal fractional losses of the amount of N applied on permanent pasture ranging between 0.04% and 11.1%. Seasonal differences are therefore usually observed and can be related to concurrent variations in parameters, such as rainfall, soil moisture, soil temperature (Dobbie et al. 1999), and to differences in management (Dobbie and Smith 2003). Table 5.5 shows a summary of the soil and meteorological conditions for the events studied above, describing the principal parameters expected to be influencing N_2O emissions. The soil water content values, at times referred to as soil moisture, used in the regression were obtained from continuous measurements made at Easter Bush using a TDR probe (see Chapter 4 and Coyle (2005)) at several depths (3.5, 7.5, 15, 30 cm). Instead the data used for the comparison of soil moisture between the two fields were obtained from analysis on extracted soil cores. The soil temperature values at 5 cm depth were collected with temperature probes as described in Chapter 4. The four fertilization events presented very different environmental conditions, which were reflected in the magnitude of the N_2O fluxes measured.

Table 5.5 Summary of environmental conditions and N_2O emissions for the cases analysed in the previous section: four fertilisation events (June 2002, August 2002, March 2003 and June 2003) and winter 2003.

	Rate of N addition (kg ha^{-1})	Total rainfall[a] (mm)	Tsoil[b] (°C)	WC[c] (m^3 m^{-3})	Soil- N[d] (mg N kg^{-1} soil)	N_2O flux range[e] (ng N_2O-N m^{-2} s^{-1})	Median N_2O daily flux (ng N_2O-N m^{-2} s^{-1})
Jun 02	120	77	11-19 (15)	nd	nd	65 - 1832	195.0
Aug 02	50	110.7	13-18 (15)	0.42	3.4	36 - 887	229.6
Mar 03	136	8	2-9 (5)	0.43	2.3	-5 - 68	6.5
Jun 03	48	10	12-17 (14)	0.34	3.3	-10 - 12	2.5
winter 03	-	14	1-8 (3)	0.44	2	-27 - 19	-5.5

a) Total rainfall during 7 days before and 8 days after fertilization

b) Temperature measured at depth of 5 cm. The value in brackets is the average temperature

c) Water content at depth of 7.5 cm

d) N available in the soil as NH_4^+ and NO_3^- as average value for 0-10 cm and 10-20 cm depth soil cores.

e) N_2O daily flux range after fertiliser application

nd = not determined

The quick and big response to fertiliser application observed on the 8 June 2002 (up to 3500 ng N_2O-N m^{-2} s^{-1} after fertiliser application) occurred in ideal conditions of relatively warm (soil average temperature 15°C) and wet soil, as 26 mm and 51 mm of rain fell during the week before the fertilization and 8 days afterwards respectively. Aided by regular rainfall events, soil temperature and soil wetness were pretty constant in the days following the fertiliser application until the break in the measurements on 17 June. These invariable environmental conditions contributed very likely to the phenomenon of regular diurnal cycle pattern of N_2O fluxes measured in the period from 10 to 17 June. By contrast, in August 2002 the rainfall measured at Easter Bush during the period of fertilization showed days with high rates of rainfall (from 5 to 20 mm) alternated by dry days and the measured response of N_2O emissions after the fertiliser application was less pronounced than in June. Nevertheless, on 12 August a maximum flux of 1800 ng N_2O-N m^{-2} s^{-1} was measured. The gaps in the N_2O flux time series just after 12 August prevented any accurate determination of the duration of the effect of the N input on the emissions for these days.

Due to a gap in the data of soil water content during the event in August 2002 an estimate was obtained as average of the neighbouring values giving a value of 0.42

m^3 m^{-3} at 7.5 cm depth (corresponding to 78% of WFPS) (Table 5.5). In June 2002 the measurements for soil moisture were not yet implemented but an approximation was obtained from the behaviour of the fractional water content measurements for August, when the soil temperature at 5 cm and the rainfall were very similar to those in June. In Figure 5.15 the soil fractional water content at several depths (3.5 cm, 7.5 cm, 15 cm, and 30 cm) and rainfall are pictured for August 2002. Considering that during the fertilization time in June the rainfall was higher than in August and that the soil response to the rainfall input was generally quick and clear (Figure 5.15), it is reasonable to assume that the fractional water content for June was > 0.4 m^3 m^{-3} (>WFPS > 75%). Nevertheless, the June data were not included in the regressions shown in Table 5.6.

March 2003 was a very dry month with only 8 mm of rainfall at the time of the fortnight of the fertiliser application, and soil average temperature of about 5°C with a maximum of 9°C. Although soil moisture was >0.4 m^3 m^{-3} N_2O losses were small after the fertilization and daily average fluxes for the whole month ranged between -5 and 68 ng N_2O-N m^{-2} s^{-1}, in spite of the high N input (136 kg N ha^{-1}). The reason for this lack of response may be due to the low temperature.

June 2003 was dry (only 10 mm during fertilization period) and warm (soil temperature of 14°C) and the water content in the soil was the lowest of all the cases studied (0.34 m^3 m^{-3}) (Table 5.5). It is likely that the absence of water in the soil inhibited denitrification and N_2O emissions, as it is described in Davidson (1991) and in many other studies (Granli and Bockman 1994). N_2O fluxes for this month were even smaller than in March. A reason for it could be that the warm temperature caused the moisture in the top few mm of the soil to dry out very quickly, preventing the formation of anaerobic conditions required for N_2O production.

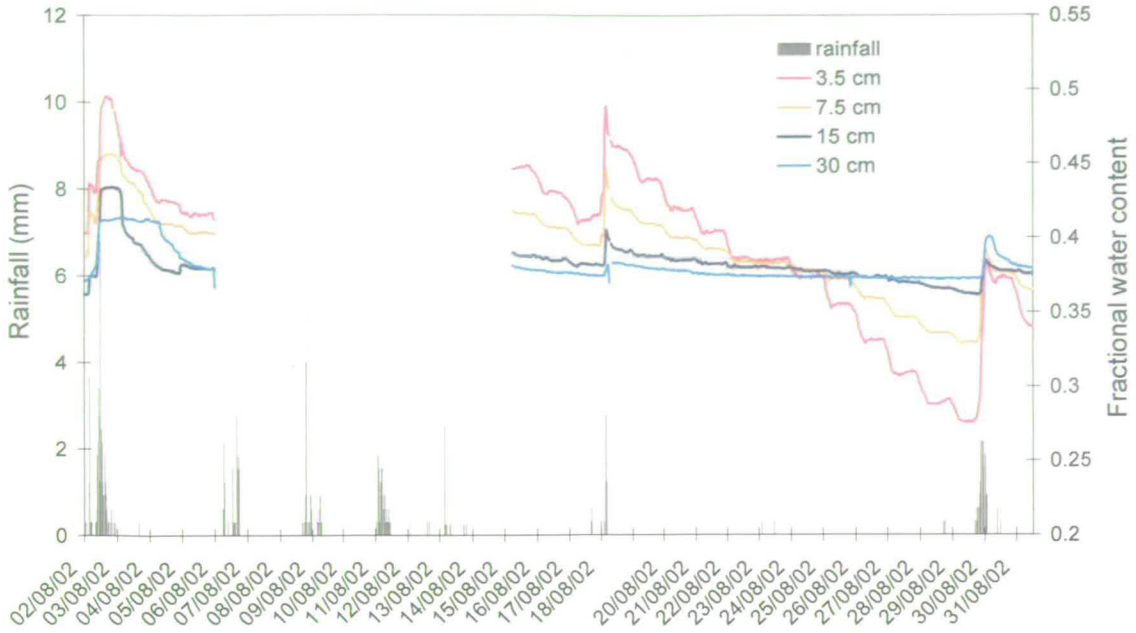

Figure 5.15 Rainfall and fractional water content at different depths at Easter Bush field.

In winter the water content in the soil was quite high (WFPS > 75%), despite the rainfall (14 mm), but the soil temperature (average of 3°C) was a limiting factor for N_2O emissions. Up to now the only microbial process know to consume N_2O is denitrification, which mainly occurs under prevailing anoxic conditions (Davidson 1991; Granli and Bockman 1994). For that reason, an increase of N_2O consumption could have occurred in winter due to an increase in soil moisture, since a raise in water content should increase anaerobiosis in soils.

An important variable related to the production of N_2O is the concentration of soil-available NH_4^+ and NO_3^-, which is often found to be one of the drivers of N_2O fluxes (Skiba et al. 1992). At Easter Bush it was measured monthly, at times before and at other times after the fertilisation events, and Table 5.5 shows that in the summer the available nitrogen concentrations were higher than in March and winter. This could also be the reason for the small fluxes observed in winter. Studies showed that N_2O consumption occurs in well aerated soil with low N availability (about 2 mg N kg^{-1} soil that compares well with the winter value for Easter Bush), mainly attributed to denitrification of heterotrophic nitrifiers (Wrage et al. 2001; Rosenkranz et al. 2005).

Analysing the relationships between N_2O median fluxes over the fertilisation periods and the soil properties for the Easter Bush site, a reasonable correlation was found with the soil moisture ($R^2 = 0.64$, $N = 4$, $p > 0.05$ based on the logarithm of the N_2O flux median) and smaller correlation coefficients with the concentration of soil-available NH_4^+ and NO_3^- ($R^2 = 0.39$, $N = 4$, $p > 0.05$) and soil temperature ($R^2 = 0.51$, $N = 5$, $p > 0.05$). In order to investigate more thoroughly the influence of these variables on the N_2O fluxes, combinations of available soil-N, water content and temperature were adopted using multiple regressions of the type:

$$Y = \beta_0 + \beta_1 X_1 + \beta_2 X_2 + \varepsilon$$

where Y is the response (median N_2O flux), X_1 and X_2 are the predictor variables, such as water content (WC), soil N and soil T, β_0, β_1 and β_2 are the regression coefficients and ε is an error term. The regressions results (Table 5.6) approximate the measured N_2O fluxes well, confirming the importance of the concurrent influence of the soil parameters. The best agreements were found using either the soil-available N or the soil temperature at 5 cm together with the soil water content at 7 cm ($R^2 = 0.99$), but very good results were also found with soil water content at 3.5 cm ($R^2 = 0.98$ and $R^2 = 0.97$) (Table 5.6). The lack of soil temperature data at depths larger than 5 cm made it impossible to perform a regression containing soil T and water content at 15 and 30 cm.

To increase the points in the regressions and after the considerations made about the soil moisture in June 2002, further calculations were made setting the water content for June as the lowest and highest value in Table 5.6 (0.34 and 0.44 respectively). The R^2 of the resulting regressions varied between 0.73 and 0.97 with p value ranging between 0.27 and 0.027 which still confirms some significant correlations. The resulting N_2O fluxes modelled with the two regressions and the measured fluxes are plotted in Figure 5.16.

The small values of p and big values of R^2 suggest that N_2O emissions are more strongly related to the N_2O production in the top layer of the soil.

Table 5.6 Multi-linear regression equations to predict N_2O flux (ng N_2O-N $m^{-2}s^{-1}$) using the water content at X depth (WC_X) (m^3 m^{-3}), the soil-available N and the soil temperature at 5 cm (T)(°C). R^2 indicates how much variation in the response (N_2O flux) is explained by the model. The p-value represents the probability of rejecting the hypothesis of null regression coefficients when it is actually true. A commonly used cut-off value for p is 0.05. In the data presented here (N = 4) the only case where the null hypothesis can be rejected is b), which represents therefore the most reliable regression.

	REGRESSION EQUATION	R^2	p
a)	N_2O flux = - 1565 + 2561 * $WC_{7.5\,cm}$ + 211 * N soil-available	0.99	0.093
b)	N_2O flux = - 1199 + 2536 * $WC_{7.5\,cm}$ + 24.2 * T	0.99	0.040
c)	N_2O flux = - 1152 + 1832 * $WC_{3.5\,cm}$ + 169 *N soil-available	0.98	0.129
d)	N_2O flux = - 843 + 1779 * $WC_{3.5\,cm}$ + 19.1 * T	0.97	0.168
e)	N_2O flux = - 3061 + 6076 * WC_{15cm} + 267 N soil-available	0.93	0.255
f)	N_2O flux = - 6174 + 14377 *$WC_{30\,cm}$ + 227 N soil-available	0.85	0.386

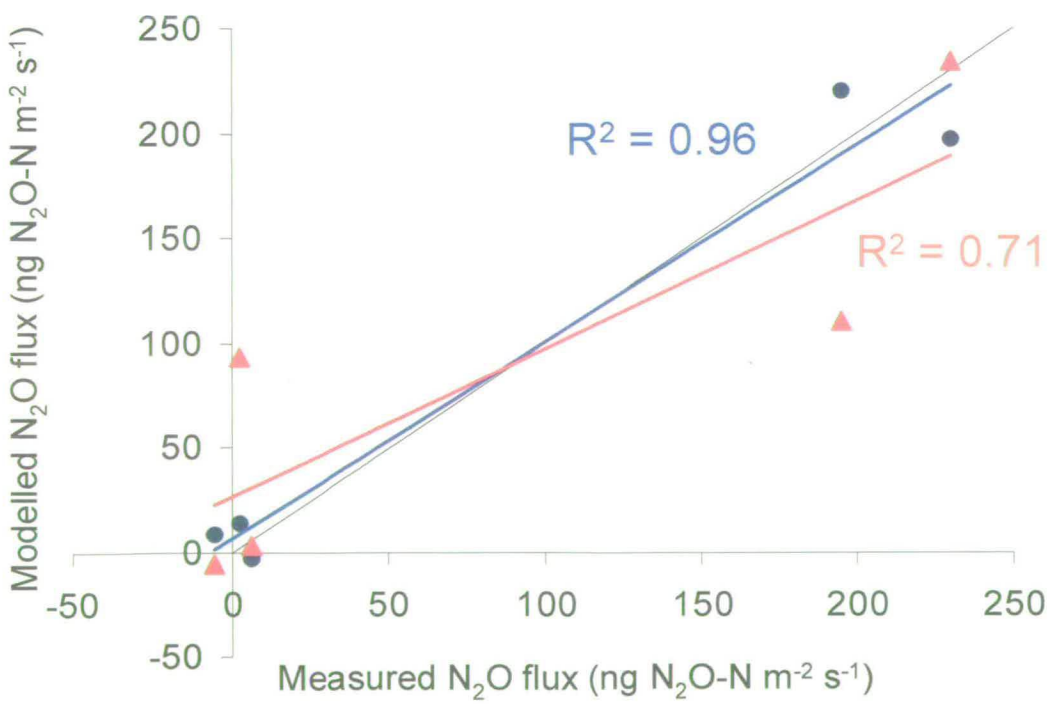

Figure 5.16 Comparison of the measured N_2O fluxes (as they appear in Table 5.5) and the fluxes obtained from two multilinear regressions containing soil water content value for June set to 0.44 m^3 m^{-3} (blue line) and to 0.33 m^3 m^{-3} (red line). The two equations are: N_2O= - 838 + 1778*$WC_{7.5cm}$ + 18.4*T (N = 5, p = 0.027) and N_2O= - 641 + 1280* $WC_{7.5cm}$ + 21.9*T (N = 5, p = 0.27) respectively.

Water content values in soil samples collected monthly (9 soil cores) in each field for the period from August 2002 to August 2003 resulted slightly higher in the north field compared to the south field (Figure 5.17). The annual pattern observed in the data in Figure 5.17 reflects the same behaviour found in the data collected with the TDR presented in Table 5.5, with wetter soil in winter and drier in summer and with values for summer 2003 much lower than soil moisture for summer 2002. Results of the monthly measurements are in reasonable agreement with the continuous measurements at fixed location made with a TDR (R^2 =0.69) (Figure 5.18).

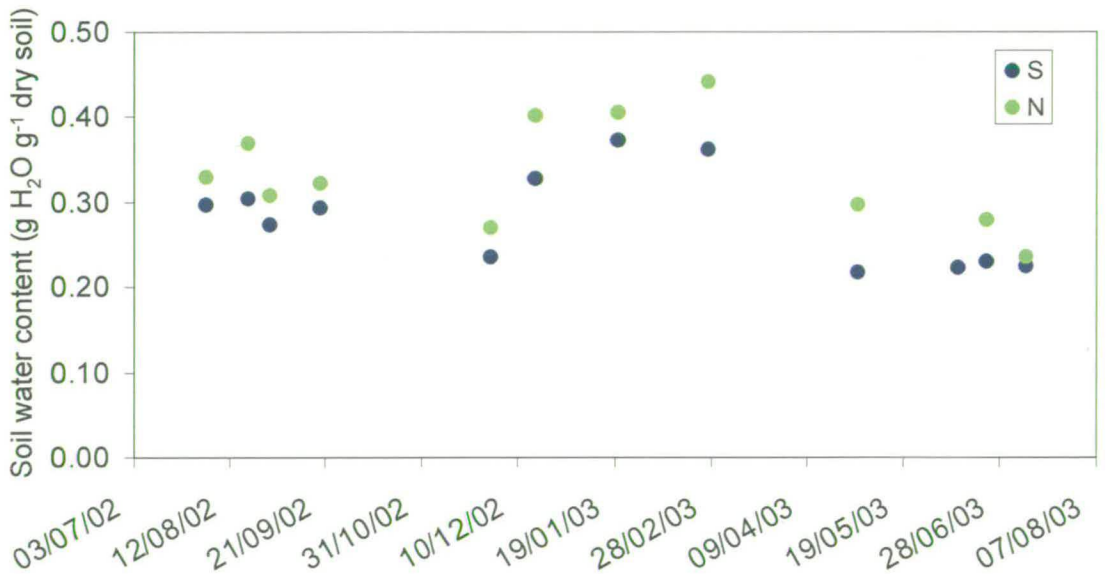

Figure 5.17 Water content in soil samples collected at Easter Bush roughly every month from August 2002 to August 2003. The value is an average of water content obtained from two layers in the soil, 0-10 cm and 10-20 cm, over 9 soil cores for each field. Values for the south (blue) and the north (green) fields are distinguished.

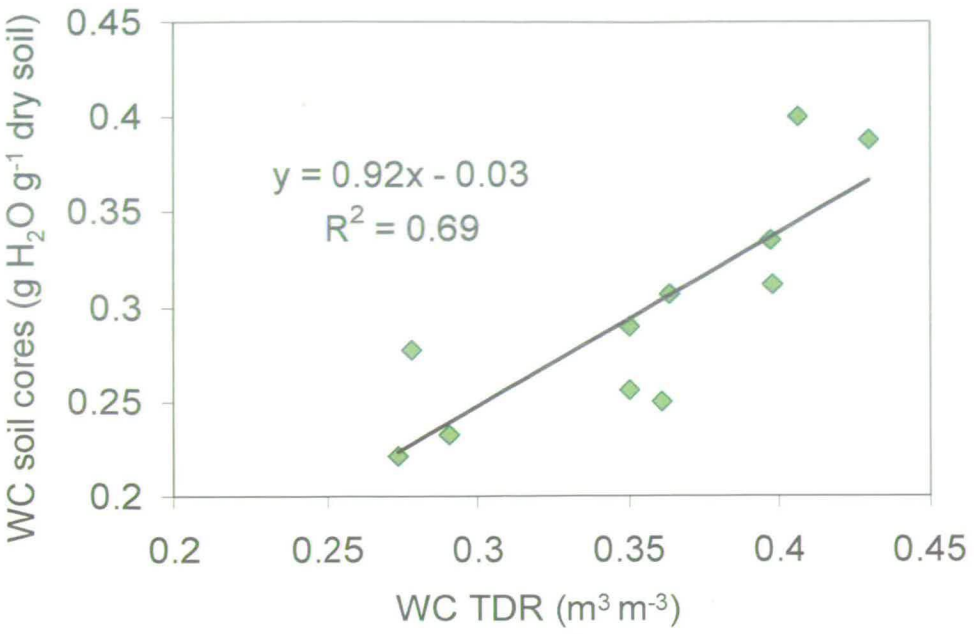

Figure 5.18 Scatter plot of soil water content measured from the soil cores collected monthly (9 samples for each field) versus water content measured continuously with a TDR probe at fixed location.

5.3.4 Diurnal variability of N_2O fluxes

The most common method to measure diurnal variations of N_2O emissions from soils is the use of auto-chambers. The system is comprised of a closable sampling chamber placed on the soil surface, a headspace delivery system that circulated headspace between the chamber and the analytical unit, and a gas analyser (Ambus and Robertson 1998). An automated soil monolith-flux chamber system was used by Thomson et al. (1997) to investigate relationships between diurnal fluxes of N_2O and other variables in a semi-controlled environment. The variation between maximum and minimum fluxes was on average 40% (~ 55 μg N_2O-N m^{-2} h^{-1} equivalent to 15 ng N_2O-N m^{-2} s^{-1}) (Thomson et al. 1997), which is much smaller than the variation observed in this study (~ 250 ng N_2O-N m^{-2} s^{-1}).

Following the initial big emission pulse after fertilisation in June 2002, emissions at Easter Bush showed a clear diurnal pattern with a maximum value at noon and minimum during the night (Figure 5.10). Similar patterns with maximum emission at noon have been reported by Smith et al. (1998) for a cut grassland less than a mile away from this study site. Laville et al. (1997) reported a N_2O flux diurnal pattern with maximum between 09:00 and 16:00 in a micrometeorological

study. Different pattern were observed by Yamulki et al. (1995) and Thomson et al. (1997) where the emissions presented a daily maximum at around 03:00 am and minimum in the late morning or early afternoon.

To further explore the mechanistic process, the diurnal cycle of the soil temperature at different depths was analysed together with the N_2O flux. Unfortunately, only soil temperature at 5 cm was measured in June 2002 and data from May 2003 with similar environmental conditions of daily soil temperature at 5 cm and soil water content were used to estimate the soil temperature at the surface. The solution for the equation for heat conduction was used (Monteith and Unsworth 1990) to obtain the temperature value at depth z and time t $T(z,t)$:

$$T(z,t) = \overline{T} + A(z)\sin(\omega t - z/D) \tag{5.3}$$

where $\overline{T}$ is the average daily temperature, $A(z)$ is the amplitude of the temperature wave at depth z, $\omega = (2\pi/24)h^{-1}$ for daily cycles, and D is the so called *damping depth* (at depth $z=D$ the amplitude of the temperature wave is $1/e$ times the amplitude at the surface).

The daily N_2O flux seems to follow the pattern of soil temperature at the surface better than the variation in a deeper layer (Figure 5.19), also confirmed by the correlation coefficient calculated for the two cases: $R^2 = 0.23$ for the soil temperature at 5 cm and $R^2 = 0.52$ for the soil temperature estimated for the surface (Figure 5.20). This implies that the N_2O emission maximum between 12:00 and 16:00 corresponded with the peak of temperature at the very surface layer of the soil (Figure 5.19).

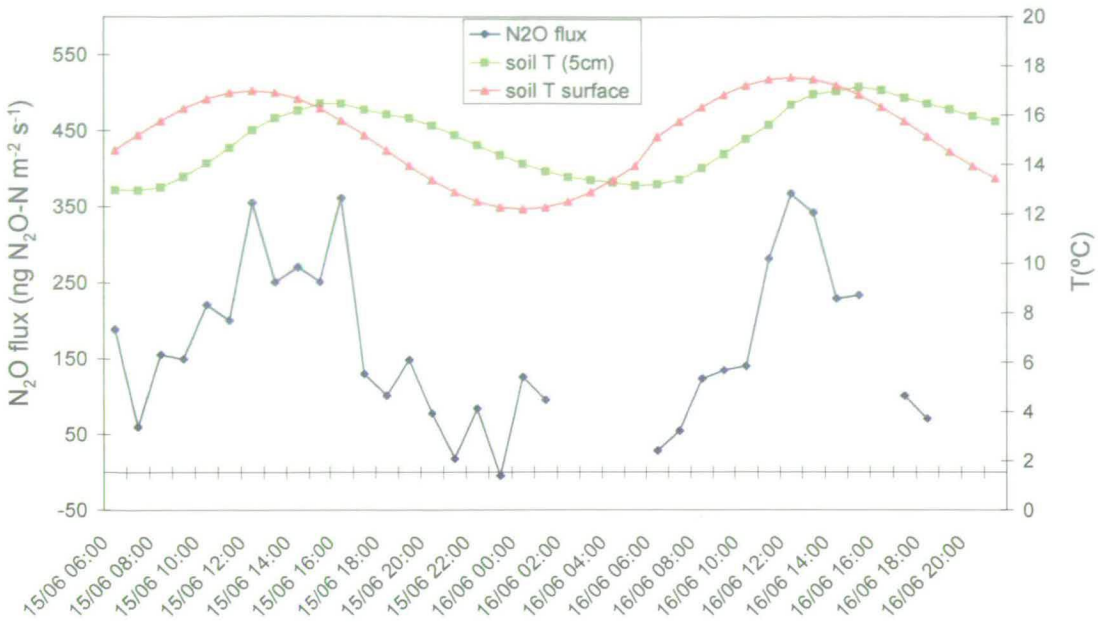

Figure 5.19 Examples of diurnal cycles of N_2O flux, measured soil temperature at 5 cm depth, and soil temperature at the surface obtained by using the damping depth method. 15-16 June 2002.

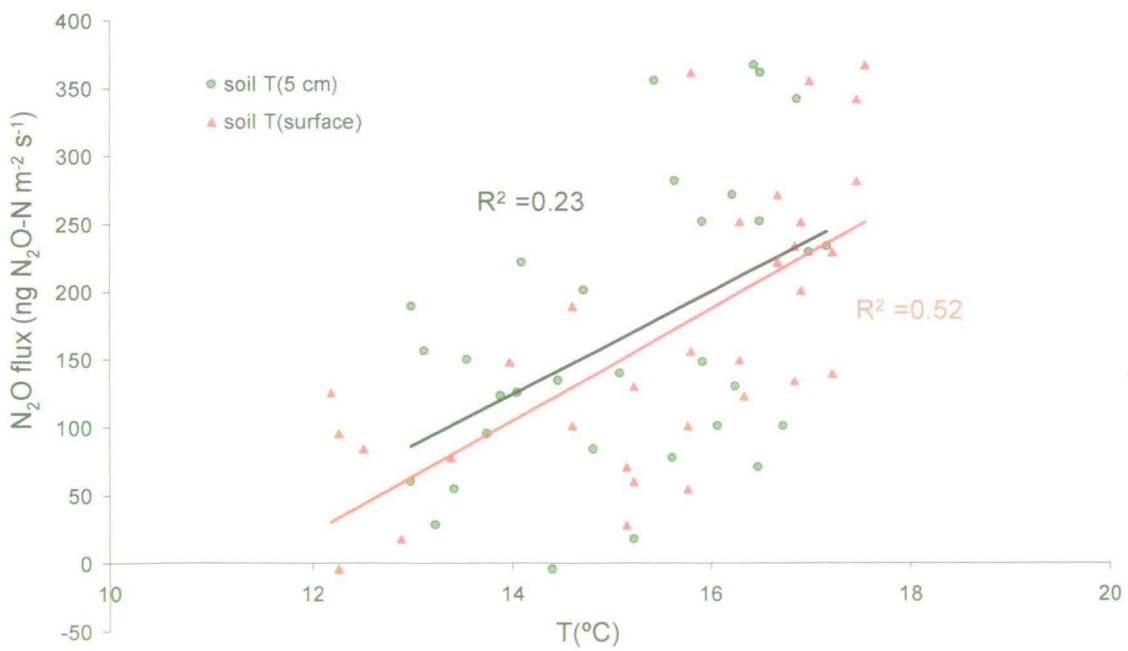

Figure 5.20. Correlation between N_2O flux and soil temperature at 5 cm (dots and black line) and the N_2O flux and temperature of the soil near the surface (triangles and red line). 15-16 June 2002.

On the other hand, a comparison of the N_2O flux with sensible heat flux (H) and friction velocity ($u*$) for the same period in June 2002 indicates that N_2O emissions are also related to the turbulent structure of the lower atmospheric layer. The structure observed in the N_2O fluxes in Figure 5.22 is noticeably correlated with H, following the same pattern. Still observable, but less evident, is the correlation with $u*$. These two turbulent parameters relate with the N_2O emissions better than the air temperature (Figure 5.21) as the correlation coefficients calculated for the days shown in the picture confirm: R^2 =0.7 for H, R^2 = 0.5 for $u*$ and R^2 = 0.2 for the air temperature.

An interpretation of the agreement between the daily N_2O flux behaviour and the micrometeorological parameters could be that the gas emission is regulated or influenced by the exchange of turbulent energy between surface and atmosphere (provided by H) and the surface stress (indicated by $u*$). In practice, the gas produced in the soil could be transported from the superficial soil layer according to the intensity of H and $u*$. However, the correlation of patterns does not necessarily mean the existence of a cause-effect relationship, so a deeper investigation is needed to relate the process of N_2O production rate in the soil and the transportation of the gas using the parameters mentioned here.

This work suggested that diurnal variations of N_2O fluxes could be controlled by changes in soil temperature and in turbulent parameters.

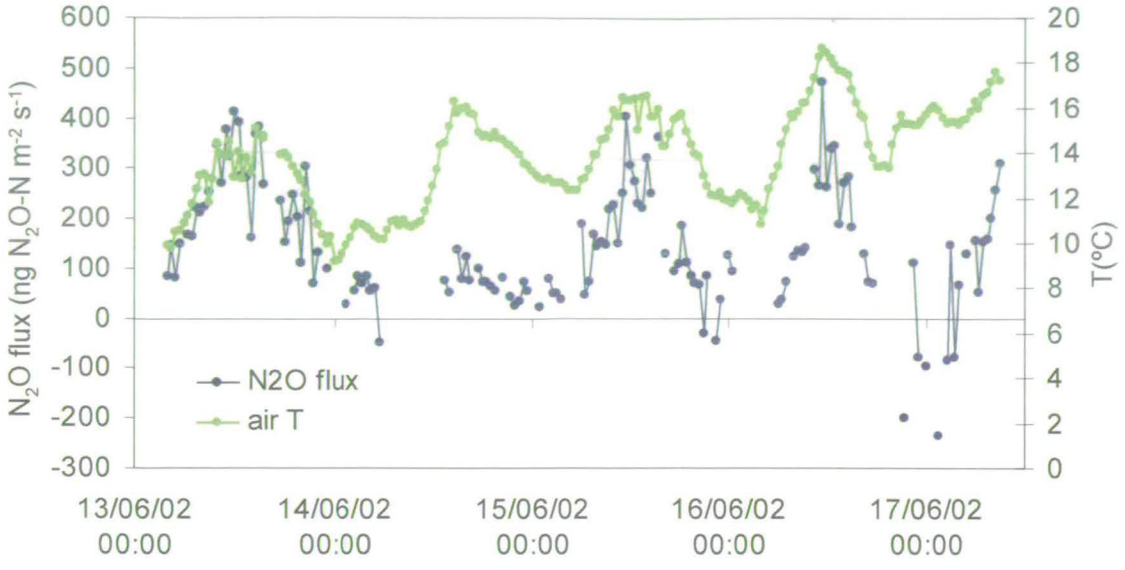

Figure 5.21 Time series of air temperature and N_2O flux measured by eddy covariance at Easter Bush in June 2002.

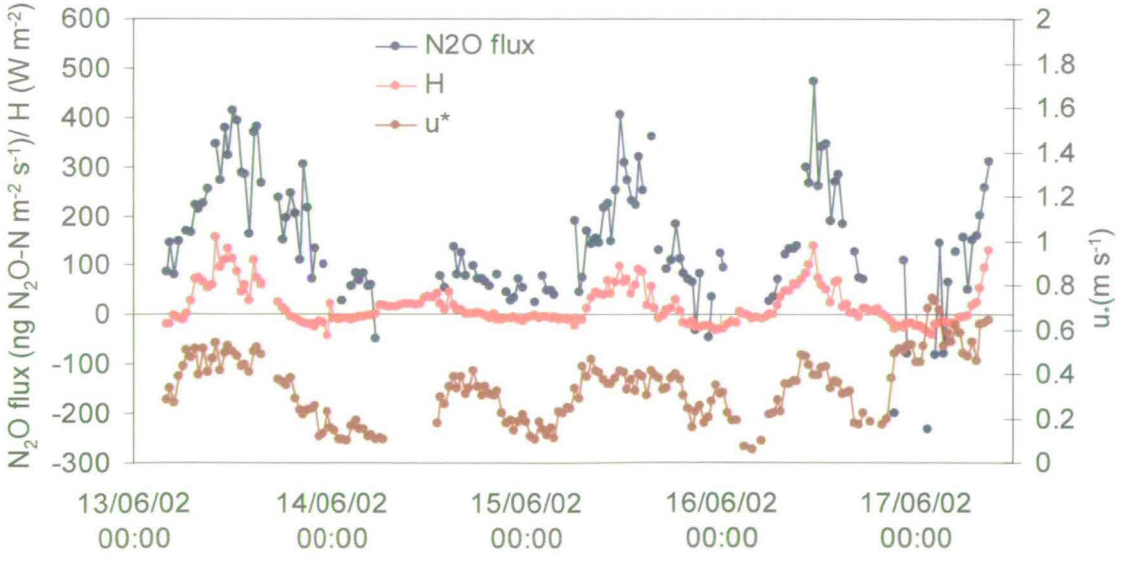

Figure 5.22 Time series of N_2O flux measured by eddy covariance, sensible heat flux (H) and friction velocity (u_*) at Easter Bush in June 2002.

5.3.5 N_2O annual budget

Long-term data series are often affected by gaps which occur as a result of system failure or inadequacy of meteorological conditions. Several approaches have been developed to fill the data gaps in long-term carbon and water flux measurements (Aubinet et al. 2000) including interpolation, parameterization and use of a non-linear regression. The approach used in this work is based on linear interpolation and it is explained in this Section.

5.3.5.1 Gap filling technique

In order to calculate the total N_2O emission from Easter Bush field over the measurements period two different techniques were used for the June 2002 fertilization period and for the rest of the year to fill the gaps in the data.

For the period July 2002-June 2003 when fluxes were mainly close to background including small emission peaks due to fertilization events such as in August 2002, March and June 2003, the daily average flux was used to calculate the cumulative flux. If less than 10 half-hour values were available for a given day a linear interpolation from the neighbouring values was performed to obtain the daily cumulative flux.

For the days close to the fertilization in June 2002 and days with a diurnal cycle of the same magnitude as observed for the 10 to 16 June, an average diurnal pattern was calculated and used as a daily pattern model to fill the gaps in the half-hourly measurements of a given day. The cumulative flux was then obtained as the sum of the half hourly values. Figure 5.23 shows the flux diurnal average pattern obtained using the data from 10 to 17 June. The noise in the flux on the left side of the daily peak is due to a smaller reliability in the eddy covariance measurements at night (see Chapter 3). In the chart the black line within the box marks the median and the red line represents the average of the 30 min flux at fixed time (e.g. 13:00) over the 8 days in June (from 10/06 to 17/06/02). The boundary of the boxes closest to zero indicates the 25^{th} percentile and the farthest from zero indicates the 75^{th} percentile. Results of the superposition of the average daily model on the measurements for 12 and 13 June 2003 are shown in Figure 5.24. The two examples show almost continuous measurements with only few gaps on 13 June and a fairly large amount of

missing data points in the measurements on 12 June. Red symbols in the chart indicate the modelled values used to fill the gaps. In both cases the result obtained with the application of the modelled cycle seems to provide a reasonable approximation to a diurnal pattern of N_2O fluxes.

5.3.5.2 Results

The total annual emission was then expressed as the sum of the daily cumulative fluxes. For the period June 2002-June 2003 the annual emission from Easter Bush estimated with the method previously described was 5.3 kg N_2O-N $ha^{-1}y^{-1}$ but a large part of it was due to the emissions from June to December 2002 (5 kg N_2O-N $ha^{-1}y^{-1}$). The second part of the year of measurements from January to June 2003 only contributed for 6% to the total cumulative flux (Table 5.7).

The N_2O emission factor (EF) defined as the amount of N emitted as N_2O per year as percentage of the total N fertilized applied (IPCC 2001b) was calculated with the following equation suggested by the IPCC:

$$EF = F_{N_2Ocumulative} / (N_{applied} * (1 - Frac_{GASF})) \quad (5.4)$$

where $Frac_{GASF}$ is the fraction of nitrogen that volatilises as NH_3 and NO_x from applied synthetic fertiliser ($Frac_{GASF}$ = 10%)(IPCC 2001b). The overall EF obtained for Easter Bush of 1.68% is 30% higher than the default value adopted by the IPCC of 1.25%, but still very similar. A large difference was noticed in the emission factors calculated for the first six months (3.29%) and for the rest of the time (0.19%) (Table 5.7). Still, the values were within the range of the N_2O emission from applied nitrogen reported in the literature (0.1-11%) (Velthof et al. 1996a; Dobbie et al. 1999; Rudaz et al. 1999). It could be argued that the reason for this discrepancy is related to the different time of the year in the two periods, the first one including the warm and more reactive (in terms of soil bacterial processes) season and the second one including the cold season and spring. Yet, both periods comprised two fertilization events including the June one. In fact, June 2002 emission represents 53% of the cumulative N_2O flux whereas in June 2003 the response to the fertiliser application was almost non-existent, due to a much drier summer season compared with 2002 (Figure 5.25). The small N_2O flux in June 2003 could be the explanation

for the difference in emission factors and reflects the different environmental conditions for the two years that lead to extremely different annual emissions. To support this argumentation, the annual cumulative N_2O flux measured during 2002 and 2003 with static chambers at Cowpark, a nearby, similarly managed grassland field, showed good agreement with the results presented here: the total emission for 2002 was 4.2 kg N_2O-N $ha^{-1}y^{-1}$ with an EF of 1.4% and for 2003 it was 0.5 kg N_2O-N $ha^{-1}y^{-1}$ with an EF of 0.1% (Jones et al. 2005).

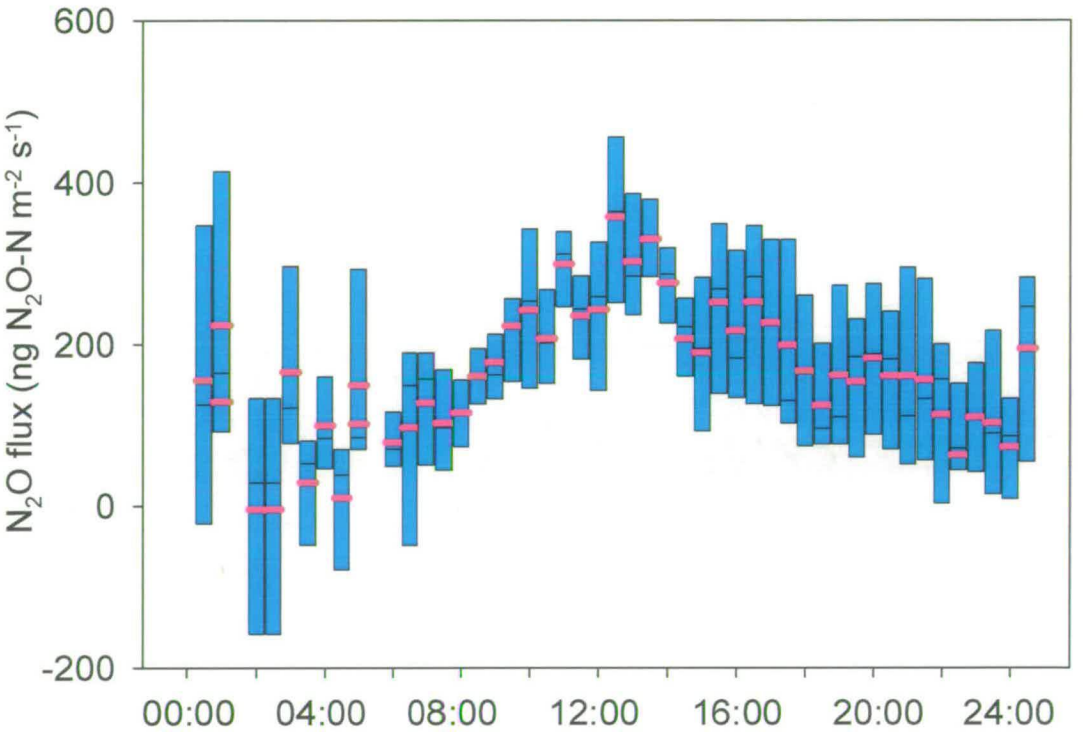

Figure 5.23 June 2002. Daily cycle pattern used as model to fill the gaps in half-hourly data and obtained as average (red line) of the diurnal cycles of the days 10-16 June. The boundary of the boxes closest to zero indicates the 25th percentile and the farthest from zero indicates the 75th percentile. The black line in between is the median.

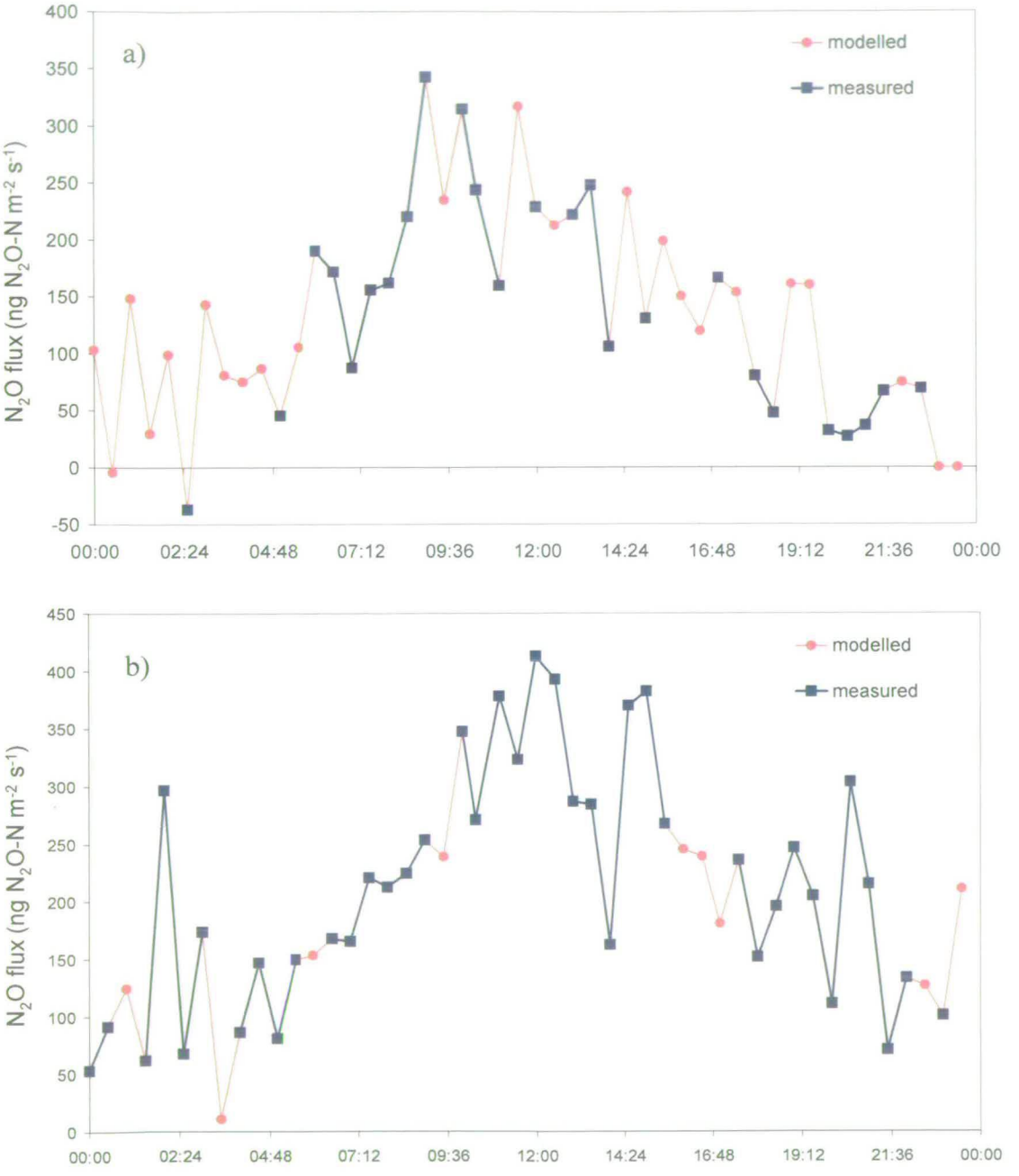

Figure 5.24. Time series of the N_2O diurnal pattern for 12 June (a) and 13 June 2002 (b). The blue symbols represent the available measurements points whereas the red dots show the modelled values used for filling the gaps and obtained with the superposition of the average diurnal cycle showed in Figure 4.21

Table 5.7 Cumulative N_2O flux and emission factors (EF) for 2002 and 2003 measurements at Easter Bush.

Interval of time	Cumulative flux (kg N_2O-N $ha^{-1}y^{-1}$)	Fertiliser applied (kg N ha^{-1})	EF (%)
Period I: June-December 2002	5.0	170	3.29%
Period II: January-June 2003	0.3	184	0.19%
Total	5.34	354	1.68%

The cumulative flux plotted in Figure 5.25 raises another aspect of the grassland N_2O emission problem: the N_2O uptake. During the winter months of December and January the field acted as a sink and in February fluxes were negligibly small (Figure 5.6). This was already highlighted in the seasonal study for winter (Section 5.3.2) where the mean N_2O flux was -5.5 ng N_2O-N $m^{-2}s^{-1}$. This illustrates how N_2O uptake can contribute to the total N_2O budget from grasslands and therefore will influence the annual emission factors.

Finally, if the correction due to the N_2O flux underestimation, found with the spectral analysis in paragraph 5.2.3, was applied to the total cumulative flux, 19% of the flux would be added resulting in a total emission of 6.36 kg N_2O-N $ha^{-1}y^{-1}$ which corresponds to an emission factor of 2%.

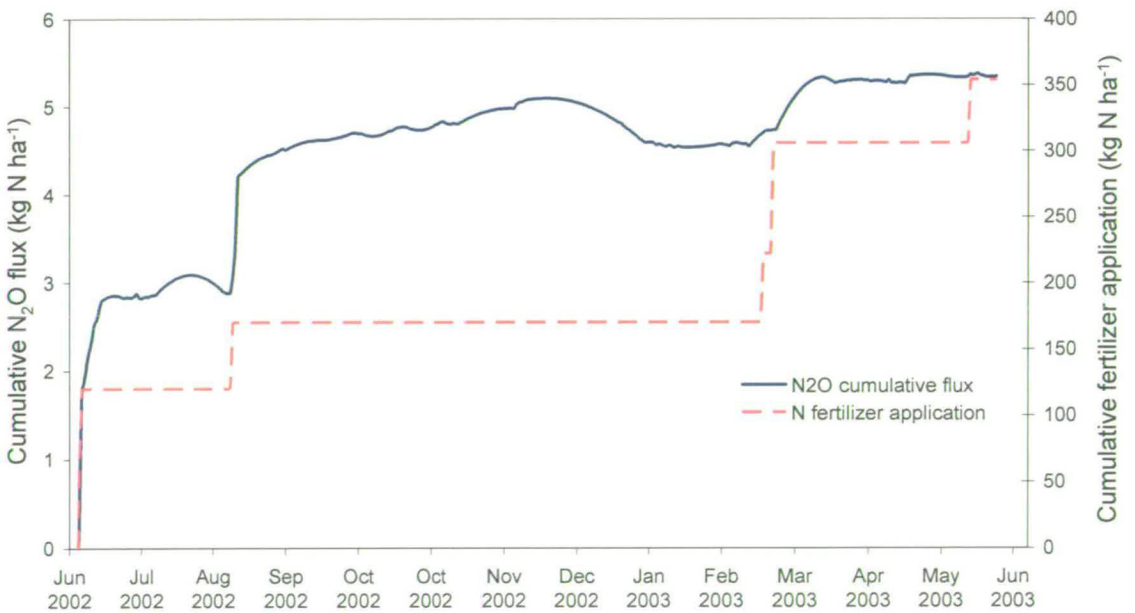

Figure 5.25 Cumulative N_2O flux and fertiliser application.

5.3.6 Comparison with static chamber measurements at Easter Bush site

Eddy covariance N_2O flux measurements were compared with the conventional static chamber methodology on 11, 12 and 13 June 2003.

The static chambers method is the most commonly used methodology by which N_2O fluxes are measured and more than 90% of our knowledge of N_2O derives from the use of static chambers. Cylindrical polypropylene chambers (volume of 0.032 m^3, cover area 0.12 m^2) of 20 cm height and 40 cm diameter were used here (Figure 5.26) (Clayton et al. 1994). Fourteen chambers were placed into the prevailing fetch of eddy covariance measurements in the south field. The chambers were arranged in a regular grid with an average distance of 20 m between two consecutive chambers as shown in the diagram in Figure 5.27. For flux measurements the chambers were closed for 60 min and gas samples were collected at the start and termination of the enclosure period using a Perspex 1ℓ syringe and were stored in Tedlar bags (3ℓ volume) until analysis by TDL using the same system setting described in Chapter 6. Measurements were taken once a day around midday. N_2O fluxes were calculated from the concentration differences between the chamber air at the end of the enclosure period (C_c) and ambient air at the beginning of the 60 min (C_a), the chamber volume (V), the time for which the chamber remained closed (t) and the surface area covered by the chamber (A):

$$F = \frac{(C_c - C_a)V}{At} \tag{5.5}$$

Over the three days, hourly N_2O fluxes from individual chambers ranged from 0.4 to 90 ng N_2O-N m^{-2} s^{-1}. The daily average flux over the 14 chambers gradually decreased from 30.6 ng N_2O-N m^{-2} s^{-1} on 11 June to 19.8 ng N_2O-N m^{-2} s^{-1} on 13 June with standard deviations as high as the flux. The decrease in the flux on 13 June was associated with a slight decrease of the soil temperature at 5 cm by 0.5 °C but a constant WFPS of about 69%. The typical high spatial variability of the measurements resulted in a large coefficient of variation (CV), calculated as the ratio of the standard deviation and the mean flux. CV values between chambers on the individual days were greater than 90% but CV's are in agreement with those found in

previous works (Ambus and Christensen 1995; Laville et al. 1997). A fairly similar pattern of N_2O emission was revealed by the measurements with chambers through the three days with hot spots remaining in the same position, although the period analysed was too short to provide a reliable picture of the spatial N_2O production of the field. Emissions were higher from chambers within 50 m from the eddy covariance mast (Figure 5.27 and Figure 5.28) compared to emissions 70 m further. This portion of field surface was often wetter than the rest and frequently flooded after heavy rainfall.

The average N_2O flux from the 14 chamber measurements for each day was compared with an hourly average from the micrometeorological values at the same time of the day (e.g. 1 pm). The results from the two methods plotted in Figure 5.29 show a reasonable agreement, with N_2O hourly fluxes from micrometeorological system within 50% of those estimated by the chamber method. This is acceptable and in agreement with previous comparisons (Christensen et al. 1996; Laville et al. 1999). The reason for the discrepancy observed is that static chambers and eddy covariance do not measure the same thing: eddy covariance estimates the N_2O emission as an integration over a large area (field) and provides usually smaller fluxes than the chamber system, which investigates a more localised area (Laville et al. 1997). In this study chambers were positioned within the footprint area for the eddy covariance mast with wind coming from the sector where they were located.

Figure 5.26 Images of the static chamber placed in the soil at Easter Bush field. The picture at the top shows the cylindrical body in polypropylene of 20 cm height and 40 cm diameter. The total volume is about 0.032 m^3 and cover area of 0.12 m^2. The chamber closed with the lid during the measurement period is shown at the bottom.

Figure 5.27 11-13 June 2003. Location of the 14 static chambers (green dots) and of the other micrometeorological instruments at the experimental site Easter Bush, already described in detail in Chapter 4.

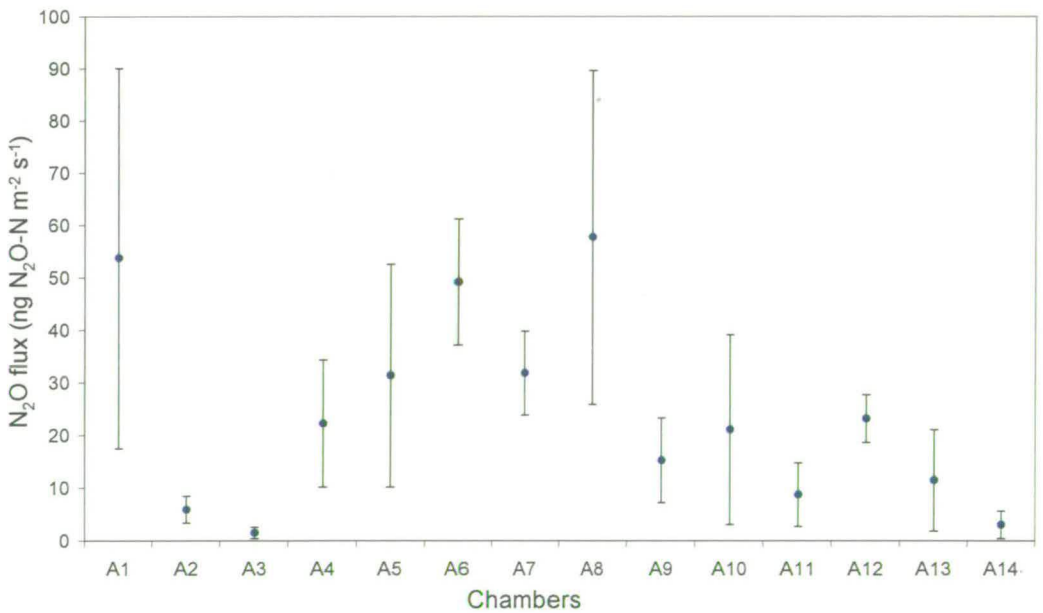

Figure 5.28 N_2O flux average over the three days of measurements (11, 12 and 13 June 2003) for each of the 14 chambers. Error bars represent the standard deviations.

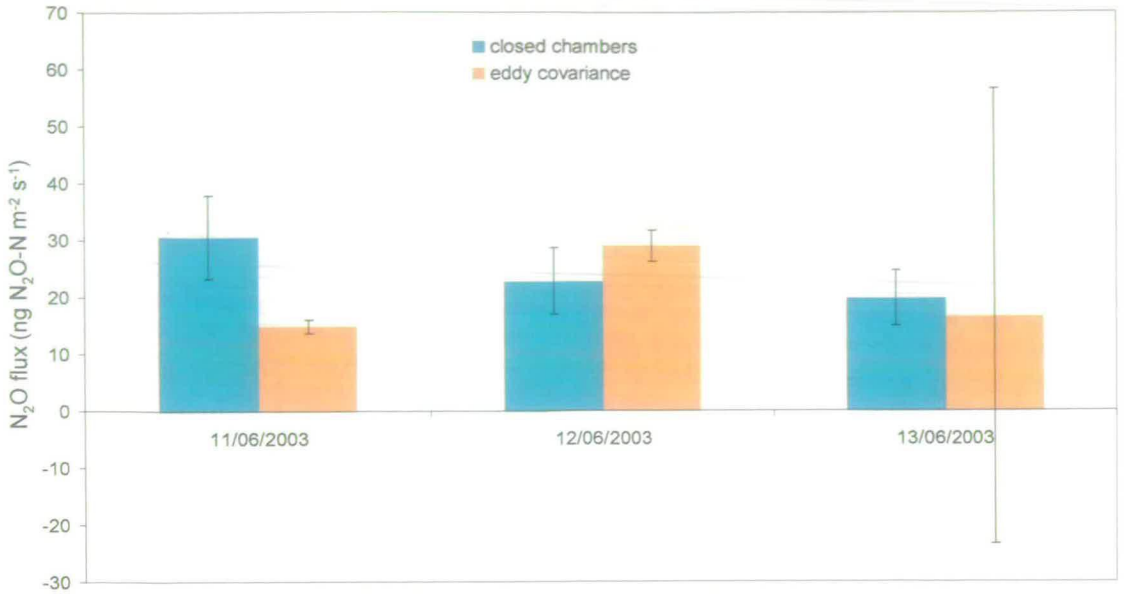

Figure 5.29 N_2O fluxes obtained with the 14 closed chambers method (green) and with eddy covariance technique (orange). Error bars represent the standard error calculated from the 14 chambers measurements and from the eddy covariance measurements.

5.4 Conclusion

One year of almost continuous N_2O flux measurements made with the eddy covariance technique at the typical managed grassland Easter Bush site have been presented in this Chapter. Results provided a picture of the field scale N_2O fluxes on the short (day) and long (seasonal) time scale. The large differences in seasonal fluxes (-5.5 – 195 ng N_2O-N m^{-2} s^{-1}), that include the 4 fertilization events and the winter, were mainly due to different environmental conditions (such as temperature, rainfall, etc.) in the periods investigated (Table 5.5). This was confirmed by the good prediction of N_2O seasonal fluxes using soil water content together with soil temperature values or soil N availability in a multi-linear regression ($R^2 = 0.96$, N = 5, $p < 0.05$) (Table 5.6 and Figure 5.16).

The maximum flux value measured in June 2002 is extraordinarily large (3800 ng N_2O-N m^{-2} s^{-1}). The fact that such large values do not appear in the literature might be explained by the methodology used here. The eddy covariance technique permits continuous measurements with fluxes calculated every 30 minutes and integrated over an area of 0.01-1 km^2 (~0.2 km^2 at Easter Bush), whereas static manual chambers provide at maximum only one flux measurement per hour and

therefore have a larger probability of missing emission peaks. Still, the large emission peak on 8 June 2002 lasted for nearly a day with fluxes than 10^2 ng N_2O-N m^{-2} s^{-1} (Figure 5.10) and could have been detected by chamber measurements.

The diurnal patterns of the N_2O fluxes were observed only after the fertilisation in June 2002, when daily average fluxes were large, ranging between 64 ng N_2O-N m^{-2} s^{-1} and 360 ng N_2O-N m^{-2} s^{-1} (Figure 5.10). Maximum fluxes up to 5 times greater than the minimum fluxes were measured around noon with peaks occurring at the same time as the temperature of the soil surface ($R^2 = 0.52$). This suggests that the production of N_2O occurred in the soil top few mm. A significant correlation of diurnal N_2O fluxes with turbulent parameters such as H ($R^2 = 0.7$) and $u*$ ($R^2 = 0.5$) suggests that diurnal variations of N_2O fluxes are controlled by changes in soil temperature but also by changes in turbulent parameters. This provides an interesting process to investigate and a different approach to use in process-based models for prediction of N_2O emissions.

In this study a sink activity was observed in winter months (seasonal average flux of -5.5 ng N_2O-N m^{-2} s^{-1}) and played a small but significant role in the total N_2O emission budget for Easter Bush. Although N_2O uptake activity is not extensively discussed in the literature (Glatzel and Stahr 2001; Flechard et al. 2005), a more thorough investigation could improve the understanding of the global N_2O sink, which could largely contribute to improve our current estimate of the atmospheric residence time of N_2O (Cicerone 1989).

The total annual (from June 2002 to June 2003) budget estimate for the field using a gap filling method presented in Section 5.3.5.1 was 5.3 kg N_2O-N ha^{-1} y^{-1} (EF = 1.68%), with EF varying from 3.29% in the first period (Jun-Dec 2002) to 0.19% in the second part of the study (Jan-Jun 2003).

The variability of the emission factors highlighted in this Chapter is one of the fundamental factors contributing to the uncertainty in the emission inventories, which is in part discussed in the next Chapter.

Chapter 6 Results from a national network for monitoring greenhouse gas concentration in the atmosphere

6.1 Introduction

The current increase of nitrous oxide (N_2O) in the atmosphere of about 0.2 to 0.3% y^{-1} (IPCC 1992) is a cause of concern for the environment. About 70% of the global anthropogenic N_2O emissions are estimated to be derived from the agricultural sector (Cole et al. 1997) e.g. from increased fertiliser use and indirectly by enhanced N deposition inputs (Granli and Bockman 1994) or land use changes (Keller et al. 1993). Furthermore there is a growing interest in various mitigation options for N_2O emissions (Velthof et al. 1998) from many countries committed to reduce their greenhouse gas emissions. Thus there is the need for continuous monitoring systems to assess changes in emissions from different sources and to estimate the success of mitigation strategies applied.

Monitoring of N_2O concentrations is important for several purposes and the approach selected may vary for each. In the first instance, it is of interest to observe trends between years with some information about seasonal variability. This might be accomplished by detailed and sophisticated systems that provide data with high temporal resolution such as a TDL, or automated Gas-Chromatographic analyser (Arah et al. 1994; Wienhold et al. 1994). However, such systems are too expensive to implement at more than a few sites. Secondly, the spatial pattern of N_2O concentrations is important and requires a large number of sampling sites. Since the principal use of the monitoring network described in this Chapter is to validate national gas emission inventories and atmospheric dispersion models, the spatial resolution of measurements is more important than high resolution in time for this purpose. Therefore a low cost sampling method can be implemented at many sites at low time resolution.

Existing monitoring networks for N_2O are mainly devoted to monitor global concentration field and to study the increase of N_2O concentration during the 20^{th} century. One example is the AGAGE (Advanced Global Atmospheric Gas

Experiment) network that includes measuring stations in several points in the world such as: Mace Head, Ireland; Pt. Barrow, Alaska (71, 16N, 156.5W); Cape Meares, Oregon (45.50N, 124W); Cape Kumukahi and Mauna Loa, Hawaii (19.30N, 154.5W); Samoa (14.10S, 179.6); Cape Grim, Tasmania (42S, 145E), Palmer Station, Antarctica (64.46S, 64.1W), and the South Pole (90S). Results from long-term atmospheric measurements show that N_2O concentration in the northern hemisphere is higher than in the southern hemisphere by about 0.7 ± 0.04 ppb (Khalil et al. 2002), and the Arctic to Antarctic difference is about 1.2 ± 0.1 ppb. Furthermore, concentrations at locations influenced by continental air are larger than at marine sites, showing the existence of large land-based emissions. Approaches used for the studies mentioned above include the employment of gas chromatography analysis of hourly or weekly samples of air (Biraud et al. 2002), which are slightly different from the one used in the present study.

Monitoring systems for ammonia (NH_3) concentration at regional and national scale have been already successfully developed in the Netherlands (Duyzer et al. 2001) and in the UK (Sutton et al. 2001a), where the National Ammonia Monitoring Network (NAMN) has provided concentration records for 7 years, allowing assessment of intra- and inter-annual trends between areas dominated by different ammonia emission source sectors. Furthermore, atmospheric chemistry and transport models were applied to improve the description of local spatial variability of ammonia concentration. The combination of model and measurements provides the basis to assess NH_3 responses across the UK to international emission controls.

Following the general concept applied for ammonia, the development of a UK monitoring network capable of detecting the enhancement in local N_2O concentration from UK sources is presented in this Chapter. The same network has been used for a similar study on methane (CH_4), but only nitrous oxide will be taken into consideration in the following sections. The very different properties of N_2O and NH_3, the first one with an atmospheric lifetime of ~120 y and the second one with a short (hours) lifetime, require different levels of detection of gas concentration differences: NH_3 atmospheric concentrations are small (0.1-10 ppb), whereas N_2O ambient concentration is large (~320 ppb) and the monitoring network needs to resolve smaller concentration differences (e.g. 1-3 ppb) than for NH_3.

6.2 Methodology

The principal requirements of a suitable method for the application are: the ability to detect spatial variation of N_2O concentration within the country (approximately 2-3 ppb as estimated by previous studies (Skiba, personal communication)); sufficiently cheap to monitor at a large number of sites (about 80); and acceptably reliable and simple to implement by local site operators.

Within the context of the above requirements, a decision was made to sample concentrations in the network on a monthly basis. This was selected in preference to weekly sampling, since it greatly reduces the workload for the network co-ordination and for site operators, but it still provides the facility to investigate major seasonal patterns in N_2O concentrations.

To fulfil the requirement of resolving the variability of the N_2O concentration, a Tuneable Diode Laser (TDL) gas analyzer (see Paragraph 4.4) was used to measure N_2O in the air samples. This instrument provides a precision of 0.2-0.3% (~1 ppb) at 1 Hz on the ambient concentration (~320 ppb), accomplishing the initial requirement of detecting 2-3 ppb of variation.

The spatial and temporal N_2O concentration differences measured by this network are likely to be very small, but well within the measurement range of the TDL instrument. Within the time and funding available for this work a national network could never cover the full variability of N_2O concentrations. However, a dense network (e.g., >2-4 sites for 100 × 100 km) of about 80 sites could be sufficient to detect most of the regional pattern.

6.2.1 Description of the system

The monitoring method used consists of monthly air samples collected into containers which are then sent to CEH-Edinburgh for analysis by TDL spectroscopy.

A very simple device is used: small cheap air pumps modified to a low flow rate (<1ml/min) by adding capillary tubing to the pump outlet for sampling the air continuously for a month period; commercially-available large metallized plastic bags, fitted with a defined airtight inlet, to collect the gas samples at 1.5 m height

(Figure 6.1). The balloons were enclosed in cardboard boxes (490 × 330 × 255 mm) when inside buildings or in plastic boxes (565 × 265 × 255 mm) of the same dimensions when placed on fields. All the sampling bags were prepared at CEH and posted or taken to the site operators. Once received at CEH the samples were stored in an unheated cabin and were measured when samples from all the sites were received, usually two weeks after the first sample arrived.

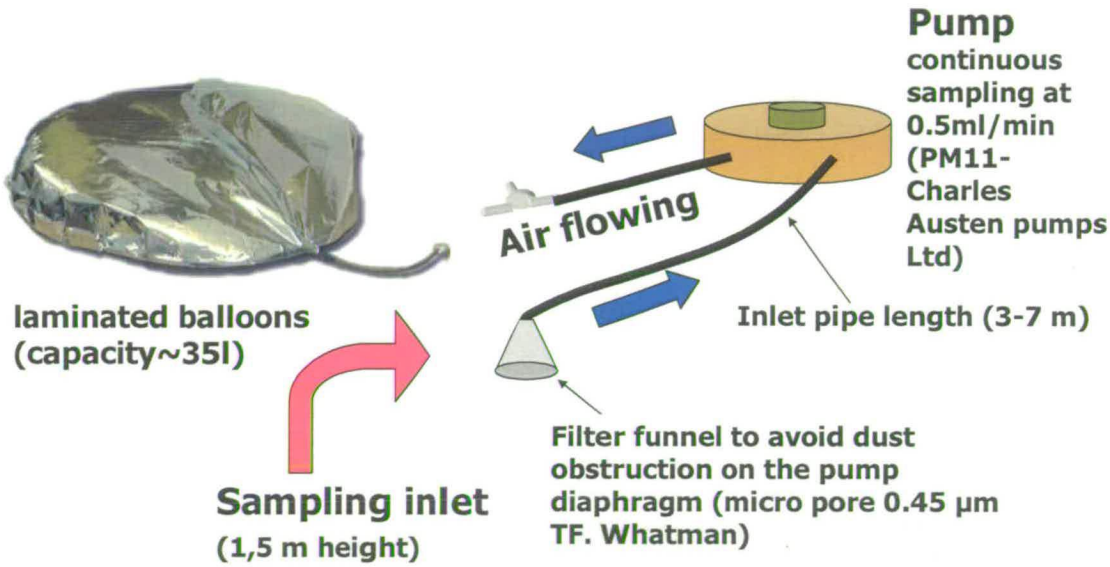

Figure 6.1 Scheme of the sampling system: the pump is connected to an inlet at 1.5 m height and to a bag where the air sample is collected. During the collection, bags were filled up with a maximum of 25 litres of air, well below their capacity

Concentrations were determined relative to compressed air calibrated by BOC gas standards. The nominal concentration suggested by BOC for this cylinder was 310 ppb (certified 357 ppb) N_2O in air, but a recalibration against a primary standard (concentration = 295 ppb, Aerodyne Res. Inc.) was made using the TDL. The resulting concentration for the BOC cylinder was 305.7 ppb. This value was used in the study when referred to standard concentration.

Every sample was measured for 30 s with the TDL operating at 1 Hz switching to the standard concentration after every sample. A running mean of 13 s was performed over the 30 s-interval and the mean value with the lowest standard deviation out of the last four records was taken as the monthly concentration of the

bag. This set up of the measuring system provides a detection limit of about 2 ppb corresponding to a rms = 0.5% for ambient concentration.

6.2.2 Quality analysis and control

Quality tests on the air-tight balloons used to collect sampled air were done at several times of the year and in different ways. On 20 August 2003 16 samples were filled with air from a cylinder at standard concentration of 306 ppb of N_2O and 1889 ppb of CH_4. The bags were analysed immediately after the collection of the air with the same TDL setting and system described in 6.2.1. After a month's time in the balloon N_2O concentration increased by 0.7% (about 2 ppb) and by about 2 % (about 6 ppb) after 2 months, whereas CH_4 concentration varied randomly by 0.4 % (about 7 ppb) in both cases, 1 and 2 months after the collection. Figure 6.2 shows N_2O concentration in August, September and October 2003. The variation in concentration over a month is mainly due to the uncertainty of the system, as the overlapping error bars show in the chart. The increase in concentration in the sampled air in the bags could be due to some release from the bag itself.

In February 2003, November 2003 and January 2004 some more tests were done on bags containing air samples from the network sites. A total of about 30 bags were tested for both N_2O and CH_4 concentrations: they were analysed immediately after they were received at CEH (i.e. about 1 month after the start of the air collection) and a month later (i.e. about 2 months after the start of the air collection). N_2O concentration varied up to 2% (about 6 ppb) in 93% of the cases and by less than 2.5% in the rest of the bags, showing a good agreement with the 2% of variation shown in the test with standard concentration filled bags (Figure 6.2) after 2 months of storage in the balloons. In 65% of the cases CH_4 concentration varied by less than 1% (about 18ppb) and in 35% of the cases it varied by an average of 2%. The variation in concentration does not seem to be related to the seasonality; in fact the changes in percentage stayed the same in winter and summer. In this study most samples were analysed within 6 weeks from the first date of sampling, avoiding storing the samples longer. In this case the tests on the balloons showed that the concentration change was comparable with the uncertainty of the measuring system

(about 2 ppb) (Figure 6.2). For this reason no corrections were applied for production rate in the bags.

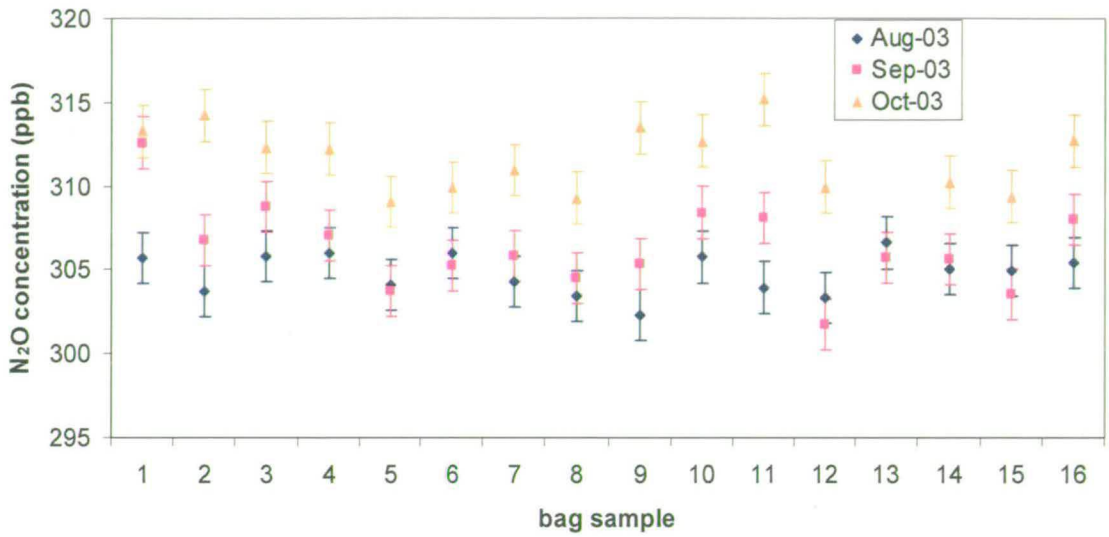

Figure 6.2. Example of 16 bags filled with standard concentration of N_2O (305 ppb) and measured on 20 August (◊) and then measured again on 18 September (■) and on 27 October 2003 (▲). Error bars refer to 0.5% of uncertainty of the system.

6.3 Network sites

N_2O concentration was measured from approx 80 sites from March 2002 until November 2003. In the areas of Cumbria and Devon a monitoring network, already utilized for the Foot & Mouth Disease project, was used, comprising 20 sampling sites for each region. In the Foot & Mouth Disease project, parallel measurements of N_2O, CH_4 and NH_3 were made to produce a more complete picture of gas emissions in the area. The remaining sites were in part included in the Ammonia National Network (33 sites) and in part used for a parallel project aiming to study methane emissions from ex-open-cast mine locations in the country (Methane-Mine project, 11 sites; see Table 6.2). In Figure 6.3 the site locations are shown in a map.

The main emission sources type in Cumbria and Devon are agricultural. The two networks include sampling sites situated in localized areas with similar characteristics of N_2O source type. The average distance between sites is 20 km in Cumbria and 17 km in Devon.

The sites from the National Network are divided into different categories depending on the dominant type of source: 2 'background' sites were located in areas of no known large sources of emissions; 15 sites were in close vicinity to livestock rearing, predominantly cattle ('agricultural'); 14 sites in locations of a mixture of urban development and agriculture ('mixed'); and 2 sites were in the city centres of Edinburgh and London ('urban'). The sites positions, examined from a previous study on ammonia (Sutton et al. 2001b), were identified using the following criteria:

- representative spatial coverage of the UK,
- relationship of the sites to local sources,
- availability and access to a willing and helpful local contact,
- co-location of the sites in relation to other air quality and ecosystem monitoring activities
- access to power

The sites from the Methane-Mine project were influenced by the presence of disused mining activities and were located in a mixture of urban and rural environment. As a consequence 3 sites were included in the mixed group and 11 in the urban group.

The location of the sites of different categories is shown in Figure 6.4. Due to budget restrictions during the second year of the experiment, the number of sites of the National Network was reduced from 33 to 13, although a representative number of sites for each type of source were maintained. Table 6.1 summarizes the features of the several networks and in

Table 6.2 the positions and names of National Network and 'mines project' sites are described.

As Figure 6.4 shows, the number of mixed sites in the south east of the country is higher than in the south west part of the UK, where there are more agricultural sites. The nature and location of the sites used for the national network is confirmed by a soil N_2O emission inventory created by CEH (Sozanska 1999; Skiba et al. 2001), taking into account the land use, N input, soil wetness and soil temperature and represented in the map in Figure 6.5. In fact, comparing the two maps (Figure

6.4 and Figure 6.5) analogies between inventory estimates of emissions and sites category used for the network are noticeable: the north of Scotland is an evident low emission region (green area) and this coincides with the location of the background sites in the national network; the area in the south-west part of the UK containing spots of the highest N_2O emission (purple and blue area in Figure 6.5) is primarily dominated by agricultural sites (green dots in Figure 6.4), which are believed to be the main soil N_2O source.

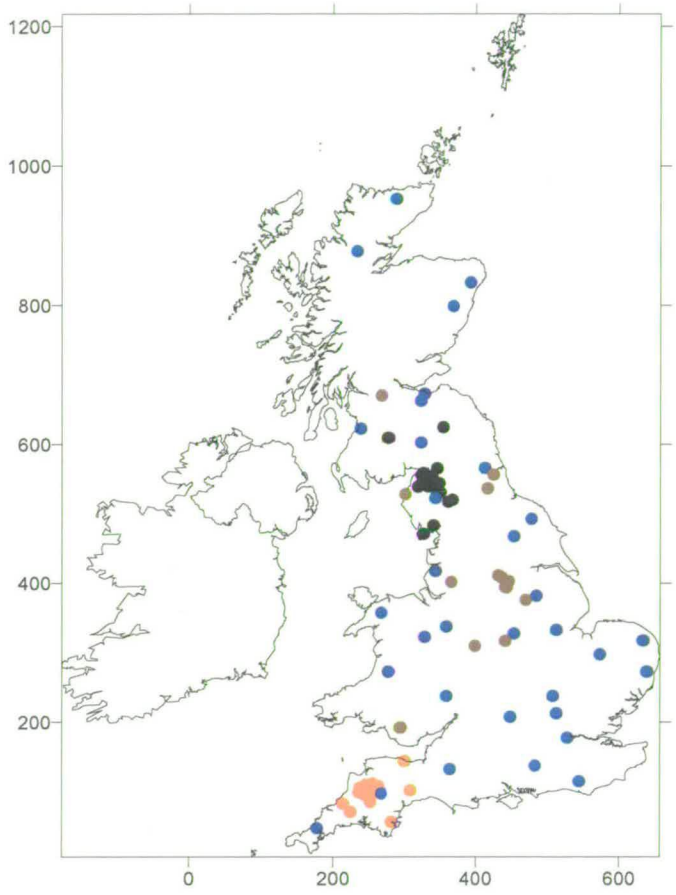

Figure 6.3. Nitrous oxide network in the UK. The red dots represent the sites from Devon network; the black dots show Cumbria sites; blue dots represent the Ammonia National Network sites and the brown dots are the sites from the 'Mines' project around the country.

Table 6.1 Summary of the monitoring networks used in this study.

Name of the network	No of measuring sites (Mar-Dec 2002)	No of measuring sites (Jan-Nov 2003)	Source type
Ammonia National Network	33	13 (from April)	Background Agricultural Mixed Urban
Cumbria	20	20	Agricultural

Devon	20	20	Agricultural
Mines project	-	13	Mixed
			Urban

Table 6.2. Summary of the sampling sites included in the National Network (NN sites) and in the Mines-project (MP sites). Positions are expressed with the national grid reference and the dominant source: 0, background; 1, agricultural and livestock; 2, mixed; 3, urban.

Site Name	Network	National Grid Ref.	Dominant source	Site Name	Network	National Grid Ref.	Dominant source
Bush	NN	nt245635	2	Sibton	NN	tm363722	2
Holme Lacy	NN	so554357	1	Edinburgh	NN	nt253734	3
Brown Moss 2	NN	sj563390	1	Cwmystwyth	NN	sn771742	1
Bure Marshes	NN	tg334161	2	Marton	NN	sk844818	2
				Gainsborough			
Mere Sands Wood	NN	sd447157	2	Pointon	NN	tf128313	1
Halladale 1	NN	nc902488	0	Auchincruive	NN	ns379234	1
Ellon Ythan	NN	nj945304	2	Lyulphs Tower	NN	ny403202	1
Llynclys Common	NN	sj2732371	1	Barcombe Mills	NN	tq438149	1
Easingwold	NN	se540675	2	Newcastle OTC's	NN	nz126658	2
North Wyke	NN	sx659983	1	Barnsley, Smithies	MP	se353080	3
Rothamstead	NN	tl123129	2	Victoria Junior Sc.	MP	nx999282	2
Wytham Woods	NN	sp452083	2	Crook, Durham	MP	nz161362	3
Alice Holt	NN	su809379	2	Car house, Rotherham	MP	sk424939	3
Dyffryn Mymbyr	NN	sh695572	1	Woolley, Pinxton	MP	se309111	3
Strathvaich Dam	NN	nh348750	0	Kibbelsworth, Durham	MP	nz243562	3
Eskdalemuir	NN	nt235030	1	Coleorton	MP	sk403168	2
High Muffels	NN	se776939	1	Cannock	MP	sj984095	3
Stoke Ferry	NN	tl700988	1	Bridgend	MP	ss935921	3
London, Crom.	NN	tq266791	3	Bolton-upon-Dearne	MP	se452026	3
Five Acres	NN	sw794486	1	Kimberworth Park	MP	sk404943	3
Silsoe	NN	tl088356	2	Gamston Aviation	MP	sk693762	2
Sutton Bonington	NN	sk505268	2	Glasgow	MP	ns681700	3
Banchory	NN	no677984	2	Newton Westpark	MP	sd644016	3
Castle Cary	NN	st609319	1				

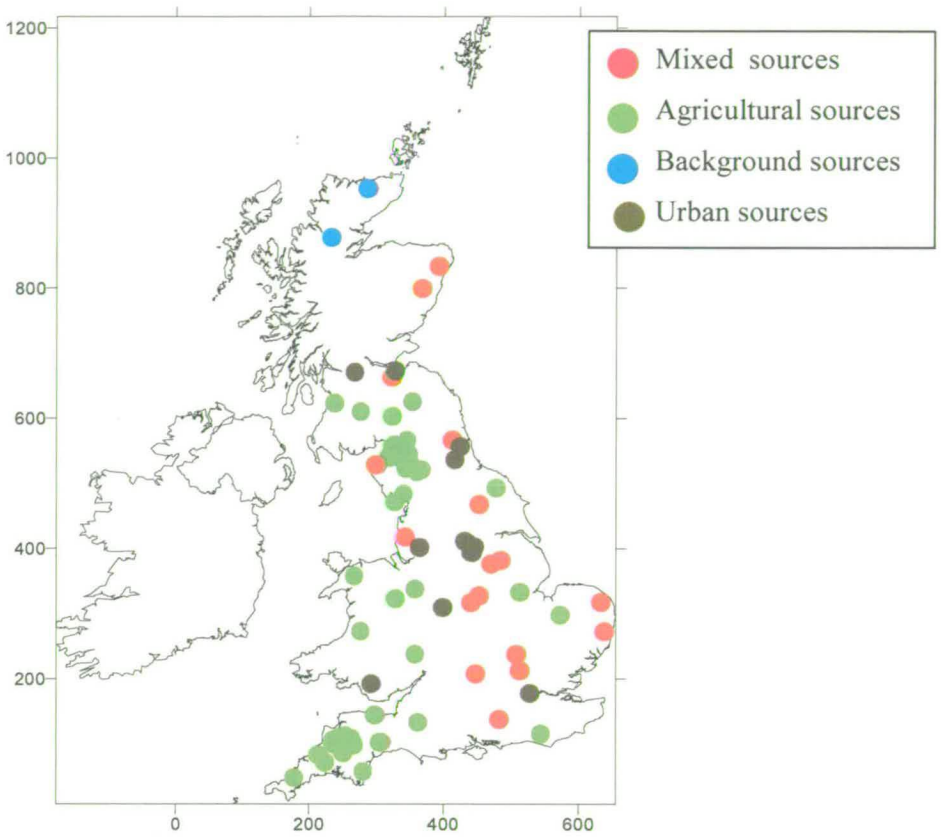

Figure 6.4. National network sites classified by type of N_2O source.

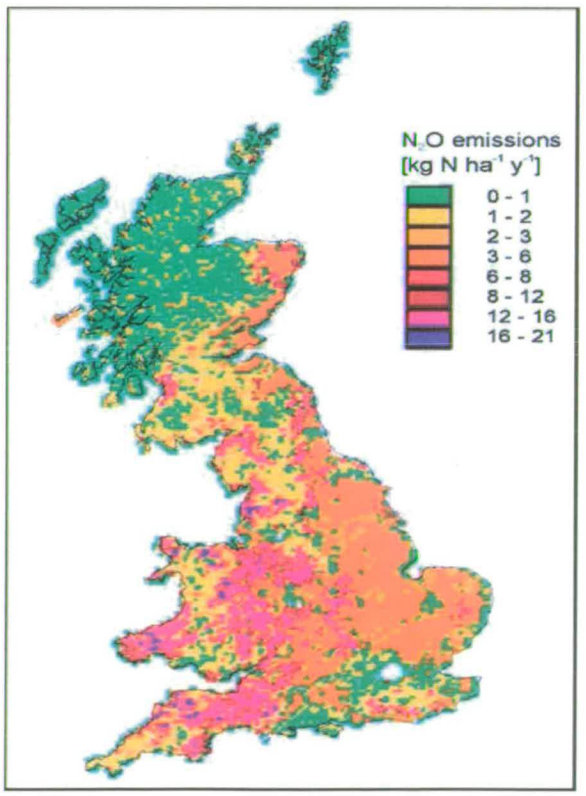

Figure 6.5. N_2O soil emission inventory developed by CEH (Sozanska et al. 2002).

6.4 Results and discussion

Samples were collected from March 2002 to November 2003. Due to problems with the TDL, concentrations for June, August and December 2002 are not taken into consideration.

Figure 6.6 shows the total monthly average concentration for the entire period of measurements. In the calculation of the monthly averages shown here, sites from all the networks were considered. Although the gaps in the data during the first year do not allow quantifying the difference, concentration seems overall a bit lower in 2002 compared to 2003 and also it varies more widely in 2003 than in 2002. Mean monthly values ranged between a minimum of 316 ± 2 ppb in April 2003 and a maximum of 340 ± 9 ppb in August 2003. The big error bars in 2003 can be due to the reduced number of sites used in the second part of the study (the number of sites is indicated in Figure 6.6). As expected, for N_2O concentrations there is no evidence of a country scale trend.

Figure 6.6. Total monthly concentrations from March 2002 to November 2003. Error bars represent the standard errors. The number of sites used for each period is indicated.

6.4.1 Spatial variation of N_2O concentration

The spatial variation of N_2O concentration is related to the very irregular spatial emission pattern, and therefore to the source types and to the atmospheric transport of the gas. The concentration distribution across the UK provides information about the influence on a large scale of the activities in the country and the impact of the weather on the diffusion of the gas in the atmosphere.

In Figure 6.7 the concentration distribution within the country in relation to the easting position of the sampling sites is shown. In the chart the points closer to the west coast have lower concentrations, whereas the sites towards the centre of the country have higher concentrations and widely spread in the scatter plot. Moving towards the east coast, concentrations slightly decrease again. This could be explained by the influence of clean marine air masses at coastal sites compared to trajectories from polluted terrestrial sources. The most frequent and strong westerly wind blowing over the UK can be the reason of lower concentrations on the west coast compared to the east. A few outliers and the sampling sites at the extremities are highlighted in the chart. The high concentration in Newton Westpark, Kimberworth Park and London, all urban sites, is mainly due to car traffic. In Auchencruive the sampling site is very close to grazing animals that contribute to increased N_2O emission. The soil compaction due to animals reduces the quantity of air available in it, facilitating the production of nitrous oxide via denitrification.

The bold line in Figure 6.7 (obtained using an inverse square smoother) shows a maximum average concentration of 330 ppb at about 300 km from the east coast, corresponding to an increase of about 11 ppb above the concentration of 319 ppb measured at the coast. In order to make a qualitative analysis of the network system a simple box model was used to estimate the N_2O flux needed to give such increase in N_2O concentration. Considering a box with a 500 km square base and height of 1 km, it is possible to simulate the air moving from the west coast towards inland (Figure 6.8). 1 km depth was chosen to allow for the air mixing within the boundary layer. A wind coming from west with a speed of 10 m s^{-1} was assumed. The flux responsible for the increase of 11 ppb in N_2O concentration after that the air travelled for 250 km inland was calculated to be about 0.9 μg N_2O m^{-2} s^{-1}, which is much larger than the

average emission obtained from the UK inventory (about $2 \cdot 10^{-3}$ μg N_2O m^{-2} s^{-1}). This suggests that the enhancement in concentration provided by using the network system could be overestimated. A reason for the overestimation could be that the measurement height (1.5 m) is too low and the air sampled is not well mixed within the boundary layer and it is highly influenced by sources in the vicinity of the sampling point. Also the measurements could be affected by the increase in atmospheric concentrations during the night, due to the nocturnal inversion and lack of air mixing. On the other hand, the box model used is very simplistic and limitations are due to the approximations applied. The height of the boundary layer was assumed to remain constant (z_i) and the air was considered to be well mixed within it. In this case the concentration increase with time was constant and given by:

$$\frac{\partial C(t)}{\partial t} = \frac{F}{z_i} \tag{6.1}$$

where the flux F is assumed to be horizontally homogeneous and constant. In practice the boundary layer depth is very variable between night and day as well as the mixing condition within it. For this reason the flux analysis discussed here is essentially a qualitative investigation.

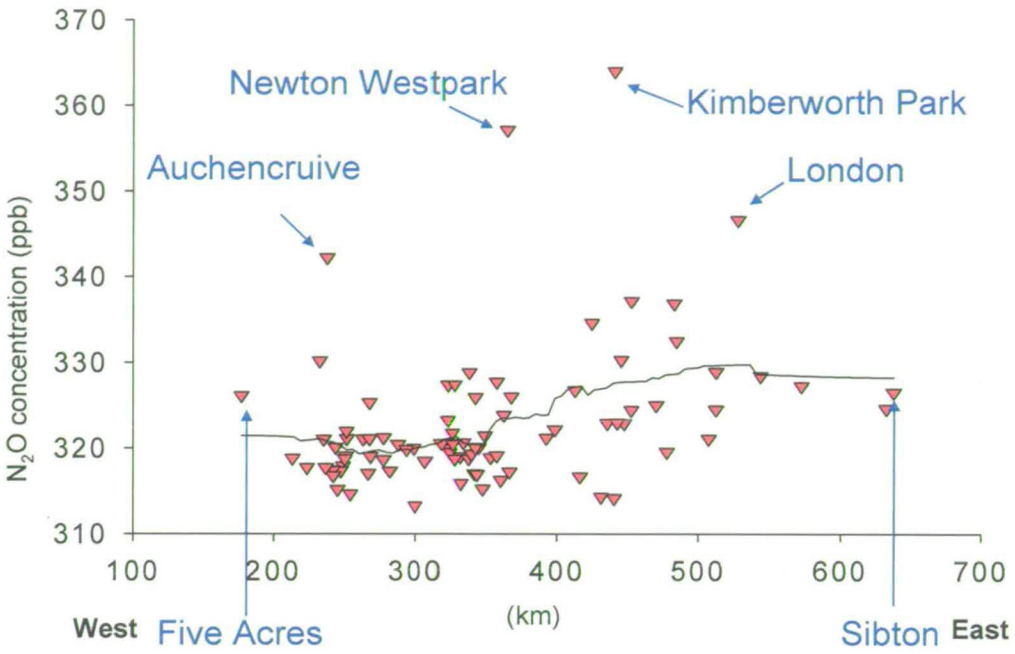

Figure 6.7 N_2O site averages over March 2002- November 2003 vs. easting length of the country. Some of the outliers are indicated as well as the most west point (Five Acres) and the most east one (Sibton). The bold line results from the application of an inverse square smoother (Sigmaplot 9) that uses a Cauchy function to weight the data..

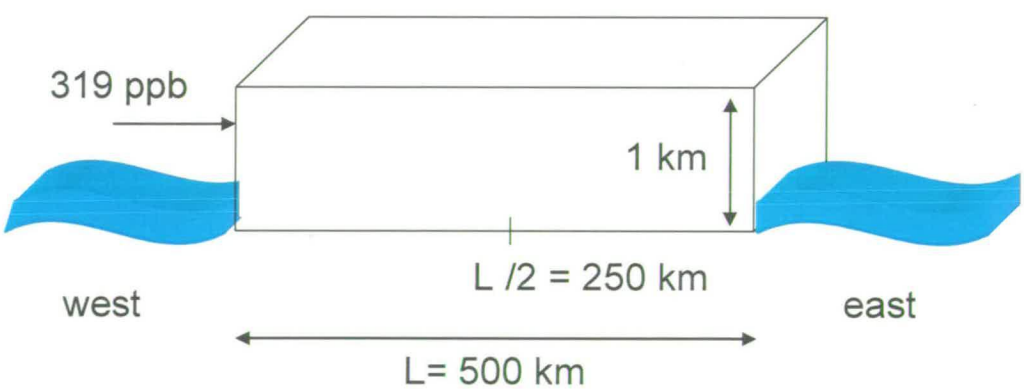

Figure 6.8 Scheme of a simple box model used to describe the mass of clean air (319 ppb of N_2O concentration) coming from the west coast towards land.

To study a bit further the spatial variation of N_2O concentration, site concentrations averaged over the period March 2002 - March 2003 were analysed. To compare values from the same category of N_2O source only sites from the National Network 'agricultural' and 'mixed' groups, Cumbria and Devon were considered.

N_2O concentrations averaged over the first year in the Cumbria cluster ranged between 316.8 ± 3.4 ppb and 325.1 ± 3.5 ppb, whereas in the Devon cluster they ranged between 314.6 ± 2.6 ppb and 324.8 ± 4.8 ppb. Concentration at the National Network sites varied more widely, ranging from 319.2 ± 3.3 ppb at High Muffles, located towards the east coast between York and Middlesbrough, to 332.5 ± 8.1 ppb in Marton Gainsborough, situated further south. The annual average value for Cumbria is 320 ppb and for Devon is 319 ppb, whereas for the National Network it is 324 ppb. Data from the National Network look more spread above the mean than data from the other two groups of sites. Figure 6.9, Figure 6.10 and Figure 6.11 show the deviation of the concentration of each site from the mean concentration of the network, respectively for Cumbria, Devon and National Network. The standard deviation from the mean is about 3.4 ppb for the National Network and about 1.9 ppb and 2.3 ppb for Cumbria and Devon, with a resulting variation of the concentration of 1.1%, 0.6% and 0.7% respectively. One reason that the concentration range varies less in Cumbria and Devon compared to the national network is the different spatial distribution of the monitoring sites. As it is shown in Figure 6.3, Cumbria and Devon sites are concentrated in small regions and consequently similarly influenced from sources. Furthermore, they will be subjected to analogous environmental conditions, such as temperature, rainfall and wind direction, that are fundamental keys for N_2O production and transport. On the contrary, national network sites analysed here, although of the same source types, are scattered over the entire country and influenced by extremely different situations contributing to N_2O emission.

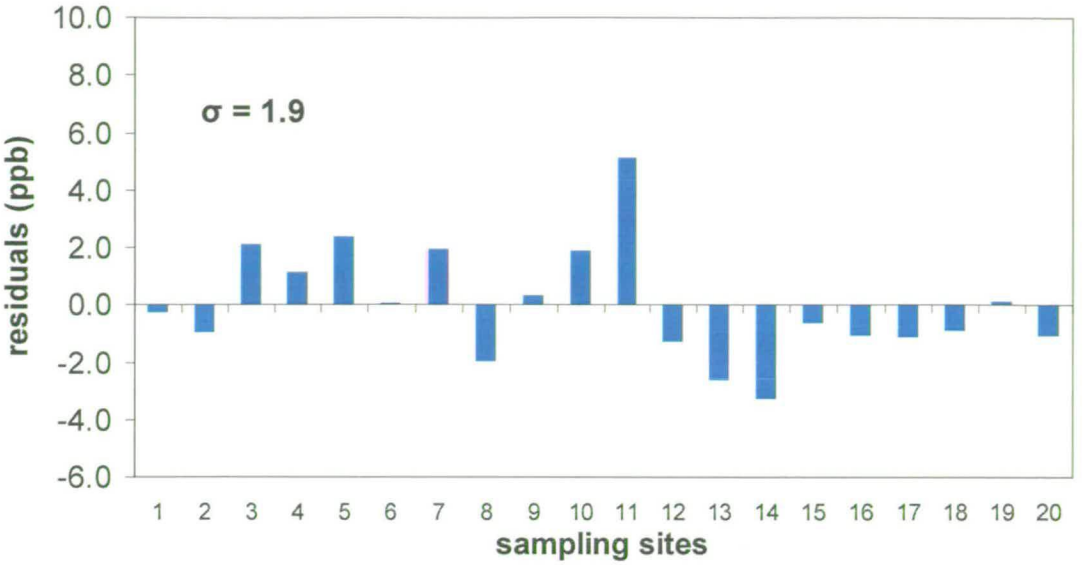

Figure 6.9. Residuals of N_2O concentrations from the Cumbria sites. σ represents the standard variation from the annual average for this category.

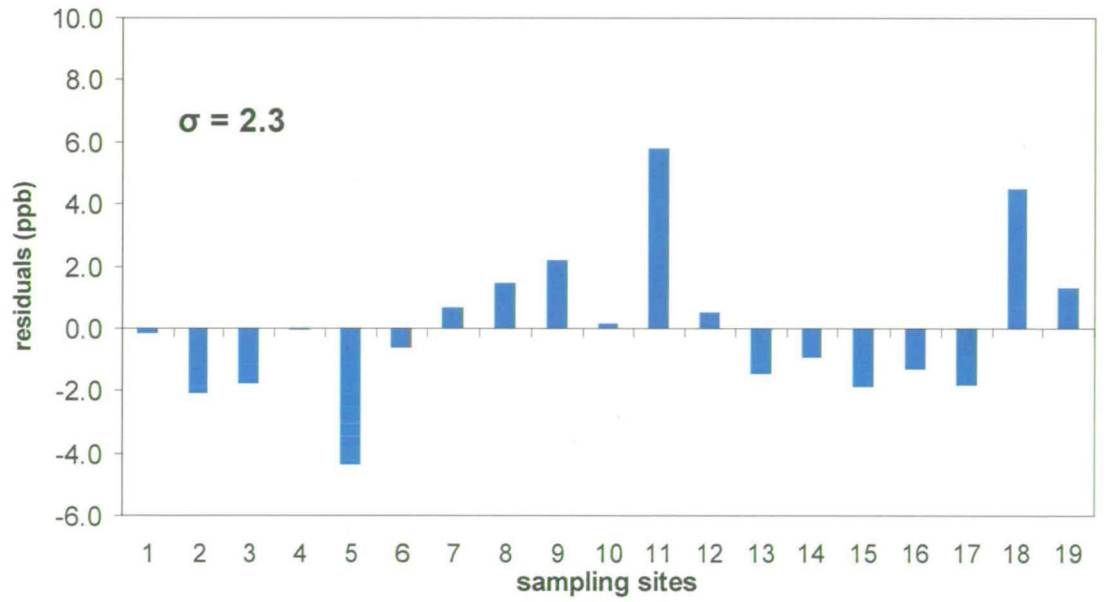

Figure 6.10. Residuals of N_2O concentrations from the Devon sites. σ represents the standard variation from the annual average for this category.

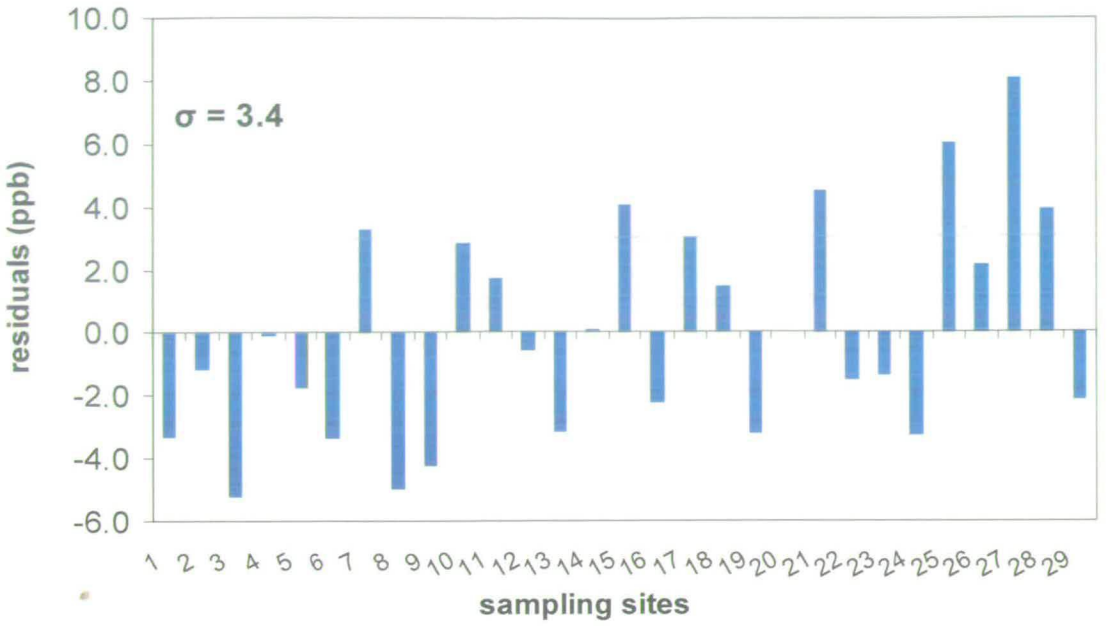

Figure 6.11. Residuals of N_2O concentrations from the national network sites. σ represents the standard variation from the annual average for this category.

The important role of location and distance between sites is taken in consideration again in a comparison of monthly N_2O values from a National Network site (Llyuphs Tower) located in Cumbria and total monthly averages from the Cumbria cluster of sites (Figure 6.12). A similar analysis was done for a National Network site situated in Devon (North Wyke) and monthly averages for the Devon network. Charts show concentrations with standard error bars. As expected, in most of the cases the error bars of the two series overlap or they differ very little. The fact that the concentration in Llyuphs Tower and the Cumbria concentrations are in agreement (correlation = 0.94) suggests that N_2O concentration in Cumbria is well represented from results of the network system. For Devon and North Wyke the accord is less clear, but still noticeable (correlation = 0.61).

This comparison suggests that the monitoring system adopted is able to detect the variation in concentration caused by spatial differences.

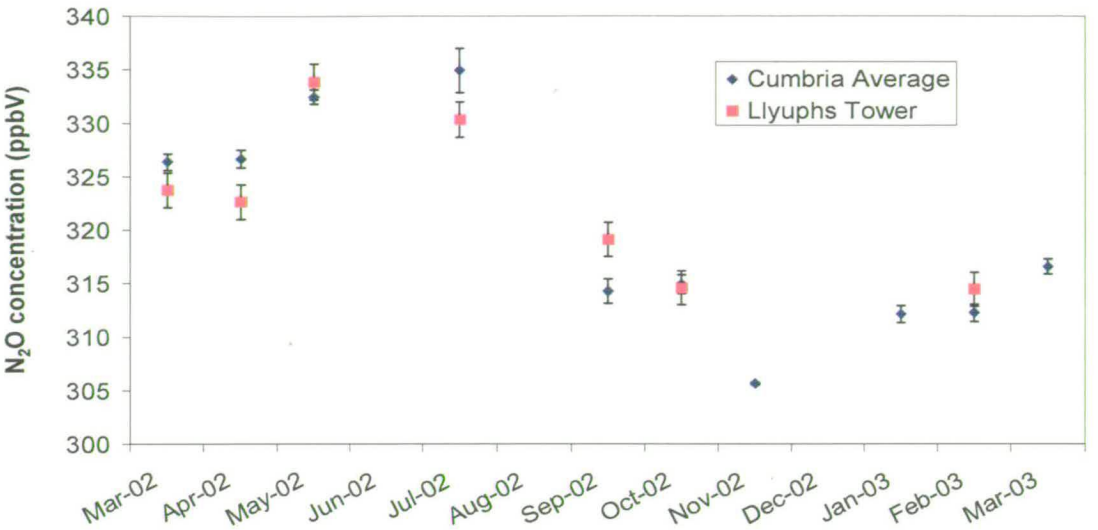

Figure 6.12. Comparison between N_2O concentrations in Llyuphs Tower (national network) and monthly average concentration from Cumbria network. Error bars for Cumbria's values represent the standard error and for Llyuphs Tower they represent the 0.5% error on the concentration measurement.

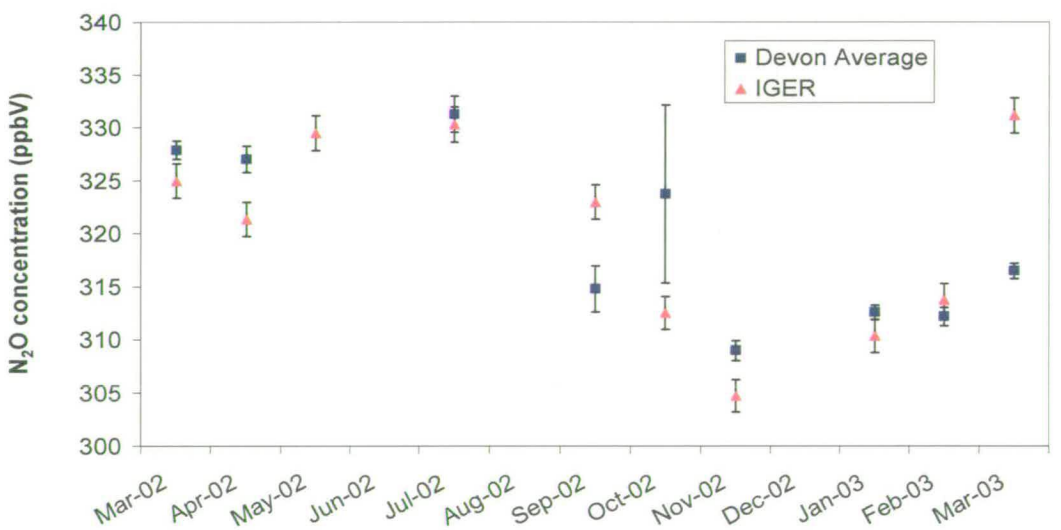

Figure 6.13. N_2O concentration in North Wyke (national network) and monthly average concentration from Devon network. Error bars for Devon's values represent the standard error and for North Wyke they represent the 0.5% error on the concentration measurement

6.4.2 Inter-annual variation in N_2O concentration

Meteorological conditions play a significant role in controlling processes for N_2O emissions and in the context of inter annual comparison it is fundamental to analyse similarities and differences between the two years. 2002 was less warm than 2003 during the summer, but the opposite situation occurred during the winter (Figure 6.14). There was a large difference between the two years in respect of rainfall. Figure 6.15 shows that 2003 in the UK was drier than 2002, especially in February, August, October and November. Statistics showed that 2003 was the driest of the last 40 years in the UK (data obtained from Met Office annual reports).

Another fundamental variable that controls the gas diffusion in the surface layer of the atmosphere is the wind. The wind speed did not vary significantly between the two years with differences of less than 0.5 m/s for the same months in 2002 and 2003. The only exception was February, when the monthly wind speed was 7.2 m/s in 2002 and 5.1 m/s in 2003. For February 2002 the only data available were from Cumbria and Devon sites and comparing them with concentrations in February 2003 no relationship was found with the monthly national wind speed. As a consequence, we could not relate discrepancies between concentrations in the two years with variations in wind speed.

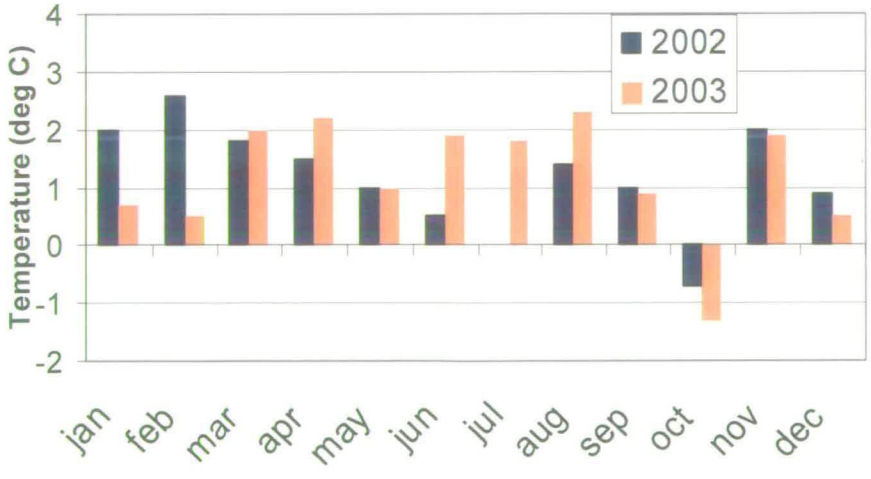

Figure 6.14. UK temperature anomaly data for 2002 and 2003. Zero is the normal value calculated as an average from 1961 to 1990 (from Met Office annual reports).

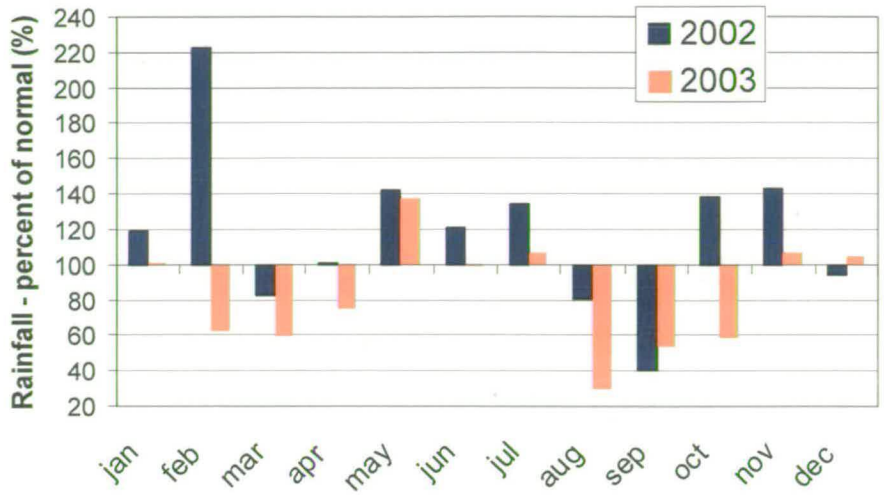

Figure 6.15. UK rainfall data for 2002 and 2003. 100% is the normal value calculated as an average from 1961 to 1990 (from Met Office annual reports).

The direction of the wind plays an important role on the monitoring N_2O concentration in the UK (Simmonds et al. 1996; Derwent et al. 1998). Previous studies (Derwent et al. 1998) showed that the baseline concentration at Mace Head, which is a research station on the western coast of Ireland, ideally located for measuring background concentration, was different depending on the wind sector of provenance of the air masses. Concentration measured in air masses coming from over polluted European continental areas was about 2 ppb higher than the one in air coming from the North Atlantic Ocean. In our study it was not possible to detect such differences, mainly because monthly samples are less adequate for this purpose than the weekly ones used in the cited study, and because wind data were not always available at our measurement sites.

Figure 6.16 shows the annual pattern of average N_2O concentration for the national network sites, Cumbria and Devon in 2002 and 2003. Values averaged over all the sites for each month are considered. N_2O concentration seems to be slightly higher in 2003, although the number of months missing could lead to an inappropriate conclusion. Concentrations look quite similar in spring and summer with differences ranging between 3 and 7 ppb, but in evident disagreement in October and November when the difference goes up to 23 ppb. This could be an effect of the difference in rainfall for those months, already highlighted in Figure 6.15.

In Figure 6.17 monthly wind speed and N_2O concentration for 2003 are shown in the same chart. The concentration increase during some of the summer months could be related to the low wind speed, typical of this period of the year, but not all the months with low wind speed showed a coincident high concentration. In September, for example, although the monthly averaged wind speed was still quite small, N_2O concentration decreased by almost 30 ppb. This suggests that other variables are involved. The high N_2O concentration in August 2003 corresponds to a high rainfall deficit for the same month (Figure 6.15) and it seems better correlated with the wind speed (Figure 6.17). No further explanation could be found for such high concentration in a very dry month. Figure 6.18 shows the relationship between monthly enhancements above N_2O background concentration (used a value of 315 ppb) and monthly wind speeds at country scale for 2002 and 2003. Although the regression poorly represents the data ($R^2 = 0.2$, $N = 17$, $p > 0.05$), it confirms the decrease of N_2O concentration with the increase of wind speed. An analysis on few days of N_2O concentration data measured at Easter Bush field site in July 2002 during the eddy covariance measurements (TDL operating at 10 Hz) (see Chapter 5), was made to better illustrate the relationship between the concentration and wind speed. Figure 6.19 shows the logarithmic decline of the variation of N_2O concentration (ΔN_2O) above a baseline concentration obtained with the minimum concentration values in those days, with the increase of wind speed (at 2.5 m height). Changes in wind speed often occur between day and night. At night the wind speed decreases and the condition of atmospheric stability causes a rise in concentration. During the day the decrease in concentration is mainly caused by the higher wind speed and unstable condition. Figure 6.20 shows a 2 day-example (2-3/07/02) where the ΔN_2O in atmospheric stable condition ($L > 0$) is generally greater than for unstable condition ($L < 0$). Although the influence of the wind speed on N_2O concentration is stronger in daily patterns (Figure 6.19) than for annual patterns (Figure 6.18), it is still possible to observe the wind influence in inter-annual differences in concentration. Also, the phenomenon of variation in concentration and wind speed between day and night could contribute largely to increase the concentration sampled continuously for a month at the network sites.

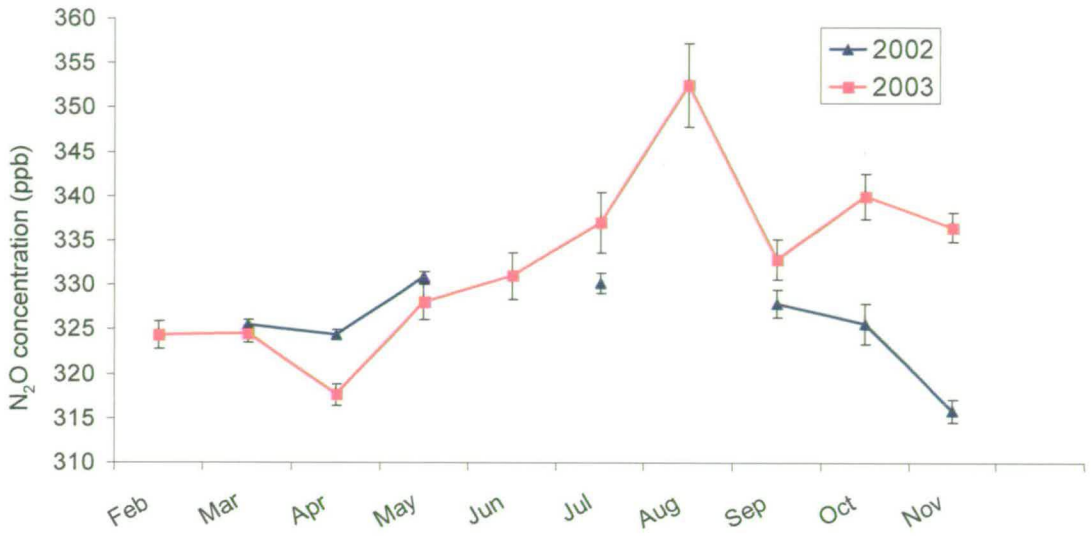

Figure 6.16. Comparison of the monthly N_2O concentrations for 2002 and 2003 in the 13 national network sites active for the entire period and Cumbria and Devon sites. Error bars represent the standard errors.

Figure 6.17. Monthly N_2O concentration and wind speed in 2003.

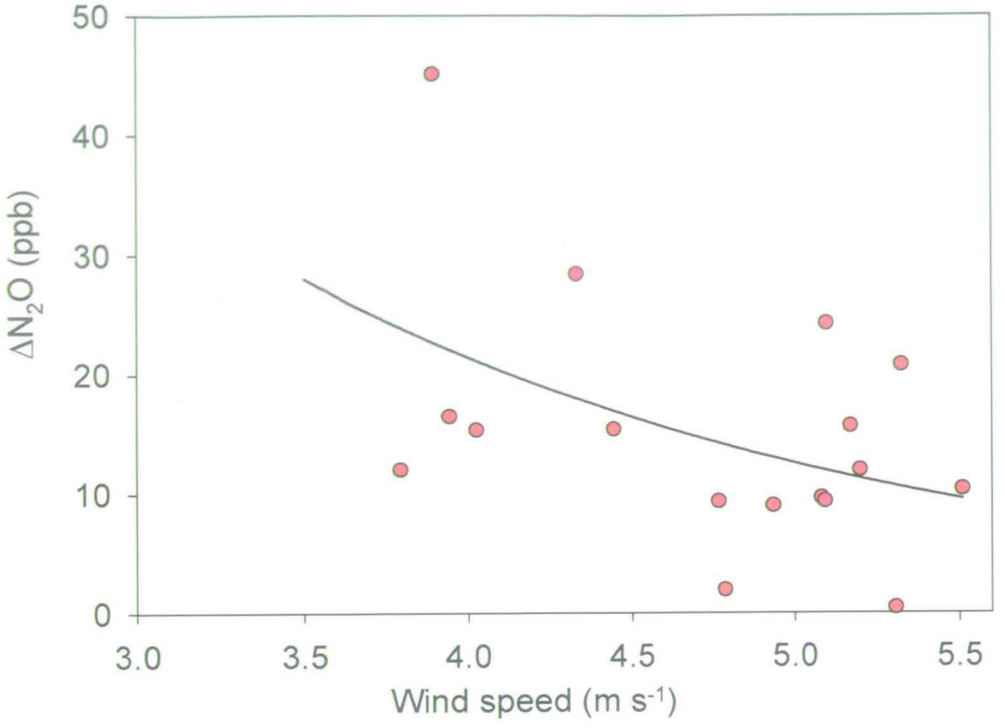

Figure 6.18 Enhancement of monthly N_2O concentrations for 2002 and 2003 above a background concentration of 315 ppb of N_2O plotted against the monthly wind speed for the whole country (R^2=0.2 p > 0.05).

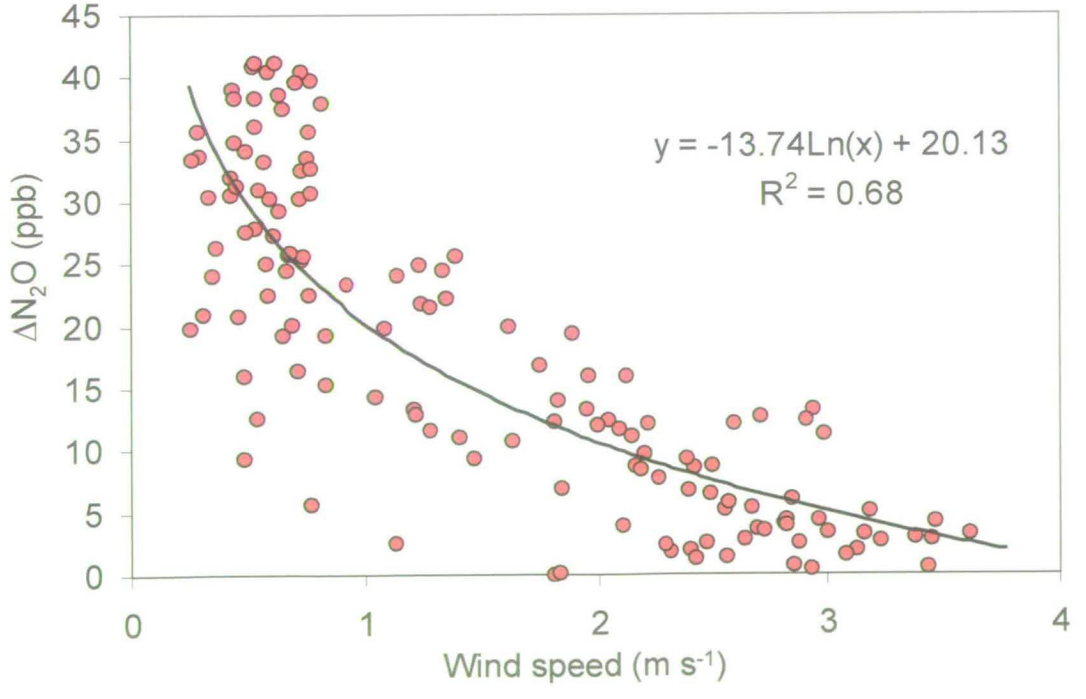

Figure 6.19 Variation of N_2O concentration (ppb) measured at Easter Bush field site (15 min average) from 3/07/02 to 5/07/02 versus wind speed (m s^{-1}). The variation in concentration was calculated above a baseline calculated with the minimum concentrations in those days.

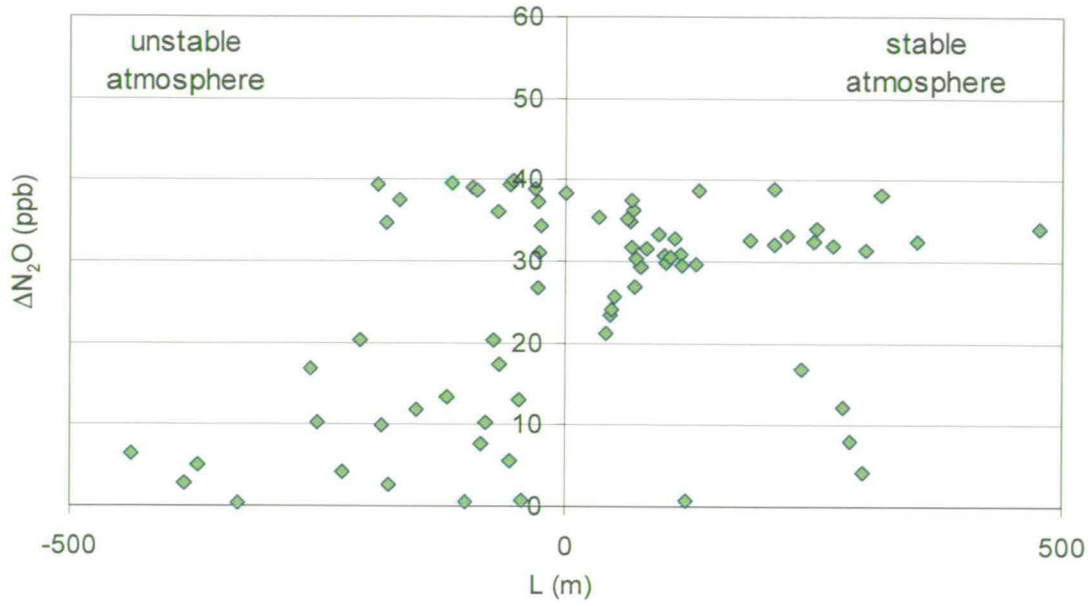

Figure 6.20 ΔN_2O in relationship to the atmospheric stability parameter L (Monin-Obhukov length).In stable atmosphere (L> 0) ΔN_2O is generally higher than in unstable condition ((L< 0).

In Figure 6.21, the sites from the National Network are divided by type of source, and the annual concentration for each site is plotted in different colours for 2002 and 2003. In general N_2O concentrations from mixed sites are higher than from agricultural ones, but still very comparable. For example, the 2002 annual averages for agricultural and mixed sources were respectively 324 and 325 ppb, whereas in urban centres annual concentrations were higher than mixed sites (335 ppb in 2002). For most of the sites monitored during both years, 2003 concentrations were higher than in 2002 with some exceptions in the agricultural sites. In two of the agricultural sites, High Muffels and Firwood Llyclys, and in Edinburgh the two annual concentrations were almost the same or within the error bars. In Llyclys Tower (agricultural site) and Woodbastwick (mixed site) 2003 concentration was lower than in 2002, but in the rest of the network sites N_2O concentrations in 2003 were higher than in 2002. This is in agreement with the monthly pattern for the two years shown in Figure 6.16. Although the small number of sites available for each category does not allow extrapolating this particular behaviour to a national one, this study provides a picture of the changes of N_2O atmospheric concentration around the country in a 2-year period. Mixed and agricultural sites did not always show a clear difference in

concentration pattern, which may be because in some of the mixed sites it is difficult to distinguish the most influential source.

It is interesting to notice that London had the largest concentration in both years with a very small variation (error bars in Figure 6.21). This indicates that the concentration in London remained high during the year unlike in Auchencruive and Alice Holt where annual 2003 concentration was high but with a wide variation due to some high monthly peaks. The variation of N_2O monthly concentration with the wind speed in London is shown in Figure 6.22. The clear decrease of concentration with the increase in wind speed ($R^2 = 0.5$, N = 7, $p > 0.05$) highlights the important role of wind in the gas diffusion in the surface layer of the atmosphere. Already discussed in Figure 6.18, the effect is more evident and significant for urban sources.

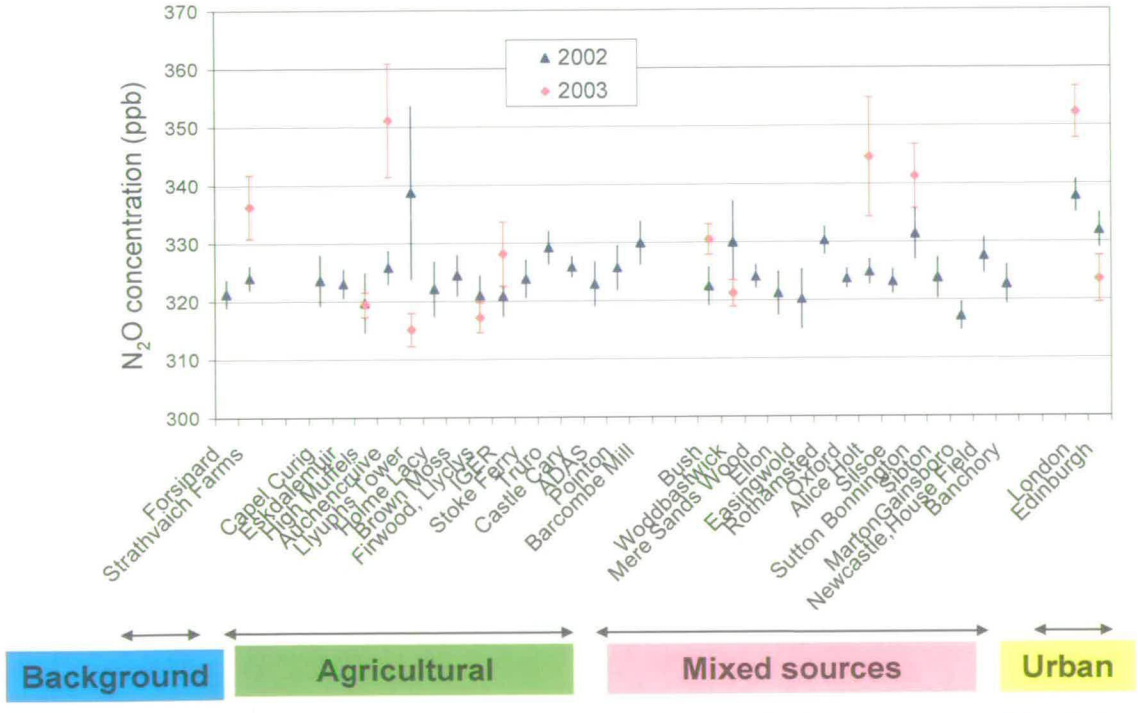

Figure 6.21. Nitrous oxide annual concentrations for all sites divided by source type. Blue dots represent 2002 concentrations and the red ones represent 2003 concentrations. Error bars represent the standard error for the annual mean value.

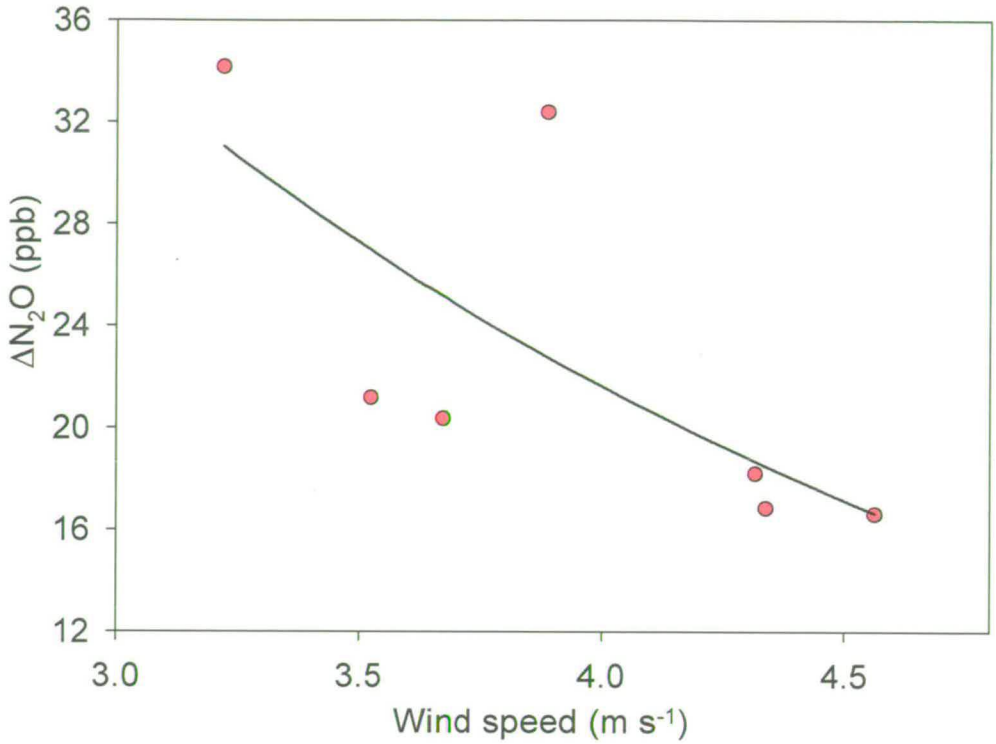

Figure 6.22 Monthly enhancement (ΔN_2O) above N_2O background concentration (set as 315 ppb) plotted against the monthly wind speed in London for 2002 ($R^2 = 0.5$, N = 7, $p>0.05$).

6.4.3 N_2O concentration in the atmosphere and type of N_2O sources

As mentioned above, in 2003, data from sites of mixed and urban type were available from a parallel project. Including these data in the mixed and urban categories, the number of sites will increase as well as the reliability of the results. In Figure 6.23 the number of urban sites is raised from 2 (Edinburgh and London from national network) to 11 and the mixed ones increased from 5 to 8. This will provide a more consistent picture of the annual urban emission cycle. Comparing the obtained plot containing monthly concentrations for each category, Figure 6.23, with a similar chart considering only the national network sites for the same period Figure 6.24 an analogous pattern can be observed. Although in the newly obtained chart the data are less spread than in the one in Figure 6.24 the main features of the plot are maintained.

In the annual pattern for 2002 and 2003 (respectively Figure 6.25 and Figure 6.23- Figure 6.24) urban concentrations have the highest values during the winter, then becoming close to the mixed and agricultural ones during the summer months,

from May to July. On the other hand, mixed and agricultural concentrations increase in May when the agricultural and live stocking activities start; they have their maximum peak in the summer (in August for 2003) and then decrease slowly in autumn.

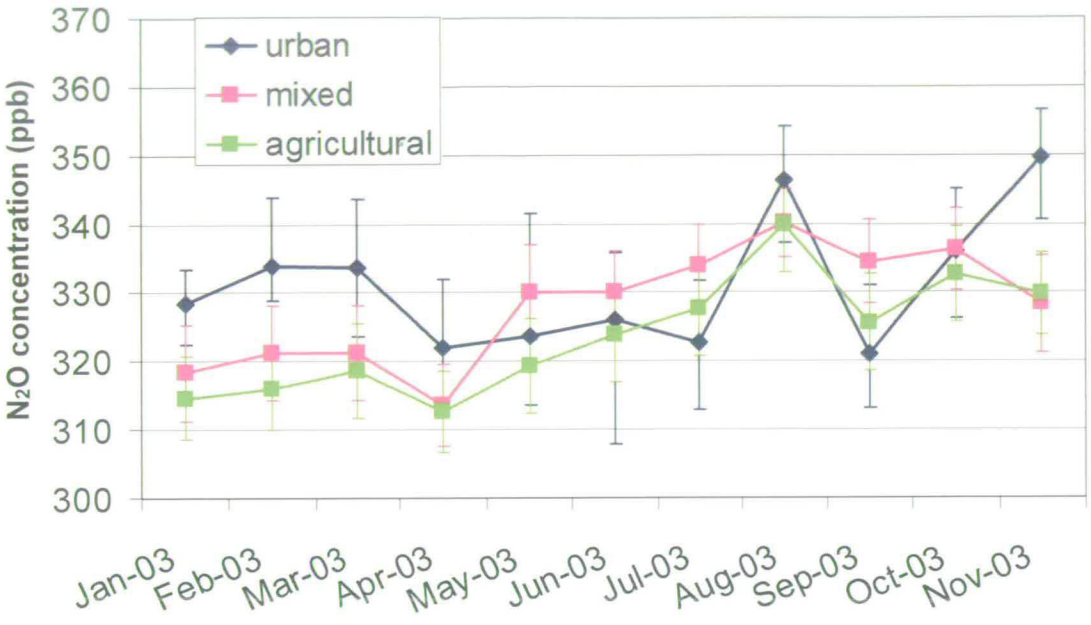

Figure 6.23. N_2O monthly concentrations for 2003. National network sites and mine project sites.

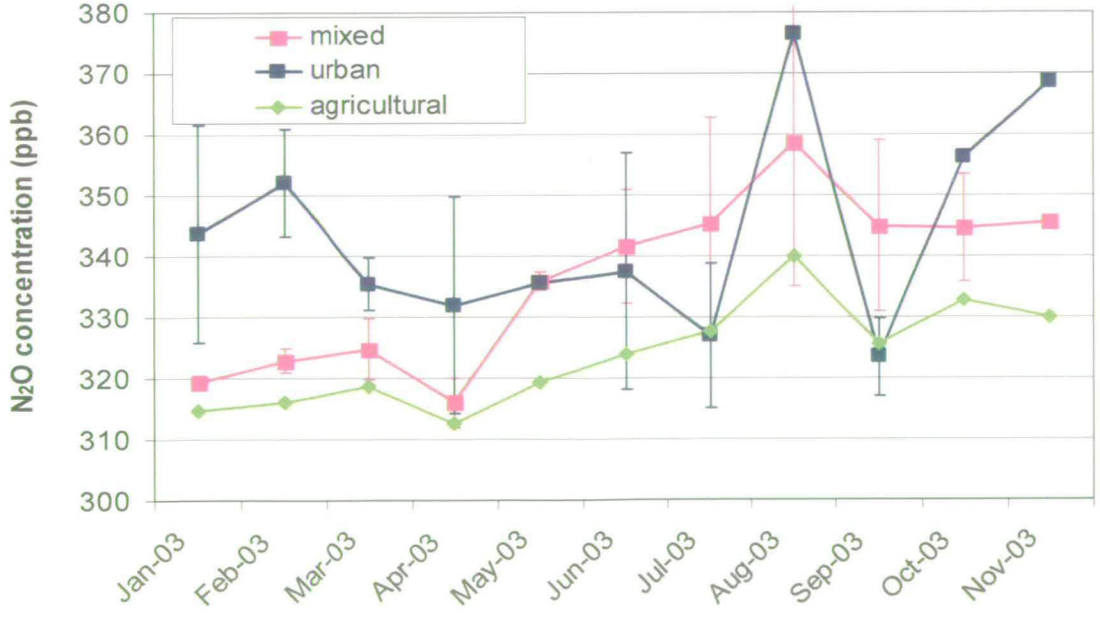

Figure 6.24. N_2O monthly concentration for 2003 in the national network sites

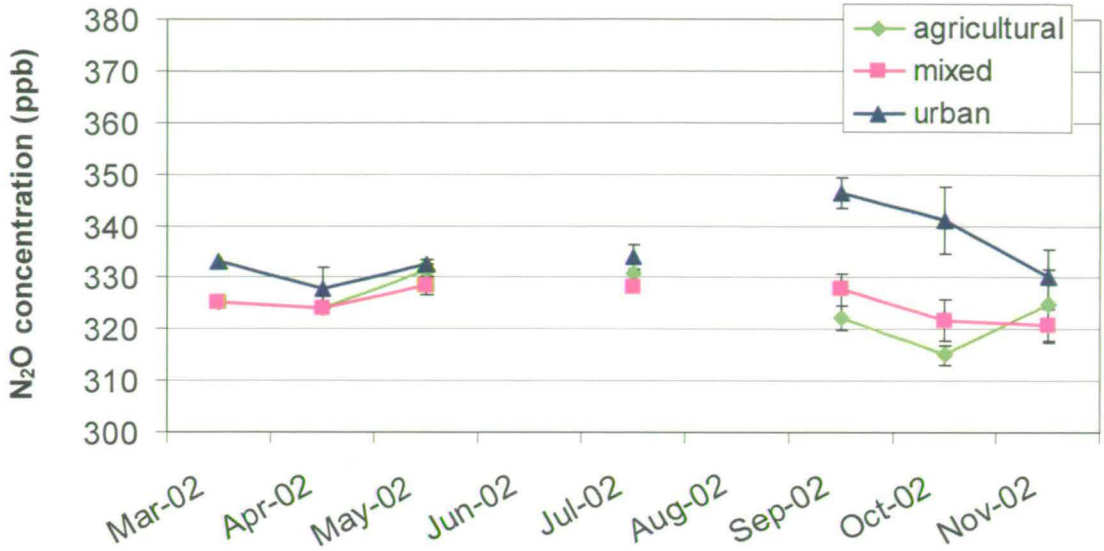

Figure 6.25. N_2O monthly concentrations in 2002 in the national network sites.

6.4.4 Effect of temperature and rainfall

Meteorological conditions are important regulators of N_2O emissions. The different combinations of rainfall, air temperature, nature of the soil and treatments applied to it lead to very different emissions. It is evident that these factors are more important for agricultural and mixed sources than for the urban ones. For some of the sites of the national network, monthly temperature and rainfall data available from meteorological stations run by the Met Office were compared with concentration measurements. Monthly rainfall values were calculated considering the rain which fell in the last 15 days of the previous month and the rain which fell in the first 15 days of the month analysed. So, for example to calculate March rainfall the last 15 daily rainfall values of February and the first 15 daily values of March were considered. The reason why this method was used is that N_2O emission depends on the wetness of the soil (Robertson 1994; Smith et al. 2003) and so is more likely to be due to recent rainfall events .

In most of the cases temperature seems to control the emissions, but for some of the sites, when the temperature is not directly correlated, rainfall correlates with the concentrations. For example, in the Bush site, a predominantly agricultural location with a few busy roads surrounding, N_2O concentration was correlated with

temperature with a coefficient R^2 of 0.41% (p = 0.006), but including the rainfall as a predictor variable in the regression the correlation coefficient increased up to 60% (p = 0.002) (Table 6.3). 2002 N_2O concentrations and the temperature pattern in the Bush site are shown in Figure 6.26. Sutton Bonington is also an agricultural site as well, with characteristics very similar to Bush site. From Figure 6.27 and Figure 6.28 it is possible to notice that in this case variation in N_2O concentration are in agreement with the temperature pattern in September, October and November 2002 and from April to November 2003, but rainfall seems to be well correlated with N_2O from January to May 2003. North Wyke is mainly a livestock dominated source in the south west of the country. In this case the concentration was better related to temperature during the 2002, but from April 2003 rainfall was in good correlation with the concentration.

In order to estimate a correlation between N_2O concentration, temperature and rainfall a multiple regression was used of the type:

$$Y = \beta_0 + \beta_1 X_1 + \beta_2 X_2 + \varepsilon$$

where Y is the response (N_2O concentration), X_1 and X_2 are the predictors variables (temperature and rainfall), β_0, β_1 and β_2 are the regression coefficients and ε is an error term. Table 6.3 contains the results obtained for sites of different nature. Although only a small number of sites were provided with rainfall and temperature data, the regression gave information on the relationship between the three variables in different conditions of emission source. As expected, nitrous oxide concentrations in agricultural and mixed sites were better correlated than urban ones with the two meteorological variables, with R^2 coefficient ranging from 32% to 81% compared to 1-2% for the cities. This confirms the importance of environmental conditions in determining N_2O emissions from agricultural sources. It should be noted, however, that the response of agricultural site to rainfall depends on the initial wetness of the soil. The fact that the main source of N_2O emission in urban environments is the traffic of vehicles fitted with catalytic converters and the very poor correlation between urban concentrations and rainfall and temperature, the factors primarily controlling N_2O emission from soil, indicates that N_2O in urban environments is more influenced by traffic rather than these meteorological parameters.

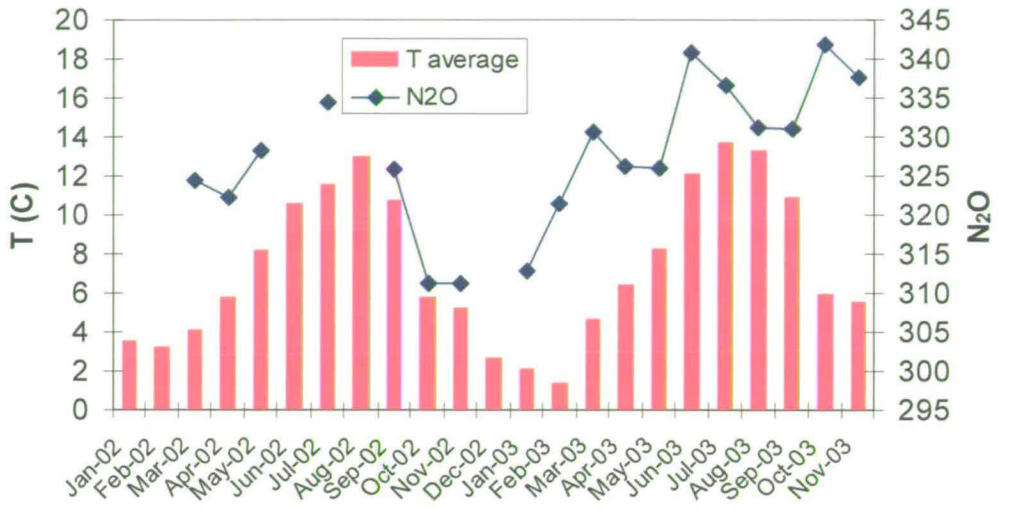

Figure 6.26. Bush site. Temperature and N_2O concentration for 2002 and 2003.

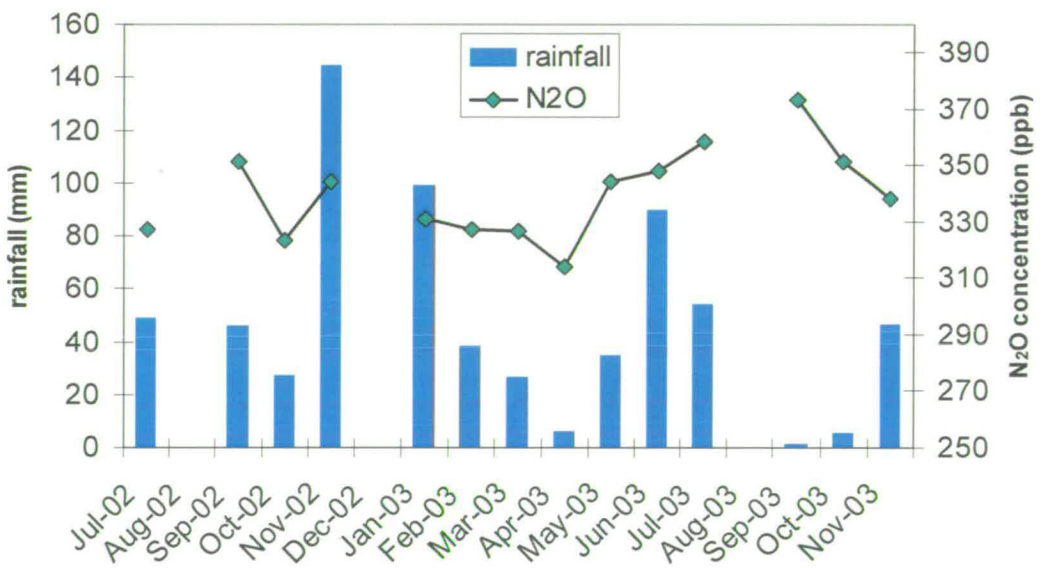

Figure 6.27 Sutton Bonington. Rainfall and N_2O concentration for 2002 and 2003.

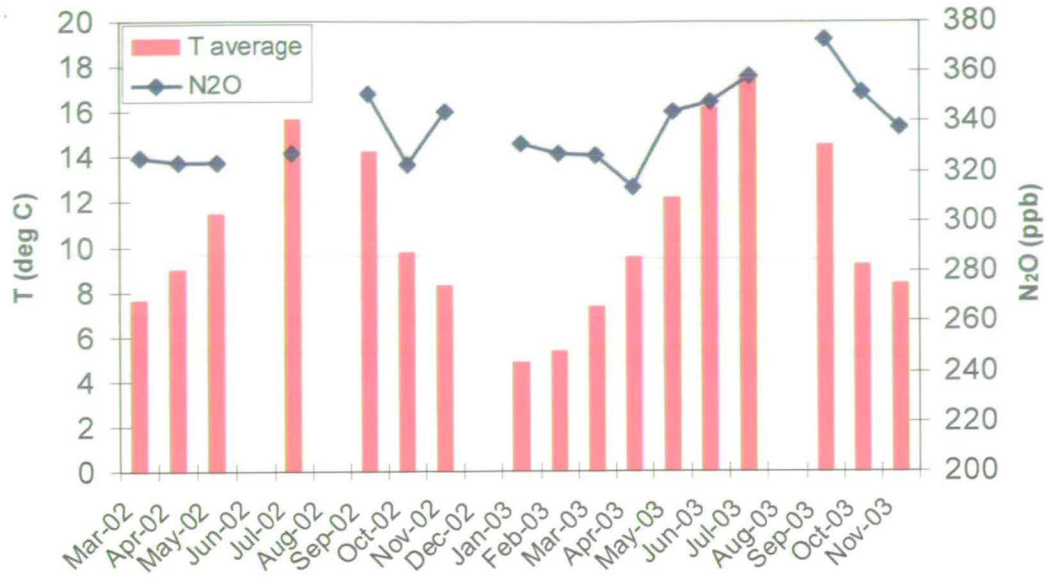

Figure 6.28. Sutton Bonington. Temperature and N_2O concentration in 2002 and 2003.

Table 6.3. Results from a multiple regression between N_2O concentration, temperature and rainfall for some sites of different nature of source. R^2 represent the coefficient of correlation and is the proportion of variability in the concentration accounted for by the predictors (rainfall and temperature). βT and βrainfall are the regression coefficients for temperature and rainfall respectively. N is the number of points used for the regression. The p-value gives information about the significance of the regression ($p<0.05$).

Type of dominant source	Site name	R^2	βT	βrainfall	N	p
Mixed	Rothamsted	81%	0.508	0.121	8	0.015
Mixed	Bush	60%	1.39	- 0.088	17	0.002
Mixed	Sutton Bonington	46%	2.74	0.032	13	0.045
Mixed	Oxford	32%	0.474	0.044	10	0.253
agricultural	North Wyke	51%	2.29	0.128	17	0.010
agricultural	Brown Moss	49%	0.344	- 0.117	7	0.263
agricultural	Capel_Curig	45%	0.637	- 0.172	9	0.166
agricultural	Eskdalemuir	34%	0.843	- 0.021	10	0.238
Urban	Edinburgh	1%	0.31	0.009	10	0.951
Urban	London	2%	-0.01	0.051	18	0.883

6.5 Conclusions

The study presented can be used as a first step to improve a monitoring network at large scale and subsequently to promote similar greenhouse gas monitoring networks at national scale in other countries.

The system is able to detect spatial variations in N_2O atmospheric concentrations confirming that they vary quite widely across the country and less broadly in localized networks such as Cumbria and Devon. Nevertheless, the national network is able to describe seasonal variations of the concentration when tested on specific points (Figure 6.12 and Figure 6.13) and compared with the more consistent Cumbria and Devon networks data. However, measured enhancements in concentrations over the atmospheric background (319 ppb) could be overestimated (Section 6.4.1). In fact, the additional average emission responsible for these enhancements as calculated from measured concentrations was much larger (0.9 μg N_2O m^{-2} s^{-1}) than the value obtained from the UK inventory (~$2 \cdot 10^{-3}$ μg N_2O m^{-2} s^{-1}). Improvements could be obtained increasing the measurement height (currently of 1.5 m) to allow a better air mixing in the boundary layer and to avoid the high influence of sources in vicinity of the sampling point. The bias introduced by including nocturnal samples characterised by high concentrations could be removed with a conditional sampling protocol to exclude stable stratification of the atmosphere, or simply sampling only by day. Alternatively, the nocturnal bias could be isolated in the data processing phase with an analysis of the monthly wind speed data for each site. Rejecting the months with average low wind speed could provide a criterion to avoid the influence of nocturnal high concentrations. A limitation of this method is the restricted availability of wind data for the sampling sites. The implementation of meteorological stations in sites where there is no coverage of data from Met-Office sites could be a solution to this problem, but it would increase the cost of the system.

When inter-annual differences are analysed, 2003 N_2O concentration were mainly larger than in 2002, both in national monthly averages and annual averages by site (Figure 6.16 and Figure 6.21). A relation between the differences in monthly concentrations for 2002 and 2003 at national scale and rainfall seems to occur (Figure 6.15 and Figure 6.16). For this reason a more detailed investigation for a few sites, including mixed, agricultural and urban types of source, was carried out (see

Section 6.4.4). Results showed that correlation of N_2O concentration with rainfall and temperature was large for mixed and agricultural types of source and almost non-existent for cities (Table 6.3), indicating different controls on urban concentration.

This study highlighted the importance of urban contributions to atmospheric N_2O concentration, especially with London that had the highest concentration in both years. The seasonal pattern of concentrations sorted by source type showed again significant values of urban concentrations during the year (Figure 6.23 and Figure 6.25).

Data from this type of monitoring network can be used to validate models and to assess changes in emission factors in inventories. In this case a comparison of the results from the national network with an atmospheric transport model (FRAME) will be described in Chapter 7.

Chapter 7 Comparison with the FRAME model

7.1 Introduction

The high spatial and temporal variability of N_2O emissions (see Chapter 2) represents one of the main problems in the production of accurate emission inventories, obtained from emission factors or regression models. The monitoring system described in Chapter 6 is a valuable tool to monitor N_2O concentrations at country scale but also provides data to validate emission inventories using atmospheric transport models. In this Chapter the N_2O concentrations measured at the national monitoring network shown in Figure 6.3, already presented in Chapter 6, are compared with concentrations modelled with a Lagrangian atmospheric transport model that uses as input the N_2O emissions estimates obtained from a disaggregated spatial inventory for the UK (Sozanska 1999; Skiba et al. 2001). The model is called FRAME: **F**ine **R**esolution **A**tmospheric **M**ulti-pollutant **Ex**change (Singles et al. 1998; Fournier et al. 2004). FRAME is a statistical Lagrangian model that simulates a stratified column of air, traversing a grid over the UK, in a series of straight line independent trajectories. From a first sequential version, processing only one trajectory at a time over Great Britain (Singles 1996), the model was further developed to cover the area of the British Isles (including Northern Ireland and Eire) and a parallel version was implemented (the different trajectories were distributed over 128 processors) with a resultant speed-up factor of 69 for the simulation time (Fournier et al. 2002). The model was used initially to assess the long-term annual mean NH_3 surface concentrations and NH_x (NH_3 and NH_4^+) wet deposition over the British Isles (Singles et al. 1998). Further developments of FRAME included increasing the angular resolution of the trajectories from 15° to 1° and the inclusion of point source emissions of sulphur dioxide (SO_2) and oxidised nitrogen (NO_X) from elevated stacks (Fournier et al. 2004). This resulted in a more robust multi-species model that was able to accurately represent the behaviour of sulphur and oxidised nitrogen as well as reduced nitrogen. In addiction, a new orographic

precipitation scheme was introduced in the model to improve the representation of the wet deposition (Fournier et al. 2005).

FRAME has been successfully used to study NH_3 deposition and concentrations in Scotland (Sutton et al. 2004b) and to investigate variation in atmospheric gas concentrations (NH_3, N_2O, CH_4) due to the reduction of livestock in the UK following the foot and mouth disease (Sutton et al. 2004a). FRAME has been used to simulate the dispersion and deposition of heavy metals (McDonald et al. 2002).

7.2 FRAME

7.2.1 Model description

The FRAME domain covers the British Isles (in the application presented here only Great Britain is taken into consideration) with a resolution of 5 km × 5 km square grid. High vertical resolution near the ground is provided by a multi-layer structure (33 layers) with a variable depth ranging from 1 m in the bottom layer to 100 m in the top layer (Fournier et al. 2004). Vertical mixing is analysed with the *K*-theory eddy diffusivity, with the exchange of material between layers calculated using the equation:

$$\frac{\partial c}{\partial t} = \frac{\partial}{\partial z}\left(K_z \frac{\partial c}{\partial z} \right) \qquad (6.1$$

Where c is the concentration of the component analysed and K_z is the vertical diffusivity and depends on the atmospheric stability (Pasquill 1961) and height.

The diffusion equation is solved using a Finite Volume Method. Individual trajectories are initiated at each edge grid cell and advected across the model domain until they exit the area of simulation. Since N_2O is generally not involved in chemical reactions in the low atmosphere and it is an insoluble gas, wet deposition was assumed to be zero and no gas phase chemical reactions were included in the calculation. Dry deposition to the surface was also considered to be zero. Thus, in the present study the model simulation was reduced to a simple representation of horizontal advection and vertical dispersion. A diurnal variation of the height of the mixing layer is included in the model. The starting times of trajectories at the edge of the model domain are cycled forward by six hours from one trajectory to the next.

The vertical diffusivity, K_z increases linearly up to a specified height, H_z, and then remains constant up to the top of the boundary layer. During the daytime, the diffusivity parameters K_z and H_z are parameterised with the boundary layer mixing height and the geostrophic wind speed to represent a combination of mechanical and convective mixing. At night time, the diffusivity parameters are determined with the geostrophic wind-speed and the Pasquill stability classes (Singles 1996).

A wind frequency rose is used to weight the trajectories according to their relative directional frequency and a wind speed rose to allocate a suitable wind speed to each trajectory direction. These were generated using radiosonde data from operational radiosonde stations in 4 different geographical locations in the British Isles: Camborne (south-west England), Hemsby (east coast of England), Stornoway (north-west Scotland) and Valentia (on the west coast of the republic of Ireland). The data, available in electronic format at the British Atmospheric Data Centre, covered a ten-year period from 1991 to 2000. To avoid strong influences by surface friction effects, an appropriate vertical layer at which to extract wind data was found to be the 950-900 hPa pressure level (approximate altitude layer 500-900 m.a.s.l). The wind speed rose used in FRAME was generated from the harmonic mean of the directionally dependent wind speeds (Vieno 2005).

The model uses a fine angular resolution of 1^{o} between trajectories. A total of 120, 000 trajectories are included in a single simulation. The model code is written in High Performance Fortran and executed on a Beowulf Linux cluster comprising 60 dual 1.0 MHz Intel Xeon processors. The run time for a single simulation is approximately 25 minutes with all processors employed.

7.2.2 Model input

Emissions for N_2O were provided by a spatially disaggregated inventory of N_2O emissions for each 5 km × 5 km grid-square, which was created for the NERC GANE programme(Skiba et al. 2005) and refers to emissions from Great Britain in 2002. The inventory includes the main sources of N_2O. Soil emissions were calculated using a multi linear regression equation from the parameters: N input, soil water content and soil temperature (Sozanska et al. 2002; Dragosits et al. 2005). Strengths of emissions from industry, transport, rivers, estuaries, atmospheric N deposition and livestock were calculated as advised by DEFRA and the IPCC (IPCC

2001b). A summary of the N_2O annual emissions from the UK used as input is presented in Table 7.1. It was assumed that emissions from rivers, estuaries, atmospheric N deposition, livestock and soil emissions were released into the lowest vertical layer of FRAME (1-2 m). Within the category of industrial emissions 10 plants were treated as point sources with known stack parameters and the remaining industrial discharges was released and diffused into several layers (1-50 m in one run of the model and 1-6 m in another run) (see Table 7.2). Traffic emissions were treated differently in several runs, released at 1 - 2 m in one case and at 1-6 m in another (Table 7.2). For the emissions of N_2O from the 10 industrial plants, stack parameters were available for three plants (data supplied by Dr Keith Vincent, NETCEN, AEA Technology). For the remaining seven point sources, default stack parameters were used for the plume rise calculation in the model (stack height 160 m, exit velocity 16 m s^{-1}, exit temperature 150°C, stack diameter 5 m). A description of the stack parameters and annual emission estimates for the main industrial plants is given in Table 7.3.

Since the exercise proposed here aimed to investigate the enhancement in N_2O atmospheric concentration due to emissions from Great Britain, the concentration of N_2O imported to the model domain was assumed to be 319 ppb, based upon the measurements of baseline concentrations of radiatively active gases at a remote site at Mace Head in Ireland (data available on the AGAGE web site: http://cdiac.ornl.gov/ftp/ale_gage_Agage/AGAGE/). The total emissions of N_2O for Great Britain used as input to FRAME are mapped in Figure 7.1.

Table 7.1 N_2O annual emissions by type of source for the UK. Values used as input for FRAME.

Sector	UK emissions (kt N y^{-1})
Transport	8.6
Industry	13.6
Estuaries	0.7
Rivers	0.6
Nitrogen deposition	4.7
Agriculture	22.2
Soils	54.6

Table 7.2 Details of the thickness and height (metres from the soil) of the layers in which N_2O emissions are released in the FRAME model for 3 different runs.

	Transport	Industry *	All the other emissions**
FRAME run 1	1-6 m	1-50 m	1-2 m
FRAME run 2	1-2 m	1-50 m	1-2 m
FRAME run 3	1-2 m	1-6 m	1-2 m

*excluding the 10 industrial plants treated as point sources (see Table 7.3)
**including estuaries, rivers, N deposition, agriculture and soils

Table 7.3 Point source emissions of N_2O from the 10 most important industrial sources. Grid coordinates refer to the centre of the relevant model 5 km grid square

Source number	E (km)	N (km)	N_2O emissions (kt N y^{-1})	Sh (m)	V (m s^{-1})	P T (°C)	Sd (m)	Production process
1	457.5	522.5	0.15	160	16	150	5	Nylon works
2	442.5	517.5	1.96	160	16	150	5	Fertilizer works
3	452.5	517.5	2.30	160	16	150	5	Nitric acid plant
4	427.5	432.5	0.21	160	16	150	5	Waste management
5	467.5	427.5	0.12	198	19	130	10	Power station
6	447.5	422.5	0.13	260	30	90	16	Power station
7	337.5	377.5	0.11	160	16	150	5	Power station
8	352.5	182.5	2.04	160	16	150	5	Power station
9	552.5	177.5	0.22	50	15	150	3.8	Oil refinery
10	397.5	87.5	0.12	160	16	150	5	Starch works

E is the Easting position
N is the Northing position
Sh is the stack height
V is the exit velocity
P T is the plume temperature
Sd is the stack diameter

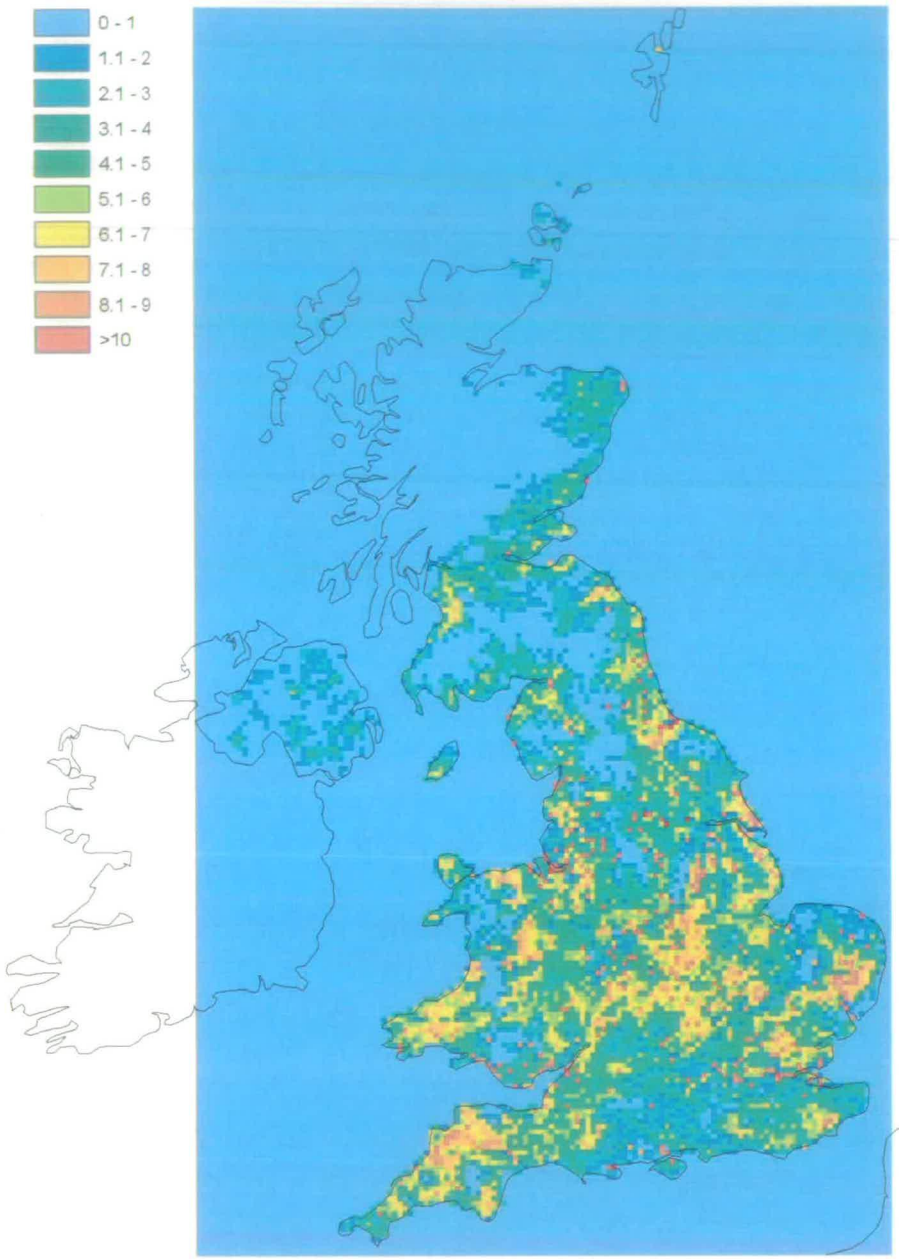

Figure 7.1 Map of annual N_2O emissions at 5 km x 5 km resolution used as input to the FRAME model (kg N $ha^{-1}yr^{-1}$) (from NAEI, Dragosits et al. 2005).

7.3 Results

The atmospheric N_2O concentrations calculated at the surface by FRAME for Great Britain are illustrated in Figure 7.2 for run 1 and in Figure 7.3 for run 3. The data refer to the enhancement of N_2O concentrations above the background level of 319 ppb. The difference between concentrations in the two maps is mainly localised in areas influenced by traffic and urban emissions and it is clearly represented in Figure 7.4, where the ratio of the enhancements in surface concentration obtained in run1 and run 2 is mapped. The maps in Figure 7.2 and Figure 7.3 display a spatial distribution of concentrations with a similar pattern to that for the emissions (Figure 7.1), but with a less fine scale variability. N_2O concentrations are larger in central England, East Anglia, Devon and north-west England and they are smaller in Scotland, coastal areas and the hill areas of Wales and the Northern Pennines.

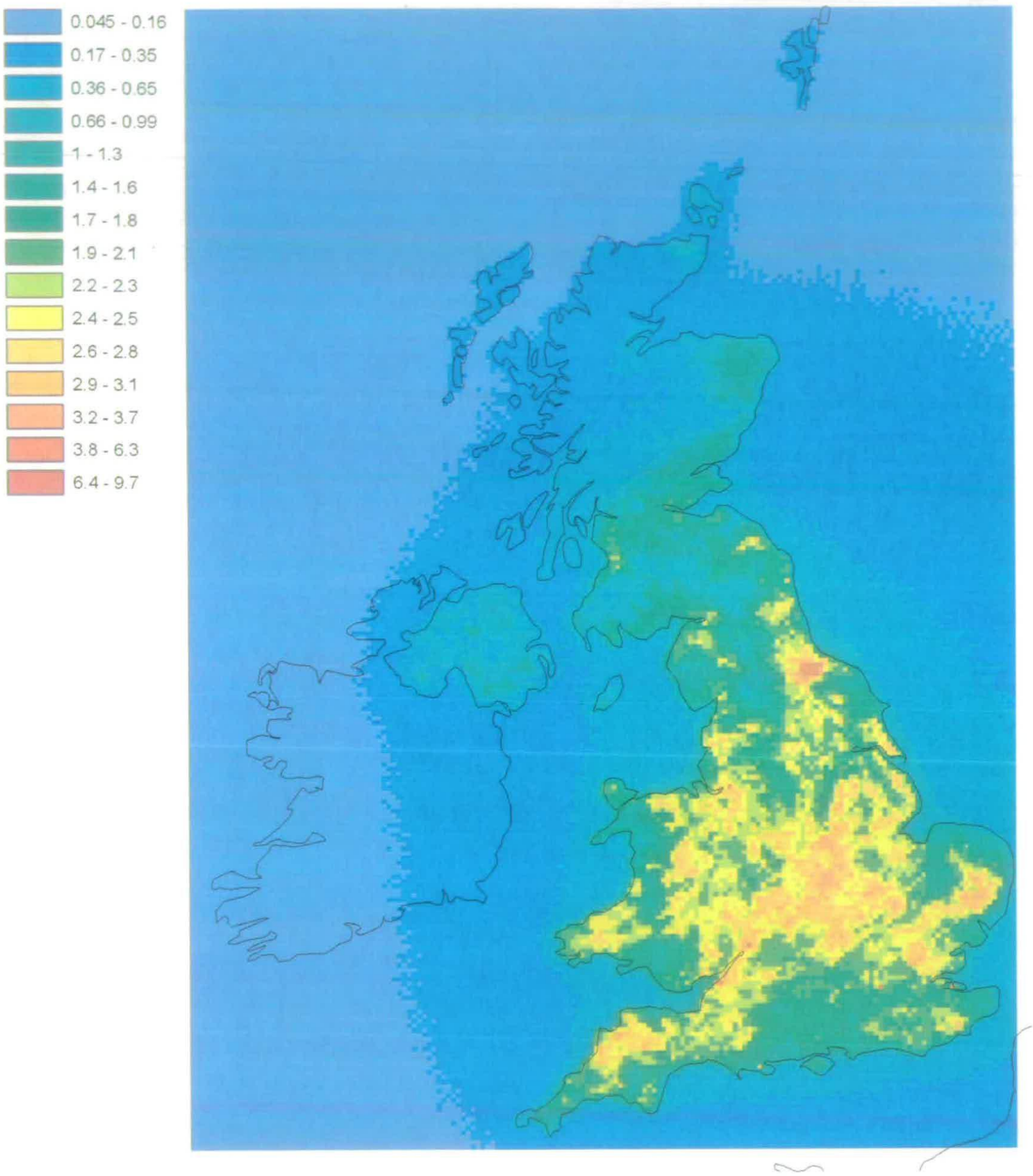

Figure 7.2 Map of the enhancement of N_2O surface (1m) concentrations (ppb) modelled by FRAME in run 1 (Map created by M. Vieno).

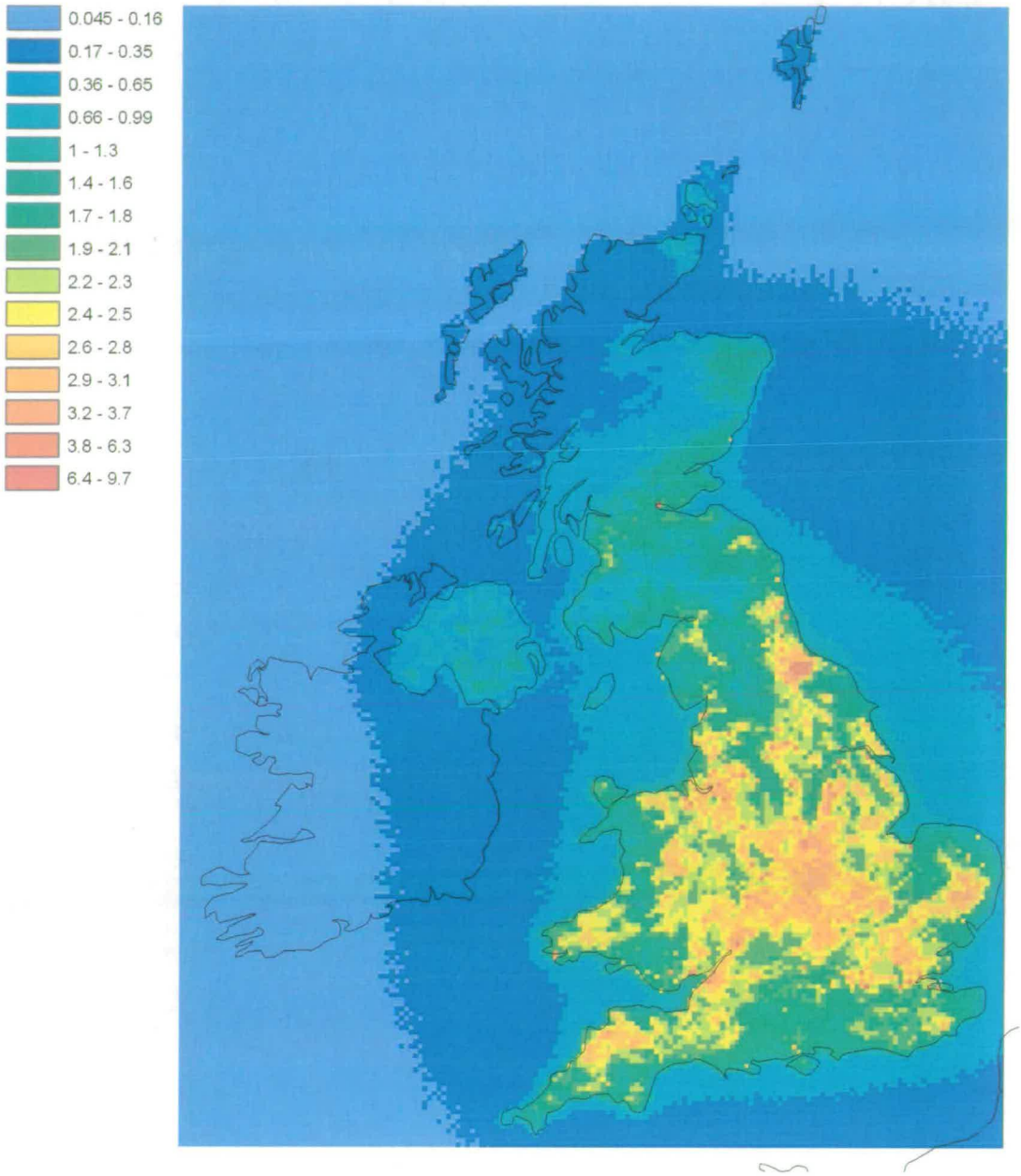

Figure 7.3 Map of the enhancement of N_2O surface (1m) concentrations (ppb) modelled by FRAME in run 3 (Map created by M. Vieno).

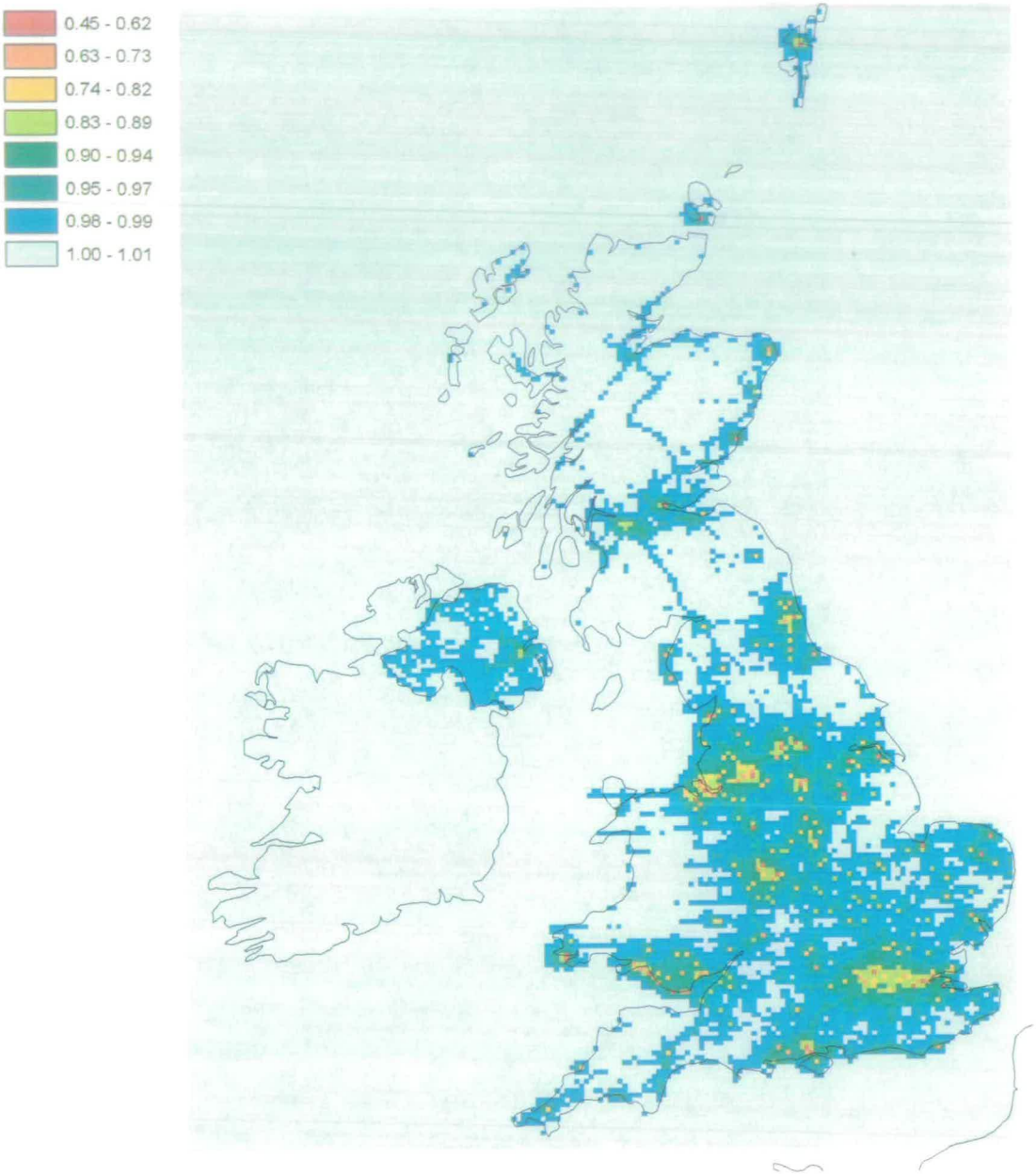

Figure 7.4 Ratio between N_2O concentration outputs of run 1 and run 3 of FRAME. It is clear that the biggest differences are in urban and industrial areas (Map created by M. Vieno).

7.3.1 Comparing measured and modelled N_2O concentrations

The simulated N_2O concentration field for Great Britain presented in Figure 7.2 and Figure 7.3 may be compared with measured long-term average concentration reported in Chapter 6 based on sampling at height of 1.5 m with Tedlar bags and analysis with TDL spectroscopy.

The correlation between the modelled and the measured enhancement in N_2O concentrations above background (319 ppb) is illustrated in Figure 7.5. Measured concentrations are obtained from measuring sites characterised by different sources (agricultural, mixed, urban and background), as explained in Chapter 6. From Figure 7.5 it is evident that there is considerably more variation in the measured concentrations than in those predicted at the measurement sites by the model. This suggests sub-grid scale local variability in N_2O emissions which can be detected by site measurements but is unresolved in a model with a 5 km grid square resolution. The scatter plot improves slightly when only measurements from agricultural sites are included in the comparison but there is still no significant correlation with the model: the urban and mixed source sites represent most of the high measured concentration values in Figure 7.5 that do not appear anymore in Figure 7.6. This aspect is further discussed in the next paragraph.

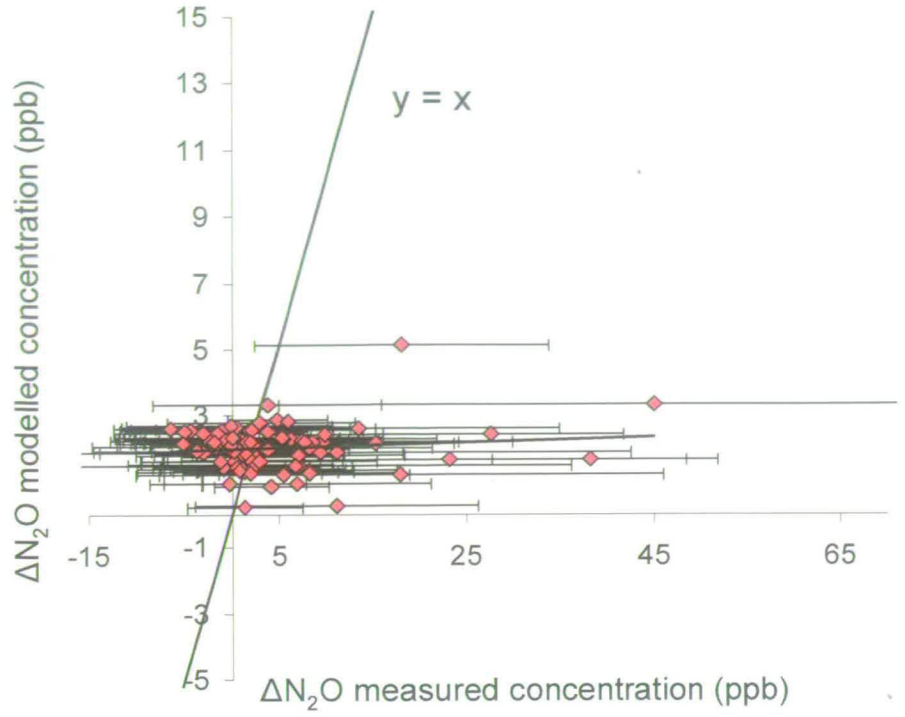

Figure 7.5 Correlation between modelled and measured enhancements of N_2O concentration above background value (319 ppb). Measured values obtained from all the measuring sites presented in Chapter 6. Error bars are the standard deviation of the annual average of sites measurements. The bold line represents the 1:1 ratio line.

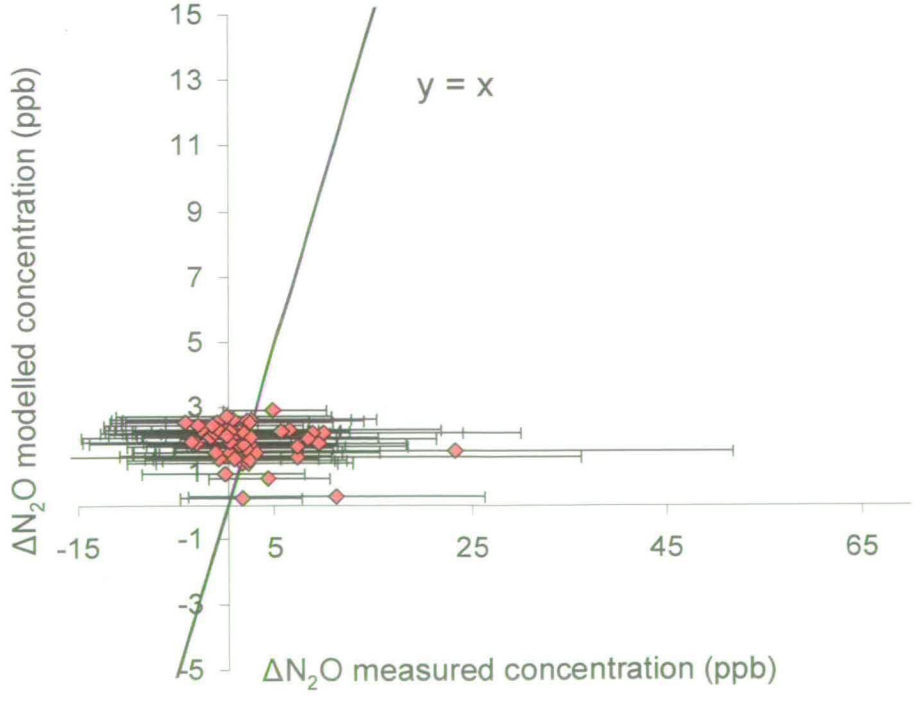

Figure 7.6 Correlation between modelled and measured enhancements of N_2O concentration above background value (319 ppb). Only measured values obtained from agricultural sites are taken into account. Error bars are the standard deviation of the annual average of sites measurements. The bold line represents the 1:1 ratio line.

Statistical parameters for measured and modelled N_2O concentrations are presented in Table 7.4. The average N_2O annual concentration calculated by FRAME over all monitoring sites is 321 ppb (standard deviation ranging 0.5-0.7 ppb for the different runs), which is lower than the average concentration calculated from the measured values of 323 ppb (standard deviation = 8.4 ppb). This may suggest that the background concentration of 319 ppb used in FRAME was an underestimate. This concentration value is obtained from measurements made at a coastal site in western Ireland, where the air masses come predominantly from the sea and they are therefore 'clean'. Derwent *et al.* (1998) observed an increase of about 2 ppb in the N_2O baseline concentration measured at the same site in Ireland when the air was flowing over Europe. Thus, it may be expected that air imported from Europe in south-easterly trajectories would contain somewhat enhanced concentrations at the south-eastern boundary of the FRAME domain that is not taken into account in this study.

For the measurements at remote locations and in livestock dominated areas the accord between measured and modelled concentrations is acceptable (Table 7.4): FRAME predicts an average annual concentration of 321 ppb and the measured data provide an annual concentration of 321 ± 0.4 ppb. The agreement for the 30 sites with urban influence (mixed and urban categories) was poorer: the average concentration modelled by FRAME was 321 ppb compared to the average annual measured concentrations of 328 ± 1 ppb. This suggests that a larger number of measurement sites subjected to urban influences are located near areas of high emissions which are either not accurately represented in the emissions inventory or are due to strong local variability in emissions which is not resolved by the 5 km grid size employed in FRAME The much wider variability in measured concentrations is represented by the large standard deviations for measured values in Table 7.4.

Table 7.4 Statistical parameters for measured and modelled N_2O annual concentrations for distinguished type of sources and overall measuring sites.

		FRAME run 1 (ppb)	FRAME run 2 (ppb)	FRAME run 3 (ppb)	Measured (ppb)
Agricultural sites (N=57)	Average	320.9	320.9	320.9	320.9
	Std dev	0.5	0.5	0.6	12.1
Mixed and urban sites (N=30)	Average	321.0	321.0	321.2	328.3
	Std dev	0.6	0.6	0.8	17.2
Total	Average	320.9	321.0	321.0	323.1
	Std dev	0.5	0.6	0.7	8.4
	Min	319.3	319	319.2	313.3
	Max	322.4	322.4	324.1	364.0

7.4 Discussion

From the results it is evident that N_2O concentrations in agricultural-livestock source dominated sites are simulated by FRAME with greater accuracy than concentrations in urban-mixed sites, although the model does not reproduce the high spatial variability observed in the measurements.

The fact that FRAME represents the measurement of NH_3 concentration better than N_2O is because in the case of NH_3 the very short atmospheric lifetime (1 – 3 h) and the relatively small urban sources reduce the effect on emissions from urban and mixed area. In the case of N_2O, the very large atmospheric lifetime (~120 y) and large urban sources extend the influence of urban (mainly traffic) sources over the entire country.

Generally FRAME produces concentrations well correlated with emissions input (e.g. for NH_3) (Vieno, pers. comm.) when released at the bottom layer (1 m), so the quality of the emissions data is highly reflected in the model output. The correlation between emissions input and concentrations output is lower when the emissions are released at higher layers and diffused throughout several layers. For the model results presented here the agreement between the N_2O concentrations provided by FRAME and the N_2O emissions ranges from $R^2 = 0.4$ for run 1 (traffic emissions released and diffused at 1-6 m and industrial emissions at 1-50 m) to $R^2 = 0.7$ for run 3 (traffic emissions released and diffused at 1-2 m and industrial emissions at 1-6 m). When sites categorised as urban and mixed type are excluded from the comparison R^2

becomes 0.8. The increase of N_2O modelled concentrations in mixed and urban sites when the height of the release and diffusion of emissions is lowered (from run 1 to run 3 of FRAME) is shown in Figure 7.7. The biggest variations are found in Sutton Bonington, Victoria school, Carhouse pumping station and Kimberworth Park where emissions peaks are mainly due to mixed-urban sources (see also Figure 7.8). In run 3 the variability of the mixed and urban concentrations increases slightly showing the sensitivity of FRAME to changes in emissions parameters. Figure 7.8 and Figure 7.9 show the modelled and measured concentrations and the N_2O emissions for the traffic-urban sites and for some agricultural sites of the network respectively. As anticipated, in Figure 7.9 the output of FRAME follows exactly the same pattern as the emissions with a fairly constant ratio between the values of the two series, whereas in Figure 7.8 the modelled concentrations present some variations from the emissions pattern. In the four sites mentioned above the large emissions due to industry are not reflected in the modelled concentration.

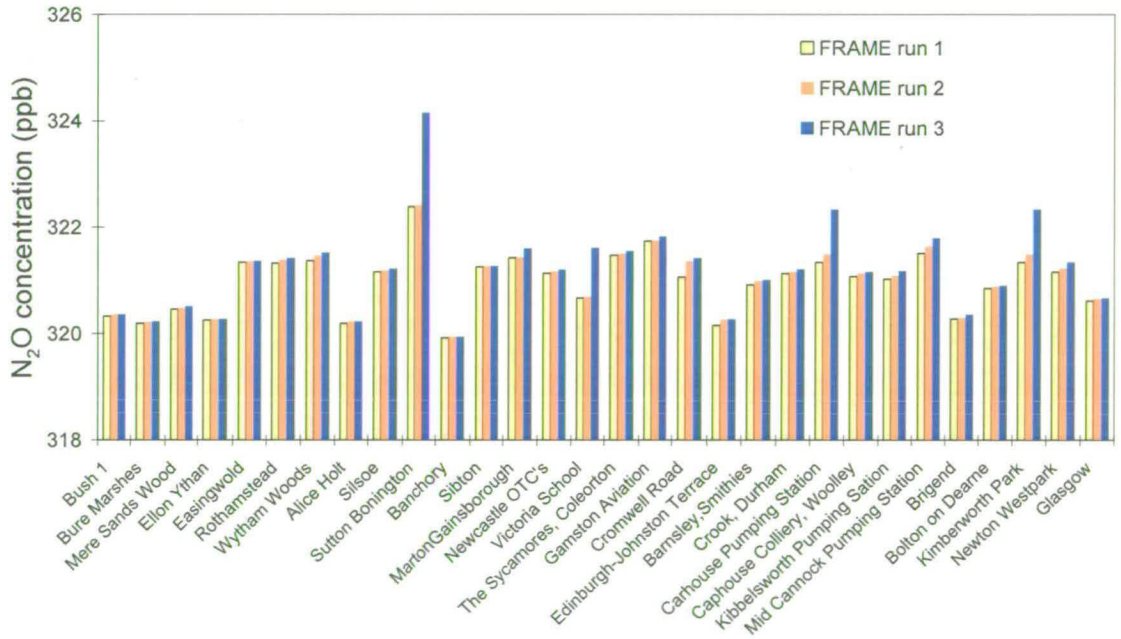

Figure 7.7 Results of the 3 runs of FRAME for N_2O concentrations at mixed and urban sites. A clear increase in concentration occurs in run 3 (blue bars) at sites where industrial sources are strong.

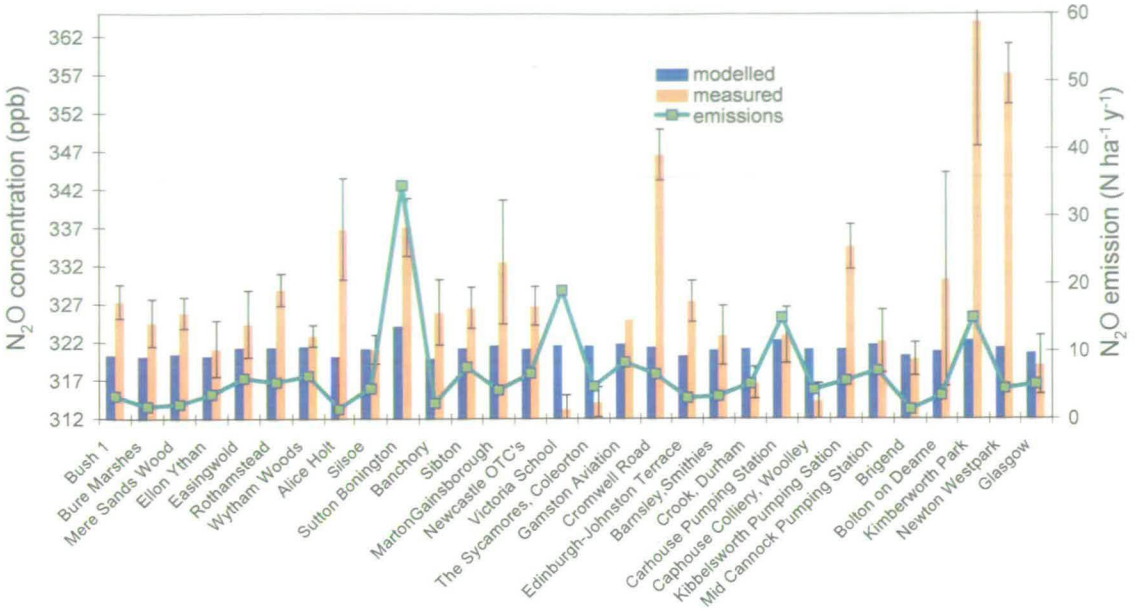

Figure 7.8 N_2O concentrations modelled with FRAME (run 3) (blue bars), measured concentrations (orange bars) and N_2O emissions from the national inventory for urban and mixed sources sampling sites. Error bars represent the standard errors.

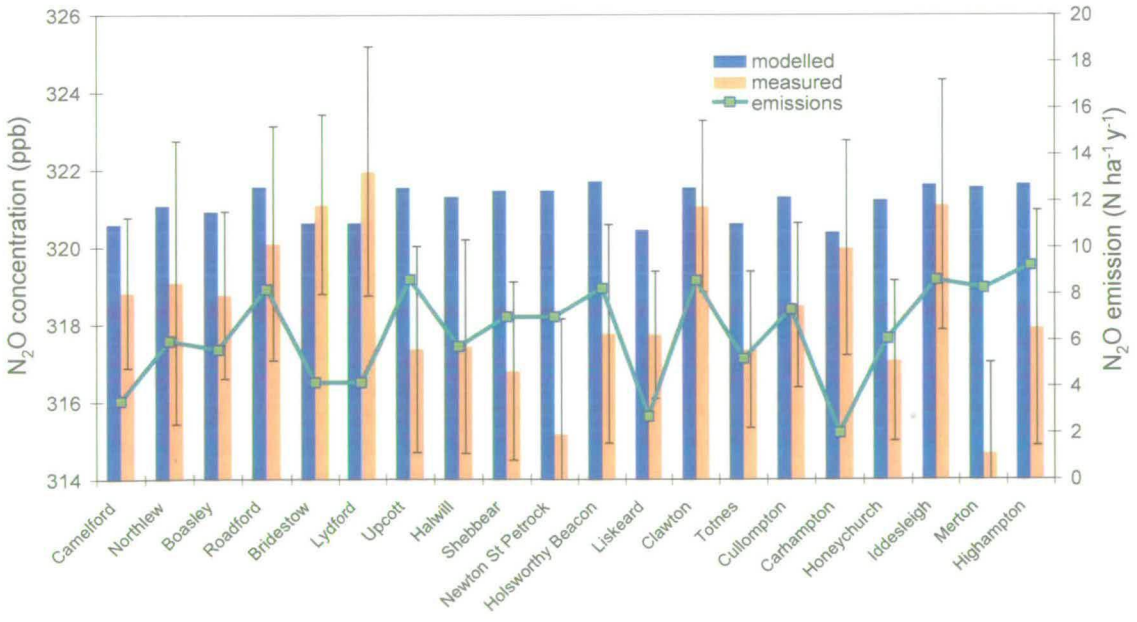

Figure 7.9 N_2O concentrations modelled with FRAME (run 3) (blue bars), measured concentrations (orange bars) and N_2O emissions from the national inventory for some of the agricultural sources sampling sites. Error bars represent the standard errors.

Generally, concentrations in locations with homogeneous surface without obstacles, such as in some agricultural and livestock sites, are better represented by the model than urban locations. The relatively better agreement for agricultural areas suggests the N_2O emissions characterised for these land surfaces, and in addition, that the spatial heterogeneity in source strength is greater and less well characterised for urban areas.

The fact that FRAME is not able to resolve spatial differences at distances smaller than 5 km is another aspect affecting the comparison between measured and modelled concentration. For example if two sampling sites are located in the same 5 km grid square the model calculates only one value of concentration, which will represent an average estimate for the grid. Measured concentrations instead can be very different even between two sites within the same grid. Figure 7.10shows some examples of measured and modelled N_2O concentration for sites within the same grid. For the agricultural sampling sites D13 and D14 in the same grid the measured concentrations differ only by 0.9 ppb and for the agricultural sites D17 and D18 by about 2 ppb. Concentrations measured at urban and mixed sites (sites 88 and 95), even if within the same grid (grid 3 in Figure 7.10) can vary largely (~ 40 ppb in the example). As it is evident from the chart the modelled concentrations do not represent the actual scale of variations in concentration. Furthermore, the vicinity of the sampling sites to a N_2O sources also determine big increases in measured concentrations that are not detected in the model output: grid 3 in Figure 7.10 is a good example of the large influence of the traffic source on the measured concentration.

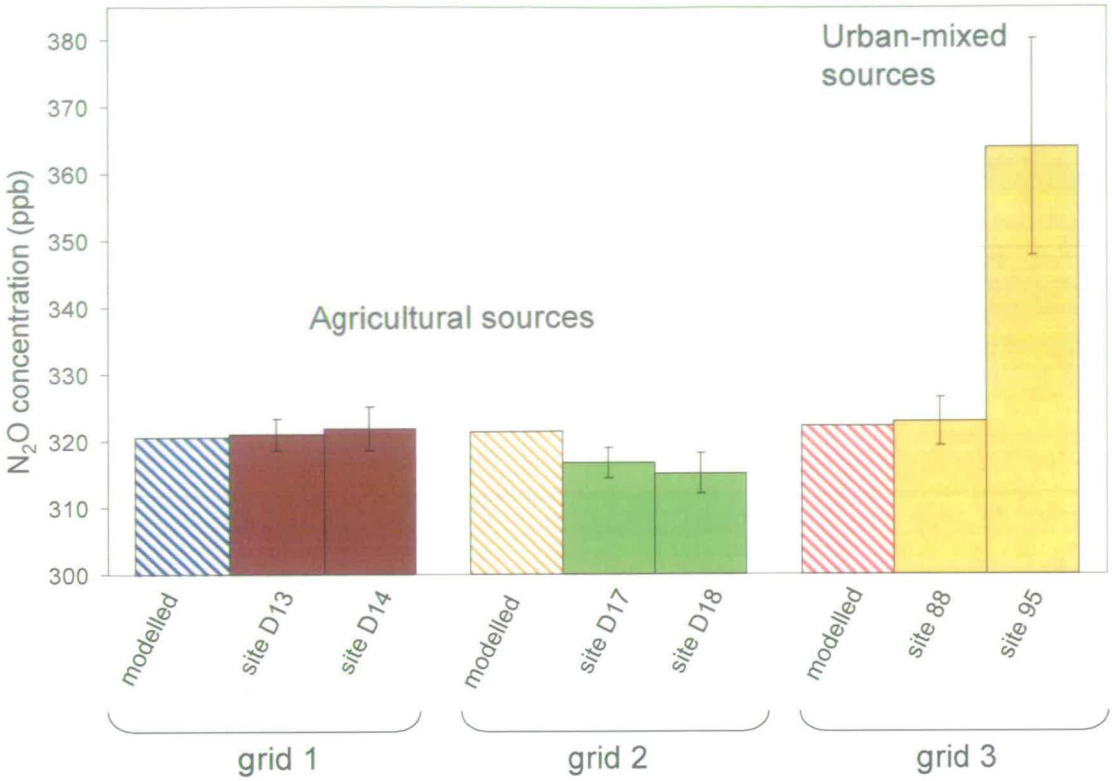

Figure 7.10 Examples of measured and modelled N2O concentrations at pairs of sampling sites within the same 5 km grid square. The first two grids are located in predominantly agricultural areas whereas grid 3 is influenced from urban and mixed sources. The difference in measured concentrations at the agricultural sites within the same grid (sites D13 and D14, and sites D17 and D18) are fairly small (~1-2 ppb of N_2O). Concentrations measured at sites 88 and 95 differ by 41ppb. Error bars represent the standard errors on measured values showing the importance of local site measurement.

7.5 Conclusion

The comparison between N_2O concentrations measured and modelled with FRAME showed consistently reasonable agreement, although the variability of modelled concentrations is smaller than in the measured ones. The systematic differences between measurements and modelling reveal important deficiencies in current understanding:

- The larger concentrations measured in the network than those modelled can be related to the accumulation of N_2O in surface air during periods of high stability. To validate national N_2O emissions, it is necessary to sample at greater height.

- The substantial emissions in urban areas and the effect of traffic sources observed in the measurements implies larger emissions spatial variability in N_2O sources than is currently included in the national inventory. A better agreement between measurements and model at agricultural sites than at urban and mixed sites suggests that the inventory for emissions from soils and agricultural sources is more accurate than for traffic and urban sources.
- The basic method to define N_2O concentration fields has merit, but stratified sampling to adapt slightly different approaches in different source areas would improve the value of the measurements for validation with FRAME.

Chapter 8 Conclusions and Perspectives

This study examined the spatial and temporal variability of N_2O emissions at the field scale (Chapter 5) and at country scale (Chapter 6 and Chapter 7) in Great Britain.

The one year of measurements of N_2O flux from the typical managed grassland at the Easter Bush site using the eddy covariance technique provided a picture of N_2O fluxes at field scale on short (day) and long (seasonal) time scale (Chapter 5). The large differences in seasonal fluxes (-5.5 – 195 ng N_2O-N m^{-2} s^{-1}) and in responses to fertiliser applications were mainly due to different environmental conditions (such as temperature, rainfall, etc.) in the periods investigated (Table 5.5). This was confirmed by the good prediction of N_2O seasonal fluxes using soil water content together with soil temperature or soil N availability in a multi-linear regression ($R^2 = 0.96$, $N = 5$, $p < 0.05$) (Table 5.6 and Figure 5.16).

The magnitude of the extraordinarily large N_2O flux measured after the fertilization in June 2002 (3500 ng N_2O-N m^{-2} s^{-1}) is rarely observed in the literature, although Clayton et al (1997) and Flechard et al. (2005) observed high emissions after fertiliser application (Table 8.1).This might be related to the fact that the commonly used static chamber method provides one flux measurement per day and therefore have some probability of missing big emission peaks. However, emission peaks as large as the one analysed here generally last a few hours, allowing the detection of most of the emission with the chamber method.

The comparison of chamber measurements and eddy covariance measurements presented in Chapter 5 showed a reasonable agreement between the two techniques. The discrepancy observed with chamber fluxes higher than eddy covariance fluxes can be related to the different surface area investigated by the two methods (Laville et al. 1997). Also, changes in soil conditions within the chambers, such as soil temperature at the surface, and changes in plant physiological processes could have influenced N_2O fluxes measured by chambers (Smith et al. 1994).

The diurnal patterns of the N_2O fluxes, observed only after the fertilisation in June 2002, showed maximum fluxes up to 5 times greater than the minimum fluxes. Daily cycles of N_2O flux correlated with the temperature of the soil surface (R^2 = 0.52) better than with soil temperature at greater depth, suggesting that the production of N_2O occurred in the top few mm. A significant correlation of diurnal N_2O fluxes with turbulent parameters such as H ($R^2 = 0.7$) and u_* ($R^2 = 0.5$) suggests that diurnal variations of N_2O fluxes are also related to changes in turbulent parameters and provides an interesting process to investigate in future studies and a different approach to use in process-based models for prediction of N_2O emissions.

Table 8.1 shows a summary of previous N_2O flux measurements with different techniques and on different ecosystems. The range of fluxes measured at the Easter Bush field during the fertilisation periods is in agreement with the results of Clayton et al. (1997) and Dobbie et al. (1999) on managed grassland in Scotland. The evidence of a net sink to the soil, which was observed at Easter Bush during winter months, is also reported by Ryden (1981), Flechard et al. (2005), Maggiotto and Wagner-Riddle (2001) on grassland, Yamulki et al. (1995) on arable soils, and Butterbach-Bahl et al. (1998) on forest soils. Although in most of these studies N_2O uptake from soil is a sporadic event, regular negative N_2O fluxes were observed in the long term study by Flechard et al. (2005) using static and automatic chambers and a photo-acoustic gas analyser. In fact, the frequency distribution of the observation presented in this last study is very similar to the frequency distribution obtained for the Easter Bush data with negative fluxes representing about 40% of the measurements. An analogous distribution of flux measurements was found by Fowler et al. (1995) during a shorter campaign (~200 hours) using eddy covariance and a TDL. The net sink to the soil played a significant role in the total N_2O emission budget for Easter Bush, highlighting the need to investigate the uptake activity more thoroughly in N_2O emission measurements.

The total annual (from June 2002 to June 2003) budget estimate for Easter Bush using a gap filling method presented in Section 5.3.5.1 was 5.3 kg N_2O-N ha^{-1} y^{-1} (corresponding to an EF of 1.68%), with EF varying largely (from 0.19% to 3.29%) during the measurement period. The variability of N_2O emission factors is a cause of

uncertainty for national emission inventories, the validation of which is discussed in Chapter 6 and Chapter 7.

Table 8.1 Summary of previous N_2O flux measurements and results from this study.

Reference	*Technique*	*Ecosystem*	*Treatments*	*Measurement*	*N_2O Fluxes range*
Ryden (1981)	Chamber technique	Temperate grassland	Untreated plot	Weekly	-4.1 to -1.2 ng N m^{-2} s^{-1}
			Fertilised plot	Weekly	-5.8- 245 ng N m^{-2} s^{-1}
Fowler et al. (1995)	EC with TDL	Arable soil (Denmark)	nd	Hourly average of 10 min meas.	-70 – 350 ng N m^{-2} s^{-1}
Yamulki et al. (1995)	Static chambers + GC	Arable soil (UK)	Fertilised	daily	-3.3 - ~45 ng N m^{-2} s^{-1}
Clayton et al. (1997)	Static chambers + GC	Temperate grassland	Background	daily	Max value~5.8 ng N m^{-2} s^{-1} [a]
			Fertilised plot	daily	Max value ~ 2033 ng N m^{-2} s^{-1}
Laville et al. (1997)	EG and EC with TDL	Arable soil (France)	Fertilised	Hourly average of 15 min meas.	-5- 50 ng N m^{-2} s^{-1}
Dobbie et al. (1999)	Static chambers + GC	Temperate grassland	Fertilised plot	daily	Max value ~1620 ng N m^{-2} s^{-1}
		Arable	Fertilised		Max value ~462 ng N m^{-2} s^{-1}
Laville et al. (1999)	EG and EC with TDL	Arable soil (France)	Fertilised	Hourly average of 15 min	Max value ~700 ng N m^{-2} s^{-1}
Esler et al. (2000) Griffith et al. (2002)	AG with FTIR gas analyser	Grazed pasture		Half-hourly	Max value ~22 ng N m^{-2} s^{-1} [b] mean value =17.4 ng N m^{-2} s^{-1}
Maggiotto et al. (2001)	AG with TDL	Grassland (Canada)	Fertilised	Daily average of hourly measurements	-7 – 82 ng N m^{-2} s^{-1}
Flechard et al. (2005)	Static and automatic chambers + photo-acoustic gas analyser [c]	Temperate grassland	Untreated plot	daily	-102 – 449 ng N m^{-2} s^{-1}
			Fertilised plot	daily	-109 – 2402 ng N m^{-2} s^{-1}
This study	EC with TDL	Temperate grassland	Background	Daily average of 30 min measurement	-27 – 19 ng N m^{-2} s^{-1}
			Fertilisation periods	Daily average of 30 min measurement	-10 – 1832 ng N m^{-2} s^{-1}
Butterbach-Bahl et al. (1998)	Static chambers + GC	Temperate forest		Daily average of hourly measurements	- 0.5 – 15 µg N m^{-2} h^{-1}
Pilegaard et al. (submitted)	Chamber technique	Forest soils [d]		Daily to monthly measurements	0.5 - 20.3 µg N m^{-2} h^{-1} [e]

AG= Aerodynamic gradient technique
EC = Eddy covariance technique
a) Monthly cumulative fluxes ranged between -15±10 g N ha^{-1} and 92 ± 42 g N ha^{-1}
b) Day time data (6:00-18:00).The authors do not consider the measured negative fluxes due to N_2O uptake, but as statistics values.
c) INNOVA Air Tech Instruments, Ballerup, Denmark;
d) 1 year-study on 15 forest sites in Europe (NOFRETETE project)
e) Range of annual averages for the 15 sites.

The study presented in Chapter 6 focused on the development of a N_2O monitoring network to use for validation of emission inventories at the national scale. The system proposed is able to detect spatial variations in N_2O atmospheric concentrations confirming that they vary quite widely across the country and less broadly in localized networks. Nevertheless, the national network is able to describe seasonal variations of the concentration when tested on specific points. However, the system overestimated the strength of N_2O sources when compared with emissions obtained from the UK inventory based on a simple box model (Section 6.4.1) and on a comparison with FRAME (Chapter 7).

Inter-annual differences in N_2O monthly concentrations in 2002 and 2003 were related to annual pattern of rainfall and wind speed at national scale. In a more detailed investigation for a few sites, including different type of sources (see Section 6.4.4), N_2O concentrations were well correlated with rainfall and temperature for mixed and agricultural sources (R^2 ranging from 0.3 to 0.8), but not for cities (R^2 = 0.01) (Table 6.3). N_2O concentrations in the urban area of London were better controlled by the variation of wind speed.

This study highlighted the importance of urban sources, which is mainly traffic to total atmospheric N_2O concentrations.

Data from the monitoring system discussed in Chapter 6 were used to validate the atmospheric transport model FRAME and the N_2O emissions inventory for the UK (Chapter 7). The comparison between measured N_2O concentrations in the national monitoring network and concentrations modelled by FRAME showed reasonable agreement, although the variability of modelled concentrations was smaller than the measured ones. This is partially because the model resolution of 5 km is not able to represent high variability of N_2O measured at the sampling sites.

The large concentrations measured in the network can be related to the accumulation of N_2O in surface air during periods of high atmospheric stability. To validate national N_2O emissions, it is necessary to sample at greater height.

A better agreement between measurements and model at agricultural sites than at urban and mixed sites suggests that the inventory for emissions from soils and agricultural sources is more accurate than for traffic and urban sources. The substantial emissions in urban areas and the effect of traffic sources observed in the

measurements imply larger emissions and spatial variability of N_2O sources than is currently included in the UK inventory.

The combination of FRAME and long term measurements with a national monitoring network has merit, but some modifications are needed to improve the value of the measurements for validation, such as the increase of sampling height, and a reassessment of the sampling sites excluding the sites that showed to be highly influenced by the vicinity of N_2O sources. The implementation of measurements of meteorological parameters (such as wind speed, wind direction and temperature) in few strategic measuring sites (maybe one per type of emission source) could provide a clearer picture of the influence of the meteorological parameters on the monthly concentration.

A simulation of monthly concentrations using FRAME could improve the comparison with measured concentrations. Furthermore, the use of transport models (e.g. NAME from Met-Office) that use the actual meteorological data in place of statistical values used by FRAME, could give a better representation of measured concentrations.

References

Affre, C., A. Lopez, et al. (2000). The analysis of energy and ozone flux data from the LANDES 94 experiment. *Atmospheric Environment* **34**(5), 803-821.

Ambus, P. (1998). Nitrous oxide production by denitrification and nitrification in temperate forest, grassland and agricultural soils. *European Journal of Soil Science* **49**(3), 495-502.

Ambus, P. and S. Christensen (1995). Spatial and Seasonal Nitrous-Oxide and Methane Fluxes in Danish Forest-Ecosystems, Grassland-Ecosystems, and Agroecosystems. *Journal of Environmental Quality* **24**(5), 993-1001.

Ambus, P. and G. P. Robertson (1998). Automated near-continuous measurement of carbon dioxide and nitrous oxide fluxes from soil. *Soil Science Society of America Journal* **62**(2), 394-400.

Anderson, I. C., M. Poth, et al. (1993). A comparison of NO and N_2O production by the autotrophic nitrifier Nitrosomonas europea and the heterotrophic nitrifier Alcaligenes faecalis. *Applied and Environmental Microbiology* **59**(11), 3525-3533.

Arah, J. R. M., I. J. Crichton, et al. (1994). Automated Gas-Chromatographic Analysis System for Micrometeorological Measurements of Trace Gas Fluxes. *Journal of Geophysical Research* **99**(D8), 16593-16598.

Aubinet, M., A. Grelle, et al. (2000). Estimates of the Annual Net Carbon and Water Exchange of Forests: the EUROFLUX methodology. *Advances in Ecological Research* **30**, 111-175.

Baggott, S. L., L. Brown, et al. (2005). Greenhouse Gas Inventories for England, Scotland, Wales and Northern Ireland: 1990-2003. National Atmospheric Emissions Inventory (NAEI),Harwell, Oxforshire, UK, pp. 73.

Baldocchi, D. (1997). Flux footprints within and over forest canopies. *Boundary-Layer Meteorology* **85**, 273–292.

Becker, K. H., J. C. Lorzer, et al. (2000). Contribution of vehicle exhaust to the global N_2O budget. *Chemosphere - Global Change Science* **2**(3-4), 387-395.

Berges, M. G. M., R. M. Hofmann, et al. (1993). Nitrous oxide emissions from motor vehicles in tunnels and their global extrapolation. *Journal of Geophysical Research* **98**(18), 527-531.

Biraud, S., P. Ciais, et al. (2002). Quantification of carbon dioxide, methane, nitrous oxide and chloroform emissions over Ireland from atmospheric observations at Mace Head. *Tellus Series B-Chemical and Physical Meteorology* **54**(1), 41-60.

Bouwman, A. F. (1996). Direct emission of nitrous oxide from agricultural soils. *Nutrient Cycling in Agroecosystems* **46**, 53-70.

Bouwman, A. F. (1999). Approaches to scaling of trace gas fluxes in ecosystems. Bilthoven, The Netherlands, Elsevier, pp. 362.

Bouwman, A. F., L. J. M. Boumans, et al. (2002). Emissions of N_2O and NO from fertilized fields: Summary of available measurement data. *Global Biogeochemical Cycles* **16**(4), 1058-1064.

Bouwman, A. F., J. A. Taylor, et al. (2000). Testing hypotheses on global emissions of nitrous oxide using atmospheric models. *Chemosphere - Global Change Science* **2**(3-4), 475-492.

Bouwman, A. F., K. W. Vanderhoek, et al. (1995). Uncertainties in the Global Source Distribution of Nitrous Oxide. *Journal of Geophysical Research* **100**(D2), 2785-2800.

Brown, L., B. Syed, et al. (2002). Development and application of a mechanistic model to estimate emission of nitrous oxide from UK agriculture *Atmospheric Environment* **36**, 917-928.

Brumme, R., W. Borken, et al. (1999). Hierarchical control on nitrous oxide emission in forest ecosystems. *Global Biogeochemical Cycles* **13**, 1137-1148.

Butler, J. H., J. W. Elkins, et al. (1998). Nitrous Oxide and Halocompounds. Summary report No. 24. US Department of Commerce,Boulder, Colorado, pp. 91-121.

Butterbach-Bahl, K., R. Gasche, et al. (1998). Impact of N-input by wet deposition on N-trace gas fluxes and CH4-oxidation in spruce forest ecosystems of the temperate zone in Europe. *Atmospheric Environment* **32**(3), 559-564.

Cant, N. W., D. E. Angove, et al. (1998). Nitrous oxide formation during the reaction of stimulated exhaust streams over rhodium, platinum and palladium catalysts. *Applied Catalysis B Environmental* **17**, 63-73.

Chalk, P. M. and C. J. Smith (1983). Chemodenitrification. In: Gaseous Losses of Nitrogen from Plant-Soil Systems. J. Freney and J. R. Simpson (eds.). The Hague, Martinus Nijhoff/Dr W Junk Publishers, pp. 65-89.

Christensen, S., P. Ambus, et al. (1996). Nitrous oxide emission from an agricultural field: Comparison between measurements by flux chamber and micrometerological techniques. *Atmospheric Environment* **30**(24), 4183-4190.

Cicerone, R. J. (1989). Analysis of sources and sinks of atmospheric nitrous oxide (N_2O). *Journal of Geophysical Research* **94**, 18265-18271.

Clayton, H., J. R. M. Arah, et al. (1994). Measurement of Nitrous-Oxide Emissions from Fertilized Grassland Using Closed Chambers. *Journal of Geophysical Research* **99**(D8), 16599-16607.

Clayton, H., I. P. McTaggart, et al. (1997). Nitrous oxide emissions from fertilised grassland: A 2-year study of the effects of N fertiliser form and environmental conditions. *Biology and Fertility of Soils* **25**(3), 252-260.

Cole, C. V., J. Duxbury, et al. (1997). Global estimates of potential mitigation of greenhouse gas emissions by agriculture. *Nutrient Cycling in Agroecosystems* **49**(1-3), 221-228.

Coyle, M. (2005). The Gaseous Exchange of Ozone at Terrestrial Surfaces: Non-stomatal Deposition to Grassland. PhD thesis, University of Edinburgh.

Davidson, E. A. (1991). Fluxes of Nitrous Oxide and Nitric Oxide from Terrestrial Ecosystems. In: Microbial production and consumption of greenhouse gases: methane, nitrogen oxides, and halomethanes. W. W. B. Rogers J.E. (eds.). Washington DC, Washington DC: American Society for Microbiology, 1991, 306p.

Davidson, E. A., M. Keller, et al. (2000). Testing a Conceptual Model od Soil Emissions of Nitrous and Nitric Oxides. *Bioscience* **50**(8), 667-680.

De Klein, C. A. M., I. P. McTaggart, et al. (1999). Measurement of nitrous oxide emissions from grassland soil using photo-acoustic infra-red spectroscopy, long-path infrared spectroscopy, gas chromatography, and continuous flow isotope- ratio mass spectrometry. *Communications in Soil Science and Plant Analysis* **30**(9-10), 1463-1477.

Denmead, O. T., R. Leuning, et al. (2000). Nitrous oxide emissions from grazed pastures: measurements at different scales. *Chemosphere - Global Change Science* **2**(3-4), 301-312.

Dentener, F., H. Dlugokencky, et al. (2001). Atmospheric Chemistry and Greenhouse Gases. In: Climate Change 2001. The Scientific Basis. D. Ehhalt and M. Prather (eds.). Cambridge, Cambridge University Press.

Dentener, F. and C. Kroeze (1994). A three-dimensional model of the global ammonia cycle. *Journal of Atmospheric Chemistry* **19**, 331-369.

Derwent, R. G., P. G. Simmonds, et al. (1998). European source strengths and northern hemisphere baseline concentrations of radiatively active trace gases at Mace Head, Ireland. *Atmospheric Environment* **32**(21), 3703-3715.

Di Marco, C., U. Skiba, et al. (2004). Field scale flux measurements from grassland using eddy covariance. *Water, Air and Soil Pollution: Focus* **4**, 143-149.

Dobbie, K. E., I. P. McTaggart, et al. (1999). Nitrous oxide emissions from intensive agricultural systems: Variations between crops and seasons, key driving variables, and mean emission factors. *Journal of Geophysical Research* **104**(D21), 26891-26899.

Dobbie, K. E. and K. A. Smith (2001). The effects of temperature, water-filled pore space and land use on N_2O emissions from an imperfectly drained gleysol. *European Journal of Soil Science* **52**(4), 667-673.

Dobbie, K. E. and K. A. Smith (2003). Impact of different forms of N fertilizer on N_2O emissions from intensive grassland. *Nutrient Cycling in Agroecosystems* **67**(1), 37-46.

Douglas, J. T. and C. E. Crawford (1993). The response of a ryegrass sward to wheel traffic and applied nitrogen. *Grass and Forage Science* **48**, 91-100.

Dragosits, U., U. Skiba, et al. (2005). Spatial estimation of CH_4 and N2O emissions from agriculture, waste and other sources for the 2002 GHG inventory. NAEI pp. 10.

Duyzer, J. H., B. Nijenhuis, et al. (2001). Monitoring and modelling of ammonia concentrations and deposition in agricultural areas of the Netherlands. *Water, air and soil pollution: Focus* **1**, 131-144.

Edwards, G. C., G. W. Thurtell, et al. (2003). A diode laser based gas monitor suitable for measurement of trace gas exchange using micrometeorological techniques. *Agricultural and Forest Meteorology* **115**(1-2), 71-89.

EIA (1998). Emission of greenhouse gases in the United States 1997. Energy Information Administration,Washington DC.

Elliott, W. P. (1958). The growth of the atmospheric internal boundary layer. *Transaction of American Geophysical Union* **39**, 1048–1054.

Esler, M. B., D. W. T. Griffith, et al. (2000). N_2O concentration and flux measurements and complete isotopic analysis by FTIR spectroscopy. *Chemosphere - Global Change Science* **2**(3-4), 445-454.

Finnigan, J. (1999). A comment on the paper by Lee (1998): "On micrometeorological observations of surface-air exchange over tall vegetation". *Agricultural and Forest Meteorology* **97**(1), 55-64.

Finnigan, J. J. (2001). Instrumentation II: vector wind sensors. In: Advanced short course on Agricultural, Forest and Micrometeorology(eds.). Bologna, Universita' di Bologna.

Finnigan, J. J. and K. T. Paw (2001). Requirements for field measurements. In: Advanced short course on Agricultural, Forest and Micrometeorology(eds.). Bologna, Universita' di Bologna.

Firestone, M. K. and E. A. Davidson (1989). Microbiological basis of NO and N_2O production and consumption in soil. In: Exchange of Trace Gases between Terrestrial Ecosystems and the Atmosphere. M. O. Andreae and D. S. Schimel (eds.). New York, John Wiley & Sons, pp.7-21.

Flechard, C., A. Neftel, et al. (2005). Bi-directional soil/atmosphere N_2O exchange over two mown grassland systems with contrasting management practices. *Global Change Biology* **11**(12), 2114-2127.

Flessa, H., P. Dorsch, et al. (1996). Influence of cattle wastes on nitrous oxide and methane fluxes in pasture land. *Journal of Environmental Quality* **25**(6), 1366-1370.

Flessa, H., U. Wild, et al. (1998). Nitrous oxide and methane fluxes from organic soils under agriculture. *European Journal of Soil Science* **49**(2), 327-335.

Fluckiger, J., A. Dallenbach, et al. (1999). Variations in atmospheric N_2O concentration during abrupt climatic changes. *Science* **285**(5425), 227-230.

Flynn, H. C., J. Smith, et al. (2005). Climate- and crop-responsive emission factors significantly alter estimates of current and future nitrous oxide emissions from fertilizer use. *Global Change Biology* **11**(9), 1522-1536.

Foken, T. and X. H. Lee (2004). Post-field data quality control. In: Handbook of Micrometeorology: A Guide for Surface Flux Measurements. X. Lee (eds.). Dordrecht, Kluwer.

Foken, T. and B. Wichura (1996). Tools for quality assessment of surface-based flux measurements. *Agricultural and Forest Meteorology* **78**, 83-105.

Fournier, N., A. J. Dore, et al. (2004). Modelling the deposition of atmospheric oxidised nitrogen and sulphur to the United Kingdom using a multi-layer long-range transport model. *Atmospheric Environment* **38**(5), 683-694.

Fournier, N., V. A. Pais, et al. (2002). Parallelisation and application of a multi-layer atmospheric transport model to quantify dispersion and deposition of ammonia over the British Isles. *Environmental Pollution* **116**(1), 95-107.

Fournier, N., K. J. Weston, et al. (2005). Modelling the wet deposition of reduce nitrogen over the British Isles using a Lagrangian multi-layer atmospheric transport model. *Quarterly Journal of the Royal Meteorological Society* **131**, 703-722.

Fowler, D. and J. H. Duyzer (1989). Micrometeorological techniques for the measurement of trace gas exchange. In: Exchange of trace gases between terrestrial ecosystems and the atmosphere M. O. Andreae and D. S. Schimel (eds.). Chichester, England, Wiley & Sons, pp 189-207.

Fowler, D., K. J. Hargreaves, et al. (1995). Measurements of CH_4 and N_2O fluxes at the landscape scale using micrometeorological methods. *Philosophical*

Transactions of the Royal Society of London Series a-Mathematical Physical and Engineering Sciences **351**, 339-355.

Fowler, D., U. Skiba, et al. (1997). Emission of nitrous oxide from grasslands. In: Gaseous nitrogen emissions from grassland. S. C. Jarvis and S. C. Pain (eds.). Wallingford, CAB International, 147-164.

Freney, J., O. T. Denmead, et al. (1978). Soil as a source or sink for atmospheric nitrous oxide. *Nature* **273**, 530-532.

Galle, B., L. Klemedtsson, et al. (1994). Application of a Fourier-Transform IR System for Measurements of N2o Fluxes Using Micrometeorological Methods, an Ultralarge Chamber System, and Conventional Field Chambers. *Journal of Geophysical Research* **99**(D8), 16575-16583.

Gash, J. H. C. (1986). A note on estimating the effect of a limited fetch on micrometeorological evaporation measurements. *Boundary Layer Meteorology* **35**, 409–414.

Glatzel, S. and K. Stahr (2001). Methane and nitrous oxide exchange in differently fertilised grassland in southern Germany. *Plant and Soil* **231**(1), 21-35.

Goodwin, J. W. L., A. G. Salway, et al. (2001). UK Emissions of Air Pollutants 1970-1999. Department for Environment, Food and Rural Affairs,London.

Goossens, A., A. De Visscher, et al. (2001). Two-year field study on the emission of N2O from coarse and middle-textured Belgian soils with different land use. *Nutrient Cycling in Agroecosystems* **60**(1-3), 23-34.

Granli, T. and O. C. Bockman (1994). Nitrous oxide from agriculture. *Norwegian Journal of Agricultural Sciences* **12**, 1-128.

Grant, B., W. N. Smith, et al. (2004). Estimated N2O and CO2 emissions as influenced by agricultural practices in Canada. *Climatic Change* **65**(3), 315-332.

Griffith, D. W. T., R. Leuning, et al. (2002). Air-land exchanges of CO_2, CH_4 and N_2O measured by FTIR spectrometry and micrometeorological techniques. *Atmospheric Environment* **36**(11), 1833-1842.

Groffman, P. M. (1991). Ecology of nitrification and denitrification in soil evaluated at scales relevant to atmospheric chemistry. In: Microbial production and consumption of greenhouse gases: methane, nitrogen oxides, and halomethanes. W. W. B. Rogers J.E. (eds.). Washington DC, American Society for Microbiology, pp. 306.

Haenel, H. D. and L. Grunhage (1999). Footprint analysis: a closed analytical solution based on height-dependent profiles of wind speed and eddy viscosity. *Boundary-Layer Meteorology* **93**, 395–409.

Hansen, S., J. R. Maehlum, et al. (1993). N_2O and CH_4 fluxes in soil influenced by fertilization and tractor traffic. *Soil Biology & Biochemistry* **25**, 621-630.

Hargreaves, K. J., F. G. Wienhold, et al. (1996). Measurement of nitrous oxide emission from agricultural land using micrometeorological methods. *Atmospheric Environment* **30**(10-11), 1563-1571.

Hinkley, E. D., R. T. Ku, et al. (1976). Techniques for detection of molecular pollutants by absorption of laser radiation. In: Laser Monitoring of the Atmosphere. E.D. Hinkley (ed.) (eds.). New York, Springer-Verlag, pp. 237-295.

Hodgson, J. M. (1974). Soil Survey Field Handbook. Describing and Sampling Soil Profiles. Soil Survey of England and Wales., Harpenden 100.

Horst, T. W. (1997). A simple formula for attenuation of eddy fluxes measured with first-order-response scalar sensors. *Boundary-Layer Meteorology* **82**(2), 219-233.

Horst, T. W. and J. C. Weil (1992). Footprint estimation for scalar flux measurements in the atmospheric surface-layer. *Boundary Layer Meteorology* **59**, 279–296.

Houghton, J. T., L. G. Meira Filho, et al. (1995). Climate Change 1994. Radiative Forcing of Climate Change and an Evaluation of the IPCC IS92. Emission Scenarios. Cambridge, Cambridge University Press, UK.

IPCC (1992). Climate change 1992:The Supplementary Report to the IPCC Scientific Assessment.,Cambridge University press, UK, pp.205.

IPCC (1995). Climate Change 1995. The Science of Climate Change. IPCC,Cambridge University press, UK, pp 572.

IPCC (1997). Stabilization of atmospheric greenhouse gases: physical, biological and socio-economic implications.Geneva, Switzerland, pp.52.

IPCC (2001a). Climate change 2001: The Scientific Basis. IPCC,Cambridge University press, UK, pp.944.

IPCC (2001b). Good Practice Guidance and Uncertainty Management in National Greenhouse Gas Inventories IPCC,Institute for Global Environmental Strategies, Japan.

Jennings, D. E. (1980). Absolute line strengths in v4, $12CH_4$: a dual-beam diode laser spectrometer with sweep integration. *Applied Optics* **19**(16), 2695-2700.

Jimenez, J. L., J. B. McManus, et al. (2000). Cross road and mobile tunable infrared laser measurements of nitrous oxide emissions from motor vehicles. *Chemosphere* **2**, 397-412.

Jones, S. K., R. M. Rees, et al. (2005). Greenhouse gas emissions from a managed grassland. *Global and Planetary Change* **47**, 201-211.

Kaimal, J. C. and J. J. Finnigan (1994). Atmospheric Boundary Layer Flows. New York, Oxford University press, pp.289.

Kaimal, J. C. and J. E. Gaynor (1991). Another look at sonic thermometry. *Boundary Layer Meteorology* **56**, 401-410.

Kaimal, J. C., J. C. Wyngaard, et al. (1972). Spectral characteristics of surface-layer turbulence. *Quarterly Journal of the Royal Meteorological Society* **98**, 563-589.

Kammann, C., L. Grunhage, et al. (1998). Seasonal variability and mitigation options for N_2O emissions from differently managed grasslands. *Environmental Pollution* **102**, 179-186.

Keller, M. and W. A. Reiners (1994). Soil-atmosphere exchange of nitrius oxide, nitric oxide, and methane under secondary succession of pasture to forest in Costa Rica. *Global Biogeochemical Cycles* **8**, 399-409.

Keller, M., E. Veldkamp, et al. (1993). Effect of pasture age on soil trace-gas emissions from a deforested area of Costa-Rica. *Nature* **365**(6443), 244-246.

Khalil, M. A. K. (2000). Special issue: Atmospheric Nitrous Oxide. *Chemosphere - Global Change Science* **2**(3-4), 233-500.

Khalil, M. A. K. and R. A. Rasmussen (1992). The global sources of nitrous oxide. *Journal of Geophysical Research* **97**, 14651-14660.

Khalil, M. A. K., R. A. Rasmussen, et al. (2002). Atmospheric nitrous oxide: patterns of global change during recent decades and centuries. *Chemosphere* **47**(8), 807-821.

Klemedtsson, L., Q. Jiang, et al. (1999). Autotrophic ammonium-oxidising bacteria in Swedish mor humus. *Soil Biology and Biochemistry* **31**(6), 839-847.

Kljun, N., R. Kormann, et al. (2003). Comparison of the Lagrangian footprint model LPDM-B with an analytical footprint model. *Boundary Layer Meteorology* **106**, 349–355.

Kormann, R. and F. X. Meixner (2001). An analytical footprint model for non-neutral stratification. *Boundary-Layer Meteorology* **99**(2), 207-224.

Kroeze, C., A. Mosier, et al. (1999). Closing the global N_2O budget: A retrospective analysis 1500- 1994. *Global Biogeochemical Cycles* **13**(1), 1-8.

Laville, P., C. Henault, et al. (1997). Field comparison of nitrous oxide emission measurements using micrometeorological and chamber methods. *Agronomie* **17**(8), 375-388.

Laville, P., C. Jambert, et al. (1999). Nitrous oxide fluxes from a fertilized maize crop using micrometeorological and chamber methods. *Agricultural and Forest Meteorology* **96**, 19-38.

Leahy, P., G. Kiely, et al. (2004). Managed grasslands: A greenhouse gas sink or source? *Geophysical Research Letters* **31**(20), art. no.-L20507.

Leclerc, M. Y. and G. W. Thurtell (1990). Footprint Prediction of Scalar Fluxes Using a Markovian Analysis. *Boundary-Layer Meteorology* **52**(3), 247-258.

Lee, X. (1999). Reply to comment by Finnigan on "On micrometeorological observations of surface-air exchange over tall vegetation". *Agricultural and Forest Meteorology* **97**(1), 65-67.

Lee, X. H. (1998). On micrometeorological observations of surface-air exchange over tall vegetation. *Agricultural and Forest Meteorology* **91**(1-2), 39-49.

Lenschow, D. H. and L. Kristensen (1985). Uncorrelated noise in turbulence measurements. *Journal of Atmospheric and Oceanic Technology* **2**, 68-81.

Lenschow, D. H. and M. R. Raupach (1991). The attenuation of fluctuations in scalar concentrations through sampling tubes. *Journal of Geophysical Research-Atmospheres* **96**(D8), 15259-15268.

Levine, J. S., R. Wesley, et al. (1988). The effect of fire in biogenic soil emissions of nitric oxide and nitrous oxide. *Global Biogeochemical Cycles* **2**, 445-449.

Li, C., S. Frolking, et al. (1992). A model of nitrous oxide evolution from soil driven by rainfall events: 1. model structure and sensitivity. *Journal of Geophysical Research* **97**(D9), 9759-9776.

Li, C., S. Frolking, et al. (1994). Modelling nitrous oxide emissions from agriculture: a Florida case study. *Chemosphere* **28**(7), 1401-1415.

Maag, M. and F. P. Vinther (1996). Nitrous oxide emission by nitrification and denitrification in different soil types and at different soil moisture contents and temperatures. *Applied Soil Ecology* **4**(1), 5-14.

Macduff, J. H. and R. E. White (1985). Net mineralization and nitrification rates in a clay soil measured and predicted in permanent grassland from soil-temperature and moisture-content. *Plant and Soil* **86**(2), 151-172.

Machefert, S. E., N. B. Dise, et al. (2002). Nitrous oxide emission from a range of land uses across Europe. *Hydrology and Earth System Sciences* **6**(3), 325-337.

Maggiotto, S. R. and C. Wagner-Riddle (2001). Winter and spring thaw measurements of N_2O, NO and NO_x fluxes using a micrometeorological method. *Water, Air and Soil Pollution* **1**, 89-90.

Malhi, S. S., W. B. McGill, et al. (1990). Nitrate losses in soils:effect of temperature, moisture and substrate concentration. *Soil Biology & Biochemistry* **22**, 733-737.

Massman, W. J. (1991). The attenuation of concentration fluctuations in turbulent flow through a tube. *Journal of Geophysical Research* **96**(D8), 15,269-215,273.

McDonald, A. G., E. Nemitz, et al. (2002). Modelling heavy metal deposition across Scotland. In: The state of Scotland's Environment & Heritage(eds.). Edinburgh, UK, The Stationery Office Ltd, pp. 111-116.

McElroy, M. B. and D. B. Jones (1996). Evidence for an additional source of atmospheric N_2O. *Global Biogeochemical Cycles* **10**, 651-659.

McElroy, M. B. and Y. X. Wang (2005). Human and animal wastes: Implications for atmospheric N_2O and NO_x. *Global Biogeochemical Cycles* **19**(4), art no. GB2008.

McMillen, R. T. (1988). An Eddy-Correlation Technique with Extended Applicability to Non-Simple Terrain. *Boundary-Layer Meteorology* **43**(3), 231-245.

McTaggart, I. P., H. Clayton, et al. (1994). Nitrous oxide flux from fertilized grassland: strategies for reducing emissions. In: Non-CO_2 Greenhouse Gases. J. van Ham, L. H. M. Janssen and R. J. Swart (eds.). Dordrecht, Kluwer Academic, pp. 441-426.

McTaggart, I. P., J. T. Douglas, et al. (1997). Nitrous oxide emissions slurry and mineral nitrogen fertilizer applied to grassland. In: Gaseous Nitrogen emissions from grasslands. S. C. Jarvis and S. C. Pain (eds.). Wallingford, UK, CAB International, pp. 201-209.

Merry, M. and H. A. Panofsky (1976). Statistics of vertical motion over land water. *Quarterly Journal of the Royal Meteorological Society* **102**, 255–260.

Milford, C. (2004). Dynamics of atmospheric ammonia exchange with intensively-managed grassland. PhD Thesis, University of Edinburgh.

Moncrieff, J. B., J. M. Massheder, et al. (1997). A system to measure surface fluxes of momentum, sensible heat, water vapour and carbon dioxide. *Journal of Hydrology* **189**(1-4), 589-611.

Monin, A. S. and A. M. Obukhov (1954). Basic Laws of turbulent mixing in the ground layer of the atmosphere. *Trans. Geophys. Inst. Akad. Nauk. USSR* **151**, 163–187.

Monteith, J. L. and M. Unsworth (1990). Principles of Environmental physics, Edward Arnold, pp.291.

Moore, C. J. (1986). Frequency-response corrections for eddy-correlation systems. *Boundary-Layer Meteorology* **37**(1-2), 17-35.

Mosier, A. and C. Kroeze (1999). Contribution of agroecosystems to the global atmospheric N2O budget. Proceedings of International Workshop on Reducing N2O Emission from Agroecosystems, Banff, Canada,

Mosier, A. and C. Kroeze (2000). Potential impact on the global atmospheric N_2O budget of the increased nitrogen input required to meet future global food demands. *Chemosphere - Global Change Science* **2**(3-4), 465-473.

Mosier, A., C. Kroeze, et al. (1998). Closing the global N_2O budget: nitrous oxide emissions through the agricultural nitrogen cycle. *Nutrient Cycling in Agroecosystems* **52**(2 - 3), 225-248.

Murakami, T. and K. Kumazawa (1987). Measurement of denitrification products in soil by the acetylene inhibition method. *Soil Science and Plant Nutrition* **33**, 143-146.

Nevison, C., R. F. Weiss, et al. (1995). Global oceanic emission of nitrous oxide. *Journal of Geophysical Research* **100**(C8), 15809-15820.

Oenema, O., G. Velthof, et al. (2001). Technical and policy aspects of strategies to decrease greenhouse gas emissions from agriculture. *Nutrient Cycling in Agroecosystems* **60**(1-3), 301-315.

Olivier, J. G. J., A. F. Bouwman, et al. (1998). Global Air Emission Inventories for Anthropogenic Sources of NO_x, NH_3 and N_2O in 1990. *Environmental Pollution* **102**, 135-148.

Panofsky, H., H. Tennekes, et al. (1977). The characteristics of turbulent velocity components in the surface layer under convective conditions. *Boundary-Layer Meteorology* **11**(3), 355-361.

Pasquill, F. (1961). The estimation of the dispersion of windborne material. *Meteorological Magazine* **90**, 33-49.

Pasquill, F. (1972). Some aspects of boundary layer description. *Quarterly Journal of the Royal Meteorological Society* **98**, 469–494.

Paw, K. T., D. D. Baldocchi, et al. (2000). Correction of eddy-covariance measurements incorporating both advective effects and density fluxes. *Boundary-Layer Meteorology* **97**(3), 487-511.

Pilegaard, K., U. Skiba, et al. (submitted). Nitrogen load and forest type determine the soil emission of nitrogen oxides (NO and N_2O). *Biogeosciences*.

Potter, C. S., P. A. Matson, et al. (1996). Process modelling of controls on nitrogen trace gas emissions from soils Worldwide. *Journal of Geophysical Research* **101**, 1361-1377.

Prather, M., R. G. Derwent, et al. (1995). Other trace gases and atmospheric chemistry. In: Climate Change 1994. Radiative Forcing of Climate Change and an Evaluation of the IPCC IS92 Emission Scenarios. J. T. Houghton, L. G. Meira Filho, J. Bruceet al (eds.). Cambridge, Cambridge University Press, pp. 73-126.

Robertson, K. (1994). Nitrous-Oxide Emission in Relation to Soil Factors at Low to Intermediate Moisture Levels. *Journal of Environmental Quality* **23**(4), 805-809.

Rosenkranz, P., N. Br¨uggemann, et al. (2005). N_2O, NO and CH_4 exchange, and microbial N turnover over a Mediterranean pine forest soil. *Biogeosciences Discussions* **2**, 673-702.

Rowell, D. L. (1994). Soil Science: Methods and Applications, Longman Scientific&Technical, pp.360.

Rudaz, A. O., E. Walti, et al. (1999). Temporal variation in N_2O and N_2 fluxes from a permanent pasture in Switzerland in relation to management, soil water content and soil temperature. *Agriculture Ecosystems & Environment* **73**(1), 83-91.

Ryden, J. C. (1981). N_2O exchange between a grassland soil and the atmosphere. *Nature* **292**, 235-237.

Scanlon, T. M. and G. Kiely (2003). Ecosystem-scale measurements of nitrous oxide fluxes for an intensely grazed, fertilized grassland. *Geophysical Research Letters* **30**(16), art. no.-1852.

Schiff, H. I., G. I. Mackay, et al. (1994). The use of tunable diode laser absorption spectroscopy for atmospheric measurements. In: Air Monitoring by Spectroscopic Techniques. M. W. Sigrist (eds.), John Wiley &Sons, Inc. **127**, 239-318.

Schmid, H. P. (1994). Source areas for scalars and scalar fluxes. *Boundary-Layer Meteorology* **67**, 293–318.

Schmid, H. P. (1997). Experimental design for flux measurements: matching scales of observations and fluxes. *Agricultural and Forest Meteorology* **87**, 179–200.

Schmid, H. P. (2002). Footprint modeling for vegetation atmosphere exchange studies: a review and perspective. *Agricultural and Forest Meteorology* **113**(1-4), 159-183.

Schuepp, P. H., M. Y. Leclerc, et al. (1990). Footprint prediction of scalar fluxes from analytical solutions of the diffusion equation. *Boundary-Layer Meteorology* **50**(1-4), 353-373.

Seitzinger, S. P. and C. Kroeze (1998). Global distribution of nitrous oxide production and N input in freshwater and coastal marine ecosystems. *Global Biogeochemical Cycles* **12**, 93-113.

Seitzinger, S. P., C. Kroeze, et al. (2000). Global distribution of N_2O emissions from aquatic systems: natural emissions and anthropogenic effects. *Chemosphere - Global Change Science* **2**(3-4), 267-279.

Shimizu, A., K. Tanaka, et al. (2000). Abatement technologies for N_2O emissions in the adipic acid industry. *Chemosphere - Global Change Science* **2**(3-4), 425-434.

Simmonds, P. G., R. G. Derwent, et al. (1996). Long-term trends in concentrations of halocarbons and radiatively active trace gases in Atlantic and European air masses monitored at Mace Head, Ireland from 1987-1994. *Atmospheric Environment* **30**(23), 4041-4063.

Singles, R. (1996). Fine resolution modelling of ammonia dry deposition over Great Britain. PhD thesis, University of Edinburgh

Singles, R., M. A. Sutton, et al. (1998). A multi-layer model to describe the atmospheric transport and deposition of ammonia in Great Britain. *Atmospheric Environment* **32**(3), 393-399.

Sitaula, B. K., S. Hansen, et al. (2000). Effects of soil compaction on N_2O emission in agricultural soil. *Chemosphere - Global Change Science* **2**(3-4), 367-371.

Skiba, U. and B. Ball (2002). The effect of soil texture and soil drainage on emissions of nitric oxide and nitrous oxide. *Soil Use and Management* **18**(1), 56-60.

Skiba, U., C. Di Marco, et al. (2005). Quantification and validation of the total annual UK nitrous oxide budget. GANE project final report. CEH,Edinburgh, UK.

Skiba, U., K. J. Hargreaves, et al. (1992). Fluxes of nitric and nitrous oxides from agricultural soils in a cool temperate climate. *Atmospheric Environment Part a-General Topics* **26**(14), 2477-2488.

Skiba, U., I. P. McTaggart, et al. (1996). Estimates of nitrous oxide emissions from soil in the UK. *Energy Conversion and Management* **37**(6-8), 1303-1308.

Skiba, U. and K. A. Smith (2000). The control of nitrous oxide emissions from agricultural and natural soils. *Chemosphere-Global Change Science* **2**, 379-386.

Skiba, U., M. Sozanska, et al. (2001). Spatially disaggregated inventories of soil NO and N_2O emissions for Great Britain. *Water, Air and Soil Pollution: Focus* **1**, 109-118.

Skiba, U., S. van Dijk, et al. (2002). The influence of tillage on NO and N2O fluxes under spring and winter barley. *Soil Use and Management* **18**(4), 340-345.

Skiba, U. M., L. J. Sheppard, et al. (1998). Some key environmental variables controlling nitrous oxide emissions from agricultural and semi-natural soils in Scotland. *Atmospheric Environment* **32**(19), 3311-3320.

Smith, K. A. (1997). The potential for feedback effects induced by global warming on emissions of nitrous oxide by soils. *Global Change Biology* **3**(4), 327-338.

Smith, K. A., T. Ball, et al. (2003). Exchange of greenhouse gases between soil and atmosphere: interactions of soil physical factors and biological processes. *European Journal of Soil Science* **54**(4), 779-791.

Smith, K. A., H. Clayton, et al. (1994). Micrometeorological and Chamber Methods for Measurement of Nitrous-Oxide Fluxes between Soils and the Atmosphere - Overview and Conclusions. *Journal of Geophysical Research* **99**(D8), 16541-16548.

Smith, K. A., P. E. Thomson, et al. (1998). Effects of temperature, water content and nitrogen fertilisation on emissions of nitrous oxide by soils. *Atmospheric Environment* **32**(19), 3301-3309.

Soussana, J. F., C. Martin, et al. (2004). GREENGRASS. Sources and sinks of greenhouse gases from managed European grasslands and mitigation strategies. Final report to the European Commission DG Research, Vth Framework Programme, Energy, Environment and Sustainable Development. INRA Clermont-Ferrand, France, pp 208.

Sozanska, M. (1999). Distribution and amounts of nitric and nitrous oxide emissions from British soils. PhD thesis, University of Edinburgh.

Sozanska, M., U. Skiba, et al. (2002). Developing an inventory of N_2O emissions from British soils. *Atmospheric Environment* **36**(6), 987-998.

Spirig, C., A. Neftel, et al. (2004). Flux measurements of biogenic VOCs during ECHO 2003. *Atmospheric Chemistry and Physics Discussions* **4**, 6603-6643.

Stull, R. B. (1988). An Introduction to Boundary Layer Meteorology. The Netherlands, Kluwer Academic, pp. 818.

Sutton, M., U. Dragosits, et al. (2004a). The potential of NH_3, N_2O and CH_4 measurements following the 2001 outbreak of Foot and Mouth Disease in Great Britain to reduce the uncertainties in agricultural emissions abatement. *Environmental Science & Policy* **7**, 177-194.

Sutton, M., Y. S. Tang, et al. (2001a). A new diffusion denuder system for long-term, regional monitoring of atmospheric ammonia and ammonium. *Water, Air and Soil Pollution: Focus* **1**, 145-156.

Sutton, M. A., U. Dragosits, et al. (2004b). Ammonia emission and deposition in Scotland and its potential environmental impacts. *The Scientific World Journal* **4**, 795-810.

Sutton, M. A., Y. S. Tang, et al. (2001b). A Spatial Analysis of Atmospheric Ammonia and Ammonium in the UK. *The Scientific World Journal* **1**(S2), 275-286.

Teepe, R., A. Vor, et al. (2004). Emissions of N_2O from soils during cycles of freezing and thawing and the effects of soil water, texture and duration of freezing. *European Journal of Soil Science* **55**(2), 357-365.

Thomson, P. E., J. P. Parker, et al. (1997). Automated soil monolith-flux chamber system for the study of trace gas fluxes. *Soil Science Society of America Journal* **61**, 1323-1330.

Veldkamp, E., M. Keller, et al. (1998). Effects of pasture management on N2O and NO emissions from soils in the humid tropics of Costa Rica. *Global Biogeochemical Cycles* **12**, 71-79.

Velthof, G., S. C. Jarvis, et al. (1997). Spatial variability of Nitrous oxide fluxes from grasslands: differences between soil types. In: Gaseous nitrogen emissions from grasslands. S. C. Jarvis and S. C. Pain (eds.). Wallingford, UK, CAB International.

Velthof, G. and O. Oenema (1994). Nitrous oxide emission from grassland on sand, clay and peat soils in the Netherlands. *Journal of Geophysical Research* **99**, 16585-16592.

Velthof, G. L., A. B. Brader, et al. (1996a). Seasonal variations in nitrous oxide losses from managed grasslands in the Netherlands. *Plant and Soil* **181**, 263-274.

Velthof, G. L., S. C. Jarvis, et al. (1996b). Spatial variability of nitrous oxide fluxes in mown and grazed grasslands on a poorly drained clay soil. *Soil Biology & Biochemistry* **28**(9), 1215-1225.

Velthof, G. L., M. L. van Beusichem, et al. (1998). Mitigation of nitrous oxide emission from dairy farming systems. *Environmental Pollution* **102**, 173-178.

Verchot, L. V., E. A. Davidson, et al. (1999). Land use change and biogeochemical controls of nitrogen oxide emissions from soils in eastern Amazonia. *Global Biogeochemical Cycles* **13**(1), 31-46.

Vieno, M. (2005). The use of an Atmospheric Chemistry-Transport Model (FRAME) over the UK and the development of its numerical and physical schemes. PhD thesis, University of Edinburgh.

Wagner-Riddle, C., G. W. Thurtell, et al. (1996). Nitrous oxide and carbon dioxide fluxes from a bare soil using a micrometeorological approach. *Journal of Environmental Quality* **25**, 898-907.

Webb, E. K., G. I. Pearman, et al. (1980). Correction of flux measurements for density effects due to heat and water vapour transfer. *Quarterly Journal of the Royal Meteorological Society* **106**, 85-100.

Weitz, A. M., E. Veldkamp, et al. (1998). Nitrous oxide, nitic oxide, and methane fluxes from soils following clearing and burning of tropical secondary forest. *Journal of Geophysical Research* **103**, 28047-28058.

Werle, P. (1998). A review of recent advances in semiconductor laser based gas monitors. *Spectrochimica Acta Part a-Molecular and Biomolecular Spectroscopy* **54**(2), 197-236.

Wienhold, F. G., H. Frahm, et al. (1994). Measurements of N_2O fluxes from fertilized grassland using a fast response tunable diode laser spectrometer. *Journal of Geophysical Research* **99**(D8), 16,557-516,567.

Wienhold, F. G., M. Welling, et al. (1995). Micrometeorological measurement and source region analysis of nitrous oxide fluxes from an agricultural soil. *Atmospheric Environment* **29**(17), 2219-2227.

Williams, D. L., P. Ineson, et al. (1999). Temporal variations in nitrous oxide fluxes from urine-affected grassland. *Soil Biology & Biochemistry* **31**(5), 779-788.

Wrage, N., G. L. Velthof, et al. (2001). Role of nitrifier denitrification in the production of nitrous oxide. *Soil Biology & Biochemistry* **33**(12-13), 1723-1732.

Yamulki, S., K. W. T. Goulding, et al. (1995). Studies on NO and N_2O fluxes from a wheat field. *Atmospheric Environment* **29**(1627-1635).

Yamulki, S. and S. C. Jarvis (2002). Short-term effects of tillage and compaction on nitrous oxide, nitric oxide, nitrogen dioxide, methane and carbon dioxide fluxes from grassland. *Biology and Fertility of Soils* **36**(3), 224-231.

Yienger, J. J. and H. Levy II (1995). Empirical model of the soil-biogenic NO_x emissions. *Journal of Geophysical Research* **100**, 11447-11464.

Zahniser, M., D. Nelson, et al. (1997). A tunable diode laser system for atmospheric trace gas flux measurements. Billerica, MA, USA, Aerodyne Research Inc.

Zahniser, M., D. Nelson, et al. (1994). Measurement of trace fluxes using tunable diode laser spectroscopy. Exchange of Trace Gases between Land and Atmosphere Philosophical Transactions of the Royal Society.

Zahniser, M., D. Nelson, et al. (1995). Measurement of trace fluxes using tunable diode laser spectroscopy. *Philosophical Transactions of the Royal Society of*

London Series a-Mathematical Physical and Engineering Sciences(351), 371-382.

FIELD SCALE N_2O FLUX MEASUREMENTS FROM GRASSLAND USING EDDY COVARIANCE

C. DI MARCO[1,2,*], U. SKIBA[1], K. WESTON[2], K. HARGREAVES[1] and D. FOWLER[1]
[1]*Centre for Ecology and Hydrology (Edinburgh), Bush Estate, Penicuik, Midlothian, UK;*
[2]*University of Edinburgh, Atmospheric Sciences, School of Geosciences, UK*
*(*author for correspondence, e-mail: cdma@ceh.ac.uk; phone: +44-131-4454343, fax: +44-131-4453943)*

Abstract. In order to assess nitrous oxide (N_2O) emissions from typical intensively managed grassland in northern Britain fluxes were measured by eddy covariance using tuneable diode laser absorption spectroscopy from June 2002 to June 2003 for a total period of 4000 h. With micrometeorological techniques it is possible to obtain a very detailed picture of the fluxes of N_2O at field scale (10^3–10^4 m^2), which are valuable for extrapolation to regional scales. In this paper three of the four fertilizer applications were investigated in detail. N_2O emissions did not always show a clear response. Hourly fluxes were very large immediately after the June 2002 nitrogen fertilizer application, peaking at 2.5 mg N_2O–N m^{-2} s^{-1}. Daily fluxes were averaging about 300 ng N_2O m^{-2} s^{-1} over the 4 days following fertilizer application. The response of N_2O emissions was less evident after the August fertilization, although 2 days after fertilizer application an hourly maximum flux of 554 ng N_2O–N m^{-2} s^{-1} was registered. For the rest of August the flux was undetectable. The differences between fertilization events can be explained by different environmental conditions, such as soil temperature and rainfall. A fertiliser-induced N_2O emission was not observed after fertilizer application in March 2003, due to lack of rainfall. The total N_2O flux from June 2002 to June 2003 was 5.5 kg N_2O–N $ha^{-1}y^{-1}$, which is 2.8% of the total annual N fertilizer input.

Keywords: eddy covariance, micrometeorological measurements, nitrous oxide emissions, tuneable diode laser

1. Introduction

Of the major greenhouse gases, N_2O emissions are the least well quantified at the country scale. The current methodology available within the IPCC process. (IPCC, 1997) assumes that a fixed fraction of the nitrogen (N) applied to land is emitted as N_2O to the atmosphere. In practice, the fraction of N applied as fertilizer that is subsequently emitted as N_2O varies with soil and environmental variables. Therefore there are still significant uncertainties associated with the estimated magnitude of sources such as agricultural soils (from 1.8 to 5.3 Tg-N y^{-1}) (Laville *et al.*, 1999) and tropical soils (from 2.7 to 5.7 Tg-N y^{-1}).

In a literature study of quantitative estimates of N_2O emission rates from a range of land-uses across Europe, Machefert *et al.* (2002) showed that the highest rates were from agricultural lands compared to forests and natural grasslands. However, managed grasslands in the UK are estimated to have one of the highest emission rates (9.35 kg N_2O–N ha^{-1} y^{-1}) compared to forest and grassland

Water, Air, and Soil Pollution: Focus **4:** 143–149, 2004.
© 2004 *Kluwer Academic Publishers. Printed in the Netherlands.*

(0–4.9 kg N_2O–N ha^{-1} y^{-1}) in the rest of Europe (Machefert *et al.*, 2002). Furthermore, managed grasslands cover 27% of UK area (Barr *et al.*, 1993), receive large rates of fertilizer (200–500 kg N $ha^{-1}y^{-1}$), tend to be in the wetter parts of the country and are trampled and compacted by animals. These factors together promote the production of N_2O by denitrification. Therefore a detailed study of N_2O fluxes from managed grassland is required to investigate diurnal and seasonal variations in N_2O emission.

So far, the spatial and seasonal influence on agricultural N_2O emissions has mostly been studied using small chambers (Clayton *et al.*, 1994; Christensen *et al.*, 1996) with the disadvantage that each chamber samples just a small area (<1 m^2). Large numbers of chambers are needed to get a representative estimate of fluxes from field sites with high spatial variability such as grasslands. This study report a micrometeorological technique that provides flux measurements integrated on large scales, depending on the sampling height and avoids the problem of spatial and temporal variability of N_2O emissions.

2. Materials and Methods

The experiment was carried out over an intensively managed grassland at Easter Bush, 10 km south of Edinburgh, Scotland (55°52′N, 3°2′W Grid Ref: NT245641). Flux measurements were made from 6 June 2002 to 20 June 2003 almost continuously. The instruments were situated on the boundary between two grassland fields of approximately 16 ha in total. The fields consist of a clay loam soil mainly covered ($>95\%$) with *Lolium perenne*, partially grazed and fertilized three times per year with NPK fertilizer. Previous studies of the wind direction frequency distribution at Easter Bush (1998–2002) showed that the dominant direction was from the SW sector, providing homogeneous fetch suitable for micrometeorological measurements (Milford *et al.*, 2001).

NPK fertilizer was applied to both fields at a rate of 60 kg N ha^{-1}on 7 June 2002 and at 50 kg N ha^{-1}on 10 August 2002. In March 2003 the two fields were fertilized on two different days: one field with NPK at 84 kg N ha^{-1} on 17 March and the other with NH_4NO_3 at 51.7 kg N ha^{-1}on 20 March. In June 2003 NPK fertilizer was applied at a rate of 48 kg N ha^{-1}.

The N_2O fluxes were determined using the eddy covariance method, which expresses the turbulent vertical flux density F of a trace gas as the covariance between the vertical wind and trace gas density fluctuations as follows:

$$F = \overline{w'c'}$$

where w' and c' are the fluctuations of the 15-minute average vertical wind velocity and trace gas density, respectively. N_2O concentrations were measured with a tuneable diode laser absorption spectrometer (TDLAS, Aerodyne Res. Inc. Billerica, Mass. U.S.A.) scanning the single N_2O line at 2209.5 cm^{-1} and wind speed

with a sonic anemometer (METEK), fixed on the same mast (2.5 m high) where the TDL inlet was positioned. Under field conditions this spectrometer allowed to measure N_2O concentrations at 10 Hz with a precision of 1%. Fluxes were calculated from 10-Hz measurements integrated over 15-minute intervals. Wind speed and concentration raw data were detrended using a linear fit to remove a possible additional low frequencies component on the signal which is not related to the local flux. No high frequency filtering was used. To avoid distortions caused by obstacles in the fetch, data from outside the good fetch sectors were removed. Only data from 200 °C to 315 °C and 25 °C to 70 °C were retained.

3. Results

Figure 1 shows the complete period of N_2O flux measurements between 6 June 2002 and 20 June 2003. A clear response to fertilization was observed the day after the 7 June (mean daily emission of 1.5 mg N_2O–N m^{-2} s^{-1}) and 10 August (69 ng N_2O–N m^{-2} s^{-1}) N application. Peaks in the emissions were also observed on 16 September (72 ng N_2O–N m^{-2} s^{1}), 24 April (63 ng N_2O–N m^{-2} s^{-1}) and 15 May (49 ng N_2O–N m^{-2} s^{-1}) when the ground was compacted and animals were moved to adjacent fields. Gaps of data were caused by inappropriate wind direction, power cuts and problems with TDL behaviour. Daily fluxes were obtained by averaging the available data. The TDL was in the field for 5712 h and provided 4452 h of data, of which 3218 h were used to calculate fluxes.

Rainfall data recorded at Easter Bush were used to investigate the relationship between soil moisture and N_2O losses. Rainfall is not always representative of the

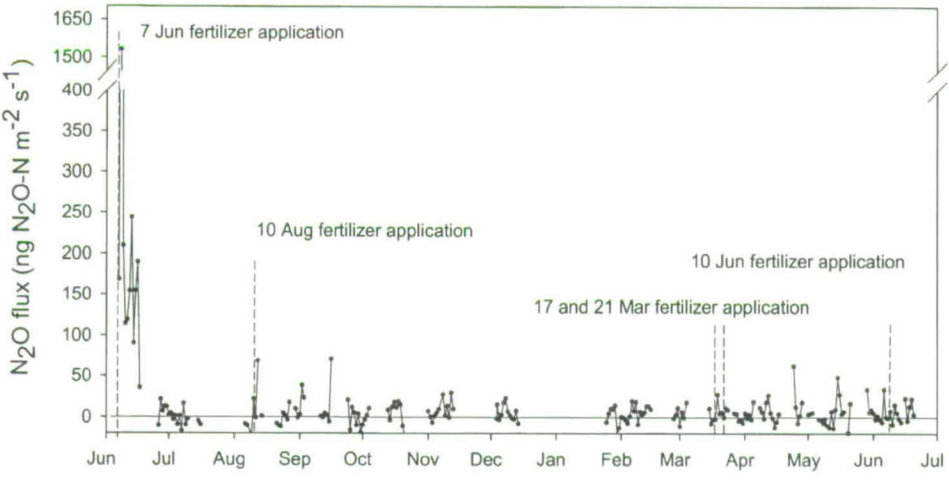

Figure 1. N_2O flux measurements at Easter Bush site. Daily values from June 2002 to June 2003. Vertical bars show fertilization events.

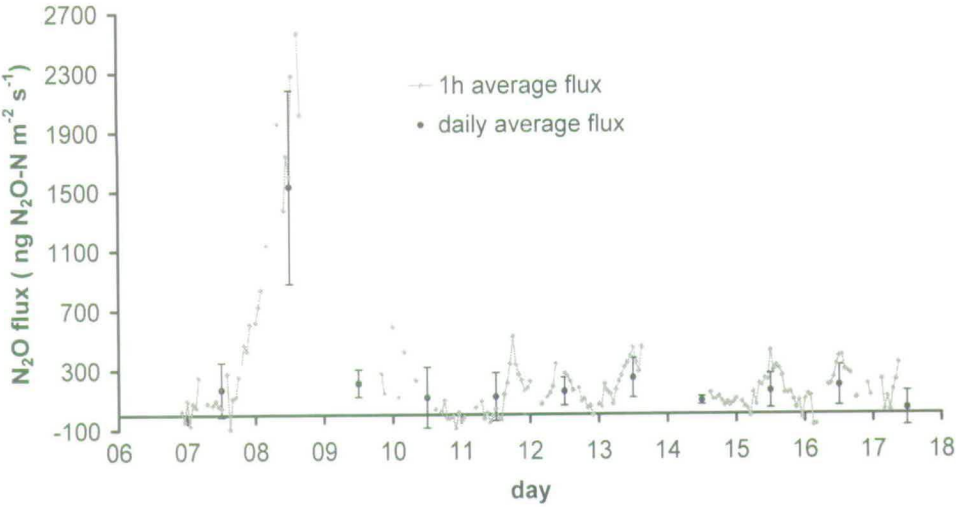

Figure 2. N_2O fluxes at Easter Bush in June 2002. Error bars show the uncertainty in a daily average flux.

soil water content because of the nature and the texture of the soil, but does give qualitative information of the soil condition.

During the month of June 2002, 107 mm of rainfall and a mean air temperature of 16 °C were registered at Easter Bush. Immediately after fertilizer application on 7 June, a quick response in N_2O losses was observed and peaked at 2.5 mg N_2O–N m^{-2} s^{-1} about 24 h after fertilizer application (Figure 2), showing an average daily emission of 1.5 mg N_2O–N m^{-2} s^{-1} on the first day after the fertilization. This pulse was equivalent to 1.3% of the total N fertilizer applied. Daily emissions then decreased, ranging from 91 ng N_2O–N m^{-2} s^{-1} to 244 ng N_2O–N m^{-2} s^{-1} for 10 days after the event. About 20 days after fertilizer application, from 26 June until 30 June, N_2O losses decreased to a daily average ranging from 7 ng N_2O–N m^{-2} s^{-1} to 21 ng N_2O–N m^{-2} s^{-1}. Negative fluxes in Figure 2 might be due to advection or storage effects that are not taken into account in this preliminary analysis.

From 11 to 17 June N_2O emissions showed a clear diurnal pattern (maximum value at noon and minimum during the night), also emphasized by the relationship with the sensible heat flux. The correlation coefficient between sensible heat flux H and N_2O flux ($r^2 = 0.72$) on 15 June (Figure 3) confirmed the air turbulence influence on N_2O fluxes, considering that sensible heat flux provides information about the exchange of turbulent energy between surface and atmosphere.

In August the rainfall measured at Easter Bush during the period of fertilization showed days with high rates of rainfall (from 5 to 20 mm) alternated by dry days. The response of N_2O emissions after the fertilizer application was less pronounced than in June. On 12 August a maximum flux of 554 ng N_2O–N m^{-2} s^{-1} was measured. For the rest of the month fluxes were mostly undetectable.

TABLE I

Summary of environmental conditions and N_2O emissions for the three-fertilisation events: June 2002, August 2002, and March 2003

	Soil temperature range (°C)	Total rainfall during 7 days before fertilization (mm)	Total rainfall during 8 days after fertilization (mm)	Rate of N addition (kg ha^{-1})	N_2O daily flux range after (ng N_2O–N m^{-2} s^{-1})
June	11–18	39	37.9	60	7–1532
August	14.5–18.5	78	32.7	50	13–44
March	2–7	0.8	–	84	4–27

March 2003 was a very dry month with 30 mm of rainfall and temperature about 2 °C above the 5.6 °C normal monthly average. The absence of water in the soil inhibited denitrification and N_2O emissions (Dobbie *et al.*, 1999) with a result of very small fluxes for the whole month (daily average ranging between 4 and 27 ng N_2O–N m^{-2} s^{-1}) in spite of the high spring N fertilizer application input (Table I).

Table I shows a summary of the soil and meteorological variables fundamental for their contribution to N_2O emissions for the months of June, August and March and N_2O flux measured. In June, 39 mm of rain was evenly distributed during 1 week, whereas in August, 78 mm of rain fell in 2 days during the week before fertilization. The differences in rainfall pattern are the most likely reason why the big "pulse" observed in June was not detected in August.

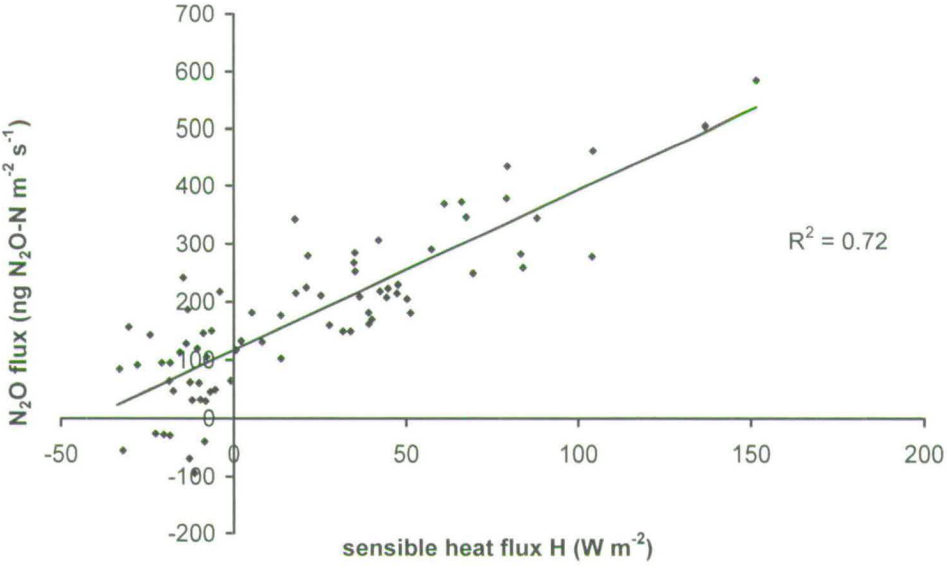

Figure 3. Correlation between N_2O fluxes and sensible heat flux at Easter Bush on 15 June 2002.

4. Discussion

The three fertilization events occurred during contrasting environmental conditions, which was reflected in the magnitude of the N_2O fluxes measured. Clear diurnal variations of N_2O emissions were only observed after N from fertilization in June and they agree with previous studies (Smith *et al.*, 1998). The maximum flux value (15-min average) measured on 8 June at 14:30 (GMT) was 3.2 mg N_2O–N m^{-2} s^{-1}, which is extraordinarily large. The fact that such large values do not appear in the literature might be explained by the methodology used here. The eddy correlation technique permits continuous measurements with fluxes calculated every 15 min integrated over an area of 0.01–1 km^2, whereas static chambers provide at maximum only one flux measurement per hour and therefore have a larger probability of missing big emission peaks.

Although calculation of annual fluxes cannot be easily generalized because of large inter annual differences in meteorological conditions, they allow us to estimate the potential emission of a particular type of field. Using 15 min average values for gap filling June 2002 data and interpolation of 1 h average values for the rest of the data total annual emission at Easter Bush were estimated to be 5.5 kg N_2O–N ha^{-1} y^{-1} or 2.8% of the fertilizer N input. This result is very similar to the cumulative N_2O flux 4.08 kg N_2O–N ha^{-1} y^{1} representing 1.36% of the fertilizer N input measured during the same period with static chambers at Cowpark, a nearby, similarly managed grassland field. (S. K. Jones, personal communication).

Acknowledgement

This work was part of the GANE project funded by NERC (NER/T/S/2000/00195).

References

Barr, C. J., Bunce, R. G. H., Clarke, R. T., Fuller, R. M., Furse, M. T., Gillespie, M. K., Groom, G. B., Hallam, C. J., Hornung, M., Howard D. C. and Ness, M. J.: 1993, *Countryside Survey 1990: Main Report*, Department of the Environment, Eastcote, 174 pp.

Christensen, S., Ambus, P., Arah, J. R. M., Clayton, H., Galle, B., Griffith, D. W. T., Hargreaves, K. J., Klemedtsson, L., Lind, A. M., Maag, M., Scott, A., Skiba, U., Smith, K. A., Welling, M. and Wienhold, F. G.: 1996, 'Nitrous oxide emission from an agricultural field: Comparison between measurements by flux chamber and micrometerological techniques', *Atmos. Environ.* **30**, 4183–4190.

Clayton, H., Arah, J. and Smith, K. A.: 1994, 'Measurements of nitrous oxide emissions from fertilized grassland using closed chambers', *J. Geophys. Res.* **99**(16), 599–516, 607.

Dobbie, K. E., McTaggart, I. P. and Smith, K. A.: 1999, 'Nitrous oxide emissions from intensive agricultural systems: Variations between crops and seasons, key driving variables, and mean emission factors', *J. Geophys. Res.* **104**(26), 891–826, 899.

IPCC (Intergovernmental Panel on Climate Change): 1997, J. T. Houghton *et al.* (eds.), *Stabilization of Atmospheric Greenhouse Gases: Physical, Biological and Socio-Economic Implications.*

Laville, P., Jambert, C., Cellier, P. and Delmas, R.: 1999, 'Nitrous oxide fluxes from a fertilized maize crop using micrometeorological and chamber methods', *Agric. Forest. Meteorol.* **96**, 19–38.

Machefert, S. E., Dise, N. B., Goulding, K. W. T. and Whitehead, P. G.: 2002, 'Nitrous oxide emission from a range of land uses across europe', *Hydrol. Earth Syst. Sci.* **6**, 325–337.

Milford, C., Theobald, M. R., Nemitz, E. and Sutton, M.: 2001, 'Dynamics of ammonia exchange in response to cutting and fertilising in an intensively-managed grassland', *Water Air Soil Pollut.* **1**, 167–176.

Smith, K. A., Thomson, P. E., Clayton, H., McTaggart, I. P. and Conen, F.: 1998, 'Effects of temperature, water content and nitrogen fertilisation on emissions of nitrous oxide by soils', *Atmos. Environ.* **32**, 3301–3309.